

**RUTHENIUM(II) COMPLEXES WITH TERPYRIDINE  
DERIVATIVES.  
WHAT IS THE LIFETIME OF THE EXCITED STATE  
DEPENDENT ON?**

by

Dott. Marco Duati,

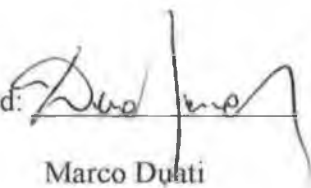
A Thesis presented to Dublin City University for the degree of Doctor of  
Philosophy.

Supervisor Prof. J.G.Vos  
School of Chemical Sciences  
Dublin City University

September 2001

I hereby certify that this material, which I now submit for assessment on the programme of Study leading to award of Doctor of Philosophy by research and thesis, is entirely my own work and has not been taken from work of others, save and to extent that such work has been cited and acknowledged within the text of my work.

Signed:



Marco Duati

I.D. No. 98970380

Date 22-01-2002

*Ai miei genitori.....*

“Seriousness is the only refuge of the shallow.”

**Oscar Wilde**

## Ringraziamenti

Lunga la lista, stretta e' la via  
Il ringraziamento e' in lingua natia.  
Prima di tutti vi voglio citare,  
Il supervisor che m'ha fatto arrivare.

Vien dall'Olanda,  
Han Vos e' chiamato,  
Di tutta la banda  
E' il prim ringraziato.

Poi la famiglia  
Vogliam nominare  
che parapiglia  
se non la dovessi citare.

Nominiam poi la folla  
Che lavora nel lab  
Con loro e' un molla  
Si va sempre al pub.

Quelli del lab tuttora presenti  
Dec , Helen, Adrian e Fiona  
Scott, Moss e l'altra Fiona  
E Wesley abbiam fatto contenti

E quelli che poi se ne son andati  
Anthea, Luke, Christine, Benedicte,  
Paolo, Johan, Peppe, Egbert.  
Davanti a me sono sfilati

Poi i crucchi anche ricordo  
Holger, Connie, Marty, Andre'  
Questi ho visto in anni tre,  
Mo qualcun so, lo scordo

Poi di Chimica Profe e studenti  
E qui nomi son piu' di venti  
Mo li vado a enumerare  
Tutti quanti li vorrei contare

Davnat Jennifer Mairead Carol

Kieran Ray Robbie Karl  
Mike Niamh Sean Kevin  
Rachel Darren Mary Ian

Noel Gerard Johnnys Cathal  
Maura Frances Brendan, Colm,  
Marion Eimear Michaela Eadaoin  
Andrea Siobhan Bronagh Lynn

Sonia Edna Clodagh ho citati  
Chissa' quanti ne ho saltati  
Nessun male me ne voglia  
Se lo lascio sulla soglia

Tutti Tecnici ricordiamo  
Forte forte li abbracciamo  
Squash e Yogha e la palestra  
Mi han salvato sai la testa

Tutti quelli che ho incontrato  
A DCU ho salutato  
Ora passo a UCD  
E forse anche a TCD

Dani Manu Monica e Mara  
Me le porto nella bara  
E gli Italici di Irlanda  
Sai li conto nella banda

Chi nel lavoro mi ha aiutato  
Ma in Irlanda non ha lavorato  
Milly, Stefano, Monica e Roberto  
Un grazie a tutti a cuore aperto.

Milioni di nomi mi volano in mente  
Ma le parole non contano niente  
A tutti quanti un grazie sicuro  
Ma il tempo passa vi scordo lo giuro.

Una cosa sola vi voglio poi dire  
Ricordate tutti dobbiamo morire. (Ha Ha)

## Abstract.

The synthesis, spectroscopic and electrochemical characterisation of ruthenium (II) polypyridyl mononuclear complexes containing 1,2,4-triazole and tetrazole moiety are described. Chapter one is an introduction relating to the work described in the thesis. The methods of characterisation, which are described in chapter two, include High Performance Liquid Chromatography,  $^1\text{H-NMR}$ , UV/Visible spectroscopy, fluorimetry, electrochemistry, spectroelectrochemistry, mass spectrometry, and lifetime emission measurements.

Chapter three describes the synthesis of the new set of ligands and their mononuclear Ruthenium (II) complexes.

Chapter four contains an extensive characterisation of  $\text{Ru(II)(bpy)}_2$  moiety complexes containing a 5-(2-pyridyl)-1,2,4-triazole ligand, ( $\Delta\text{py}$ ), or a 5-(2-pyridyl) tetrazole ligand, ( $\square\text{py}$ ), and their comparison with the archetype  $\text{Ru(bpy)}_3^{2+}$ . The examination of the acid-base chemistry of the complexes by UV/Visible spectroscopy revealed important information about the location of the excited state

Chapter five explores the spectroscopic, photophysical and electrochemical properties of the new  $[\text{Ru(tpy)(}\Delta\text{py}\Delta)]$  complexes, where  $(\Delta\text{py}\Delta)^{2-}$  is the 2,6 di-(1,2,4-triaz-3-yl)-pyridine ligand. The new species was exhaustively studied especially because it revealed to be one of the few example, available in literature, of emitting Ru(II) terpyridine complexes, with a lifetime of the excited state in the order of 100 nanoseconds.

Chapter six describes the synthesis of complexes containing  $(\Delta\text{py}\Delta)^{2-}$  and terpyridine derivatives or vice-versa terpyridine and  $(\Delta\text{py}\Delta)^{2-}$  derivative ligands. One of them will be used as a photosensitiser in a photovoltaic cell. Attachment of the  $[\text{Ru(II)(tctpy)(}\Delta\text{py}\Delta)]$  complex to nanocrystalline  $\text{TiO}_2$  films indicates incident photon-to-current efficiency (IPCE) of greater than 60%.

Chapter seven explores the use of a new 2,6 di-(tetraz-5-yl)-pyridine ligand, ( $\square\text{py}\square$ ) $^{2-}$ , and the spectroscopic, photophysical and electrochemical properties of its Ru(II) complexes.

Chapter eight is an attempt to rationalise the collected data of the Ru(tpy) moiety. The change of the energy levels in relation to the different ligands is analysed. The correlations between spectroscopic, photophysical and electrochemical data of the new complexes and the existent ones created an extensive knowledge of the tridentate Ru(II) complexes, that increases their availability as a photosensitive building block for a supramolecular system. Some suggestions for future work are also considered in the final Chapter.

Finally two appendices are included in this thesis. The first is a literature survey which synopsis the last ten years scientific papers, on the Ru-tpy moiety, including investigations of their properties, use in analytical research or their use as building blocks in supramolecular systems. The second appendix refers to the publications, poster presentations and oral presentations made during the course of the research.

---

## Table of Contents

---

<b>Chapter 1: Introduction</b>	<b>1</b>
1.1 Introduction	2
1.2 Unimolecular Complexes	4
1.2.1 Light Absorption	6
1.2.2 Excited State Processes	8
1.3 Supramolecular Systems	12
1.3.1 Localisation of Excitation Energy	15
1.4 Intercomponent Processes	16
1.5 Photochemical Molecular Devices	28
1.5.1 Photoinduced Electron Transfer PMDs	29
1.5.2 Electronic Energy Transfer PMDs	31
1.5.3 Photoinduced Structural Change PMDs	32
1.5.4 Design of Supramolecular Systems as Semiconductor Sensitisers	33
1.6 Ruthenium Polypyridine Complexes	43
1.7 Scope of the Thesis	50
1.8 Bibliography	53
<b>Chapter 2: Experimental Procedures</b>	<b>58</b>
2.1 Introduction	59
2.2 Chromatographic Techniques	59
2.3 Absorption and Emission Spectroscopy	60
2.4 Luminescent lifetime	61
2.5 Nuclear Magnetic Resonance	61
2.6 Electrochemistry	62
2.7 Mass Spectroscopy	63
2.8 Spectroelectrochemistry	63
2.9 Elemental Analysis	64
2.10 Titanium Dioxide Solar Cells	65
<b>Chapter 3: Synthesis of Ligands and Complexes</b>	<b>65</b>
3.1 Synthesis of 4,4',4'' methoxy carbonyl 2,2';6', 2'' terpyridine (tctpy)	66
3.2 Synthesis of 4' (pyrid-4''-yl) 2,2';6', 2'' terpyridine (py-tpy)	68
3.3 Synthesis of di-2,6(1,2,4, triaz-3-yl) pyridine ( $\Delta$ py $\Delta$ )	70
3.4 Synthesis of di-2,6[5 phenyl (1,2,4, triaz-3-yl)] pyridine ( $\Phi$ $\Delta$ py $\Delta$ $\Phi$ )	73
3.5 Synthesis of di-2,6(tetraz-5-yl) pyridine ( $\square$ py $\square$ )	74
3.6 Synthesis of [Ru(x-tpy)Cl <sub>3</sub> ]	75
3.7 Synthesis of [Ru(tctpy)Cl <sub>3</sub> ]	75
3.8 Synthesis of [Ru( $\Delta$ py $\Delta$ )Cl <sub>3</sub> ]	76

---

3.9	Synthesis of [Ru(py-tpy)Cl <sub>3</sub> ]	76
3.10	Synthesis of Na <sub>3</sub> [Ru(tctpy)(ΔpyΔ)]	77
3.11	Synthesis of [Ru(tpy)(ΔpyΔ)]	77
3.12	Synthesis of [Ru(Cl-tpy)(ΔpyΔ)]	78
3.13	Synthesis of [Ru(tpy)(ΦΔpyΔΦ)]	79
3.14	Synthesis of [Ru(tpy)(□py□)]	80
3.15	Synthesis of [Ru(Cl-tpy)(□py□)]	80
3.16	Synthesis of [Ru(py-tpy)(□py□)]	81
3.17	Synthesis of [Ru(bpy) <sub>2</sub> (Δpy)][PF <sub>6</sub> ]	81
3.18	Synthesis of [Ru(bpy) <sub>2</sub> (□py)][PF <sub>6</sub> ]	82
3.19	Preparation of Titanium Dioxide	83
<b>Chapter 4: Bpy Base Complexes</b>		<b>92</b>
4.1	Introduction	93
4.2	The Archetype: [Ru(bpy) <sub>3</sub> ] <sup>2+</sup>	97
4.2.1	Characterisation and NMR Spectroscopy	97
4.2.2	Electrochemistry and Electronic Spectroscopy	99
4.2.3	Lifetime Temperature Dependence	100
4.3	The Triazolate Model: [Ru(bpy) <sub>2</sub> (Δpy)] <sup>+</sup>	101
4.3.1	NMR Spectroscopy	106
4.3.2	Redox Properties	107
4.3.3	Electronic Spectroscopy	109
4.3.4	Acid-Base Properties	116
4.3.5	Temperature Dependence	121
4.4	The Tetrazolate Model: [Ru(bpy) <sub>2</sub> (□py)] <sup>+</sup>	123
4.4.1	NMR Spectroscopy	124
4.4.2	Electronic Spectroscopy	129
4.4.3	Redox Properties	131
4.4.4	Lifetime Temperature Dependence	133
4.5	Conclusions	134
4.6	Bibliography	136
<b>Chapter 6: The Prototype: [Ru(tpy)(ΔpyΔ)]</b>		<b>139</b>
5.1	Introduction	140
5.2	Synthesis and Purification	142
5.3	NMR Spectroscopy	148
5.4	Electronic Spectroscopy	151
5.5	Redox Properties and Spectroelectrochemistry	161
5.6	Lifetime Temperature Dependence	164
5.7	Solute Solvent Interaction	173
5.8	Conclusions	184
5.9	Bibliography	186



---

<b>Chapter 6: The Triazolate Family</b>	<b>189</b>
6.1 Introduction	190
6.2 [Ru(Cl-tpy)( $\Delta$ py $\Delta$ )]	192
6.2.1 Synthesis and Purification	193
6.3 [Ru(tctpy)( $\Delta$ py $\Delta$ )] <sup>5-</sup>	197
6.3.1 Synthesis and Purification	201
6.4 Synthesis and Characterisation of [Ru(tpy)( $\Phi$ $\Delta$ py $\Delta$ $\Phi$ )]	209
6.5 Bibliography	225
<b>Chapter 7: The Tetrazolate Family</b>	<b>227</b>
7.1 Introduction	228
7.2 Synthesis and Purification	231
7.3 NMR Spectroscopy	232
7.4 Electronic Spectroscopy	239
7.5 Redox Properties and Spectroelectrochemistry	245
7.6 Temperature Dependence of the MLCT Energy and Lifetime	248
7.7 Solute Solvent Interaction	251
7.8 Conclusions	255
7.9 Bibliography	256
<b>Chapter 8: Final Discussion, Conclusions and Future Work</b>	<b>258</b>
8.1 Introduction	259
8.2 Discussion	261
8.3 Future Work	276
<b>Appendix I : Literature Survey 1991-2001</b>	<b>277</b>
<b>Appendix II : Publications and Presentations</b>	<b>289</b>

---

## **Chapter One**

### **“ The Introduction ”**

“Nothing is as easy as it looks.  
Everything takes longer than you think”  
**Murphy**

## 1.1 Introduction

The first pioneering studies on the photochemical behaviour of co-ordination compounds date back to the late 1950s<sup>1,2,3,4</sup>. In these five decades, the field has experienced an enormous growth and the photochemistry of co-ordination compounds stands now as a well-known and active research field<sup>5,6,7,8</sup>. The first period of this development, in the seventies, saw strong activity in the qualitative and quantitative characterisation of the photoreactivity of several classes of co-ordination compounds, notable examples being Cr(III) and Co(III) complexes. Parallel efforts were devoted, in the same period, to the characterisation of the photophysical behaviour of several classes of co-ordination compounds based on metal ions such as: Cr(III), Ru(II), Os(II), Rh(III) and Ir(III) complexes. An important goal in the field was the recognition that excited state compounds can easily be involved in bimolecular processes such as energy and electron transfer; in this last process<sup>9</sup>, co-ordination compounds are extremely versatile because of their easily tunable redox properties<sup>10,11,12</sup>. This has permitted an extraordinary blossoming of studies on bimolecular processing.  $\text{Ru}(\text{bpy})_3^{2+}$ , one of the most popular single molecules of the whole chemical scene over the last thirty years, has surely played the leading role<sup>13,14</sup>. The problem of chemical conversion of solar light into energy has provided additional driving force to the field<sup>15,16,17,18</sup>. At the end of these four decades, it can be fairly stated that for several classes of simple co-ordination compounds, a satisfactory

degree of understanding of the excited state properties (photophysical behaviour, unimolecular reactivity and bimolecular processes) has been reached.

With this background firmly established, it's possible now to start to shift towards the study of more complex systems. This tendency, that is part of a more general trend of today's chemical research from the molecules towards supramolecular systems<sup>19,20</sup>, has brought into the photochemical scene polynuclear co-ordination, i.e. relatively large molecules containing two or more transition metal complex subunits (components) linked together by suitable bridging ligands.

Moreover, interesting developments of this field can be imagined if the spatial organisation inherent to polynuclear complexes coupled to the possibility of performing appropriate sequences of intercomponent transfer processes is considered. It is indeed conceivable that research in this area can lead in the future to the development of a polynuclear system capable of performing valuable light induced functions such as charge separation and vectorial transport of electronic energy (Photonic Molecular Devices)<sup>21,22</sup>.

## 1.2 Unimolecular complexes

Molecules are multielectron systems, where the electronic Schrodinger equation can not be solved exactly. Approximate electronic wavefunctions of a molecular system can be conveniently written as products of one electron wavefunctions, each consisting of an orbital and a spin part

$$\Psi = \Phi S = \prod_i \phi_i s_i \quad (1.1)$$

The  $\phi_i$  are appropriate molecular orbitals (MO) and  $s_i$  is one of the two possible spin eigenfunctions. The orbital part of this product multielectron wavefunction defines the electronic configuration to which the electronic state belongs.

Typical inorganic molecules of photochemical interest are co-ordination compounds of transition metals. A schematic MO diagram for an octahedral transition metal is shown in Fig. 1.1

The various MOs can be conveniently classified according to their predominant atomic orbital contribution as:

- i. strongly bonding, ligand centred  $\sigma_L$  orbitals
- ii. bonding, ligand centred  $\pi_L$  orbitals
- iii. essentially non bonding  $\pi_M(t_{2g})$  metal centred, predominantly d orbitals
- iv. antibonding  $\sigma_M^*$  ( $e_g$ ) metal centred, predominantly d orbitals
- v. ligand centred antibonding  $\pi_L^*$  orbitals
- vi. strongly antibonding, metal centred  $\sigma_M^*$  orbitals.

In the electronic ground configuration state of an octahedral complex of a  $d^n$  metal ion, orbitals of type (i) and (ii) are completely filled, while  $n$  electrons occupy the orbitals of type (iii) and (iv). As usual, excited configurations can be obtained from the ground configurations by promoting one electron from occupied to vacant MOs.

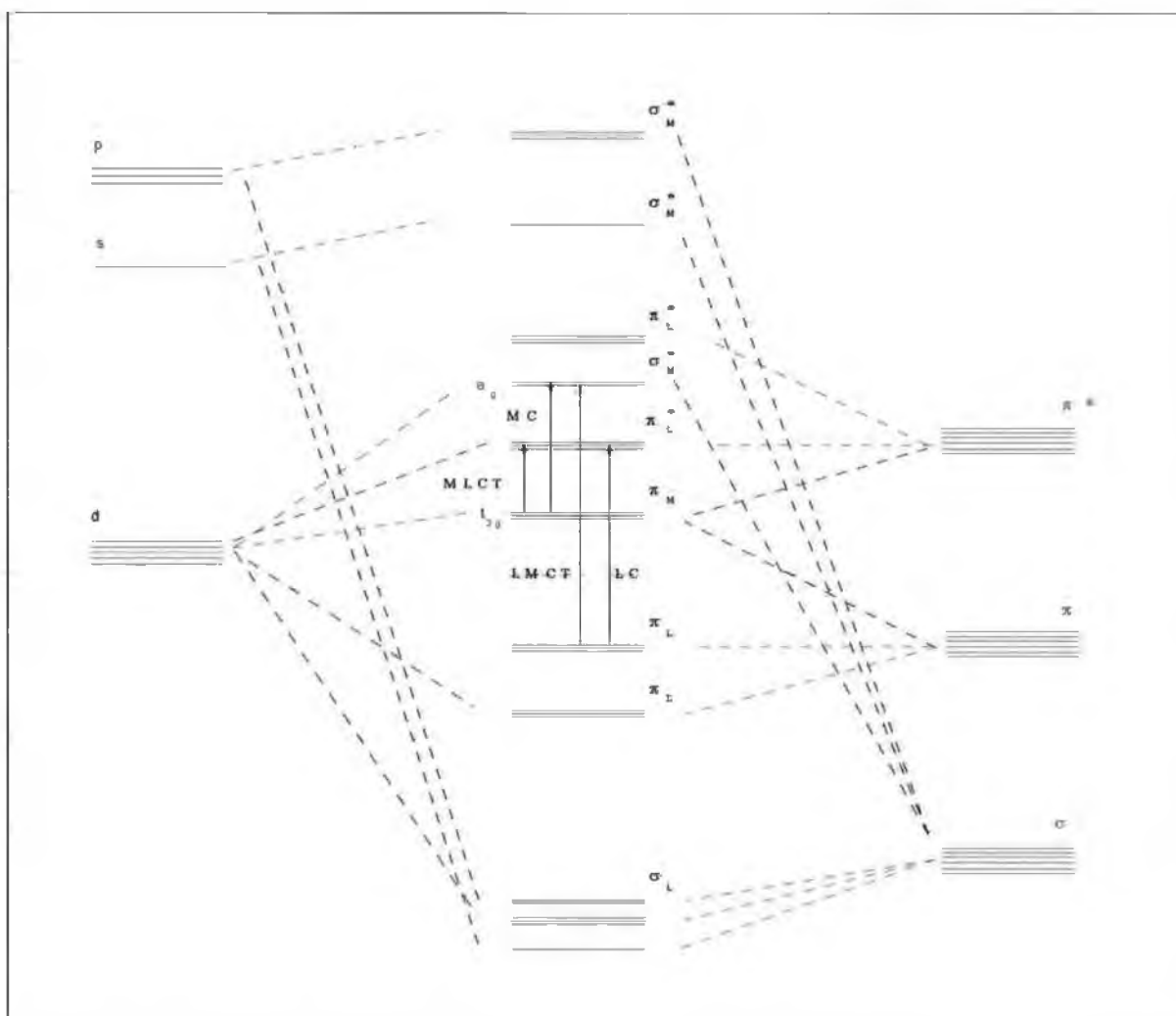


**Figure 1.1 MO diagram for an octahedral metal complex, the arrows indicate the types of transitions based MO configuration.**

At relatively low energies it's possible to find electronic transitions of this type:

- a) metal centred, MC, transitions from of type (iii) to orbitals of type (iv)
- b) ligand centred, LC, transitions from (ii) to (v)
- c) ligand to metal charge transfer, LMCT, from (iii) to (v)
- d) metal to ligand charge transfer, MLCT, from (ii) to (iii)

The relative energy ordering of these types of configurations in any particular complex depends on the nature of the metal and the ligands.

### 1.2.1 Light absorption

A molecule can be promoted from the ground electronic state to an electronically excited state by the absorption of a quantum of light, if the photon energy,  $h\nu$ , matches the energy gap between the two states. This energy gap, for low energy states of inorganic molecules corresponds to light in the visible and near ultraviolet regions.

The probability of transition from the ground state  $\Psi_i$  to the excited state  $\Psi_f$  is proportional to the square of the transition moment

$$M_{if} = \langle \Psi_i | \mu | \Psi_f \rangle \quad (1.2)$$

where  $\mu$  is the dipole moment operator<sup>23</sup>.

The equation (1.2) can be elaborated in the form:

$$M_{if} = \langle \Phi_i | \mu | \Phi_f \rangle \langle s_i | s_f \rangle \sum_n \langle x_{i,n} | x_{f,n} \rangle \quad (1.3)$$

The dipole-moment operator is considered to be independent of nuclear co-ordinates, Frank Condon approximation, and spin; it only appears in the integral containing the orbital part of the electronic wave function.

From the equation (1.3) it becomes possible to identify typical cases in which the first or second term are expected to vanish, thus leading to a zero predicted intensity of the electronic transition. The rules defining such cases are known as the selection rules for light absorption. Because of the orthogonality of spin wavefunctions, the second term in (1.3) is expected null whenever the initial and the final states have different multiplicity; those electronic transitions are called spin-forbidden.

Departure from this approximation can be dealt with in terms of a perturbation called spin-orbit coupling, by which states of different spin multiplicity can be mixed. This perturbation will increase as the fourth power of the atomic number of the atoms involved.

If the product  $\Phi_i\Phi_f$  does not belong to the same irreducible representation of the point group of  $\mu$ , the first term of the equation (1.3) is zero; in these cases the transition is said to be symmetry forbidden. An example of symmetry forbidden transitions is the d-d transitions of centre-symmetric co-ordination compounds. In practice, such transitions have low but sizeable intensity because of the poor separability of electronic and nuclear functions. This can be dealt with as a perturbation, called vibronic coupling.



### 1.2.2 Excited states processes

Light absorption by molecules will generate excited states and the electronically excited molecules can return to the ground state by emission of a quantum of light or without emission of radiation.

When the process of deactivation between one electronically excited state and the Ground State is generated by emission of light:



the process is known as a spontaneous emission, it depends on the third power of the frequency of the radiation and on the transition moment. Therefore the emission is affected by the same rules of symmetry and spin, which hold for the absorption process. When the emission process will be a spin allowed process it is called fluorescence, when it will be forbidden, phosphorescence.

In radiative deactivation, energy conservation is provided by the emission of light.

If an excited state is to be converted into the ground state without emission of radiation, a two step mechanism must operate:

- a) isoenergetic conversion of the electronic energy of the upper state into vibrational energy of the lower state
- b) vibrational relaxation of the lower state.

The first step normally is the rate determining process. It is dependent on the Fermi's Golden Rule:

$$k_{nr} = \left( \frac{2\pi}{h} \right) \langle \Psi_i | H^1 | \Psi_f \rangle^2 \langle X_{i,0} | X_{f,n} \rangle^2 \quad (1.4)$$

where  $H^1$  is the spin orbit coupling (vibronic) perturbation operator, that is the promoter of the transition.

As for the emission process, the radiationless transition assumes a different name if it would be spin allowed or spin forbidden. When the transition is spin allowed it is called internal conversion, when spin forbidden it is inter system crossing.

For a given ground state vibrational frequency, the probability of radiationless transition decreases exponentially with the energy gap between the states, energy gap law. The higher the energy gap, the higher is the vibrational quantum number of the isoenergetic level of the ground state and the smaller is the overlap between the vibrational functions.

At constant energy gap, the probability will depend on the vibrational energy spacing of the ground state, since the smaller is the energy spacing, the higher the vibrational quantum number of the isoenergetic level of the ground state, and the smaller the overlap. Therefore, high energy vibrations such as C-H stretching, are more effective than low frequency ones as energy accepting modes<sup>24</sup>. (Deuteration, which lowers the vibrational frequency, is used as a tool for reducing the rate of radiationless transition.)

Radiative and radiationless processes do not cause any chemical change in the light absorbing molecule and can thus be classified as photophysical processes. However excited states can achieve deactivation to ground state species, also by a variety of chemical processes, because energy rich species, such as excited states, are expected to be more reactive than those of the corresponding ground states.

The radiative and radiationless processes as described in this chapter compete for deactivation of any excited state of a molecule.

In absence of other processes, an excited state ( $^*A$ ) will decay according to an overall first order kinetics, with lifetime,  $\tau(^*A)$  given by equation (1.5)

$$\tau(^*A) = \frac{1}{k_r + k_{nr} + k_p} = \frac{1}{\sum_i k_i} \quad (1.5)$$

Where  $k_r$  is the radiative rate constant,  $k_{nr}$  is the non-radiative one and  $k_p$  is the rate constant of possible reactions.

For each process of the  $^*A$  excited state, an efficiency  $\eta_i(^*A)$  can be defined as in :

$$\eta_i(^*A) = \frac{k_i}{\sum_j k_j} = k_i \tau(^*A) \quad (1.6)$$

The quantum yield  $\Phi_i$  of a given process originating from the excited state is defined as the ratio between the number of molecules undergoing the process per unit time and the number of photons absorbed per unit time;

$$\Phi_i = \eta_i(^*A) \prod_n \eta_n \quad (1.7)$$

Where  $\eta_n$  terms represent the efficiencies of the various steps involved in the population of  $^*A$ .

Kasha<sup>25</sup> has expressed in a rule the outcome of the competition between excited state unimolecular processes of a typical organic molecule: "the emitting level of a given multiplicity is the lowest excited level of that multiplicity". Kasha's rule has been extended by Crosby<sup>26</sup> to typical transition metal complex; "in the absence of photochemistry from upper excited states, emission from a transition metal complex

with an unfilled d-shell will occur from the lowest electronic excited state in the molecule or from those states that can achieve a significant Boltzmann population relative to the lowest electronic excited state.”

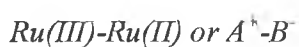
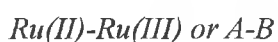
### 1.3 Supramolecular Systems

The term “supramolecular” was originally coined for multicomponent systems, where molecular components are clutched together by weak intramolecular forces such as: hydrogen bonds, electrostatic or host-guest interaction<sup>27</sup> and donor acceptor interactions. Now the definition of supramolecular systems also include systems, which have molecular components covalently bonded. In a supramolecular system the intercomponent bond would only have a structural role and will not change the essential individual component properties. However, the properties of a supramolecule will generally not be a simple superposition of those of the component molecules. It is possible to form new processes, which can include energy and electron transfers or complexation of new species.

A covalently linked molecular system can be defined supramolecular<sup>16,19,28</sup>, when the interactions of the molecular components are weak enough to preserve their individual properties. The problem of the degree of electron de-localisation in a complex chemical system must be addressed, especially for the class of complexes containing the same metal in different oxidation states (mixed valence compounds). The problem can explained using a simple two component model, A-B, as the binuclear complex  $(\text{NH}_3)_5\text{Ru-L-Ru}(\text{NH}_3)_5^{5+}$ , where L represents a symmetrical bridging ligand<sup>29,30</sup>.

In a valence localised description, in terms of integral oxidation states of the metal centres, this overall charge implies that the complex is a Ru(II)-Ru(III) species.

Otherwise, in a fully delocalised description the species will result with both Rutheniums in a oxidation state of 2.5. The factors, who will determine the localised or delocalised nature of the complex, can be easily appreciated following the approach developed by Hush-Satin<sup>31</sup>. Consider the two valence localised electronic isomers:



a specific equilibrium geometry corresponds to each of these species, in terms of inner (Ruthenium-Ammonia distance) and outer (solvent molecules orientation around the centres) nuclear degrees of freedom. Using parabolic potential energy curves for the two electronic isomers and a generalised nuclear co-ordinate, involving inner and outer nuclear displacements, it is possible to distinguish three different situations. (Fig. 1.2 points out the fact that at the equilibrium geometry of each electronically excited state). The energy separation between these two states at the equilibrium is usually called reorganisational energy and is indicated by  $\lambda$ . The two electronic isomers can be principally inter-converted by an electron exchange process; at the equilibrium geometry, electron exchange may only occur with concomitant absorption of a photon of energy  $\lambda$ . Otherwise, energy conservation is fulfilled by a radiationless process at the nuclear geometry of the crossing point, which can be thus viewed as the classical transition state for the classical transition state for electron exchange. Its energy is in the model  $\lambda/4$ .

When the electronic interaction between the metal centres,  $H_{AB}^{el}$ , is absolutely negligible, (it could be due to very long centre to centre distance or isolating character of the bridge, L), the curves in Fig.1.2 a represent the system at any geometry along the nuclear co-ordinates.

In most cases, however, some intercomponent electronic interaction is likely to be present, either as a consequence of direct orbital overlap between the metal centres, or through some bridge mechanism. In this case, Fig. 1.2a will represent only the zero order situation. The electronic interaction has almost no effect on the zero order curves in the proximity of the equilibrium geometry where the difference in energy between the electronic isomers is much larger than  $H_{AB}^{el}$ , but causes mixing of the zero order states nearer the crossing point.

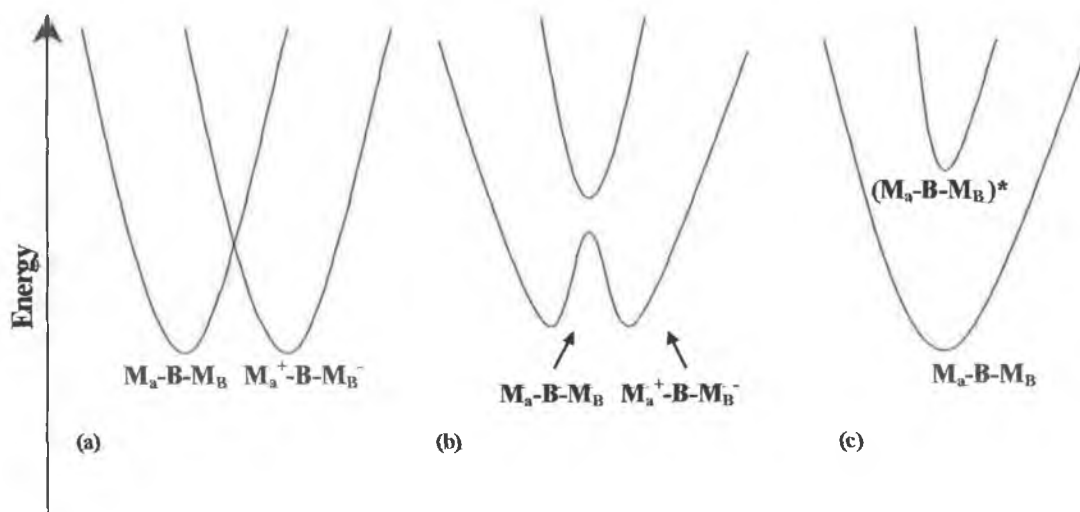


Figure 1.2 Potential energy curves for mixed-valence compounds with negligible (a), weak (b) and strong (c) electronic coupling.

These kind of systems can be still considered as valence localised and will still exhibit the properties of the isolated component, but new properties and

processes promoted by the two centres can be observed, such as optical transition or thermally activated electron transfer. The barrier to thermal electron transfer is only negligibly smaller than that calculated on the basis of the zero order curves  $\lambda/4$ .

When a strong electronic coupling is provided by the bridging ligand, the zero order levels can be substantially perturbed even in the proximity of their equilibrium geometry, in the limit of a very large electronic coupling the first order curves will show a single minimum and an intermediate geometry. The binuclear complex can be considered fully delocalised, Fig. I.2c.

### 1.3.1 Localisation of Excitation Energy

The conceptual scheme used above to discuss the oxidation states can be extended to analyse the location of excitation energy in a supramolecular system. In the two component system A-B, it is again, possible to distinguish three possible situations, whose are depending on the magnitude of the relevant centre to centre electronic coupling  $H_{AB}^{en}$ . In the ideal case of  $H_{AB}^{en}=0$  the excitation is fully localised on one of the centres, either  $^*A-B$  or  $A-B^*$ , but there would be no possibility for intercomponent energy transfer; otherwise, for big electron coupling, the system is a whole excited "large molecule"  $(A-B)^*$ . When  $H_{AB}^{en}$  is not negligible but smaller than the vibrational trapping energy, the excitation can be still regarded as essentially localised, but now a intercomponent energy transfer processes of the  $^*A-B$  to the  $A-B^*$  type are allowed.

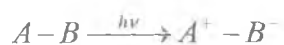


In this extension of the localisation argument from the electron transfer to the energy transfer field, the difference between the quantities involved should not be overlooked. At first the difference between the  $H_{AB}^{el}$  and  $H_{AB}^{en}$ , but also it should be remembered that trapping energies for electronic excitation are expected to involve mainly reorganisation of internal vibrational modes. Reorganisation of solvent modes, which is always an important part of  $\lambda$  in electron transfer, is expected to be small for energy transfer unless the ground and excited state have had much more different dipole moments.

#### **1.4 Intercomponent Processes**

The previous discussion about the localisation of oxidation states and excitation energy will help the discussion under which a covalently linked chemically complex system can be classified as supramolecular

Sometimes the absorption spectrum of a supramolecule can differ from the sum of the spectra of the molecular components such as new bands appearing in its spectrum. These bands are due to the optical electron transfer process (Fig. 1.3, 1.4.). This process must be clearly distinguished from photoinduced electron transfer, which corresponds to thermal electron transfer following electronic excitation of a single component.:



In this case the reorganisational energy  $\lambda$  is defined as a virtual, rather than real, energy difference, pertaining to a hypothetical isoenergetic system with the same nuclear displacements.

According to the Hush theory the energy of an optical electron transfer transition,  $E_{op}$ , is correlated to the energy between the minima of the A-B and A<sup>+</sup>-B<sup>-</sup> curves,  $\Delta E$ , and to the reorganisational energy,  $\lambda$ .

$$E_{op} = \Delta E + \lambda \quad (1.8)$$

Whether or not electron transfer transitions are actually observed in the supramolecular spectra depends on several factors. Except for systems exhibiting large interactions, the intensities of these bands are expected to be low with respect to those of the components. Therefore to be observable these bands require need to occur in a region of the spectrum free from absorption bands of the components, usually the visible or the near infrared.

Cases are possible, however, where, because of an  $\Delta E$  greater than  $\lambda$ , the relaxed state  $A^+ \cdot B^-$  remains an excited state, so an emission analogue of the absorption process is possible. Emission from electron transfer state in some supramolecular systems have indeed been observed.

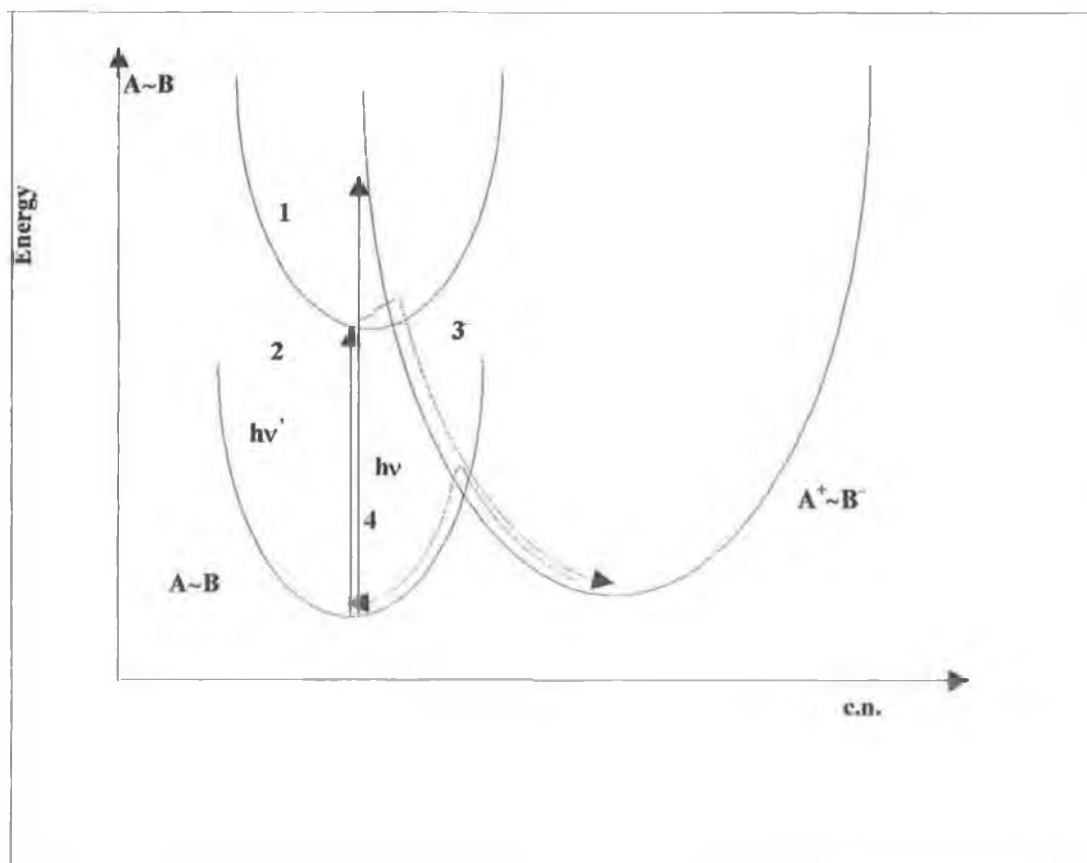


**Figure 1.3** Schematic representation of different type of electron transfer processes in a two-centre system: 1. Optical, 2-3 Photoinduced, 4 Thermal.

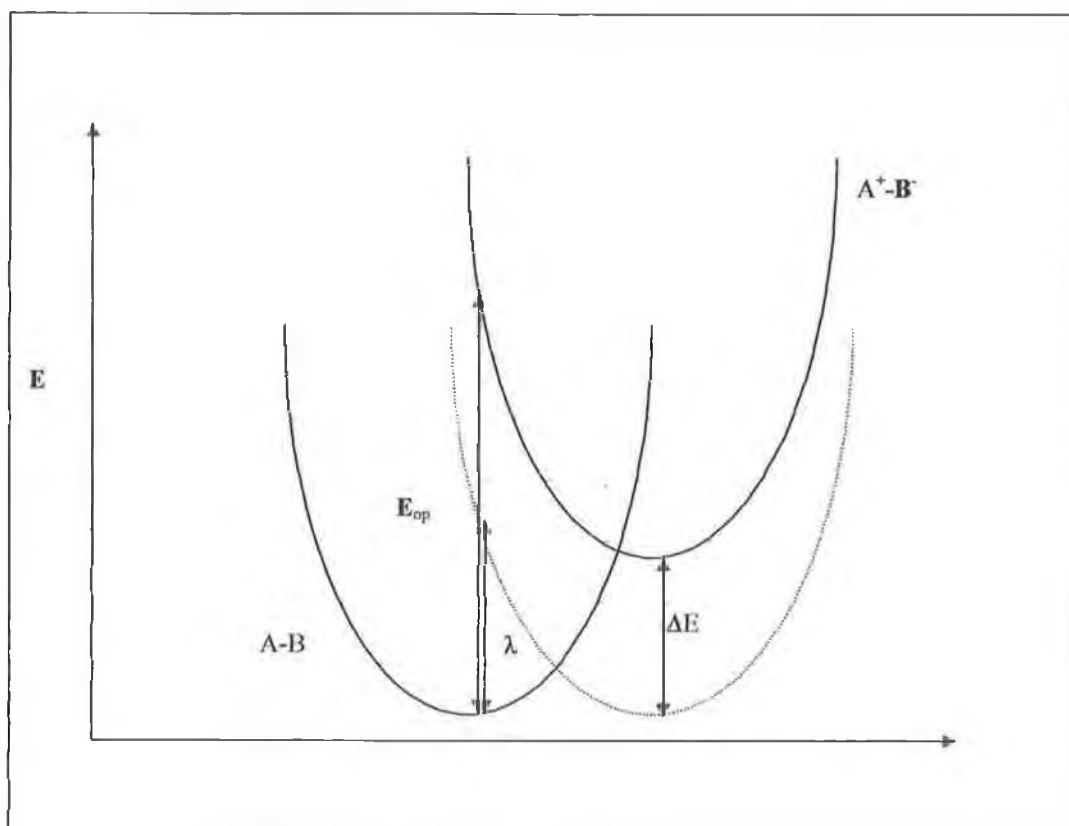


Figure 1.4 Energy profiles and parameters relevant to optical electron transfer.

Photoinduced electron transfer and charge recombination are both examples of electron transfer.



As for any radiationless transition between weakly interacting electronic states of a molecule, the probability is given by an expression of the type:

$$k_{el} = \left( \frac{2\pi}{h} \right) (H_{AB}^{el})^2 FCWD \quad (1.9)$$

where  $H_{AB}^{el}$  is the electronic coupling between the two states interconverted by the electron transfer process and FCWD is the Frank-Condon weighted density states.

It is possible to consider  $H_{AB}^{el}$  as a one-electron matrix element involving the HOMO of the electron donor centre and the LUMO of the electron acceptor centre. In a supramolecular system, this matrix element is expected to depend exponentially on the distance between the two components; the law is:

$$H_{AB}^{el} = H_{AB}^{el}(0) \exp\left[ -\frac{\beta(r-r_0)}{2} \right] \quad (1.10)$$

The variable  $r$  is the intercomponent distance<sup>32</sup> if a direct intercomponent orbital overlap is assumed. It could be better regarded as the effective distance, where the interaction is assumed to be mediated by a bridging unit;  $H_{AB}^{el}(0)$  is the interaction at the minimal intercomponent distance  $r_0$  and  $\beta$  is the attenuation parameter, dependent on nature of the bridge.

The FCWD term is a thermally averaged Frank-Condon factor connecting the initial and final states. It contains a sum of the overlap integrals between the nuclear wavefunctions including the vibrational modes (inner) and the solvent reorganisation modes (outer).

The expression of FCWD, which is normally very complicated, becomes relatively simple in ideal situations. In a simple approximation in which the solvent modes ( $\nu_0$ ) are thermally excited and treated classically ( $h\nu_0 \ll k_B T$ ), and internal

vibrations ( $\nu_i$ )<sup>33</sup> are frozen and treated quantum mechanically ( $k_B T \ll h\nu_i$ ), the FCWD term becomes:

$$FCWD = \left( \frac{1}{4\pi\lambda_0 k_B T} \right)^{\frac{1}{2}} S_m \left( \frac{S^m e^{-S}}{m!} \right) \exp \left[ - \frac{(\Delta G^0 + \lambda_0 + m h \nu_i)^2}{4\lambda_0 k_B T} \right] \quad (1.11)$$

$$S = \frac{\lambda_i}{h\nu_i} \quad (1.12)$$

In equation 1.11, the sum extends over  $m$ , the number of quanta of the inner vibrational mode in the product state,  $\Delta G^0$  is the thermodynamic driving force of the process and  $\lambda_0$  is the outer sphere (solvent) reorganisational energy, in its simplest form will be:

$$\lambda_0 = e^2 \left[ \left( \frac{1}{2r_a} \right) + \left( \frac{1}{2r_b} \right) - \left( \frac{1}{r} \right) \right] \left[ \frac{D_s - D_{op}}{D_{op} D_D} \right] \quad (1.13)$$

where  $e$  is the electron charge,  $D_{op}$  and  $D_s$  are the optical and static dielectric constants of the solvent,  $r_A$  and  $r_B$  are the radii of the two molecular components, and  $r$  the intercomponent distance;  $\lambda_i$  is the innersphere reorganisational energy given, in the single mode approximation, by

$$\lambda_i = \frac{1}{2} k (\Delta Q_e)^2 \quad (1.14)$$

Where  $k$  is an average force and  $\Delta Q_e$  is the change in the equilibrium geometry along the vibrational mode considered.

It could be demonstrated that in the high temperature limit, the nuclear factor takes the form:

$$FCWD = \left( \frac{1}{4\pi\lambda k_B T} \right)^{\frac{1}{2}} \exp \left[ - \frac{(\Delta G^0 + \lambda)^2}{4\lambda k_B T} \right] \quad (1.15)$$

The exponential term of this equation is the same as predicted by the classical model of Marcus<sup>34</sup>, where parabolic energy curves, such as those of Fig.1.5, are considered. The activation free energy of the process is that required going from the equilibrium geometry of the reactants to the crossing point.

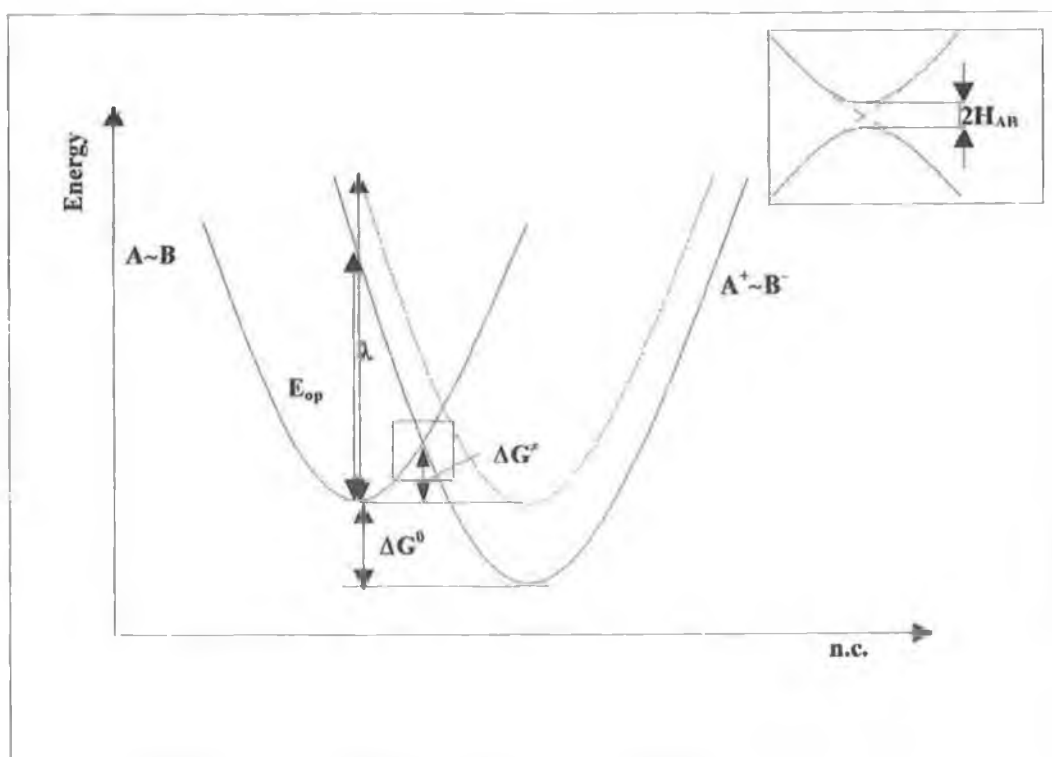


**Figure 1.5 Energy profiles and parameters relevant to photoinduced electron transfer.**

The equations contain an important prediction, namely, that of three typical kinetic regimes depending on the driving force range:

- (a) a normal regime for small driving forces ( $-\lambda < \Delta G^0 < 0$ ), the process is thermally activated and is promoted by an increase of driving force
- (b) an activation less regime ( $-\lambda = \Delta G^0$ ), the rate can not be increased by changing the driving force
- (c) an inverted region regime for a strongly exoergonic reaction ( $-\lambda > \Delta G^0$ ), the process slows down with increasing driving force.

Increasing  $\lambda$  slows down the process in the normal regime, but accelerates it in the inverted regime. The main difference between the high temperature limit expression and the full quantum mechanical expression of FCWD lies in the type of quantitative free energy dependence predicted in the inverted region. The classical limit predicts a parabolic decrease of  $\ln(k_{et})^{35}$  with increasing driving force, as compared with the linear decrease predicted by the quantum mechanical models, but definite proofs for the existence of the inverted region have been accumulating in the last years<sup>36,37</sup>.



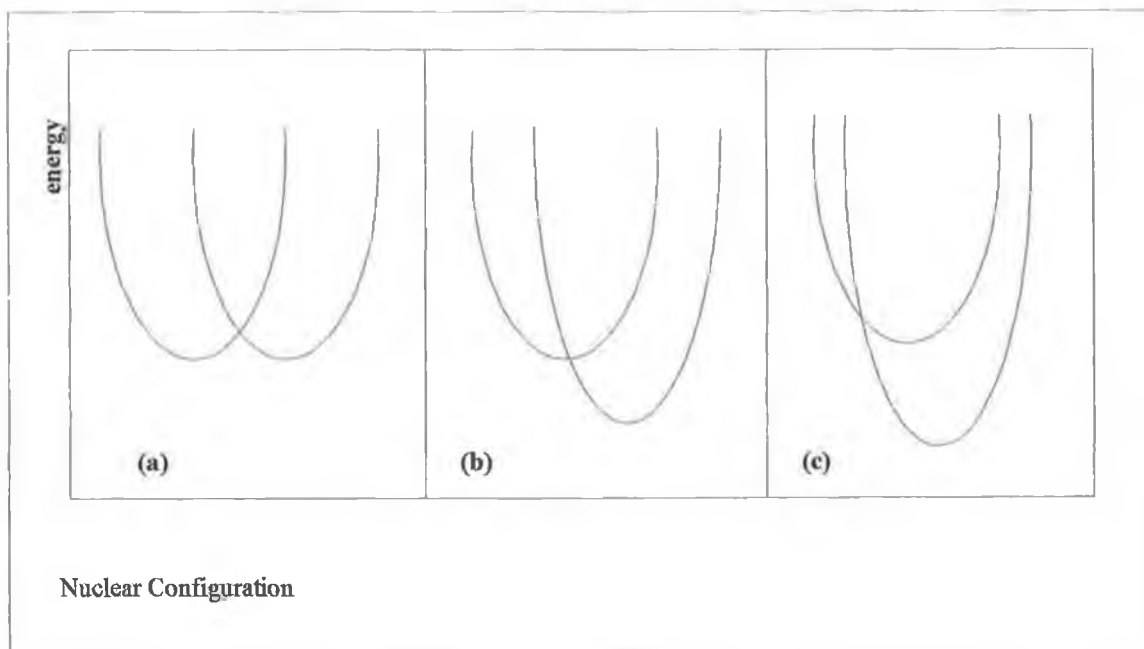


**Figure 1.6** Potential energy curves for reactant and product states of an electron transfer process in the three archetypal free energy ranges of the Marcus model.

Energy transfer is another type of radiationless transition between the electronic states of the supramolecule.



Thus, the rate constant for energy transfer is given by the golden rule expression, formally identical to that used for electron transfer,

$$k_{en} = \left( \frac{2\pi}{\hbar} \right) (H_{AB}^{en})^2 FCWD \quad (1.16)$$

where  $H_{AB}^{en}$  is the electronic coupling between the two excited states interconverted by the energy transfer process and FCWD is an appropriate Frank Condon factor.

Analogously to what happens for electron transfer processes, the Frank Condon factor for energy transfer processes can be cast either in quantum mechanical<sup>38,39</sup> or in classical terms<sup>40</sup>. Although the nature of the reorganisational energy can be somewhat different in the two cases, large contributions from solvent reorganisation are generally not expected for energy transfer. It will be an exception if the process involves large dipole moment changes upon local excitation, the effects of  $\lambda$  and  $\Delta G^0$  are qualitatively the same as in electron transfer, including the prediction of activated, activationless and inverted regime.

As to the electronic factor, a major difference exists between the detailed structure of  $H_{AB}^{el}$  and  $H_{AB}^{en}$ . Whereas the first one is a one electron, connecting the HOMO of the electron donor and the LUMO of the electron acceptor, the  $H_{AB}^{en}$  is a two-electron matrix element involving HOMOs and LUMOs on both the energy donor and energy acceptor centres.

In general case,  $H_{AB}^{en}$  may contain two terms: coulombic (Forster) and exchange (Dexter). The two terms have different dependencies on a various parameters of the system and each of them can become predominant depending on the specific system and experimental situation. The coulombic mechanism<sup>41</sup> is a long-range mechanism that does not require physical contact between donor and acceptor. It can be shown that the most important term within the coulombic interaction is the dipole-dipole term, that obeys the same selection rules as the corresponding electric

dipole transitions of the two partners. The typical example of efficient coulombic mechanism is that of a singlet to singlet energy transfer:



between large aromatic molecules, a process used by nature in the antenna device of the photosynthetic system<sup>42</sup>.

The exchange mechanism is a short mechanism that requires orbital overlap, and therefore physical contact, between donor and acceptor. The exchange interaction can be visualized as a simultaneous exchange of two electrons between the donor and the acceptor via LUMOs and HOMOs. The spin selection rules for this type of mechanism arise from the need to obey spin conservation in the reacting pair as a whole. This allows this mechanism to be operative in many cases in which, as in coordination compounds, the relevant excited states are forbidden in the usual spectroscopic sense.

An interesting question is that concerning the relative rates of electron and exchange energy transfer in an ideal system, where both processes are thermodynamically allowed. Generally speaking, energy transfer tends to have smaller re-organisation barriers than electron transfer, due to the much smaller solvent re-polarisation required for the former process. As far as the electronic term is concerned, the two-electron versus the one-electron nature of the interaction implies more severe overlap requirements for energy than for electron transfer. In a number of

elegant studies on covalently linked organic donor-acceptor systems, Closs and Miller<sup>43</sup> have recently probed the relationship between electron and exchange energy transfer, showing that rates of energy transfer decrease with increasing bridge length much faster than those of corresponding electron transfer processes.

## 1.5 Photochemical Molecular Devices

An assembly of molecular components capable of performing light induced functions can be called a photochemical molecular device<sup>44,45</sup>, (PMD).

PMDs are present in nature where they perform functions essential to life such as photosynthesis and vision. Important progress towards the understanding of such natural PMDs has been made in recent years<sup>46,47,48,49</sup>. For example, the structure of the reaction centre of bacterial photosynthesis is known and its function is reasonably well understood<sup>50,51</sup>. The very efficient photo induced charge separation achieved in this system arises from the successful competition of forward over back electron transfer reactions, which is made possible by the very specific supramolecular organisation reached as the result of evolution.

To perform a particular function and to be useful for a specific application, a PMD needs to be constructed of suitable molecular components, each having a specific role. It's possible to distinguish three fundamental kind of molecular components:

active components, which perform an elementary act or a sequence of elementary acts directly related to the desired function

perturbing components, which can be used to modify the properties of the active components

connecting components, which can be used to link together components in the desired spatial arrangement.

The first requisite of any PMD is chemical stability. Only stable devices are able to process a large number of photons and can thus be useful for practical applications.

From the previous chapters we have seen that polynuclear complexes are made of components with individual photochemical and photophysical properties and the behaviour of the polynuclear complex is determined by the spatial arrangement and relative energies of the components. Polynuclear complexes clearly have some of the distinctive features of PMDs. Whether or not a given polynuclear complex is to be considered a PMD depends, of course, on the extent to which its behaviour can be considered as useful light induced function.

Generally speaking, it's possible to divide the PMDs by the functions performed:

- photoinduced electron transfer
- electronic energy transfer
- photoinduced structural change.

### **1.5.1 Photoinduced Electron Transfer PMDs**

PMDs can perform conversion of light into chemical energy (artificial photosynthesis) like those shown in Fig 1.7. The principal components of the device must have appropriate relative redox potentials (ground and, or excited state) and must be assembled in a correct energy sequence. Photoinduced charge separation can occur either between two relay components as in [Fig.1.7.(a) a] or between the photosensitizer and a relay as in [Fig.1.7.(a) b]. If connected with electrodes, these

devices can convert light into electrical energy and constitute the fundamental elements of the molecule-based photovoltaic cells.

**Figure 1.7 Photo Molecular Devices**

Photosensitisation of an electron transfer process between remote reactant is another important application of PMDs based on photoinduced electron transfer process (Fig 7(a) c). This process may become useful in the case of a spontaneous overall electron transfer process that is prevented by intermediate step having a high energy barrier. At last, the potential application of photoinduced electron transfer can be applied to the switching of electric signals. The Relay (Rel) components are connected to electrodes and separated by an electron transfer photosensitiser (Pel).

Application of a potential difference to the electrodes does not allow electronic migration when the PeI is kept in the dark because its HOMOs and LUMOs lie at too high energy with respect to the Fermi levels of the electrodes. Under light excitation, it becomes possible to transfer one electron between the HOMO and LUMO of the photosensitizer, consequently it is possible the transfer of an electron between the two relays and therefore the two electrodes. Because of the possibility of modifying its electrical resistance with light, this PMD can be considered as a phototransistor

### **1.5.2 Electronic Energy Transfer PMDs**

Light absorption by a component of a PMD generates localised electronic energy. The possibility of transmitting this electronic energy to another component of the PMD, where the energy can be used for chemical purposes or reconverted into light. This function can only be obtained upon elaboration of the light energy input in the dimension of energy, space and time by means of an appropriate sequence of suitable components.

Energy transfer PMDs can include:

- spectral sensitisation
- antenna effect
- remote photosensitisation
- light-energy up-conversion



For this group of PMDs, the interface toward light will be an energy transfer photosensitizer (Pen), a molecular species capable of absorbing light and donating electronic energy to a different device's component.

Spectral sensitisation is important when a luminescent or photoreactive species can not be excited in a desired wavelength, because it does not absorb light in a particular spectrum region; the suitable device could be a simple dyad as in Fig. 1.7. The antenna effect, Fig. 1.7(b) b, is an enhanced light sensitivity obtained by an increase in the overall cross section for light absorption. The result is obtained using several Pens, whose will convey the energy to another component. The final component can be a luminophore, obtaining an emission a different wavelength, but it can play also a different role, as electron transfer photosensitizer.

In the remote energy transfer photosensitisation, the component interfacing the PMD towards use can be either an energy transfer relay (ren) or a luminophore. To obtain migration over long distances, the PMD should involve a sequence of energy transfer processes along a vectorial array of components. A PMD, who is able of performing light energy up conversion so as to obtain anti-stokes luminescence, is an another potential use of electronic energy transfer (Fig.1.7)

### **1.5.3 Photoinduced Structural Changes PMDs**

The characteristic active-components of this kind of PMDs are photoisomerizable components, Pi. Important requirements for the Pi are possibility of being excited

either by light absorption or energy transfer, chemical and photochemical stability and possibility of reverting the photoinduced structural change by athermal or photochemical reaction. The nature of the other components of a PMD performing this function depend on its specific utilisation, which include:

- switching electrical signals,
- switching receptor ability,
- modification of cavity size,
- activation of coreceptor catalysis

#### **1.5.4 Design of Supramolecular Systems as Semiconductor**

##### **Sensitisers**

The use of solid state materials for conversion of solar energy into electricity is a topic of much interest to scientists. Colloids and nanocrystalline films of several semiconductor systems have been employed in the direct conversion of solar energy into chemical or electrical energy<sup>52,53</sup>. In the 1950s the improvements of silicon purity and solid-state junctions created a revolution in the development of solar cells. Silicon solar cell efficiencies improved of an order of magnitude in the 1950s up to reach 24% in 1995<sup>54</sup>. In the 1990s a major photoelectrochemical solar cell development was obtained with the introduction of thin film dye sensitized solar cells devised by Grätzel<sup>55</sup>. For the first time a solar energy device operating on a molecular

level showed the stability and the efficiency required for potential practical applications<sup>56,57,58</sup>.

Although the general principles of dye sensitization of wide-band-gap semiconductors were already well established in the 1970s<sup>59</sup>, progress in the application of such techniques, to light energy conversion, has been initially very slow due to the limited light absorption showed by monolayer of dyes on electrodes of small surface roughness. Substantial advances in conversion efficiencies, obtained with sensitized semiconductor electrodes, started with the development of high surface area nanocrystalline semiconductors<sup>60</sup> and of suitable molecular sensitizers<sup>61,62</sup>.

Most of the nanocrystalline semiconductors studied up to now are metal oxides or chalcogenides, such as TiO<sub>2</sub>, ZnO, SnO<sub>2</sub>, Nb<sub>2</sub>O<sub>5</sub>, WO<sub>3</sub>, SrTiO<sub>3</sub>, Ta<sub>2</sub>O<sub>5</sub> or CdS. Films based on these materials are constituted by a network of mesoscopic particles which are in close contact with each other and allow for an efficient electronic migration. Because of their high roughness factor and relative good conductivity, these materials are ideal candidates for a number of interesting applications such as photoelectrochemical solar cells, sensors, electro- and photochromic materials, and photocatalytic devices<sup>63</sup>. Wide band gap n-type semiconductors such as TiO<sub>2</sub> and ZnO, are materials that do not undergo decomposition upon irradiation or heating and are therefore generally utilized in dye sensitized photoelectrochemical solar cells<sup>64,61</sup>. The developments of these materials and of efficient molecular sensitizers have caused a sharp acceleration in the field and

active research on several aspects of this technology is now being performed in many laboratories.

Dye sensitization, i.e. charge injection from an electronically excited adsorbed dye, is a well-established technique that allows photoelectrochemical and photocatalytic processes on wide band-gap semiconductors using sub band-gap excitation. The energy gradient initially stored in the interfacial charge separated pair  $\text{TiO}_2(\text{e}^-)/\text{D}^+$  can be utilized to drive chemical reactions as well as to convert visible light into electricity<sup>65</sup>.

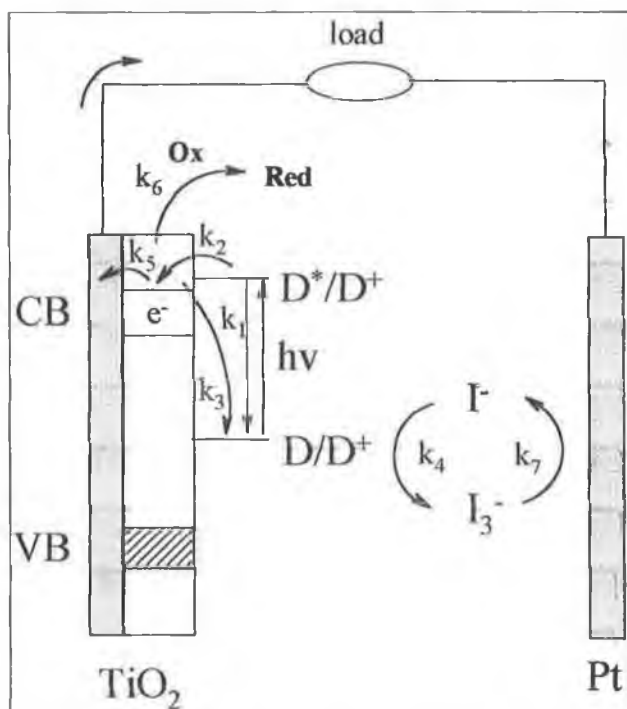


**Figure 1.8** Schematic representation of the elementary steps involved in a regenerative photoelectrochemical cell for light conversion based on dye sensitization of semiconductors

An accepted model for dye sensitization in regenerative photoelectrochemical cells is shown in Figure 1.8. The cell consists of a molecular sensitizer anchored to the semiconductor surface, a solution containing a relay electrolyte, and a counter electrode. Light excitation promotes the sensitizer to upper lying electronic excited states that convert very rapidly and efficiently to the lowest-lying electronic excited state. The excited dye injects an electron into the conduction band of the semiconductor from a normal distribution of donor levels at a rate  $k_2$ , and becomes oxidized. An electron donor ( $I^-$ ) acting as relay electrolyte then reduces the oxidized dye, at a rate  $k_4$ . The electron flows ( $k_5$ ) through an external circuit to perform useful work. Reduction of the oxidized donor ( $I_3^-$ ) occurs at the counter electrode ( $k_7$ ) and the solar cell is therefore regenerative. Radiative decay, nonradiative decay ( $k_1$ ) of the excited dye molecule, and recombination of the photoinjected electron with the oxidized dye ( $k_3$ ), represent loss mechanisms. Additional loss mechanisms, such as recombination of the conduction band electrons with the oxidized electron donor, are represented by the rate constant  $k_6$ . Other loss mechanisms, as chemical reactions taking place from the oxidized or excited dye sensitizer, are not shown in Figure 1.8.

The performance of the cell can be quantified on a macroscopic level with parameters such as Incident Photon to Current Efficiency (IPCE), open circuit photovoltage ( $V_{oc}$ ), and the overall efficiency of the photovoltaic cell,  $\eta_{cell}$ . The parameter measuring directly how efficient incident photons are converted into electrons is the incident photon to current conversion efficiency (IPCE)<sup>66,67</sup>. The wavelength dependent IPCE term can be expressed as a product of the quantum yield

for charge injection ( $\Phi$ ), the efficiency of collecting electrons in the external circuit ( $\eta$ ), and the fraction of radiant power absorbed by the material or «light harvesting efficiency» (LHE), eq.1.19:

$$IPCE(\lambda) = LHE(\lambda) \Phi \eta \quad (1.19)$$

While  $\Phi$  and  $\eta$ , can be rationalized on the basis of kinetic parameters, LHE depends on the active surface area of the semiconductor and on the cross section for light absorption of the molecular sensitiser. In practice the IPCE measurements are performed with monochromatic light and calculated according Eq. 1.20.

$$IPCE(\lambda) = \frac{1.24 \cdot 10^3 (V \cdot nm) \times \text{photocurrent density} (\mu A \cdot cm^{-2})}{\text{wavelength (nm)} \times \text{photon flux} (W \cdot m^{-2})} \quad (1.20)$$

The maximum open-circuit photovoltage, attainable in the dye-sensitized solar cell, is the difference between the Fermi level of the solid under illumination and the Nernst potential of the redox couple in the electrolyte. However, for these devices this limitation has not been realized and  $V_{oc}$  is in general much smaller. It appears that  $V_{oc}$  is kinetically limited and for an n-type semiconductor in a regenerative cell the diode

$$V_{oc} = \left( \frac{kT}{e} \right) \ln \left( \frac{I_{inj}}{n \sum_i k_i [A_i]} \right) \quad (1.21)$$

equation 1.21 can be applied.<sup>68</sup>

where  $I_{inj}$  is the electron injection flux,  $n$  is the concentration of electrons in  $TiO_2$ , and the summation is for all electron transfer rates to acceptors  $A_i$ . One successful strategy for increasing  $V_{oc}$  has been to add pyridine derivatives to the electrolyte. Pyridine is thought to adsorb on the  $TiO_2$  surface and to inhibit recombination of injected electrons with  $I_3^-$  ( $k_6$ ). An alternative approach, which will be discussed in section 4, involve the use of supramolecular systems containing a sensitizer unit covalently bound to a suitable electron donor unit that allows to translate the positive charge from the oxidized form of the sensitizer.

The overall efficiency of the photovoltaic cell,  $\eta_{cell}$ , is given by eq. 1.22

$$\eta_{cell} = \frac{i_{ph} \times V_{oc} \times ff}{I_s} \quad (1.22)$$

where  $i_{ph}$  is the integrated photocurrent density,  $ff$  the cell fill factor, and  $I_s$  the intensity of the incident light. The integrated photocurrent density represents the overlap between the solar emission and the monochromatic current yield. The maximum overall efficiencies reported so far are in the 7-11% range, depending on the fill factor of the cells. Under optimal current collection geometry, minimizing ohmic losses due to the resistance of the conductive glass, and under reduced solar irradiance, fill factors of 0.8 have been obtained.

Photosensitization of  $TiO_2$  with transition metal complexes, chlorophyll derivatives, and related natural porphyrins have been reported. Besides these studies,

a different approach involving coupling of two semiconductor particles with different energy levels, such as CdS-ZnO and CdSe-TiO<sub>2</sub>, has been proposed by Kamat<sup>69</sup>.

In order to be useful in a photoregenerative cell, the molecular sensitiser should fulfil several requirements, including:

1. the ability to adsorb firmly on the semiconductor.
2. efficient light absorption in the visible region.
3. an excited-state redox potential negative enough for electron injection into the conduction band.
4. a ground-state redox potential as positive as possible, compatible with b) and c)
5. small reorganizational energy for excited- and ground-state redox processes, so as to minimize free energy losses in primary and secondary electron transfer steps.



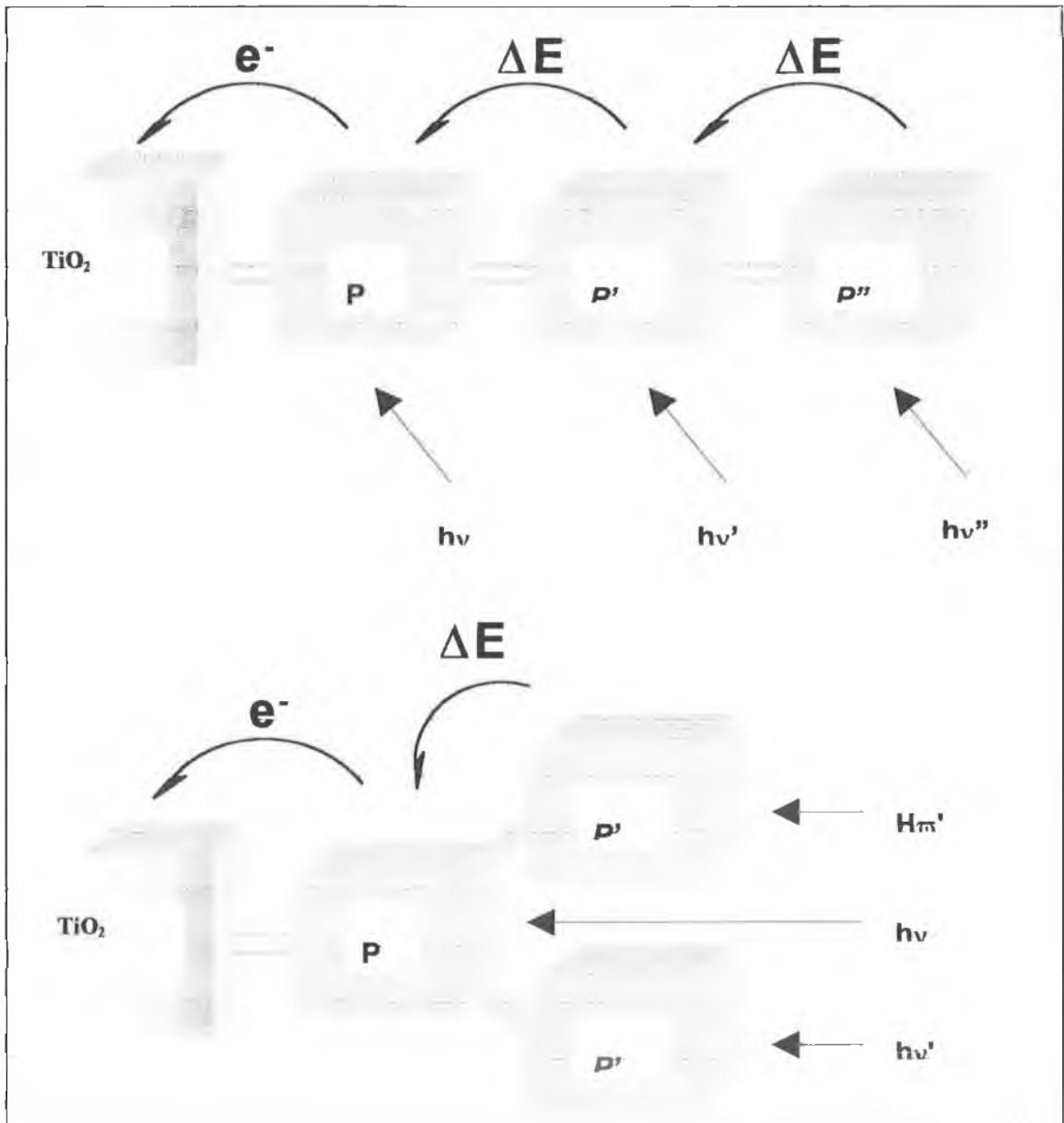


**Figure 1.9 Possible sequences of intramolecular and interfacial electron-transfer (a) linear and (b) branched antenna systems adsorbed on a semiconductor#**

It should be noticed that the photoregenerative device, described in the previous section (see Figure 1.7), has the peculiarity of operating with molecular sensitizers

having short lived excited-states, and with sensitizers showing photochemical instability or irreversible ground-state redox behaviour. This peculiarity is satisfied when charge injection processes to the semiconductor are very fast and competitive with deactivation or chemical reactivity of the excited sensitizer. A fast reduction of the sensitizer-oxidized form can be obtained by increasing the concentration of iodide in the electrolytic solution.

The most successful sensitizers, used so far, are based on polypyridine complexes of  $d^6$  metal ions, such as Ru(II), Os(II), and Re(I) showing intense metal to ligand charge transfer transitions in the visible region, leading to MLCT states. The energies of these states can be varied systematically by changing the substituents at the chromophoric ligands (electron-withdrawing substituents tend to decrease the energy of the  $\pi^*$  orbitals of the polypyridine ligand, while the opposite effect is observed with electron donating substituents) as well as by changing the non-chromophoric ligands. For bis-chelate complexes of the type *cis*-[Ru<sup>II</sup>(bpy)<sub>2</sub>(X)<sub>2</sub>], as well as for the analogous Os<sup>II</sup> complexes, MLCT absorption bands shift to higher energy changing X from  $\pi$  donating ligands to  $\pi$  accepting ligands. The main effect, in this case, is a direct perturbation of the electronic density at the metal center. With this kind of system, open circuit photovoltages of ca 0.6 Volt, short circuit photocurrents of about 8-10 mA/cm<sup>2</sup>, and overall solar energy conversion efficiency of the order of 10% can be obtained in laboratory experiments.

An additional strategy to increase the light absorption efficiency of a sensitised semiconductor could be to replace the sensitizer molecule at the

semiconductor solution interphase with an antenna sensitiser molecular device (Fig.1.9). In principle, this device should take advantage of efficient intracomponent electron transfer from a number of light absorbing (antenna) units to an energy collecting unit, which is at the same time a good photosensitiser for charge injection. In this way, the light energy absorbed by all the components can be used to effect charge injection. In this way, the light energy absorbed by all the components can be used to effect to effect charge injection, with an increase in the overall cross section for light absorption compared to the case of a simple molecular sensitiser. How this increase is actually distributed over the action spectrum depends on the spectral characteristics of the antenna and sensitiser chromophores, subject to the obvious condition,  $h\nu' < h\nu$ .

## 1.6 Ruthenium Polypyridine Complexes

In the last twenty years Ru(II)-polypyridine complexes have attracted the attention of several research groups because of a unique combination of ground and excited state properties<sup>14</sup> (Fig. 1.10). The prototype of these complexes is the well-known  $[\text{Ru}(\text{bpy})_3]^{2+}$  which is extensively used as :

a photoluminescent compound,

an excited state reactant in energy and electron transfer processes,

an excited state product in chemiluminescent and electrochemiluminescent reactions

a mediator in interconversion of light and/or chemical energy.

Paris and Brandt<sup>70</sup> first reported  $[\text{Ru}(\text{bpy})_3]\text{Cl}_2$  as a luminescent species, in fluid solution, in 1959 and since then this molecule has become the building block for an ever-expanding array of photoactive molecules of dilating complexity.

The absorption spectra of bipyridiles complexes of ruthenium are dominated by a metal to ligand charge transfer (MLCT) band in the visible region, as it showed in Fig. 1.11(a), the maximum wavelength of asobrtn for  $[\text{Ru}(\text{bpy})_3]^{2+}$  is 450 nm. Transitions within the ligand  $\pi$ -bonding or  $\pi^*$ -antibonding orbital labelled  $\pi$ - $\pi^*$  or ligand centred transitions usually lie at higher energies (185, 285 nm.) have high extinction coefficients and are substantially ligand in character. In addition, transitions such as promotion of an electron from a  $t_{2g}$  to a  $e_g$  orbital are possible and such d-d or metal centered transiction give rise to weak absorption bands (322, 344 nm, spin-forbidden)<sup>71</sup>.

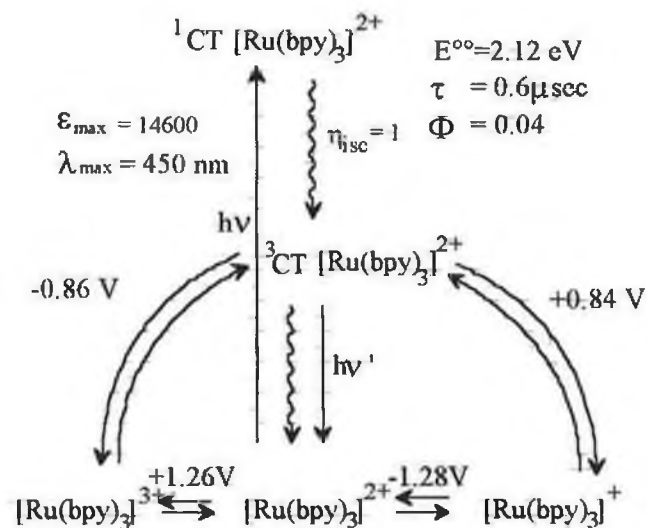


Figure 1.10 Photophysical and redox properties of the complex  $[\text{Ru}(\text{II})(\text{bpy})_3]^{2+}$ .

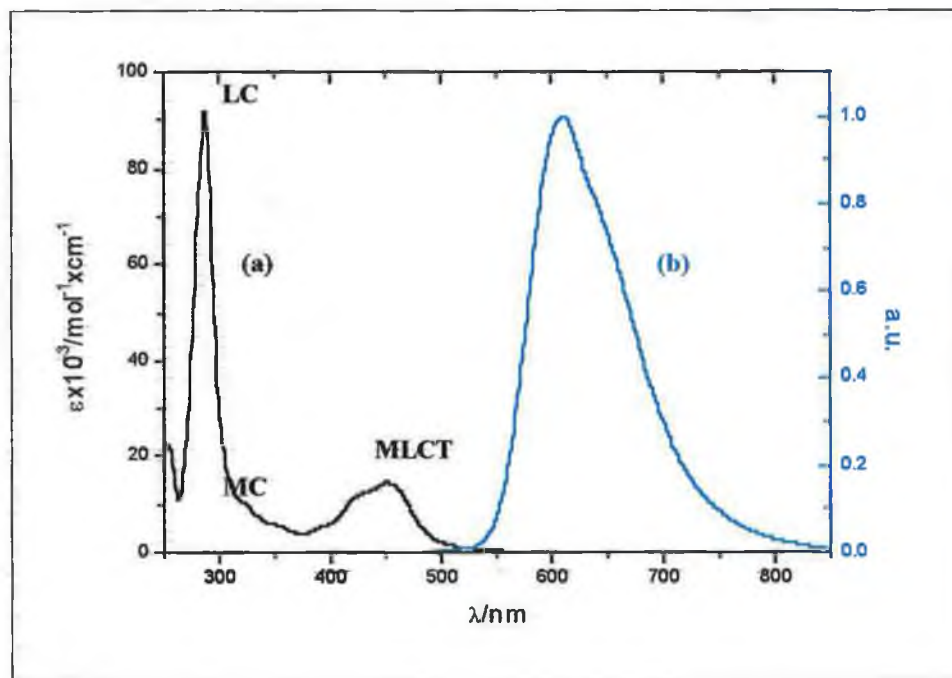


Figure 1.11 Absorption (a) and emission spectra (b) of  $[\text{Ru}(\text{II})(\text{bpy})_3]^{2+}$ , at r.t. in acetonitrile solution.

For  $[\text{Ru}(\text{bpy})_3]^{2+}$  the lowest excited state is a  $^3\text{MLCT}$  excited state; the efficiency of population from the upper singlets, obtained by excitation, to the lowest triplet state is essentially unity (Crosby rule). The  $^3\text{MLCT}$  excited state<sup>72</sup> is the emissive state (Fig. 1.11 b), low temperature measurements of the banded emission indicate the presence of three electronic components in the emitting with the upper two members situated approximately 10 and 60  $\text{cm}^{-1}$  above the lowest. The excited state lifetime is temperature dependent and increases dramatically as the temperature is decreased<sup>73</sup>. The large energy gap between the lowest excited states and the ground state allows radiative processes (phosphorescence) to compete with non-radiative ones. Population of  $^3\text{MC}$  states following MLCT excitation by internal conversion from the  $^3\text{MLCT}$  to the  $^3\text{MC}$  excited states, can lead to at best non-radiative decay, but can also lead to ligand-loss photochemistry (Fig. 1.13).

Oxidation of  $[\text{Ru}(\text{bpy})_3]^{2+}$  complexes usually involves a metal centred orbital, with formation of Ru(III) centres, which are inert to ligand substitution.

The oxidation potential in this complex fall in a rather narrow range around +1,25 V versus NHE, but substitution of one or more bipyridine ligands by another similar type ligand can drastically change their potential.

Reduction of  $[\text{Ru}(\text{bpy})_3]^{2+}$  takes place on a ligand  $\pi^*$  orbital (-1,46 V), that is usually the same involved in the MLCT transition; correlation exist between the electrochemical and spectroscopic data (Fig. 1.10). Because of its higher energy content, the excited state is a both a stronger reductant and a stronger oxidant than the corresponding ground state.

Excited state redox potentials can be tuned by changing the ground state redox potential and-or excited state energy. Since reduction usually takes place on a ligand, the ground state reduction potential will be roughly related to the reduction potential of the free ligand. However, the ability of a co-ordinated ligand to accept an electron also depends on the amount of charge transferred to the metal or received from the metal via the  $\sigma$  and  $\pi$  bonding by the other ligands. A change in the oxidation potential of the ground state causes a change in the excited state oxidation potential.

From the viewpoint of the excited state properties bipyridyl and phenanthroline are much better ligands than terpyridine for ruthenium complexes. It is well known that at room temperature, in fluid solution,  $\text{Ru}(\text{bpy})_3^{2+}$  exhibits a strong and long lived luminescence,  $^3\text{MLCT}$  lifetime in the order of one thousand nsec, whereas  $\text{Ru}(\text{tpy})_2^{2+}$  does not show any luminescence and a  $^3\text{MLCT}$  lifetime of 250 psec. That is because the main radiationless decay path at room temperature is in all the case an activated crossing to an upper lying, distorted  $^3\text{MC}$  excited state. Since the terpyridine ligand has a bad bite angle for octahedral co-ordination, the ligand field strength in terpyridine complexes is weaker than in bipyridyl type complexes. As a consequence, the energy gap between the  $^3\text{MLCT}$  and  $^3\text{MC}$  levels is smaller and the deactivating radiationless decay through the  $^3\text{MC}$  is faster. At 77 K the activated radiationless decay through the  $^3\text{MC}$  levels is stopped and the luminescence lifetime between tpy and bpy type complexes is comparable.

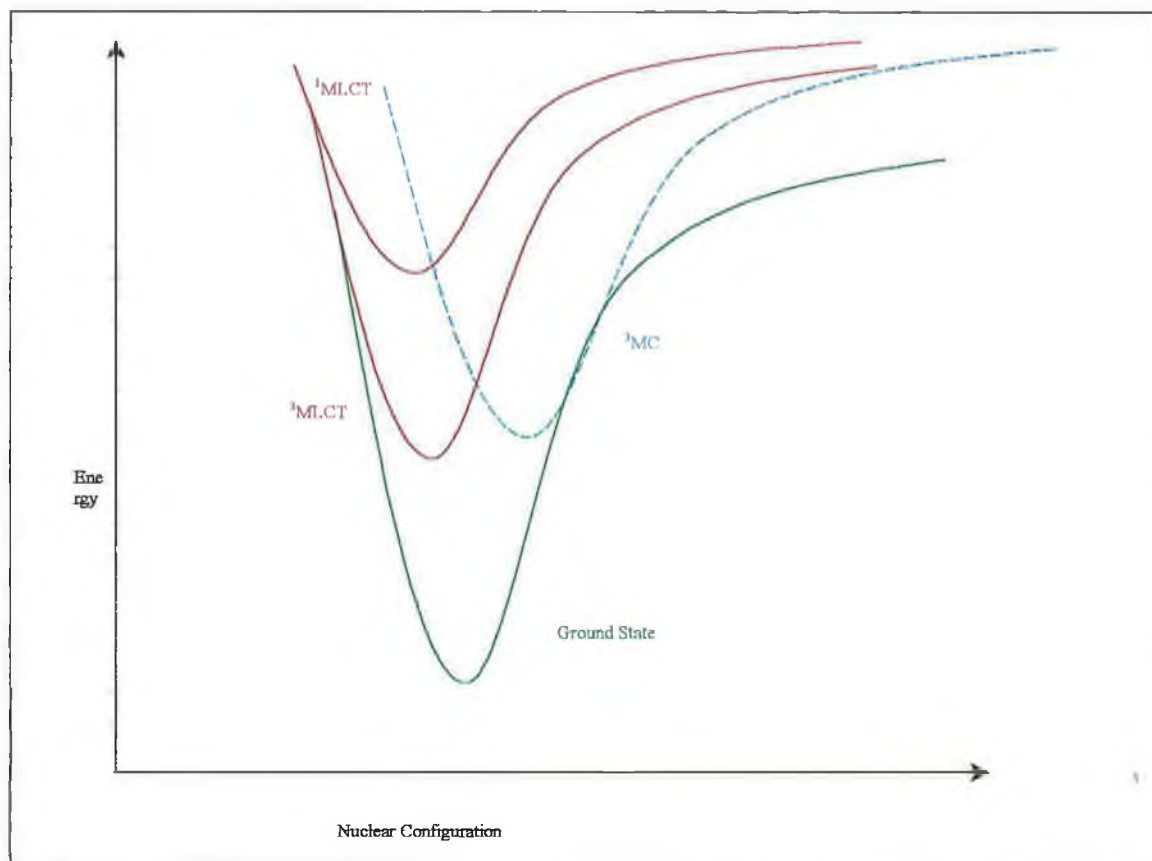


**Figure 1.12** Schematic representation of the photophysical pathways of  $[\text{Ru}(\text{bpy})_3]^{2+}$ .

From the viewpoint of structure, however, bridging ligands based on tpy, are much more appealing than those based on bidentate ligands. One reason is that there are important differences concerning the co-ordination to the metal centres. This is highlighted in Fig.1.13 where the structures of ruthenium bidentate and tridentate polypyridine complexes are illustrated. The bidentate ligands give rise to stereoisomerism at six-coordinated centres due to its bidentate nature and therefore an  $\text{M}(\text{bpy})_3^{2+}$  complex exists in two enantiomeric forms ( $\Delta$  and  $\Lambda$ ). If the two co-



ordinating nitrogens are not equivalent, as it happens for mono-substituted bpy, two geometrical isomers are possible (*fac* and *mer*); furthermore each of them can exist as one of the two enantiomers. In contrast of this behaviour, an octahedral co-ordinate metal forms an achiral  $[\text{Ru}(\text{tpy})_2]^{2+}$  complex upon reaction with terpyridine. The introduction of single substituent in the 4' position of each terpyridine ligands does not present any change of global symmetry or formation of geometrical isomers.

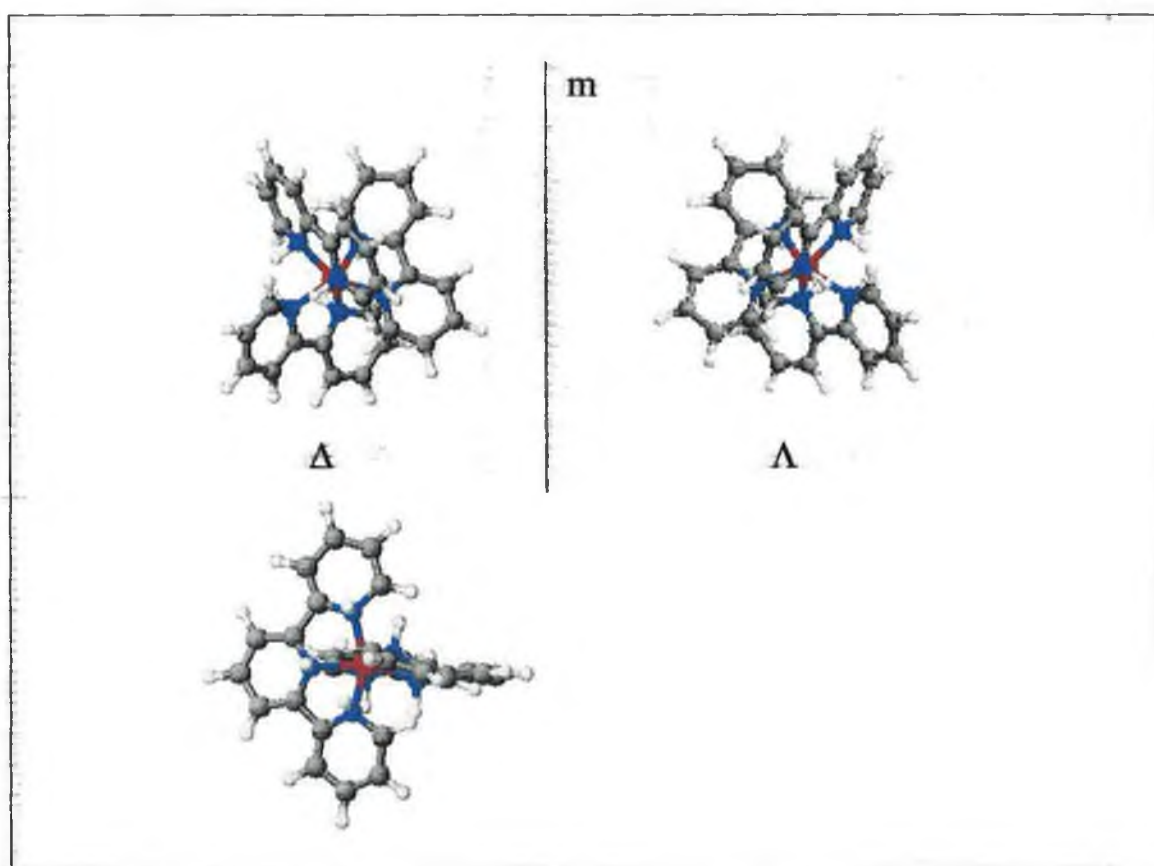


**Figure 1.13** Schematic representations of the two chiral isomers of  $[\text{Ru}(\text{bpy})_3]^{2+}$  complex and the unique form of  $[\text{Ru}(\text{tpy})_2]^{2+}$ .

Another important structural difference is that connection between bidentate type ligands with a spacer cannot occur along the co-ordination axis, whereas this can

be obtained by 4' substitution of the tpy ligand. The tridentate tpy ligand is therefore more appealing than the bidentate bipyridine and phenantroline ligands from the point of view of constructing linear, rodlike polynuclear complexes.

From the above discussion, the optimum would be a complex with the photophysical properties of Ru(II)(bpy)<sub>3</sub> complex and the structural properties of Ru(II)(tpy)<sub>2</sub> complex. Until now, in order to increase the excited state lifetime of Ru-tpy base chromophoric unit two different pathways have been used:

1. substitution in 4' position of the tpy by electron acceptor groups such as -MeSO<sub>2</sub> (at r.t. the luminescence lifetime is 36 nsec)<sup>74</sup>
2. use of ancillary ligands, which can increase the ligand field strength, as -CN (r.t. luminescence lifetime is 40 nsec.)<sup>75</sup>

## 1.7 Scope of the Thesis

The synthesis, spectroscopic and electrochemical characterisation of ruthenium (II) polypyridyl mononuclear complexes containing 1,2,4-triazole and tetrazole moiety will be described. Chapter one is an introduction relating to the work described in the thesis. The methods of characterisation, which are described in chapter two, include High Performance Liquid Chromatography,  $^1\text{H-NMR}$ , UV/Visible spectroscopy, fluorimetry, electrochemistry, spectroelectrochemistry, mass spectrometry and lifetime emission measurements.

Chapter three will describe the synthesis of the new set of ligands and their mononuclear Ruthenium (II) complexes.

Chapter four will describe an extensive characterisation of  $\text{Ru(II)(bpy)}_2$  moiety complexes containing a 5-(2-pyridyl)-1,2,4-triazole ligand, ( $\Delta\text{py}$ ), or a 5-(2-pyridyl) tetrazole ligand, ( $\square\text{py}$ ), and their comparison with the archetype  $\text{Ru(bpy)}_3^{2+}$ . The examination of the acid-base chemistry of the complexes by UV/Visible spectroscopy will reveal important information about the location of the excited state

Chapter five will explore the spectroscopic, photophysical and electrochemical properties of the new  $[\text{Ru(tpy)(}\Delta\text{py}\Delta)]$  complexes, where  $(\Delta\text{py}\Delta)^{2-}$  is the 2,6 di-(1,2,4-triaz-3-yl)-pyridine ligand. The new specie will be exhaustively studied especially because it will be revealed to be one of the few examples available in literature, of emitting Ru(II) terpyridine complexes, with a lifetime of the excited state in the order of 100 nanoseconds.

Chapter six will describe the synthesis of complexes containing  $(\Delta\text{py}\Delta)^{2-}$  and terpyridine derivatives or vice-versa terpyridine and  $(\Delta\text{py}\Delta)^{2-}$  derivative ligands. One of them will be used as a photosensitiser in a photovoltaic cell. Attachment of the  $[\text{Ru}(\text{II})(\text{tctpy})(\Delta\text{py}\Delta)]$  complex to nanocrystalline  $\text{TiO}_2$  films indicates incident photon-to-current efficiency (IPCE) of greater than 60%.

Chapter seven will explore the use of a new 2,6 di-(tetraz-5-yl)-pyridine ligand,  $(\square\text{py}\square)^{2-}$ , and the spectroscopic, photophysical and electrochemical properties of its Ru(II) complexes.

Chapter eight will be an attempt to rationalise the collected data of the Ru(tpy) moiety. The change of the energy levels in relation to the different ligands will be analysed. The correlations between spectroscopic, photophysical and electrochemical data of the new complexes and the existent ones will create an extensive knowledge of the tridentate Ru(II) complexes, that will increase their availability as a photosensitive building block for a supramolecular system.

Some suggestions for future work will be considered and developed in the final Chapter.

Finally two appendices will be included in this thesis:

- The first will be a literature survey which synthesises the last ten years scientific papers, on the Ru-tpy moiety, including investigations of their properties, use in analytical research or their use as building blocks in supramolecular systems.

- The second appendix will refer to the publications, poster presentations and oral presentations made during the course of the research.

## 1.8 Bibliography

- 
- <sup>1</sup> Plant R A, Hunt J P, **J. Am. Chem. Soc.** 1957, 79, 3343
- <sup>2</sup> Schäfer H L, **Z. Physik. Chem. Frankfurt** 1957, 11, 65
- <sup>3</sup> Adamson A W, Sporer A H, **J. Am. Chem. Soc.** 1958, 80, 3865
- <sup>4</sup> Carassiti V, Claudi B, **Ann. Chim., Rome**, 1959, 49, 1697.
- <sup>5</sup> Balzani V, Carassiti V, **Photochemistry of coordination compounds**, (1970) Academic London.
- <sup>6</sup> Adamson A W, Fleischauer P D, **Concept of inorganic photochemistry**. (1975) Wiley, New York.
- <sup>7</sup> Geoffroy G L, Wrighton M S, **Organometallic photochemistry**, (1973) Academic, New York.
- <sup>8</sup> Balzani V, Juris A, **Coordination Chem. Rev.** 2001, 211, 97
- <sup>9</sup> Demas J N, Adamson A W, **J. Am. Chem. Soc.** 1971, 93, 1800
- <sup>10</sup> Balzani V, Moggi L, Manfrin M F, Bolletta F, Laurence G S, **Coord. Chem. Rev.** 1975, 15, 321.
- <sup>11</sup> Scandola F, Balzani V, **J. Chem Educ.** 1983, 60, 814
- <sup>12</sup> Sutin N, **J. Chem. Educ.** 1983, 60, 809.
- <sup>13</sup> Seddon E A, Seddon K R, **The chemistry of the Ruthenium**, Elsevier, (1984) Amsterdam
- <sup>14</sup> Juris A, Balzani V, Barigelletti F., Campagna S, Belser P, von Zelewsky A, **Coord. Chem. Rev.** 1988, 84, 85

- 
- <sup>15</sup> Grätzel M, **Energy resources through photochemistry and catalysis**, (1983)  
Academic New York
- <sup>16</sup> Norris J R, Meisel D, **Photochemical energy conversion**, (1989) Elsevier, New  
York
- <sup>17</sup> Belser P, Bernhard S, Blum C, Beyder A, De Cola L, Balzani V, **Coordination  
Chem Rev.** 1999, 192, 155
- <sup>18</sup> Ballardini R, Balzani V, Credi A, Gandolfi M T, Venturi M, **Molecular Machine  
and Motors** 2001, 99, 163
- <sup>19</sup> Lehn J M, **Angew. Chem. Int. Ed. Engl.** 1988, 27, 89
- <sup>20</sup> Cram D J, **Angew Chem. Int. Ed. Engl.** 1988, 27, 1009
- <sup>21</sup> Kohnke F H, Mathias J P, Stoddart J F, **Angew. Chem. Ed. Engl.** 1989, 28, 1103
- <sup>22</sup> Balzani V, Scandola F, **Supramolecular Photochemistry.** (1991) Ellis Horwood,  
London
- <sup>23</sup> Kauzmann W, **Quantum Chemistry Academic** (1957)
- <sup>24</sup> Henry B R, Siebrand W, **Organic Molecular Photophysics**, (1973), Wiley
- <sup>25</sup> Kasha M, **Faraday Soc. Discussion** 1950, 9, 14.
- <sup>26</sup> Crosby GA, **J. Chem. Ed.** 1983, 60, 791.
- <sup>27</sup> Lehn J M, **Science** 1985, 227, 849.
- <sup>28</sup> Vogtle F, **Supramolecular Chemistry**, (1991) Wiley, Chichester
- <sup>29</sup> Brown D B, **Mixed Valence Compounds**, (1980) Ed Reindel, Dordrecht
- <sup>30</sup> Creutz C, **Prog. Inorg. Chem.**, 1983, 30, 1.
- <sup>31</sup> Hush N S, **Inorg. Chem.** 1967, 8, 391.

- 
- <sup>32</sup> Jortner J, **J. Chem. Phys.** 1976, 64, 4860.
- <sup>33</sup> Marcus R A, Sutin N, **Biochim. Biophys. Acta**, 1985, 811, 265.
- <sup>34</sup> Marcus R A, **Ann. Rev. Phys. Chem.**, 1964, 15, 155.
- <sup>35</sup> Closs G L, Miller J R, **Science**, 1988, 240, 440.
- <sup>36</sup> Gould I R, Moser J E, Armitage B, Farid S, **J. Am. Chem. Soc.**, 1989, 111, 1917.
- <sup>37</sup> Orlandi G, Monti S, Barigelletti F, Balzani V, **Chem. Phys.**, 1980, 52, 313.
- <sup>38</sup> Murtaza Z, Zipp A P, World L A, Graff D, Jones W E, Bates W D, Meyer T J, **J. Am. Chem. Soc.**, 1991, 111, 1917.
- <sup>39</sup> Balzani V, Bolletta F, Scandola F, **J. Am. Chem. Soc.**, 1980, 102, 2152
- <sup>40</sup> Closs G L, Piotrowiak P, Mac Innis J M, Fleming G R, **J. Am. Chem. Soc.** 1988, 110, 2652
- <sup>41</sup> Turro NJ, **Modern Molecular photochemistry**, (1978) Benjamin, Menlo Park, Ca
- <sup>42</sup> Witt H, **Nouv. J. Chem.** 1987, 11:91
- <sup>43</sup> Cloos G L, Johnson M D, Miller J R, Piotrowiak P, **J. Am. Chem. Soc.**, 1989, 111, 3751 & references there in.
- <sup>44</sup> Balzani V, Moggi L, Scandola F, **Supramolecular Photochemistry**, (1987) Reidel
- <sup>45</sup> Hader DP, Tevini M, **General Photobiology**, (1987) Pergamon.
- <sup>46</sup> Breton J Vermeglio H, **The photosynthetic Bacterial Reaction Centre**, (1988) Plenum.
- <sup>47</sup> Deisenhofer J, Michel H, **Angew. Chem. Int. Ed. Engl.**, 1989, 28, 829.
- <sup>48</sup> Huber R, **Angew. Chem. Int. Ed. Engl.**, 1989, 28, 848.



- 
- <sup>49</sup> Boxer S G, Goldstein R A, Lockhart D J, Middenford T R, Takiff L, **J. Phys. Chem.** 1989, 93, 8280.
- <sup>50</sup> Friesner RA, Won Y. **J. Photochem. Photobiol.** 1989, 50, 83.
- <sup>51</sup> Feher G, Allen J P, Okamura M Y, Rees D C, **Nature** 1989, 339, 111.
- <sup>52</sup> Bard A J, **J. Phys. Chem.**, 1982, 86, 172
- <sup>53</sup> Hagfeldt A, Grätzel M, **Chem Rev.**, 1995, 95, 49.
- <sup>54</sup> Wenham R S , Green M. A, **Progr. Photovolt.**, 1995, 4 , 3.
- <sup>55</sup> O'Regan B, Grätzel M, **Nature**, 1991, 353, 737.
- <sup>56</sup> Smestad G, Bignozzi C A, Argazzi R, **Sol. Energy Mater. Sol. Cells**, 1994, 32, 259.
- <sup>57</sup> Nazeeruddin M.K, Kay A, Grätzel M, **J. Am. Chem. Soc.**, 1993, 115, 6382.
- <sup>58</sup> Gerisher H, **Photochem. Photobiol.** , 1972, 16, 243.
- <sup>59</sup> Argazzi R, Meyer G J, **Inorg. Chem.**, 1994, 33, 5741.
- <sup>60</sup> Santangelo P G, Lewis S, **J. Phys. Chem. B**, 1992, 96, 834..
- <sup>61</sup> H. Gerisher, **J. Photochem. Photobiol.** , (1972), 16, 243.
- <sup>62</sup> Gerfin T, Grätzel M, in "Molecular Level Artificial Photosynthetic Materials", **Prog. Inorg. Chem.**, 1997, 44, 345.
- <sup>63</sup> Bignozzi C A, Schoonover J R, Scandola F, in "Molecular Level Artificial Photosynthetic Materials", **Prog. Inorg. Chem.**, 1997, 44, 1.
- <sup>64</sup> Bard A J, **J. Phys. Chem.**, 1982, 86, 172
- <sup>65</sup> Grätzel M, in **Semiconductor Nanoclusters, Studies in Surface Science and Catalysis**, P.V. Kamat and D. Meisel (eds). Elsevier Science B.V. 1996, 103, 353.,

- 
- <sup>66</sup> Gerisher H, **J. Photochem. Photobiol.** 1972, 16, 243.
- <sup>67</sup> Gerfin T, Grätzel M in "Molecular Level Artificial Photosynthetic Materials",  
**Progr. Inorg. Chem.**, 1997, 44, 345.
- <sup>68</sup> Hotchandani S, Kamat P V, **J. Phys. Chem.**, 1992, 96, 6834.  
D. Liu, and P. V. Kamat, **J. Phys. Chem.**, 1993, 97, 1076.
- <sup>69</sup> Kamat P V, Meisel D, **Elsevier Science B.V.** 1996, 103, 353.
- <sup>70</sup> Paris J P, Brandt W W, **J. Am. Chem. Soc.**, 1959, 81, 5001.
- <sup>71</sup> Kalyanasundaram N, **Coord. Chem. Rev.**, 1982, 46,159.
- <sup>72</sup> Hage R, Haasnot J G, Reedijk, Vos J G., **Inorg. Chem.**, 1992, 4, 75.
- <sup>73</sup> Lytle F E, Hercules D M, **J. Am. Chem. Soc.**, 1969, 91, 253.
- <sup>74</sup> Maestri M, Armaroli N, Balzani V, Constable E C, Cargill Thompson A M W,  
**Inorg. Chem.** 1995, 34, 2759.
- <sup>75</sup> Indelli M T, Bignozzi C A, Scandola F, Collin J P, **Inorg. Chem.**, 1998, 37, 6084.

## **Chapter 2**

### **“Experimental Procedures”**

“Anything that can go wrong will go wrong”

**Murphy**

## **2.1 Introduction**

Synthetic procedures are described in each chapter. All synthetic reagents were of commercial grade and no further purification was employed, again unless otherwise stated.

All solvents employed in spectroscopic measurement were HPLC or spectroscopic grade.

## **2.2 Chromatographic techniques**

High performance liquid chromatography (HPLC) was carried out on a Waters 510 HPLC using a Waters 990 photodiode array detector equipped with a NEC PAC III computer, a 20  $\mu$ l injector loop and a Partisil SCX radial PAK cartridge. The detection wavelength used was 280 nm. The chromatography was achieved using a mobile phase, which consisted of acetonitrile/ water, 80/20 (v/v) containing 0.08 M LiClO<sub>4</sub>. The flow rate for routine work was 1.8 cm<sup>3</sup> min<sup>-1</sup>.

Semi-preparative HPLC was performed using an ACS pump, a 1 cm<sup>3</sup> injection loop and a Waters Partisil SCX 10  $\mu$ m cation exchange column (25 x 100 mm). The mobile phase used 0.12 M Ammonium Acetate in methanol. The flow rate used 2.0 cm<sup>3</sup>/min.

## **2.1 Introduction**

Synthetic procedures are described in each chapter. All synthetic reagents were of commercial grade and no further purification was employed, again unless otherwise stated.

All solvents employed in spectroscopic measurement were HPLC or spectroscopic grade.

## **2.2 Chromatographic techniques**

High performance liquid chromatography (HPLC) was carried out on a Waters 510 HPLC using a Waters 990 photodiode array detector equipped with a NEC PAC III computer, a 20  $\mu$ l injector loop and a Partisil SCX radial PAK cartridge. The detection wavelength used was 280 nm. The chromatography was achieved using a mobile phase, which consisted of acetonitrile/ water, 80/20 (v/v) containing 0.08 M LiClO<sub>4</sub>. The flow rate for routine work was 1.8 cm<sup>3</sup> min<sup>-1</sup>.

Semi-preparative HPLC was performed using an ACS pump, a 1 cm<sup>3</sup> injection loop and a Waters Partisil SCX 10  $\mu$ m cation exchange column (25 x 100 mm). The mobile phase used 0.12 M Ammonium Acetate in methanol. The flow rate used 2.0 cm<sup>3</sup>/min.

## 2.1 Introduction

Synthetic procedures are described in each chapter. All synthetic reagents were of commercial grade and no further purification was employed, again unless otherwise stated.

All solvents employed in spectroscopic measurement were HPLC or spectroscopic grade.

## 2.2 Chromatographic techniques

High performance liquid chromatography (HPLC) was carried out on a Waters 510 HPLC using a Waters 990 photodiode array detector equipped with a NEC PAC III computer, a 20  $\mu\text{l}$  injector loop and a Partisil SCX radial PAK cartridge. The detection wavelength used was 280 nm. The chromatography was achieved using a mobile phase, which consisted of acetonitrile/ water, 80/20 (v/v) containing 0.08 M  $\text{LiClO}_4$ . The flow rate for routine work was  $1.8 \text{ cm}^3 \text{ min}^{-1}$ .

Semi-preparative HPLC was performed using an ACS pump, a  $1 \text{ cm}^3$  injection loop and a Waters Partisil SCX 10  $\mu\text{m}$  cation exchange column (25 x 100 mm). The mobile phase used 0.12 M Ammonium Acetate in methanol. The flow rate used  $2.0 \text{ cm}^3/\text{min}$ .

## 2.3 Absorption and Emission Spectroscopy

UV/Vis spectra were carried out on a Shimadzu UV-3100 spectrophotometer. Emission spectra were obtained by a Perkin Elmer LS50 luminescence spectrometer; at room temperature the measurements were taken using an excitation slide of 10 mm and emission slit of 10 mm. At 77 K, different mixtures were used and the excitation and emission slit widths were set to 5 mm. In both absorption and emission spectroscopy deprotonation was achieved using diethylamine or concentrated aqueous ammonia, and protonation using 60 % (w/v) perchloric acid.

The ground state pK<sub>a</sub>s were measured by manipulating the observed changes in the UV/Vis absorption intensity as a function of pH. The excited state acid-base equilibria were measured by manipulating the changes in the emission intensity as a function of pH. The excitation wavelength for the emission titration was chosen from a suitable isobestic point determined from the absorption acid/base titration spectra. The samples were dissolved in a few drops of acetonitrile ( $\approx 10^{-5}$  M) and diluted with 100 cm<sup>3</sup> of Britton-Robson buffer (0.04 M boric acid, 0.04 M acetic acid, 0.04 M phosphoric acid). The pH was adjusted by adding conc. NaOH or conc. H<sub>2</sub>SO<sub>4</sub> and was measured using a Corning 240 digital pH meter. The pK<sub>a</sub>s were determined from the sigmoidal fitting of change in absorbance versus pH.

## 2.3 Absorption and Emission Spectroscopy

UV/Vis spectra were carried out on a Shimadzu UV-3100 spectrophotometer. Emission spectra were obtained by a Perkin Elmer LS50 luminescence spectrometer; at room temperature the measurements were taken using an excitation slide of 10 mm and emission slit of 10 mm. At 77 K, different mixtures were used and the excitation and emission slit widths were set to 5 mm. In both absorption and emission spectroscopy deprotonation was achieved using diethylamine or concentrated aqueous ammonia, and protonation using 60 % (w/v) perchloric acid.

The ground state pK<sub>a</sub>s were measured by manipulating the observed changes in the UV/Vis absorption intensity as a function of pH. The excited state acid-base equilibria were measured by manipulating the changes in the emission intensity as a function of pH. The excitation wavelength for the emission titration was chosen from a suitable isobestic point determined from the absorption acid/base titration spectra. The samples were dissolved in a few drops of acetonitrile ( $\approx 10^{-5}$  M) and diluted with 100 cm<sup>3</sup> of Britton-Robson buffer (0.04 M boric acid, 0.04 M acetic acid, 0.04 M phosphoric acid). The pH was adjusted by adding conc. NaOH or conc. H<sub>2</sub>SO<sub>4</sub> and was measured using a Corning 240 digital pH meter. The pK<sub>a</sub>s were determined from the sigmoidal fitting of change in absorbance versus pH.



## 2.3 Absorption and Emission Spectroscopy

UV/Vis spectra were carried out on a Shimadzu UV-3100 spectrophotometer. Emission spectra were obtained by a Perkin Elmer LS50 luminescence spectrometer; at room temperature the measurements were taken using an excitation slide of 10 mm and emission slit of 10 mm. At 77 K, different mixtures were used and the excitation and emission slit widths were set to 5 mm. In both absorption and emission spectroscopy deprotonation was achieved using diethylamine or concentrated aqueous ammonia, and protonation using 60 % (w/v) perchloric acid.

The ground state pK<sub>a</sub>s were measured by manipulating the observed changes in the UV/Vis absorption intensity as a function of pH. The excited state acid-base equilibria were measured by manipulating the changes in the emission intensity as a function of pH. The excitation wavelength for the emission titration was chosen from a suitable isobestic point determined from the absorption acid/base titration spectra. The samples were dissolved in a few drops of acetonitrile ( $\approx 10^{-5}$  M) and diluted with 100 cm<sup>3</sup> of Britton-Robson buffer (0.04 M boric acid, 0.04 M acetic acid, 0.04 M phosphoric acid). The pH was adjusted by adding conc. NaOH or conc. H<sub>2</sub>SO<sub>4</sub> and was measured using a Corning 240 digital pH meter. The pK<sub>a</sub>s were determined from the sigmoidal fitting of change in absorbance versus pH.

## **2.4 Luminescent lifetime**

Luminescent lifetimes were carried out on a Q-switched Nd-Yag System. Room temperature measurements were carried out in methanol, unless otherwise stated.

For laser work samples were of low concentration ie  $10^{-4}$  or  $10^{-5}$ M. Samples were degassed by bubbling dry argon through the sample for at least 20 minutes. Lifetimes conforming to single exponential decays were analysed with Microcal Origin Software. The lifetime errors are estimated to be less than 8%

Short-lived measurements were carried out with a Single Photon Counter of Edinburgh Analytical Instrument in a T setting. The lamp were a nF900, in a Nitrogen setting, the monochromators were J-yA models, the detector was a Single Photon Photomultiplier Detection System, model S 300, with a MCA card type Norland N5000 and a PC interface Cd900 serial. The program used for the data correlation and manipulation is F900 Program, Version 5.13.

## **2.5 Nuclear Magnetic Resonance**

$^1\text{H}$ -NMR spectra were recorded on a Bruker AC400 (400 MHz) instrument. The solvent used for the complexes was mainly deuteriated acetonitrile. Deuterium oxide was used in some of the spectra but this is clearly stated. Deuteriated dimethyl sulphoxide was used for the ligands. The chemical shifts were recorded relative to the standard tetramethylsilane (TMS). The spectra

## **2.4 Luminescent lifetime**

Luminescent lifetimes were carried out on a Q-switched Nd-Yag System. Room temperature measurements were carried out in methanol, unless otherwise stated.

For laser work samples were of low concentration ie  $10^{-4}$  or  $10^{-5}$ M. Samples were degassed by bubbling dry argon through the sample for at least 20 minutes. Lifetimes conforming to single exponential decays were analysed with Microcal Origin Software. The lifetime errors are estimated to be less than 8%

Short-lived measurements were carried out with a Single Photon Counter of Edinburgh Analytical Instrument in a T setting. The lamp were a nF900, in a Nitrogen setting, the monochromators were J-yA models, the detector was a Single Photon Photomultiplier Detection System, model S 300, with a MCA card type Norland N5000 and a PC interface Cd900 serial. The program used for the data correlation and manipulation is F900 Program, Version 5.13.

## **2.5 Nuclear Magnetic Resonance**

$^1\text{H-NMR}$  spectra were recorded on a Bruker AC400 (400 MHz) instrument. The solvent used for the complexes was mainly deuteriated acetonitrile. Deuterium oxide was used in some of the spectra but this is clearly stated. Deuteriated dimethyl sulphoxide was used for the ligands. The chemical shifts were recorded relative to the standard tetramethylsilane (TMS). The spectra

## **2.4 Luminescent lifetime**

Luminescent lifetimes were carried out on a Q-switched Nd-Yag System. Room temperature measurements were carried out in methanol, unless otherwise stated.

For laser work samples were of low concentration ie  $10^{-4}$  or  $10^{-5}$ M. Samples were degassed by bubbling dry argon through the sample for at least 20 minutes. Lifetimes conforming to single exponential decays were analysed with Microcal Origin Software. The lifetime errors are estimated to be less than 8%

Short-lived measurements were carried out with a Single Photon Counter of Edinburgh Analytical Instrument in a T setting. The lamp were a nF900, in a Nitrogen setting, the monochromators were J-yA models, the detector was a Single Photon Photomultiplier Detection System, model S 300, with a MCA card type Norland N5000 and a PC interface Cd900 serial. The program used for the data correlation and manipulation is F900 Program, Version 5.13.

## **2.5 Nuclear Magnetic Resonance**

$^1\text{H}$ -NMR spectra were recorded on a Bruker AC400 (400 MHz) instrument. The solvent used for the complexes was mainly deuteriated acetonitrile. Deuterium oxide was used in some of the spectra but this is clearly stated. Deuteriated dimethyl sulphoxide was used for the ligands. The chemical shifts were recorded relative to the standard tetramethylsilane (TMS). The spectra

were converted from their Free Induction Decay (FID) profiles using a Bruker WINNMR software package.

The 2-D COSY (correlated spectroscopy) experiments involved the accumulation of 128 FIDs of 16 scans. Digital filtering was sine-bell squared and the FID was zero filled in the F1 dimension. Acquisition parameters were  $F1 = \pm 500$  Hz,  $F2 = 1000$  Hz and  $t_{1/2} = 0.001$  s. The cycle time delay was 2 s.

## **2.6 Electrochemistry**

For electrochemistry all organic solvents were HPLC grade, dried over molecular sieves. The electrolyte used was TetrabutylAmmonium EsaFluoroPhosphate (TBAPF<sub>6</sub>). The working electrodes were or a 3 mm diameter Teflon shrouded glassy carbon electrode or a platinum electrode, the reference electrode was a saturated calome electrode and auxiliary electrode was a platinum gauze. The electrochemical cell was a three-electrode cell compartmentalised with glass frits. The analyte was degassed with argon in order to measure the cathodic potential. pH was adjusted using perchloric acid or dry tryethylamina.

For cyclic voltammetry an EG&G PAR model 362 scanning potentiostat, and a Linseis, model 17100 x-y recorder, at scan rate of 100 mVs<sup>-1</sup>.

were converted from their Free Induction Decay (FID) profiles using a Bruker WINNMR software package.

The 2-D COSY (correlated spectroscopy) experiments involved the accumulation of 128 FIDs of 16 scans. Digital filtering was sine-bell squared and the FID was zero filled in the F1 dimension. Acquisition parameters were  $F1 = \pm 500$  Hz,  $F2 = 1000$  Hz and  $t_{1/2} = 0.001$  s. The cycle time delay was 2 s.

## 2.6 Electrochemistry

For electrochemistry all organic solvents were HPLC grade, dried over molecular sieves. The electrolyte used was TetrabutylAmmonium HexafluoroPhosphate (TBAPF<sub>6</sub>). The working electrodes were or a 3 mm diameter Teflon shrouded glassy carbon electrode or a platinum electrode, the reference electrode was a saturated calome electrode and auxiliary electrode was a platinum gauze. The electrochemical cell was a three-electrode cell compartmentalised with glass frits. The analyte was degassed with argon in order to measure the cathodic potential. pH was adjusted using perchloric acid or dry triethylamina.

For cyclic voltammetry an EG&G PAR model 362 scanning potentiostat, and a Linseis, model 17100 x-y recorder, at scan rate of 100 mVs<sup>-1</sup>.

were converted from their Free Induction Decay (FID) profiles using a Bruker WINNMR software package.

The 2-D COSY (correlated spectroscopy) experiments involved the accumulation of 128 FIDs of 16 scans. Digital filtering was sine-bell squared and the FID was zero filled in the F1 dimension. Acquisition parameters were  $F1 = \pm 500$  Hz,  $F2 = 1000$  Hz and  $t_{1/2} = 0.001$  s. The cycle time delay was 2 s.

## 2.6 Electrochemistry

For electrochemistry all organic solvents were HPLC grade, dried over molecular sieves. The electrolyte used was TetrabutylAmonium EsaFluoroPhosphate (TBAPF<sub>6</sub>). The working electrodes were or a 3 mm diameter Teflon shrouded glassy carbon electrode or a platinum electrode, the reference electrode was a saturated calome electrode and auxiliary electrode was a platinum gauze. The electrochemical cell was a three-electrode cell compartmentalised with glass frits. The analyte was degassed with argon in order to measure the cathodic potential. pH was adjusted using perchloric acid or dry tryethylamina.

For cyclic voltammetry an EG&G PAR model 362 scanning potentiostat, and a Linseis, model 17100 x-y recorder, at scan rate of  $100 \text{ mVs}^{-1}$ .

## **2.7 Mass Spectrography**

The experiments were performed on a timing MAT equipped with an electro spray interface (ESI) in Technische Universitaet Berlin or in DCU University with the assistance of Mr. Maurice Burke.

Spectra are collected by constant infusion of the analyte dissolved in a mixture of 80:20, methanol: water, in presence of Acetic Acid ( 1%).

ESI is a soft ionisation technique, resulting in protonated, sodiated species in positive ionisation mode and deprotonated, chlorinated or acetate salt in negative ionisation mode.

## **2.8 Spectroelectrochemistry.**

Spectroelectrochemistry was carried out as using a home-made pyrex glass thin layer cell (1 mm), a platinum gauze as working electrode , a Ag/AgCl quasi-reference electrode and a platinum wire as counter electrode. The electrolyte used was 0.1 M TEAP in acetonitrile and the UV/Visible/NIR spectra were recorded using the Shimadzu 3100 UV/NIR spectrometer interfaced to an Elonex PC433 computer. The working electrode was held at the required potential during the spectral scan using a CH instrument Model 660 potentiostat electrochemical workstation interfaced to an Elonex 486 PC. Scans at anodic potentials required degassing of the samples.



## **2.7 Mass Spectrography**

The experiments were performed on a timing MAT equipped with an electro spray interface (ESI) in Technische Universitaet Berlin or in DCU University with the assistance of Mr. Maurice Burke.

Spectra are collected by constant infusion of the analyte dissolved in a mixture of 80:20, methanol: water, in presence of Acetic Acid ( 1%).

ESI is a soft ionisation technique, resulting in protonated, sodiated species in positive ionisation mode and deprotonated, chlorinated or acetate salt in negative ionisation mode.

## **2.8 Spectroelectrochemistry.**

Spectroelectrochemistry was carried out as using a home-made pyrex glass thin layer cell (1 mm), a platinum gauze as working electrode , a Ag/AgCl quasi-reference electrode and a platinum wire as counter electrode. The electrolyte used was 0.1 M TEAP in acetonitrile and the UV/Visible/NIR spectra were recorded using the Shimadzu 3100 UV/NIR spectrometer interfaced to an Elonex PC433 computer. The working electrode was held at the required potential during the spectral scan using a CH instrument Model 660 potentiostat electrochemical workstation interfaced to an Elonex 486 PC. Scans at anodic potentials required degassing of the samples.

## **2.7 Mass Spectrography**

The experiments were performed on a timing MAT equipped with an electro spray interface (ESI) in Technische Universitaet Berlin or in DCU University with the assistance of Mr. Maurice Burke.

Spectra are collected by constant infusion of the analyte dissolved in a mixture of 80:20, methanol: water, in presence of Acetic Acid ( 1%).

ESI is a soft ionisation technique, resulting in protonated, Sodiated species in positive ionisation mode and deprotonated, chlorinated or acetate salt in negative ionisation mode.

## **2.8 Spectroelectrochemistry.**

Spectroelectrochemistry was carried out as using a home-made pyrex glass thin layer cell (1 mm), a platinum gauze as working electrode , a Ag/AgCl quasi-reference electrode and a platinum wire as counter electrode. The electrolyte used was 0.1 M TEAP in acetonitrile and the UV/Visible/NIR spectra were recorded using the Shimadzu 3100 UV/NIR spectrometer interfaced to an Elonex PC433 computer. The working electrode was held at the required potential during the spectral scan using a CH instrument Model 660 potentiostat electrochemical workstation interfaced to an Elonex 486 PC. Scans at anodic potentials required degassing of the samples.

## **2.9 Elemental analysis.**

C,H,N elemental analyses were carried out by the Microanalytical laboratories at University College Dublin.

## **2.10 Titanium dioxide solar cells.**

Solar energy conversion studies were performed in Ferrara University with the assistance of Monica Alebbi from the group of Prof. Carlo Bignozzi.

## **2.9 Elemental analysis.**

C,H,N elemental analyses were carried out by the Microanalytical laboratories at University College Dublin.

## **2.10 Titanium dioxide solar cells.**

Solar energy conversion studies were performed in Ferrara University with the assistance of Monica Alebbi from the group of Prof. Carlo Bignozzi.

## **2.9 Elemental analysis.**

C,H,N elemental analyses were carried out by the Microanalytical laboratories at University College Dublin.

## **2.10 Titanium dioxide solar cells.**

Solar energy conversion studies were performed in Ferrara University with the assistance of Monica Alebbi from the group of Prof. Carlo Bignozzi.

## **Chapter 3**

### **“Synthesis of Ligands and Complexes”**

“If there is a possibility of several things going wrong,  
the one that will cause the most damage will be the one to go wrong.  
If there is a worse time for something to go wrong, it will happen then.”

**Murphy**

### **3.1 Synthesis of 4, 4', 4'' methoxy carbonyl-2, 2', 6', 2''-terpyridine. [H<sub>3</sub>(tctpy)]**

The synthesis was a modification of the one in literature<sup>1</sup> (Scheme 1)

#### **3.1.1 Synthesis of 4, 4', 4'' ethyl-2, 2', 6', 2''terpyridine**

Freshly distilled 4-ethyl pyridine (50 cm<sup>3</sup>) was refluxed (170°C) under argon with 4g of 10% Pd on activated carbon. After 9 days the mixture was cooled down to room temperature and 500 cm<sup>3</sup> of CH<sub>2</sub>Cl<sub>2</sub> added. The carbon catalyst was filtered, washed with 100 cm<sup>3</sup> of CH<sub>2</sub>Cl<sub>2</sub> and the solution rotary evaporated to dryness. The bpy Et<sub>2</sub> was distilled out of the mixture under vacuum leaving 9.5g of tpyEt<sub>3</sub>. Yield 20%. The tpyEt<sub>3</sub> ligand was used without further purification.

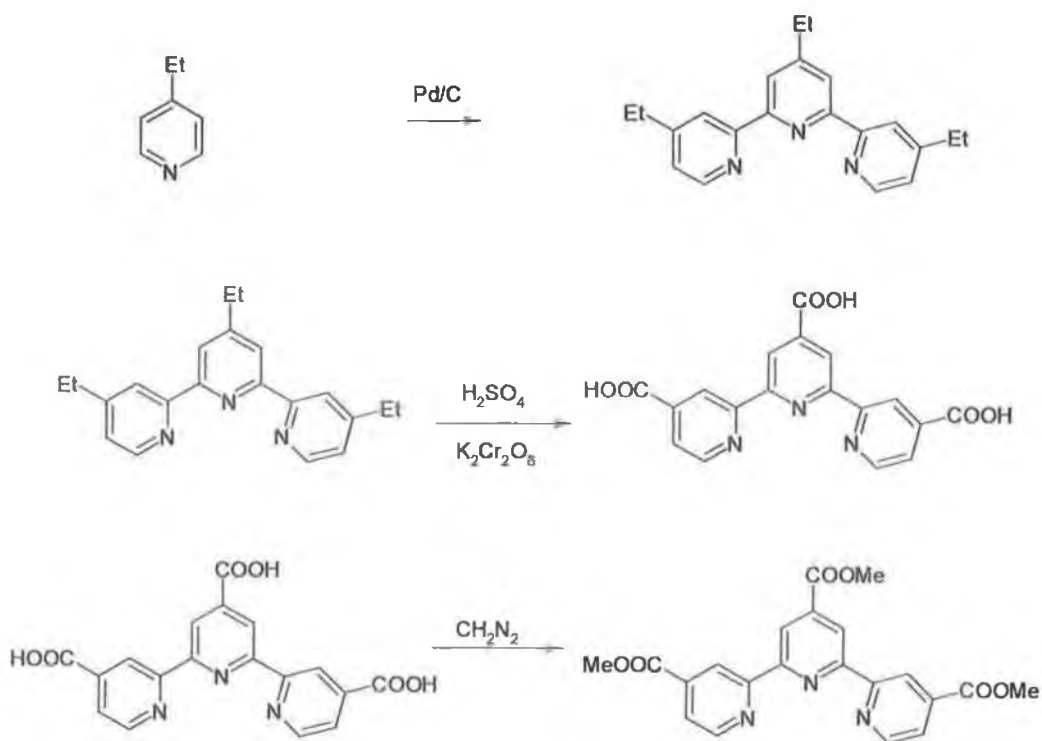
<sup>1</sup>H NMR (200 MHz, CDCl<sub>3</sub>) ppm: 1.35 (6H, t, *J* 7.6 Hz), 1.37 (3H, t, *J* 7.6 Hz), between 2.75 and 2.89 (6H, two partially overlapped quartets, *J* 7.6 Hz), 7.18 (2H, d, *J* 5.0 Hz), 8.29 (2H, s), 8.44 (2H, s), 8.59 (2H, d, *J* 5.0 Hz).

#### **3.1.2 Synthesis of 4, 4', 4'' carboxy-2, 2', 6', 2''terpyridine**

The oxidation of 4, 4', 4'' ethyl-2, 2', 5', 2''terpyridine (0.8g.) was carried out in H<sub>2</sub>SO<sub>4</sub> (4 cm<sup>3</sup>, 96 % w/w), with K<sub>2</sub>Cr<sub>2</sub>O<sub>6</sub> (3.5g.) at 60 °C.. After two hours, the reaction was added to a mixture of ice and water, yielding (60%) of 4, 4', 4'' carboxy-2, 2', 5', 2''terpyridine. <sup>1</sup>HNMR(NaOD/D<sub>2</sub>O): 7,52 (2H, d), 8,13 (2H, s) 8,31 (2H,s), 8,31 (2H, s), 8,43 (2H, d)

### 3.1.3 Synthesis of 4, 4', 4'' methoxy carbonyl-2, 2', 6', 2''terpyridine

The 4, 4', 4'' carboxy-2, 2', 5', 2''terpyridine (127 mg) was esterified reacting with  $\text{CH}_2\text{N}_2$  in diethyl ether ( $25 \text{ cm}^3$ ). When all the diazomethane had reacted (change of the solution colour from bright yellow to brown) the white solid precipitate was filtered, dissolved in chloroform and recrystallised, yield 80%.  $^1\text{HNMR}(\text{CDCl}_3)$ : 4.04 (3H,s), 4.05 (6H,s), 7.94 (2H, d), 8.90 (2H,d),9.03 (2H,s), 9.13 (2H,s). Mp.: 238-239°



Scheme 1 Synthesis of 4, 4', 4'' methoxy carbonyl, 2, 2', 6', 2'' terpyridine



### **3.2 Synthesis of 4' (pyrid-4''-yl) -2, 2', 6', 2''-terpyridine. [py-tpy]**

The ligand 4' (4''pyrdyl) -2, 2', 6', 2''-terpyridine, (py-tpy) was a modification of the Kroenke preparation, as described in literature<sup>2</sup>.

#### **3.2.1 Synthesis of 1.5-Bis(2 pyridyl) pentane -1,5-dione (dione).**

A solution of 2-acetylpyridine (8.4 cm<sup>3</sup>, 0.074 mol), pyridine 4 carbaldehyde (3.0 cm<sup>3</sup>, 0.032 mol) and sodium hydroxyde (2.0 gr) in water (25 cm<sup>3</sup>) and ethanol (35 cm<sup>3</sup>) was stirred for 1 hour at room temperature. After this period water (30 cm<sup>3</sup>) was added and a white precipitate obtained. This was collected by filtration, washed well with cold ethanol and dried to give the molecule as a white solid (4.5 gr, 45 %). <sup>1</sup>HNMR(CDCl<sub>3</sub>): 3.77 (4H, m), 4.20 (1H, m) 7.37 (2H,dd), 7.51 (2H, ddd), 7.86 (2H, td), 8.02 (2H, dt) 8.52 (2H, dd) 8.70 (2 H, m)

#### **3.2.2 Synthesis of 4' (4''pyrdyl) -2, 2', 6', 2''-terpyridine. [py-tpy]**

A solution of the dione (0.40 g, 1.21 mmol) and ammonium acetate (5.00 g) in water was heated to reflux for 2 hours. After this period, the pale coloured solution was cooled to give an off-white precipitate, which was collected by

filtration. Recrystallisation from ethanol gave small white needles of 4'-(4''pyranyl)-2, 2', 6', 2''-terpyridine (0.30gr, 50 %)  $^1\text{H NMR}(\text{CDCl}_3)$ : 7.37 (1H,t), 7.79 (1H, dd), 7.89 (1H, t), 8.68 (1H, dd) 8.73 (1H, dd) 8.76 (2 H, m) , mp 233-235 C $^\circ$

### **3.3 Synthesis of di 2, 6 (1,2,4, triazol-3-yl) pyridine. [H<sub>2</sub>(ΔpyΔ)]**

The synthesis is a modification of the one in literature<sup>3</sup> for similar molecules.

#### **3.3.1 Synthesis of Pyridine-2, 6-dicarboxy acid diethylester**

10 g (0.080 mmol) of Pyridine-2,6-dicarboxylic acid were dissolved in 70 cm<sup>3</sup> of ethanol containing 1.3 cm<sup>3</sup> concentrated sulphuric acid. The resulting mixture was refluxed overnight. The excess ethanol was removed in vacuo and the residue neutralised with a NaHCO<sub>3</sub> saturated solution and extracted with CH<sub>2</sub>Cl<sub>2</sub>. The organic layer was washed twice with NaCl saturated solution. After removal, the product was obtained as oil, which solidified on standing. Yield: 78%

<sup>1</sup>H-NMR, CDCl<sub>3</sub> (1.40-1.55 (t), 3H, J=12 Hz; 4.40-4.60, (q), 2H, J=18 Hz; 8.00-, 8.01 (t), 0.5H, J=19 Hz; 8.02-8.04 (d), 1H;)

#### **3.3.2 Synthesis of Pyridine-2, 6-dicarboxy diamide**

3.5 g of the Pyridine-2, 6-dicarboxylic acid diethylester (3.3.1) was dissolved in 3 cm<sup>3</sup> methanol and added to 15 cm<sup>3</sup> of a stirring aqueous solution of NH<sub>3</sub> (d=0.88), immersed in an ice-bath. Precipitation occurred after a half-hour. Another 7 cm<sup>3</sup> of methanol was added and the resulting mixture stirred overnight at room temperature. The product was collected by filtration and washed with cold methanol. Yield: 77% <sup>1</sup>H-NMR d<sup>6</sup>DMSO(3.403.55(s),3H;7.68-7.76 (s), 1H; 8.09-8.22 (m), 1.5H; 8.85-8.93 (s), 1H).

### **3.3.3 Synthesis of Pyridine-2, 6-dicarbonitrile**

A mixture of 2g of the Pyridine-2,6-dicarboxylic-acid-diamide and 50 cm<sup>3</sup> DMF were warmed up until a clear solution was obtained. The solution was immersed in an ice bath and 4 cm<sup>3</sup> of POCl<sub>3</sub> was slowly added. The resulting clear, yellow solution was stirred for 3h by room temperature. The residue was diluted with CH<sub>2</sub>Cl<sub>2</sub> and mixed with water. The organic layer was collected and washed one more time with water. The solvent was reduced under vacuum. The product was crashed out from the resulting thick mixture by adding a small amount of ice, filtered off, washed with water and dried. Yield: 72%

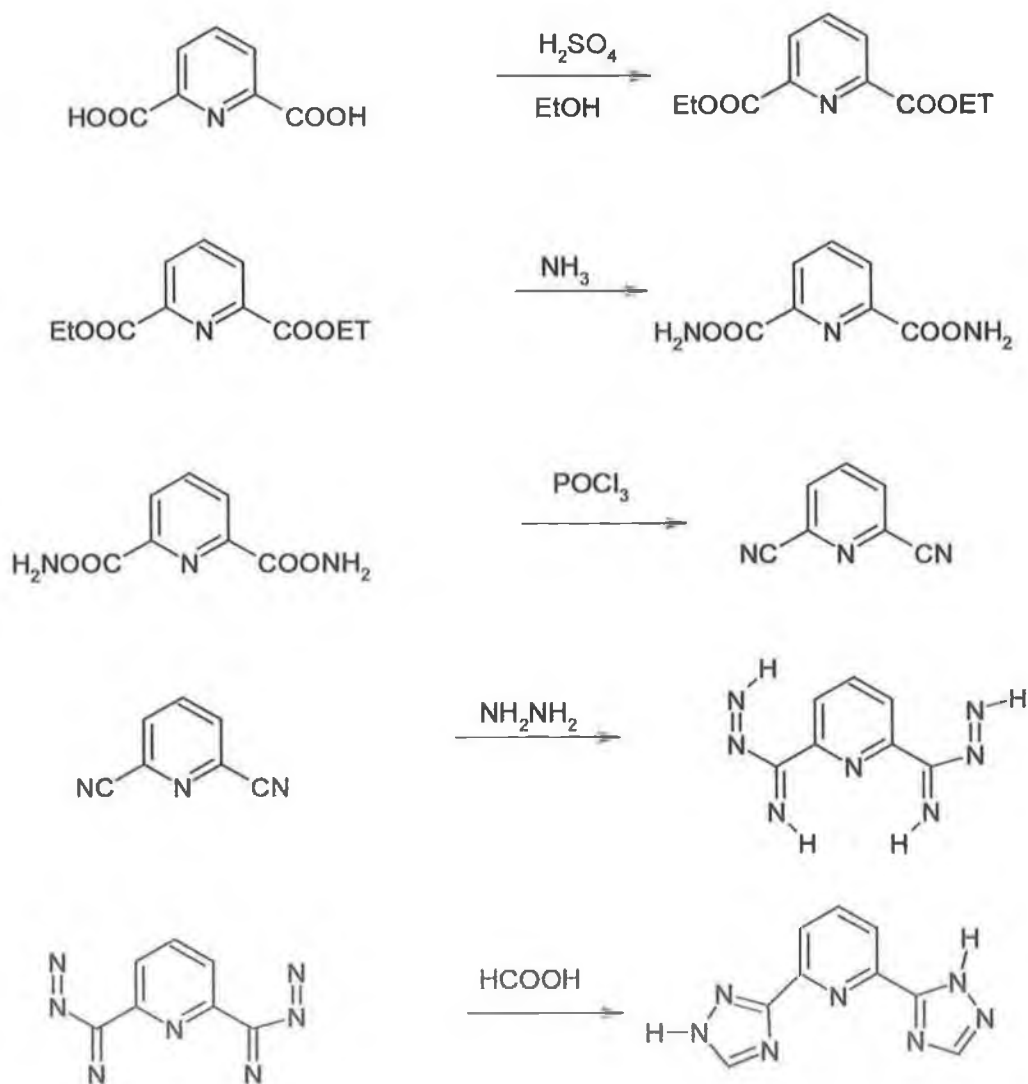
<sup>1</sup>H-NMR d<sup>6</sup>- DMSO (7.85-7.92, (d), 2H, J=20 Hz, 7.99-8.06, (t), 1H, J=19 Hz)

(Fig. 3.1)

### **3.3.4 Synthesis of Pyridine-2, 6 diimidrazone**

A 20-fold excess of hydrazine monohydrate (26 cm<sup>3</sup>) was added to a stirring solution of 3.6 g (27.9 mmol) of pyridine-2, 6-dicarbonitrile and 70 cm<sup>3</sup> of ethanol. The resulting yellow solution was stirred for two hours at 60 °C. A precipitation occurred which was collected by filtration, washed with a small portion of very cold methanol (-4 C<sup>o</sup>) and dried. Yield: 81%

<sup>1</sup>H-NMR-d<sup>6</sup>-DMSO (5.10-5.35, (s), 2H, 5.90-6.15, (s), 2H, 7.63-7.69, (t), 2H, J=19 Hz, 7.78-7.83, (d), 2H, J=20 Hz) (Fig 3.2)



**Scheme 2 Synthesis of the di-2, 6 (1,2,4, triaz-yl) pyridine. [ $\text{H}_2(\Delta\text{py}\Delta)$ ]**

### 3.3.5 Synthesis of the H<sub>2</sub>(ΔpyΔ) ligand

3 g (0.016 mmol) of the diimidrazone was carefully added step wise to 38 cm<sup>3</sup> of formic acid at 0 °C. The resulting mixture was stirred for three hours, after which the acid was removed under reduced pressure. The resulting oil was dissolved in 23 cm<sup>3</sup> of 1,2-Ethandiol and refluxed for 70 min. The solution was allowed to cool, mixed with a small amount of ice (water) and left in the fridge overnight. A precipitation occurred, which was collected by filtration and washed with small amounts of diethyl ether. Yield: 70%

<sup>1</sup>H-NMR-d<sup>6</sup>-DMSO( 8.00-8.15, (m), 2H; 8.20-8.50, (s), 1H) (Fig. 3.5)

Mass Spec found (214), teoric. (214.4) (Fig. 3.3)

### 3.4 Synthesis of the di-2,6 [**phen-3-yl (1',2',4', triazol-5-yl)**] **pyridine. [H<sub>2</sub>(ΦΔpyΔΦ)]**

2 g (0.0105) of the diimidrazone (obtained from synthesis 3.3.5) were dissolved in 18 cm<sup>3</sup> THF, 2 cm<sup>3</sup> triethylamina and 40 cm<sup>3</sup> of ethanol. The resulting yellow mixture was stirred overnight. The intermediate was collected by filtration. After recrystallisation the resulting solid was dissolved in 1,2-ethandiol and refluxed for two hours. The solution was allowed to cool down, mixed with a small amount of ice water and left in the fridge overnight. Precipitation occurred, which was collected by filtration and washed with a small portion of diethylether. The yield was almost quantitative, 80 %. M.Spec found 365, calc 365 (Fig 3.4)

$^1\text{H-NMR-d}^6$ -DMSO(7.40-7.65, (m), 6H; 8.10-8.20, (d), 4H,  $J=22$  Hz;8.20-8.40, (s), 3H) (Fig. 3.6)

### **3.5 Synthesis of the di-2,6 (tetraz-5-yl) pyridine. [ $\text{H}_2(\square\text{py}\square)$ ]**

The synthesis above present modification to the one reported in literature<sup>4</sup>

In a double necked 100 cm<sup>3</sup> flask equipped with a condenser, 2,6 pyridine dicarbonitrile (2.0 g 15.5 mmol), NaN<sub>3</sub> (2.1g 32.5 mmol), NH<sub>4</sub>Cl (1.8 g 34.1mmol) and LiCl (1.9 g 46.5mmol) were charged. DMF (20 cm<sup>3</sup>) was added and the stirred suspension was maintained at 110-120° for 8-10 hrs under nitrogen atmosphere. After cooling at r.t., evaporation of the solvent afforded a residue which was re dissolved in water. Dropwise addition of HCl 1M afforded a white precipitate which was collected by filtration and dried under vacuum. [during HCl addition volatile HN<sub>3</sub> could be formed; the flask was connected to a bubbler with a concentrate NaOH solution]. The product, (FW 215; 3.2 g; 97%) obtained in quantitative yield, was recrystallised from water/ethanol 1/1 solution.

$^1\text{H-NMR-d}^6$ -DMSO( 8.00-8.15,) (m), 3H) (Fig 3.7)

$^{13}\text{C-NMR-d}^6$ -DMSO (154, 1C; 143, 2C; 140, 2C; 123, 2C)

### 3.6 Synthesis of Ru(X-tpy)(Cl<sub>3</sub>)

The synthesis of these complexes are already reported in literature<sup>5</sup>

1 g (0.044 mmol) of RuCl<sub>3</sub>.2H<sub>2</sub>O were dissolved in 150 cm<sup>3</sup> of ethanol, the solution was refluxed and 1 equivalent of 4'-X 2, 2'; 6',2'' terpyridine (X-tpy), where X can either be H or Cl, dissolved in 20 cm<sup>3</sup> of ethanol, were dropped in the reaction bulk. The reaction was heated for 2 h. and filtered hot. A Siena's burned earth solid was collected and washed with ethanol, water and diethyl ether. Yield 80%.

The complex was used without any further purification.

### 3.7 Synthesis of Ru[tcttpy](Cl<sub>3</sub>)

The synthesis of this complex is already reported in literature.<sup>1</sup>

The complex was synthesised by adding a solution of 4, 4', 4'' methoxy-2, 2', 5', 2'' terpyridine (40 mg, 1\*10<sup>-4</sup> mmol), in dichloromethane (20 cm<sup>3</sup>), to a solution of a hydrated ruthenium trichloride (26 mg) in ethanol (30 cm<sup>3</sup>). The reaction mixture was refluxed for 2 hours and the solution was concentrated to 20 cm<sup>3</sup>. The precipitated complex was collected and washed thoroughly with ethanol water and diethyl ether. (Yield 80%)

The complex was used without any further purification.



### 3.8 Synthesis of Ru( $\Delta$ py $\Delta$ )(Cl<sub>3</sub>)

1 g of RuCl<sub>3</sub>.2H<sub>2</sub>O was dissolved in 150 cm<sup>3</sup> of ethanol, the solution was refluxed and 1 g of 2, 2'; 6', 2'' terpyridine, was suspended in the reaction bulk. The reaction was heated for 2 h. and filtered hot. A pale okra-yellow solid was collected and washed with ethanol, water and Diethyl Ether. Yield 80%.

[Ru( $\Delta$ py $\Delta$ )Cl<sub>3</sub>] (H<sub>2</sub>O) Anal. calcd. H 1.62 C 24.76 N 22.46 found H 1.99 C 24.62 N 21.62

<sup>1</sup>H-NMR (d<sup>6</sup>-DMSO) 8.55 (2H, d), 8.45 (H, t).

### 3.9 Synthesis of Ru(py-tpy)(Cl<sub>3</sub>)

The ligand 4' (4'''pyrdyl) -2, 2', 6', 2''-terpyridine, (py-tpy), was precipitated as its PF<sub>6</sub> salt, dissolving it in hydrochloric aqueous solution (pH 2) and by adding an excess of NaPF<sub>6</sub> salt. 1 g of RuCl<sub>3</sub>.2H<sub>2</sub>O was dissolved in 150 cm<sup>3</sup> of ethanol, the solution was refluxed and 2 g of [4' (4'''pyrdyl)-2, 2'; 6', 2''][PF<sub>6</sub>] terpyridine, was suspended in the reaction bulk. The reaction was heated for 2 h. and filtered hot. A Marijuana-green solid was collected and washed with ethanol, water and Diethyl Ether. Yield 80%.

### 3.10 Synthesis of $\text{Na}_3[\text{Ru}(\text{tctpy})(\Delta\text{py}\Delta)]$

The  $\text{Ru}(\text{tctpy})$  complex was obtained by heating  $[\text{Ru}(\text{tctpy})]\text{Cl}_3$  (160 mg,  $3 \cdot 10^{-4}$ ) and a stoichiometric amount of the ligand  $\text{H}_2(\Delta\text{py}\Delta)$  (70 mg,  $3 \cdot 10^{-4}$ ) in water containing a slight molar excess of  $\text{NaOH}$  and few drops of *N*-ethylmorpholine. The reaction mixture was refluxed for two hours; the dark green solution was evaporated. Purification of the solid by column chromatography on Sephadex LH20 (methanol) gave a 30% yield.

Elemental analysis suggests  $\text{Na}_3[\text{Ru}(\text{tctpy})(\Delta\text{py}\Delta)](\text{H}_2\text{O})_2$  Anal. calcd. C 41.6, H 2.2, N 17.97; found C 42.7 H 2.60 N 18.03.

$^1\text{H-NMR}$  ( $\text{CD}_3\text{OD}$ ) 9.20 (2H, s), 8.77 (2H, s), 8.41 (2H, d), 8.31 (1H, t), 8.02 (2H, s), 7.70 (2H, d), 7.23 (2H, d)

### 3.11 Synthesis of $[\text{Ru}(\text{tpy})(\Delta\text{py}\Delta)]$

The  $\text{Ru}(\text{tpy})$  complex was obtained by heating  $[\text{Ru}(\text{tpy})]\text{Cl}_3$  (1 g,  $2.2 \cdot 10^{-3}$ ) and a stoichiometric amount of the ligand  $\text{H}_2(\Delta\text{py}\Delta)$  (0.5 g,  $2.2 \cdot 10^{-3}$ ) in water containing a slight molar excess of  $\text{NaOH}$  and few drops of *N*-ethylmorpholine. The reaction mixture was refluxed for two hours; the dark green solution was concentrated, acidified to pH 2 with  $\text{HCl}$  and an excess of  $\text{NH}_4\text{PF}_6$  was added. Purification by column chromatography on alumina (acetonitrile/methanol 50:50) gave a 30% yield. Elemental analysis suggests that a mixture of monoprotonated

/deprotonated (80:20) complex is formed after recrystallization from acetone/water. For a mixture of  $[\text{Ru}(\text{tpy})\text{H}(\Delta\text{py}\Delta)][\text{PF}_6]$ :  $[\text{Ru}(\text{tpy})(\Delta\text{py}\Delta)]$ , (80:20), Anal. calcd. C 43.52, H 2.56, N 21.15; found C 43.7 H 2.60 N 21.03.

$^1\text{H-NMR}$  ( $\text{CD}_3\text{OD}$ ) 8.6 (2H, q), 8.4 (2H, q), 8.2 (H, m), 8.1(3H, m), 7.73 (2H, t), 7.6 (H, d), 7.25 (2H, t of d), 7.06 (2H, m), 6.98 (H, d)

### 3.12 Synthesis of $[\text{Ru}(\text{Cl-tpy})(\Delta\text{py}\Delta)]$

The  $\text{Ru}(\text{Cl-tpy})$  complex was obtained by heating  $[\text{Ru}(\text{Cl-tpy})]\text{Cl}_3$  and a stoichiometric amount of the ligand  $\text{H}_2(\Delta\text{py}\Delta)$  in DMF containing a slight molar excess of NaOH and few drops of N-ethylmorpholine. The reaction mixture was refluxed for two hours; the brown green solution was concentrated, acidified to pH 3 with HCl and aqueous solution of  $\text{NH}_4\text{PF}_6$  was added. A Cayenne red complex precipitated, it was recrystallise from a acidic water acetone (1:1) solution. For  $\text{H}_2[\text{Ru}(\text{Cl-tpy})(\Delta\text{py}\Delta)][\text{PF}_6]_2 (\text{DMF})_{1/2}$  Anal. calcd. C 29.13, H 2.35, N 28.74; found C 30.10 H 2.60 N 28.70. For NMR discussion see chapter 6.

### 3.13 Synthesis of {Ru(tpy)( $\Phi\Delta\text{py}\Delta\Phi$ )}

[Ru(tpy)Cl<sub>3</sub>] (250 mg, 0.57 mmol), AgBF<sub>4</sub> (331 mg, 1.70 mmol) were refluxed for 2 hours in dry acetone (75 ml). The solution was filtered in order to remove AgCl, DMF (50 ml) was added and the acetone was evaporated. A suspension of ( $\Phi\Delta\text{py}\Delta\Phi$ ) (208 mg, 0.57 mmol) and N-ethylmorpholine (5 drops) in DMF (120 cm<sup>3</sup>) were heated till complete dissolution of the ligand. Then, the DMF solution containing the Ru complex was slowly added and the resulting solution was refluxed for 4h. The solvent was removed under reduced pressure and the residue mixture was dissolved in the minimum amount of methanol and separated on an alumina column with acetonitrile/acetone (80/20) as the eluent. This resulted in three fractions. The second fraction contained the desired complex, 23 % of yield. However a TLC of this fraction showed the presence of two coordination isomers. Further attempts were necessary in order to separate this second fraction into its two components (See Chapter 6 for separation and NMR spectroscopy of the two coordination isomers).

Mass Spec (m/z) {H[Ru(tpy)( $\Phi\Delta\text{py}\Delta\Phi$ )]<sup>+</sup> calcd. (699) found (699)

[Ru(tpy)( $\Phi\Delta\text{py}\Delta\Phi$ )]Anal. calcd. C 51.19 H 3.10 N 16.58 found C 50.19 H 3.41 N 15.81.

### 3.14 Synthesis of [Ru(tpy)(py)]

The complex was obtained by heating [Ru(tpy)]Cl<sub>3</sub> (1 g, 2.2 \*10<sup>-3</sup>) and a stoichiometric amount of the ligand H<sub>2</sub>(py), (0.5 g, 2.2 \*10<sup>-3</sup>), in 20 cm<sup>3</sup> of ethylene glycol containing a slight molar excess of NaOH and few drops of N-ethylmorpholine. The reaction mixture was refluxed for two hours, by adding water a crab brown solid precipitated. The complex was recrystallised from DMF:Water solution (1:1). The final Yield was 40%

[Ru(tpy)(py)] (H<sub>2</sub>O) Anal. calcd. C 46.73 H 2.85 N 29.72 found C 46.9 H 2.60 N 29.03.

<sup>1</sup>H-NMR (d<sup>6</sup>-DMSO) 9.00 (d), 8.80 (2H, dd), 8.55 (2H, d), 8.45 (H, t), 8.45 (2H, t) 8.0(2H, dd), 7.38 (2H, d), 7.30 (H, dd).

### 3.15 Synthesis of [Ru(Cl-tpy)(py)]

The Ru(Cl-tpy) complex was obtained by heating [Ru(Cl-tpy)]Cl<sub>3</sub>, (1 g, 2.1 \*10<sup>-3</sup>), and a stoichiometric amount of the ligand H<sub>2</sub>(py)(0.44 g, 2.1 \*10<sup>-3</sup>), in 20 cm<sup>3</sup> of ethylene glycol containing a slight molar excess of NaOH and few drops of N-ethylmorpholine. The reaction mixture was refluxed for two hours, by adding water a moroccan brown solid precipitated. The complex was recrystallised from DMF:Water solution (1:1). The final Yield was 42%

[Ru(tpy)(py)] (DMF) Anal. calcd. C 45.41 H 2.25 N 28.88 found C 45.49 H 2.35 N 28.83.

$^1\text{H-NMR}$  ( $d^6$ -DMSO) 9.34 (2H, s), 8.91 (2H, dd), 8.56 (2H, d), 8.49 (H, t), 8.06 (2H, dd), 7.73 (2H, d), 7.36 (H, dd).

### **3.16 Synthesis of $[\text{Ru}(\text{py-tpy})(\text{py})]$**

The complex was obtained by heating  $[\text{Ru}(\text{py-tpy})]\text{Cl}_3$  (1g, 20mmol) and a stoichiometric amount of the ligand  $\text{H}_2(\text{py})$  (0.46g, 20 mmol) in 20  $\text{cm}^3$  of DMF containing a slight molar excess of NaOH and few drops of N-ethylmorpholine. The reaction mixture was refluxed for two hours, by adding a acidic aqueous solution (  $\text{HClO}_4$  6M) a dark blood red solid precipitated. The complex was recrystallised from Acetonitrile:Water solution (1:1). Finally the complex was precipitated as esafluorophosphate salt, by dissolving it in the smallest amount of acetone and adding an acidic (pH 2) aqueous solution of sodium esafluorophosphate. The final Yield was 20 %.

Mass Spec (m/z)  $\{[\text{Ru}(\text{py-tpy})(\text{py})][\text{ClO}_4]\}^{2+}$  calcd. (361) found (361) (Fig 3.9)

$^1\text{H-NMR}$  ( $d^6$ -DMSO) 9.07 (2H, s), 8.97 (2H, d), 8.66 (2H, d), 8.14 (2H, d), 7.97 (2H, dd), 7.43 (2H, d), 7.20 (H, dd).

### 3.17 Synthesis of $[\text{Ru}(\text{bpy})_2(\Delta\text{py})]\text{PF}_6$

The complex was made following literature<sup>6</sup>

0.395 g (1.41 mmol) of  $\text{H}\Delta\text{py}$  ligand was dissolved in 50  $\text{cm}^3$  ethanol:water (1:1 v/v). This was heated to reflux until the ligand was fully dissolved. 0.520g (1 mmol)  $\text{cis-}[\text{Ru}(\text{bpy})_2\text{Cl}_2]\cdot 2\text{H}_2\text{O}$  was added and the reaction allowed to reflux for 5-8 hours. After the solution was allowed to cool the reaction was filtered and the volume reduced to ca 15  $\text{cm}^3$ . The complex was precipitated by addition of a concentrated aqueous solution of ammonium hexafluorophosphate. The precipitate was filtered and washed with a small volume of water (10-15  $\text{cm}^3$ ). The product was dried by washing with diethylether and left under vacuum for a few hours. The dry complex was recrystallised from acetone/water (2:1 v/v). Yield = 0.53 g (60 %). Calcd. for  $[\text{Ru}(\text{bpy})_2(\Delta\text{py})]\text{PF}_6\cdot 3\text{H}_2\text{O}$ : C: 42.30; H: 3.10; N: 14.80 %. Anal. Found: C: 42.8; H: 3.10; N: 4.10 %.

### 3.18 Synthesis of $[\text{Ru}(\text{bpy})_2(\square\text{py})][\text{PF}_6]$

0.395 g (1.41 mmol) of  $\text{H}\square\text{py}$  ligand was dissolved in 50  $\text{cm}^3$  methanol. This was heated to reflux until the ligand was fully dissolved. 0.520g (1 mmol)  $[\text{Ru}(\text{bpy})_2\text{Cl}_2]\cdot 2\text{H}_2\text{O}$  was added and the reaction allowed to reflux for 3 hours. After the solution was allowed to cool the reaction was filtered and the volume reduced to ca 15  $\text{cm}^3$ . The complex was precipitated by addition of a

concentrated aqueous solution of ammonium hexafluorophosphate. The precipitate was filtered and washed with a small volume of water (10-15 cm<sup>3</sup>). The product was dried by washing with diethylether and left under vacuum for a few hours. The dry complex was recrystallised from acetone/water (2:1 v/v). Yield = 0.70 g (70 %). Calcd. for [Ru(bpy)<sub>2</sub>(□py)]PF<sub>6</sub>.H<sub>2</sub>O: C: 40.80; H: 3.10; N: 21.80 %. Anal. Found: C: 41.2; H: 3.18; N: 20.5 %.

### **3.19 Preparation of Titanium Oxide.**

Preparation of transparent TiO<sub>2</sub> membranes supported on conducting glass sheets was produced by deposition of colloidal particles on a conducting glass support. The procedure applied was similar to that used in literature<sup>7,8</sup>.

TiO<sub>2</sub> colloid solutions were prepared by hydrolysis of titanium isopropoxide, Ti(OCH(CH<sub>3</sub>)<sub>2</sub>)<sub>4</sub> as follows: Under a stream of dry argon, 125 cm<sup>3</sup> of Ti(OCH(CH<sub>3</sub>)<sub>2</sub>)<sub>4</sub> was added to 150 cm<sup>3</sup> dropping funnel containing 20 cm<sup>3</sup> of 2-propanol. The mixture was added over a period of 30 min. to a solution of 750 cm<sup>3</sup> of deionised water while undergoing vigorous stirring. It was then autoclaved for 12 hours at 220 C under an argon current. The mixture was then stirred for 8 hours at 90 C and the water was evaporated until 700 cm<sup>3</sup> of colloidal sol was obtained.

A portion of the above gel (100 cm<sup>3</sup>) was concentrated and added to a mixture of ethyl cellulose in ethanol (100 cm<sup>3</sup>) and terpineol (20 cm<sup>3</sup>), stirred for 3 hrs. in a broyer machine, in order to obtain a serygraphic paste. The deposition of a



7 $\mu$ m thickness film on optically transparent glass (CTO glass, fluorine-doped SnO<sub>2</sub>) was obtained through a serygraphic technique. After the deposition the glass heated under oxygen enriched air for 20 minutes at 400 C. High resolution scanning electron microscopy revealed TiO<sub>2</sub> to be composed of a three-dimensional network nanoscale particle (15-20 nm.).

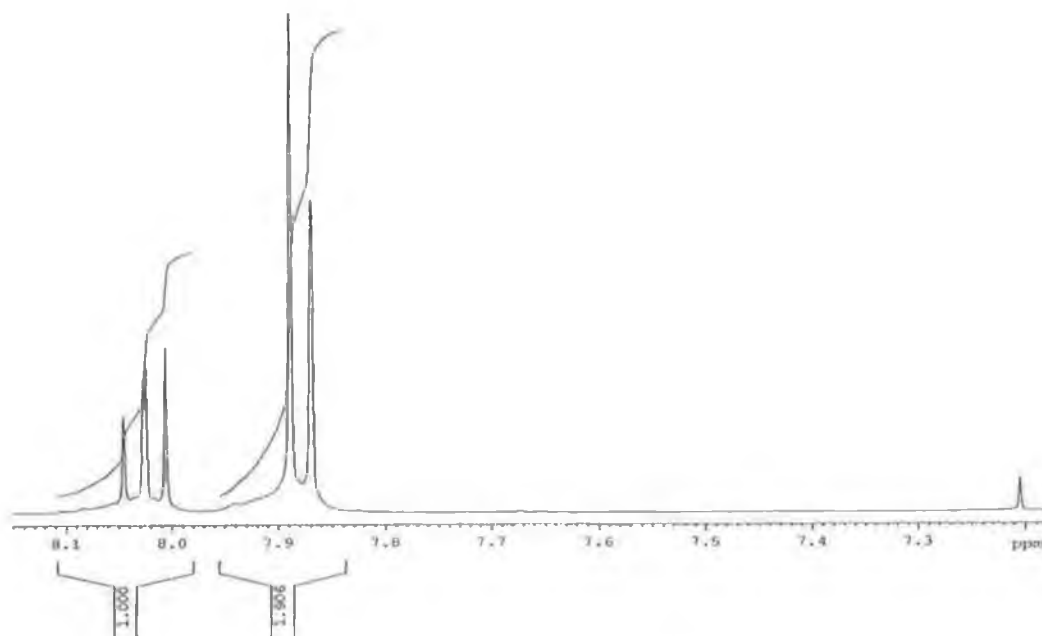


Figure 3.1 <sup>1</sup>H NMR of Pyridine-2, 6-dicarbonitrile in d<sup>6</sup>-DMSO

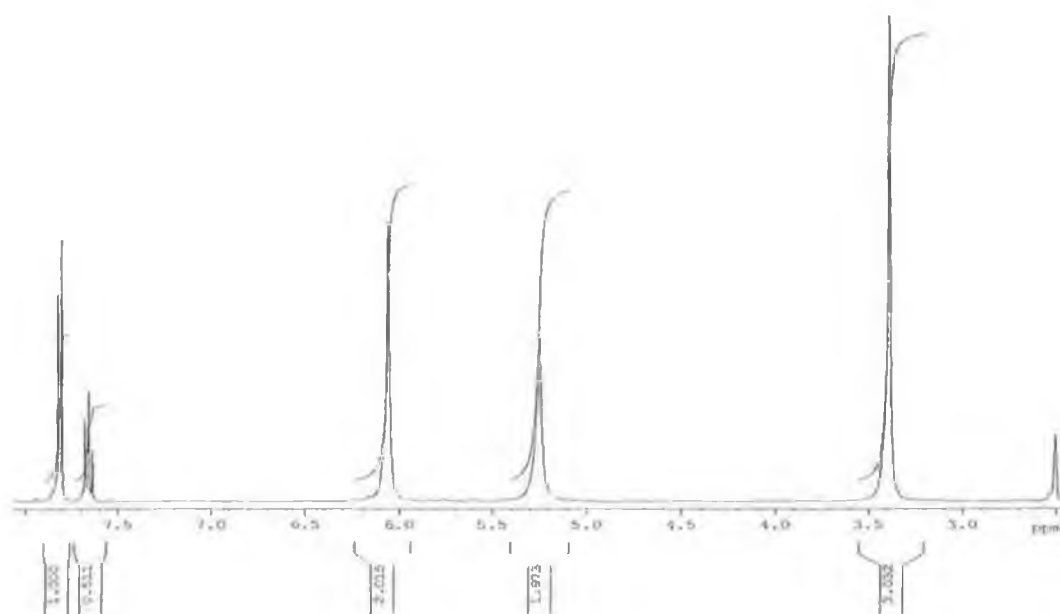


Figure 3.2 <sup>1</sup>H NMR of Pyridine-2, 6-imidrazone in d<sup>6</sup>-DMSO

SPEC: sery314 01-Feb-99 Elapse: 00:00:20.9 4  
 Samp: sample 1 Start: 11:23:02 6  
 Comm: 213  
 Mode: BSI +VE +MR BSCAN (LINE) OF PROP  
 Oper: Bertil Hoffe Client: bedri Inlet:   
 Base: 214.2 Inten: 971270 Masses: 100 - 400  
 Norm: 214.3 RIC: 5358801 #peaks: 2  
 Peak: 1000.00 mmu  
 Accu: 1 - 6 Smth: 3

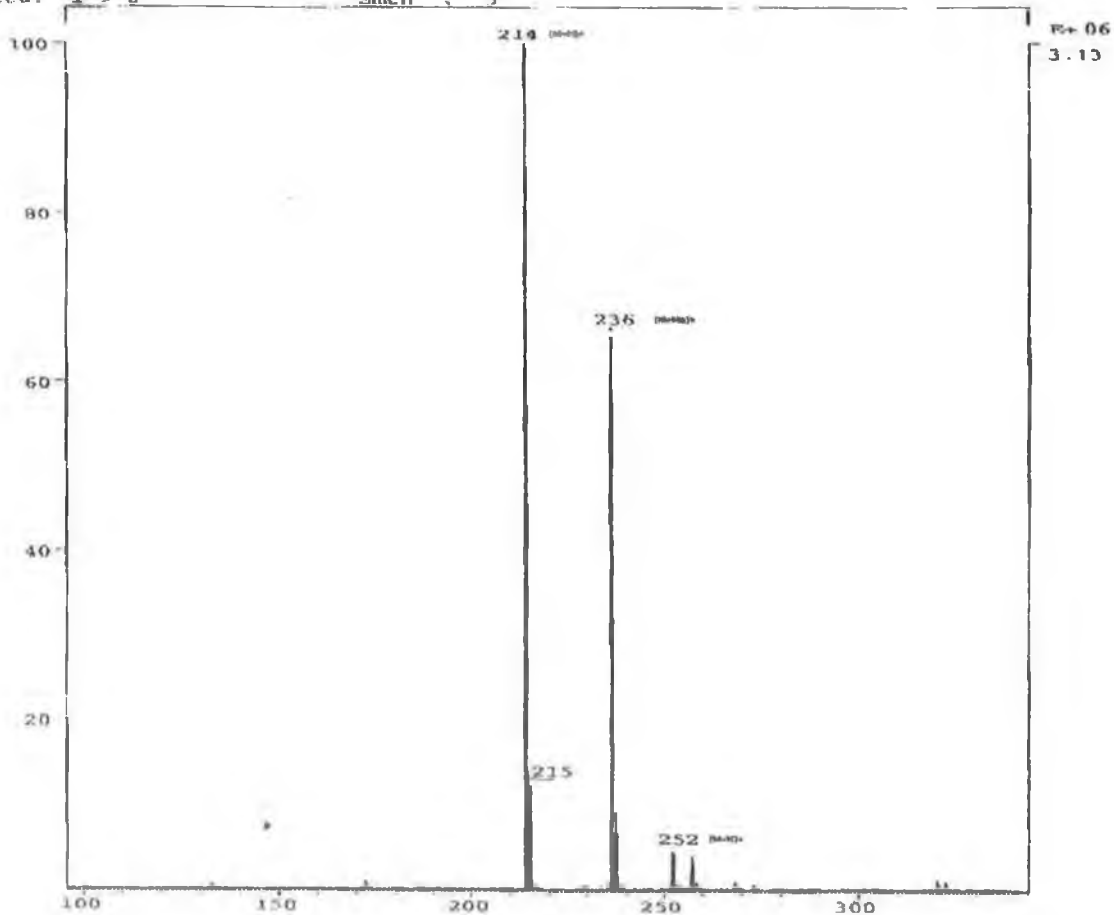


Figure 3.3 Mass Spectrum of  $H_2(\Delta py\Delta)$

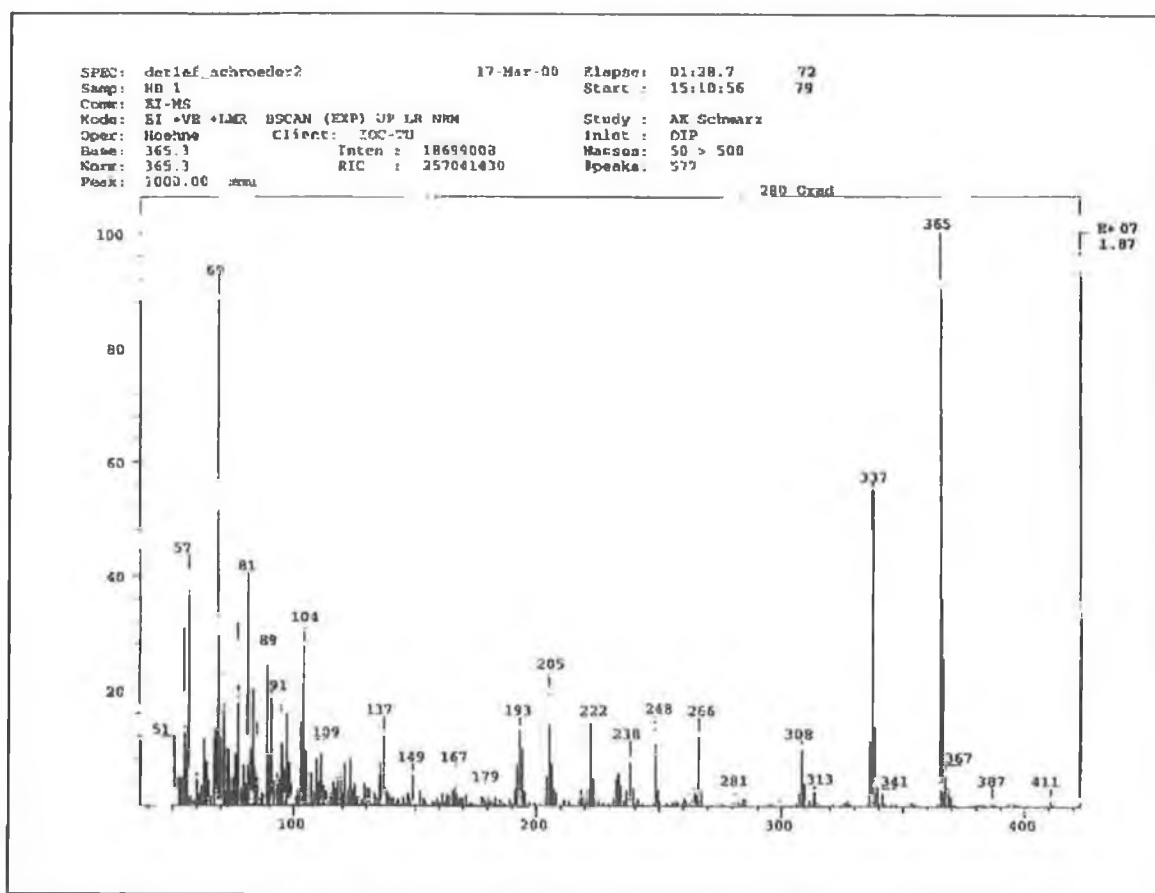


Figure 3.4 Mass spectrum of  $[H_2(\Phi\Delta py\Delta\Phi)]$

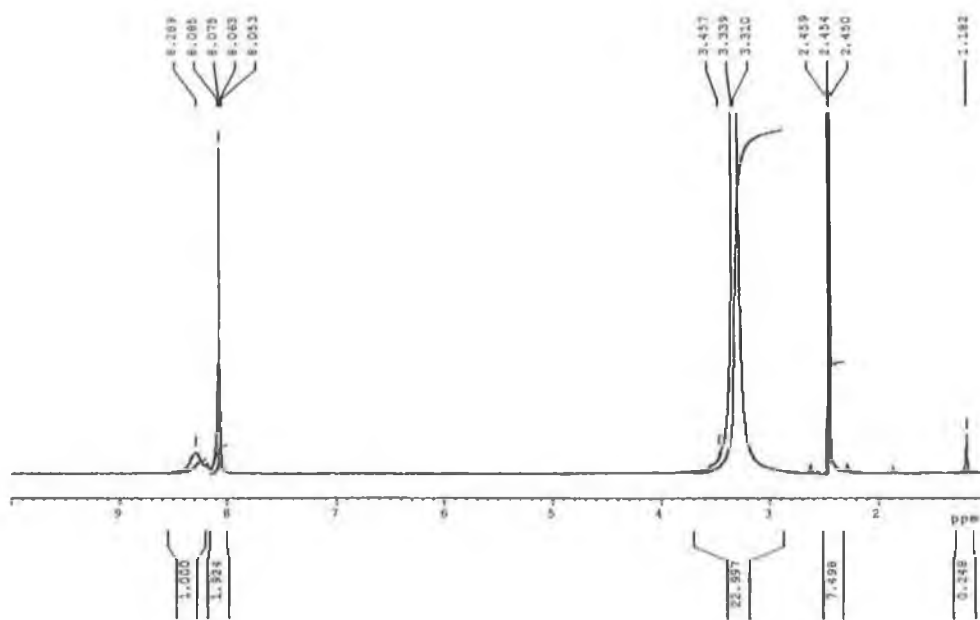


Figure 3.5  $^1\text{H}$ -NMR spectrum of  $\text{H}_2(\Delta\text{py}\Delta)$  ligand in  $d^6$ -DMSO

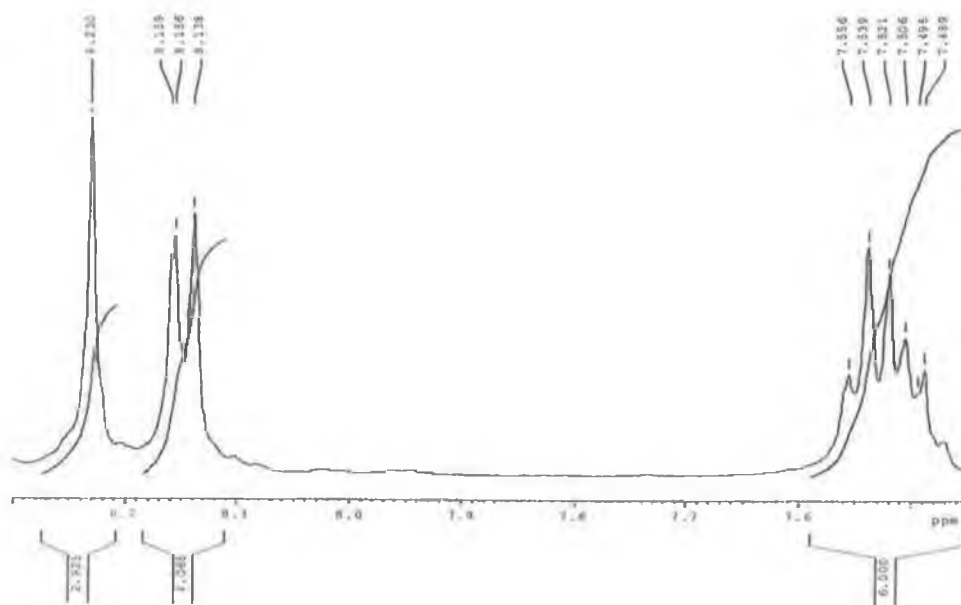


Figure 3.6  $^1\text{H}$ -NMR spectrum of  $\text{H}_2(\Phi\Delta\text{py}\Delta\Phi)$  ligand in  $d^6$ -DMSO

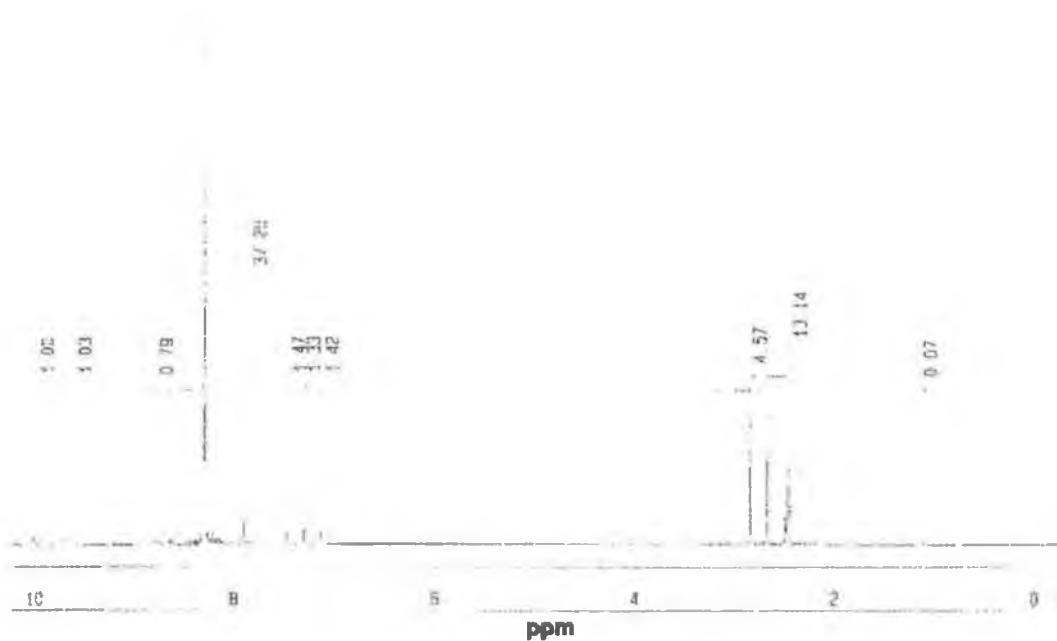


Figure 3.7  $^1\text{H-NMR}$  spectrum of  $\text{H}_2(\square\text{py}\square)$  ligand in  $\text{d}^6\text{-DMSO}$

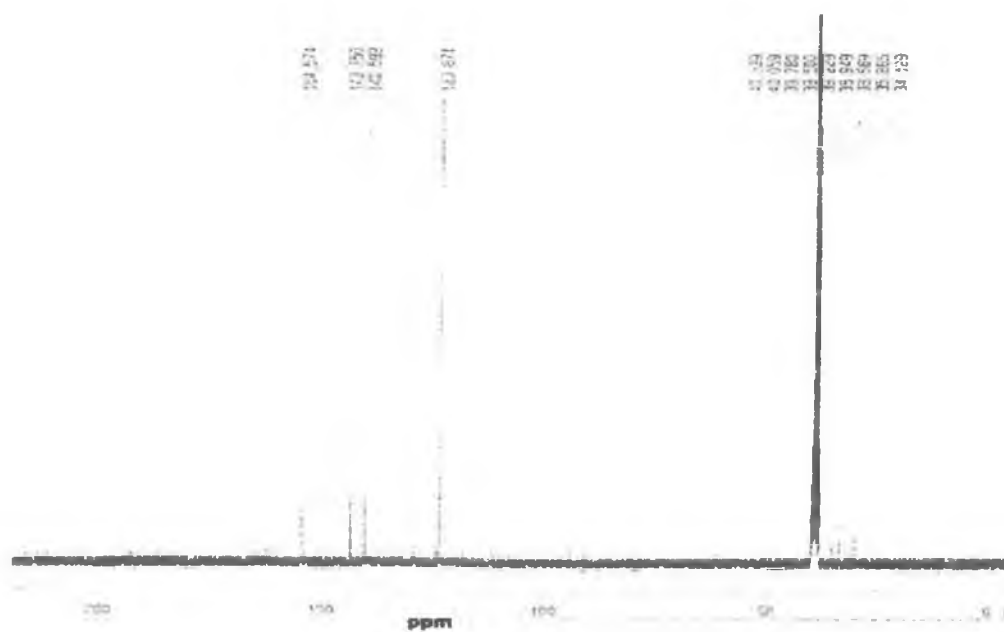


Figure 3.8  $^{13}\text{C-NMR}$  spectrum of  $\text{H}_2(\square\text{py}\square)$  ligand in  $\text{d}^6\text{-DMSO}$

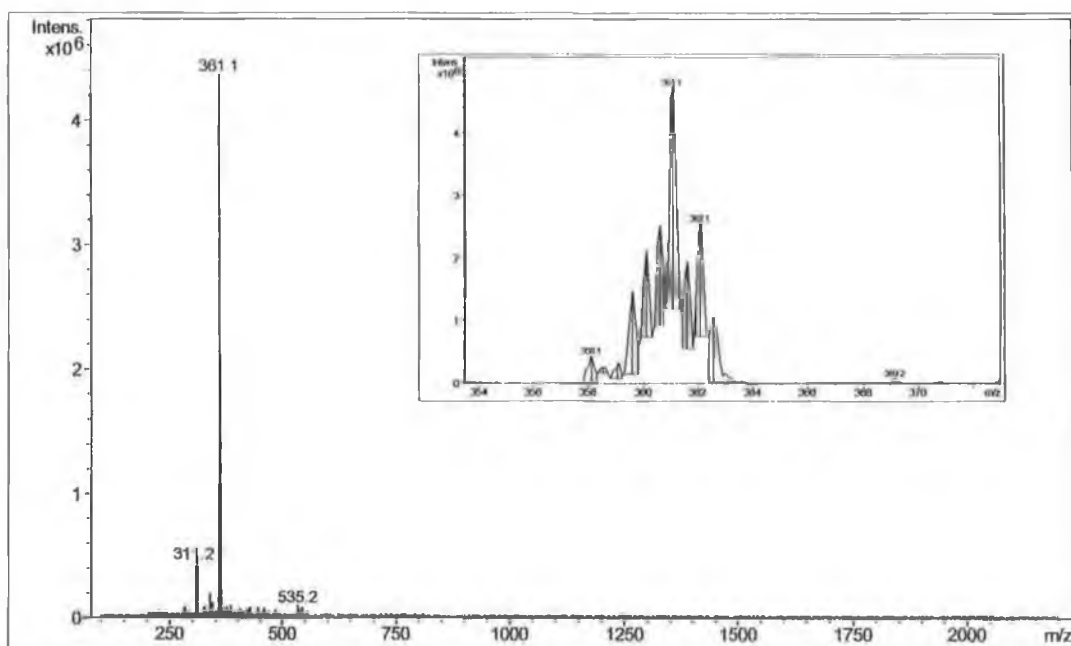


Figure 3.9 Mass spectrum of  $\{H_2[Ru(py-tpy)(\square py \square)](ClO_4)\}^{2+}$

### 3.20 Bibliography

---

- <sup>1</sup> Nazeeruddin MK, Pechy P, Gratzel M, **Chem Comm** 1997, 18, 1705
- <sup>2</sup> Constable EC, Cargill Thompson **J chem. Soc. Dalton Trans.** 1992, 2947.
- <sup>3</sup> Suyiyarto K H, Craig D C, Rae D C, Rae A D, Goodwin H A, **Aust. J. Chem.** 1993, 46, 1269
- <sup>4</sup> Finnegan, W A; Henry, R A, Lofquist, R., **J. Am. Chem. Soc.**, 1958, 80, 3908.
- <sup>5</sup> Constable E C, Cargill Thopson, Tocher D A, Daniels M A M, **New J Chem**, 1992, 16, 855.
- <sup>6</sup> O'Connor C, **Ph D Thesis**, 1999, Dublin City University, Dublin
- <sup>7</sup> O'Reagan B, Gratzel M., **Nature** 1991, 353, 737
- <sup>8</sup> Hacque S A, Tachibana Y, Willis R L, Moser J E, Gratzel M, Klug D R, Durrant J R, **J Phys. Chem. B.** 2000, 104, 538



## **Chapter 4**

### **“Bpy Based Complexes”**

“If anything simply cannot go wrong, it will anyway.  
If you perceive that there are four possible ways in which  
a procedure can go wrong, and circumvent these,  
then a fifth way, unprepared for, will promptly develop.”

**Murphy**

## 4.1 Introduction

Aromatic nitrogen heterocycles represent an important class of ligands in transition metal coordination chemistry<sup>1,2</sup>. The major division in the classification of aromatic nitrogen heterocycles is according to ring size. The six member ring nitrogen heterocycles (azines, pyridine) are  $\pi$ -deficient with relatively low energy  $\pi^*$  orbitals, which allow good metal-to-ligand, back bonding from the d-orbitals of the metal to the  $\pi$ -system of the ligand. The five member aromatic nitrogen cycles (azoles), on the other hand, are  $\pi$ -rich,  $\pi$ -donors and can also form anionic ligands by deprotonation of acidic NH groups.

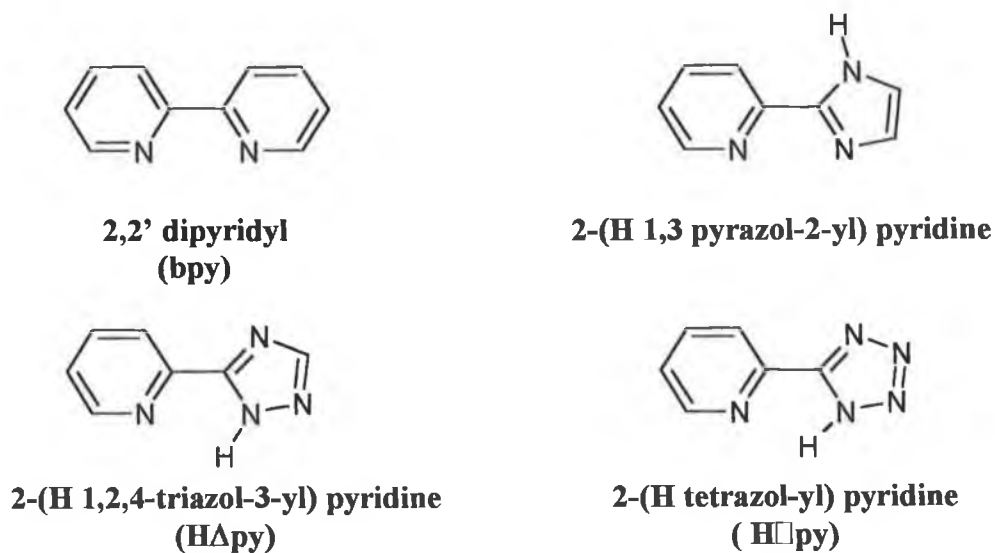


Figure 4.0-1 Ligands cited in text.

Heterocycles with more than one nitrogen atom in six member (diazine, triazine, etc.) or five member (diazoles, triazoles, tetrazoles) rings are also useful as ligands, and have quite different electronic properties to those of pyridine. In addition, they possess multiple coordination sites and are therefore potentially capable of bridging more than one metal centre.

The most well studied chelating heterocyclic ligand is 2,2'-bipyridine (bpy). This ligand was first synthesized over 100 years ago<sup>3</sup>, and has been extensively used in preparative and analytical coordination chemistry because of the stable bidentate complexes it forms with most transition metals<sup>4</sup>. In recent years, many bidentate chelating ligands related to bpy have been synthesized in which one or both of the pyridine rings are replaced with either azines or azoles<sup>5</sup>. These ligands form complexes with properties, which depend markedly on the specific heterocycles incorporated. Thus, by the appropriate choice of ligand, it is possible to tune, in a predictable manner, the ground and the excited state properties of the complex such as in the well studied  $[\text{Ru}(\text{bpy})_3]^{2+}$  complex<sup>6</sup>.

There have been several recent studies of the metal complex of 2-(pyrazol-yl) pyridine with particular emphasis on its ruthenium(II) complexes<sup>7</sup>. Replacement of one of the pyridine rings of bpy by a pyrazole ring, as in figure 1, results in significant changes in the physicochemical properties of the complexes<sup>8</sup>. Similarly, there have been many recent reports of ruthenium (II) and osmium (II) complexes of chelating ligands containing triazole rings., e.g. 2-(H1,2,4-triazol-yl) pyridine (H $\Delta$ p)<sup>9,10</sup>. Again the triazole ring alters the chemical and physical behaviours of the complexes. The presence of the acidic

NH proton allows pH control of the electronic and electrochemical properties of the complexes. Furthermore, the deprotonated triazole ring has more than one nitrogen available for coordination, and such ligands can lead to the formation of coordination isomers.

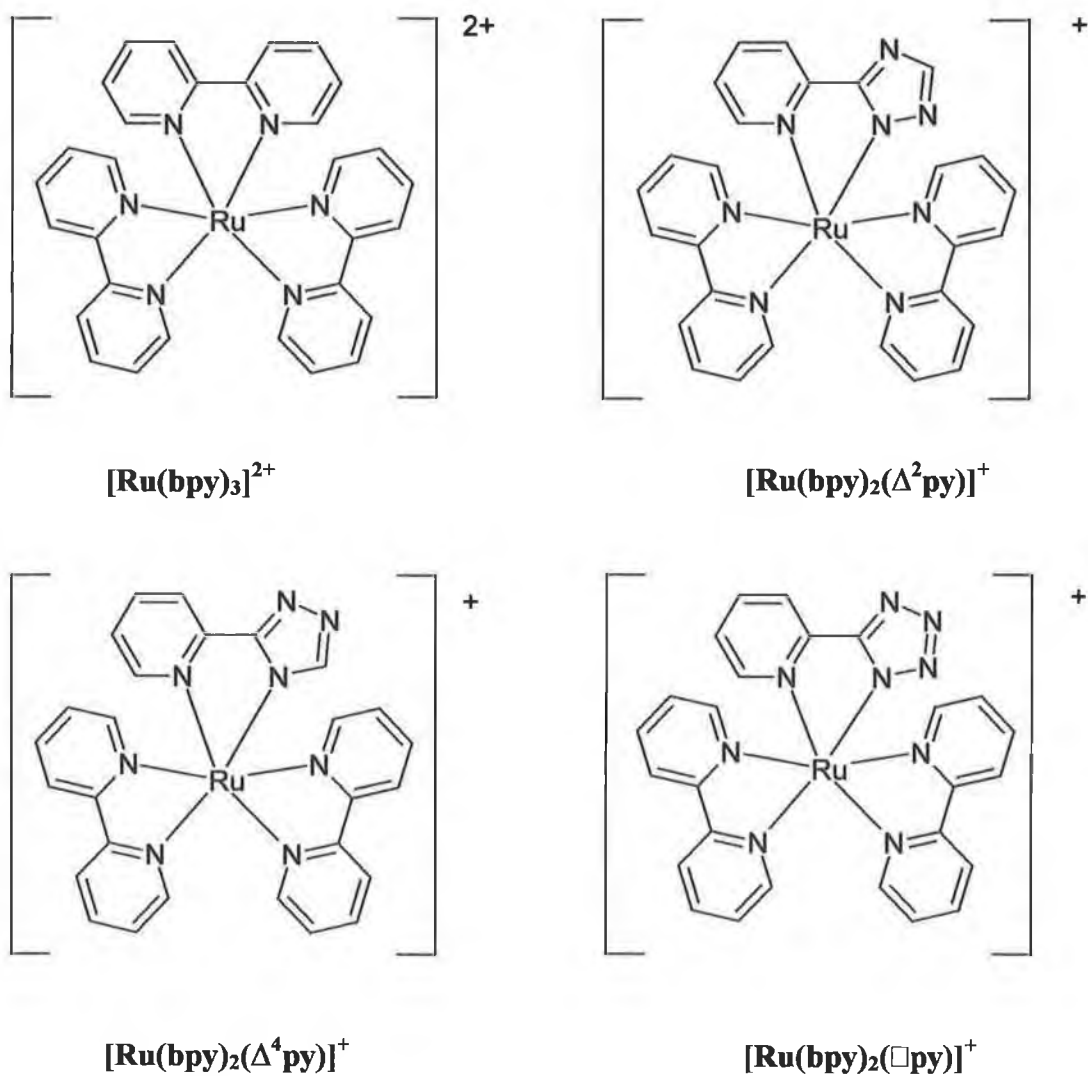


Figure 4.2 Ruthenium Complexes

The present chapter describes the preparation and the photophysical characterisation of complexes of bidentate heterocyclic ligands which incorporate triazolate or tetrazolate rings and their comparison with  $[\text{Ru}(\text{bpy})_3]^{2+}$  complex. The triazole complex was previously studied, but a new set of measurements of their properties was carried out, under the same experimental condition, to facilitate an accurate comparison. This comparison will act as a model for the new terpyridine type complexes discussed in the following chapters.

## 4.2 The Archetype: $[\text{Ru}(\text{bpy})_3]^{2+}$

$[\text{Ru}(\text{bpy})_3]^{2+}$  complex has certainly been one of the molecules most extensively studied during the last 20 years. A unique combination of chemical stability, redox properties and excited state lifetime has attracted the attention of many research workers. The preparation and purification of the complex are facile and fully described in literature<sup>11</sup>.

### 4.2.1 Characterisation and NMR Spectroscopy

By X-ray crystallography the Ru-N bond length was found to be 205.6 pm., somewhat shorter than the 210.4 pm value of the  $[\text{Ru}(\text{NH}_3)_6]^{2+}$  indicating a significant back bonding between Ru(II) and the  $\pi^*$  orbitals of bpy.

A five-line  $^{13}\text{C}$ -NMR spectrum is observed for the solvated species<sup>12</sup> (158, 151, 137, 127 and 124.5 ppm  $\text{C}^5$ ,  $\text{C}^3$ ,  $\text{C}^4$  and  $\text{C}^2$ , respectively) and the  $^1\text{H}$ -NMR spectrum can be interpreted in terms of four coupled spins in each of the six equivalent pyridine rings. The NMR spectra are therefore consistent with retention of  $D_3$  symmetry for the solvated species. The complex structure in its hexafluorophosphate salt is a low spin  $d^6$  system<sup>13</sup> and the bpy ligands are colourless molecules possessing  $\sigma$  donor orbital localized on the nitrogen and  $\pi^*$  acceptor orbital delocalised on the aromatic rings.

Following Orgel's notation<sup>14</sup>, the  $\pi^*$  orbitals may be symmetrical ( $\chi$ ) or antisymmetrical ( $\psi$ ) with respect to the  $C_2$  rotation axis retained by each  $\text{Ru}(\text{bpy})$  unit. A more detailed picture of the highest occupied and lowest empty orbital is shown in fig. 4.3. The highest filled molecular orbitals are

$\pi_{M a_1}(d)$  and  $\pi_{M e}(d)$ , which are predominantly localized on the metal. The lowest unoccupied molecular orbitals (LUMO) are  $\pi_{L a_2}^*(\psi)$  and  $\pi_{L e}^*(\psi)$ , which are localised on the ligands. The ground state of the complex is a singlet, derived from the  $\pi_{M e}(d)^4 \pi_{M a_1}(d)^2$  configuration. The high energy excited states transition metal complexes undergo fast radiationless deactivation. Thus, only the lowest excited state and the upper one, which can be populated on the basis of the Boltzmann equilibrium law, may play a role in the luminescence emission and in bimolecular processes.

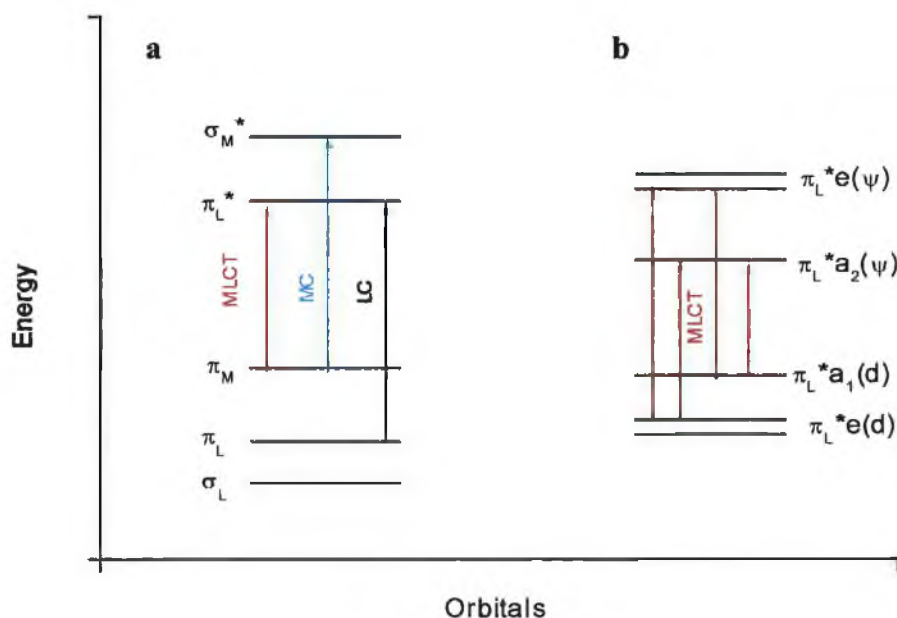


**Figure 4.3 a** Simplified molecular orbital diagram for  $[\text{Ru}(\text{L})_3]^{2+}$  complexes in octahedral symmetry showing the three types of electronic transitions occurring at low energies; **b**, detailed representation of the MLCT transition in  $D_3$  symmetry.

The  $[\text{Ru}(\text{bpy})_3]^{2+}$  cation shows remarkable chemical stability. For example it can be stored in aqueous solution for months and is reported to be unaffected by boiling concentrated HCl or 50% aqueous sodium hydroxide solution<sup>15,16</sup>.

#### 4.2.2 Electrochemistry and Electronic Spectroscopy

The cyclic voltammogram of the complex in acetonitrile presents one oxidation and three reduction processes, all monoelectronic and reversible. The redox potentials are more or less solvent independent.

The absorption spectrum of the compounds is shown in figure 4 with the proposed assignments. The bands at 185 nm (not shown in the picture) and 285 nm have been assigned to LC  $\pi\text{-}\pi^*$  transitions by comparison with the spectrum of protonated dipyridile. The two remaining intense bands at 240 and 450 nm have been assigned to singlet MLCT  $d\text{-}\pi^*$  transitions. In the long wavelength of the absorption spectrum a shoulder is present at about 550 nm ( $\epsilon = 600$ ) when the absorption measurement is made in an ethanol-methanol glass at 77 K. This absorption feature is thought to correspond to the lowest  $^3\text{MLCT}$  excited state.

Because of the presence of the heavy ruthenium atom, it is reasonable to assign the electronic transition of the complex as being to triplet or singlet states, a singlet character slightly less than 10% has been estimated for the lower-lying excited states. The maximum of the  $^1\text{MLCT}$  at 450 nm is slightly solvent sensitive, suggesting the formation of the dipolar excited state  $[(\text{Ru}^{3+})(\text{bpy})_2(\text{bpy}^-)]$ .

Excitation of the complex in any of its absorption bands leads to a luminescence emission, whose intensity, lifetime and energy positions are temperature dependent. Detailed studies on the temperature dependence of the luminescence lifetime and quantum yield in the temperature range 2-70 K has



shown<sup>17,18,19,20,21</sup> that luminescence originates from a set of three closely spaced levels (10 and 61 cm<sup>-1</sup>) in thermal equilibrium. The theoretical description of these levels continues to be a matter of debate. Recent results suggest that the best description is that which assumes a substantial triplet character and a single localized excitation. In rigid alcoholic glass at 77 K the emission lifetime is approximately 5 μsec. and the quantum emission is 0.4.

### 4.2.3 Lifetime Temperature Dependence

With increasing temperature, the emission lifetime and quantum yield decrease. This behaviour can be fitted with the equation 4.1.

$$\frac{1}{\tau} = (k_0^r + k_0^{nr}) + \sum_i A_i e^{-\frac{\Delta E_i}{RT}} \quad (4.1)$$

The values of the various parameters (Table 5) are somewhat dependent on the nature of the solvent. Included in the first term are the radiative  $k_0^r$  and nonradiative  $k_0^{nr}$  rate constants at 84 K.

From the room-temperature luminescence lifetimes and quantum yields, it is possible to obtain the rate constants for the radiative ( $k_r = \Phi/\tau$ ) and non radiative ( $k_{nr} = (1-\Phi)/\tau$ ).

A first Arrhenius term, represented by  $A_1$  and  $\Delta E_1$  in that range of magnitude, is thought to correspond to the thermal equilibration with a level lying slightly higher in energy and having the same electronic nature. The

second Arrhenius term is thought to correspond to a thermally activated surface crossing to an upper-lying  $^3\text{MC}$  level which undergoes fast deactivation. Identification of this higher level as a  $^3\text{MC}$  state is based upon the observed photosubstitution behaviour at elevated temperatures, consistent with its established photoreactivity.

### 4.3 The Triazolate Model: $[\text{Ru}(\text{bpy})_2(\Delta\text{py})]^+$

The ligand 2-(pyridin-2-yl)-1,2,4-triazole, ( $\Delta\text{py}$ ), and its protonated form ( $\text{H}\Delta\text{py}$ ) were chosen for their  $\sigma$ -donor and  $\pi$ -acceptor properties and of interest is how these different properties affect the excited states of the complex.

The synthesis of the ( $\text{H}\Delta\text{py}$ ) has been previously reported by Hage et al.<sup>22,23,24</sup>, which illustrated that the complex resulting from the coordination of this ligand, not only formed coordination isomers but also formed a very pH sensitive complex. Indeed an UV spectrum analysis of the complex, prior to the addition of acid or base, shows the presence of two species, one protonated and the other deprotonated. Also when obtaining a  $^1\text{H}$ -NMR of the complex the solution has to be pH controlled in order to obtain a clear spectrum.

Initially the complex obtained was analysed on an analytical HPLC system, see figure 4.9 which shows the chromatograms of the two isomers after separation on the alumina column. The chromatogram portrays the two coordination isomers at their different retention times but with similar UV spectra from the photodiode array detector. The isomer separation is due to their different acid-base properties, as shown previously. The separation was

successfully achieved on neutral alumina columns using 100 % acetonitrile to isolate the first and 100 % methanol to isolate the second fraction. In the elucidation of the structures of ruthenium polypyridyl complexes  $^1\text{H-NMR}^{25,26,27,28}$  has proven to be a very powerful technique $^{29,30,31,32,33}$ .

	$\text{H}^3$ /ppm (CIS Value)	$\text{H}^4$ /ppm	$\text{H}^5$ /ppm	$\text{H}^6$ /ppm	$\text{H}^5'$ /ppm
bpy	8.48	7.93	7.42	8.67	
$\text{H}\Delta\text{py}$	8.09	7.98	7.51	8.70	8.27
$\text{H}\square\text{py}$	8.31	8.05	7.06	8.79	
$[\text{Ru}(\text{bpy})_3]^{2+}$	8.33	7.83	7.10	7.60	
$[\text{Ru}(\text{bpy})_2(\Delta^2\text{py})]^+$	8.32 (0.23)	7.99 (-0.4)	7.34 (-0.17)	7.57 (-1.13)	8.11 (-0.16)
$[\text{Ru}(\text{bpy})_2(\Delta^4\text{py})]^+$	8.08 (-0.01)	7.84 (-0.14)	7.11 (-0.40)	7.49 (-1.21)	7.90 (-0.37)
$\text{Ru}(\text{bpy})_2(\text{H}\Delta^2\text{py})^{2+}$	8.23	8.00	7.26	7.70	8.65
$\text{Ru}(\text{bpy})_2(\text{H}\Delta^4\text{py})^{2+}$	8.05	7.90	7.16	7.62	8.38
$\text{Ru}(\text{bpy})_2(\square\text{py})^+$	8.53 (0.007)	8.023 (-0.06)	7.44 (-0.3)	7.95 (-1.17)	

**Table 4.1**  $^1\text{H-NMR}$  spectroscopic data for  $\text{d}^3$ -acetonitrile solutions of Ruthenium complexes, values in parenthesis represent change in shift of complex compared to free ligand (CIS)

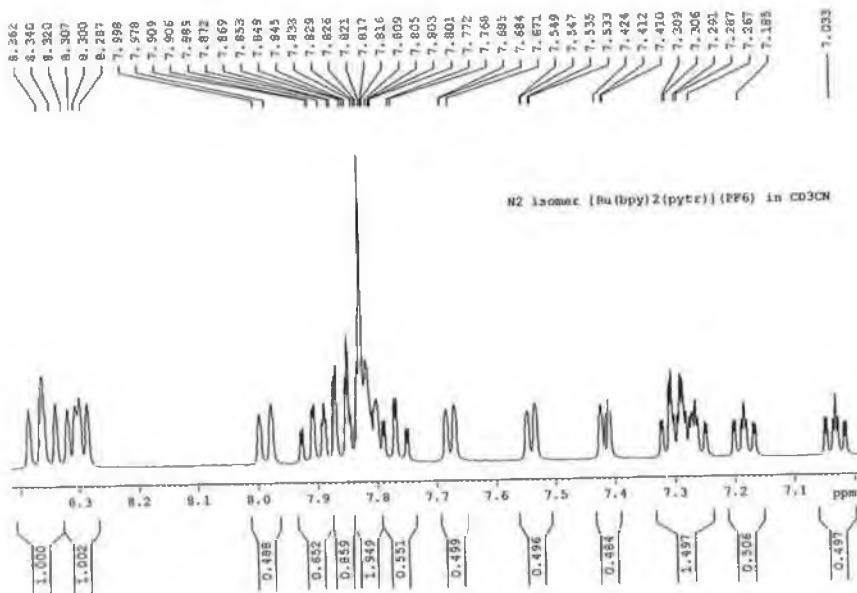


Figure 4.4  $^1\text{H-NMR}$  spectrum of the complex  $[\text{Ru}(\text{bpy})_2(\Delta^2\text{py})]^+$  in  $d^3$ -acetonitrile

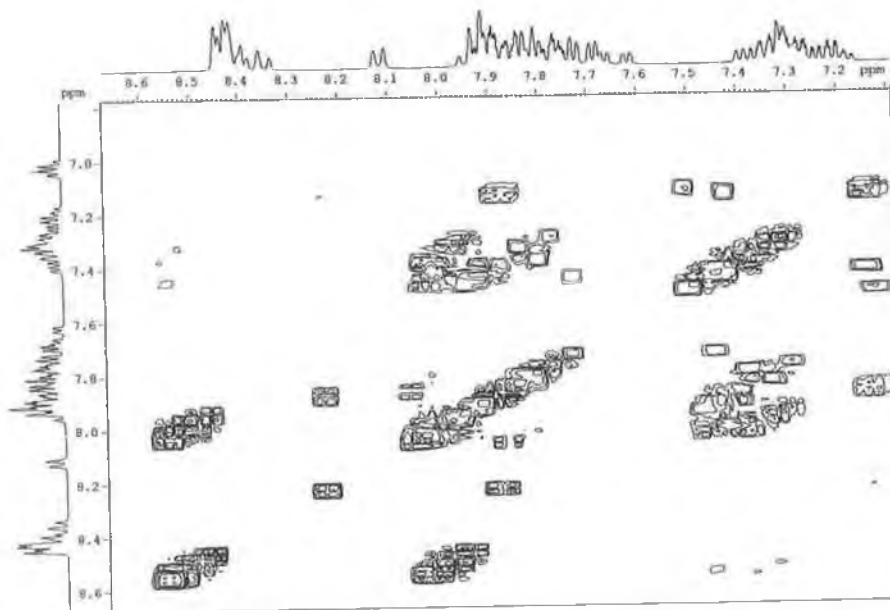


Figure 4.5  $^1\text{H COSY-NMR}$  spectrum of the complex  $[\text{Ru}(\text{bpy})_2(\Delta^4\text{py})]^+$  in  $d^3$ -acetonitrile

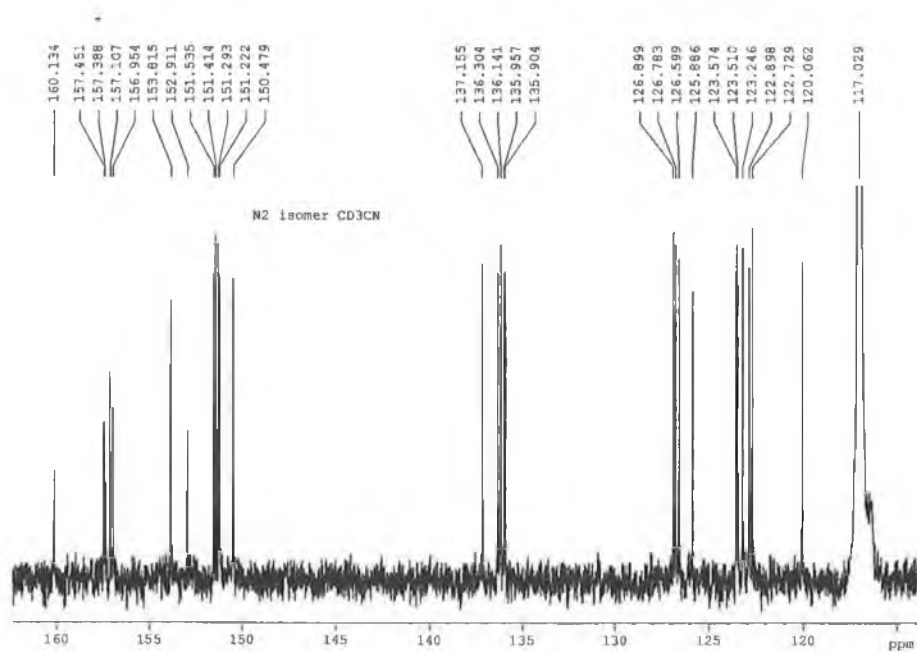


Figure 4.6  $^{13}\text{C}$ -NMR spectrum of the complex  $[\text{Ru}(\text{bpy})_2(\Delta^2\text{py})]^+$  in  $d^3$ -acetonitrile

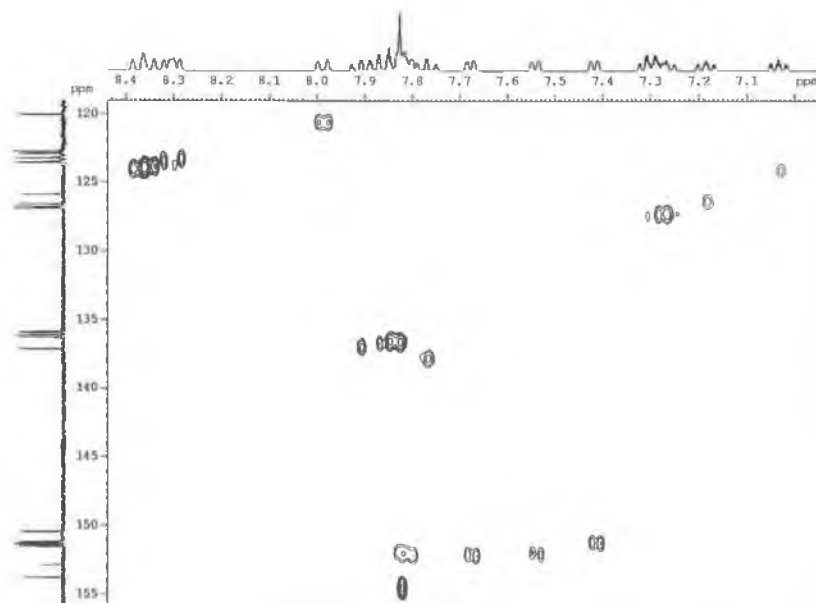


Figure 4.7 C-H correlation -NMR Spectrum of the complex  $[\text{Ru}(\text{bpy})_2(\Delta^2\text{py})]^+$  in  $d^3$ -acetonitrile

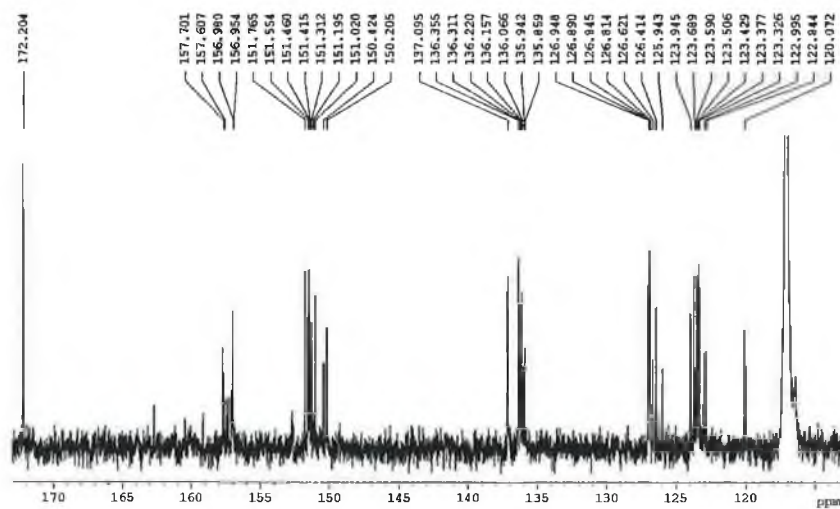


Figure 4.8 C-NMR Spectrum of the complex  $[\text{Ru}(\text{bpy})_2(\Delta^4\text{py})]^+$  in  $\text{d}^3$ -acetonitrile

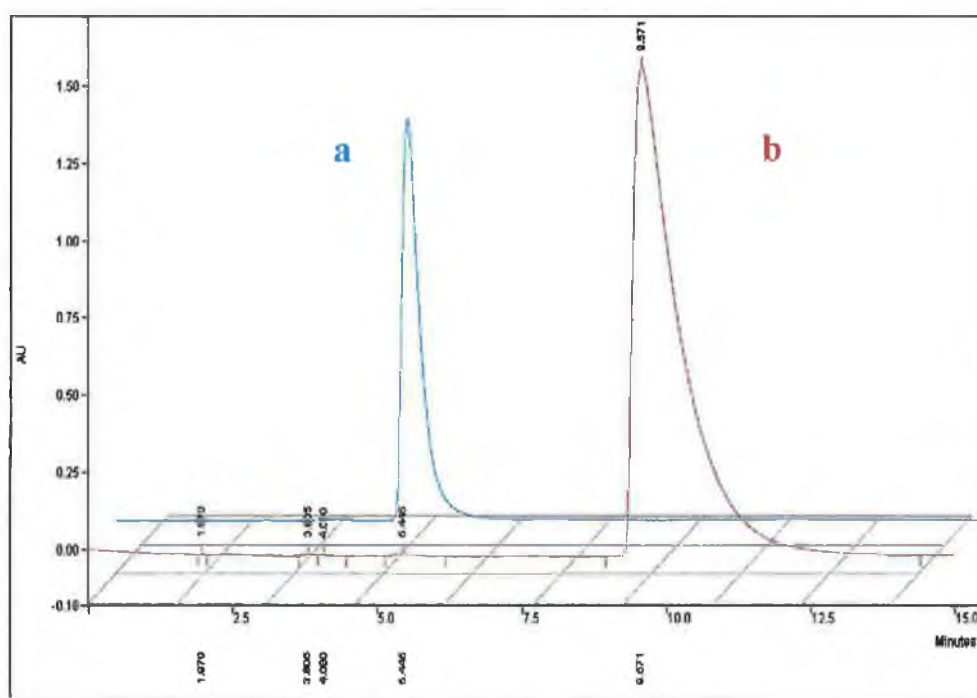


Figure 4.9 HPLC chromatograms of  $[\text{Ru}(\text{bpy})_2(\Delta^2\text{py})]^+$  (a) and  $[\text{Ru}(\text{bpy})_2(\Delta^4\text{py})]^+$  (b) in phase a solution of  $\text{LiClO}_4$  (0.08 M) in acetonitrile/water (80/20)

### 4.3.1 NMR Spectroscopy

Table 4.1 summarises the NMR data for  $H\Delta py$  and its complexes (Fig 4.5 and 4.6) in acetonitrile and includes the coordination induced shift values ( $CIS = \delta_{\text{complex}} - \delta_{\text{ligand}}$ ). Some dramatic upfield shifts are observed for the  $\Delta py$  pyridine proton signal on coordination to ruthenium. Previously, a number of factors have been identified that contribute to the sign and magnitude of the CIS values in such ruthenium complexes. Ligand to metal  $\sigma$ -donation, metal to ligand  $\pi$ -back donation, chelation imposed conformational changes, coordinative disruption of inter ring conjugation and interligand through space ring current anisotropy effects have all been invoked to explain CIS values of tris (biheteroaromatic) ruthenium(II). By far the largest upfield CIS is experienced by  $H^6$ . This is undoubtedly due to through-space ring-current anisotropy effect since the proton lies directly over the shielding plane of one of the bpy pyridine rings. When comparing the protons of the isomers the  $H^5$  signal has the most indicative shift. For  $N^4$  isomer (-0.37), which is double of that  $N^2$  isomer (-0.16). The signal of the  $H^{5'}$  proton of the triazole ring undergoes a large shift up field when a  $Ru(bpy)_2$  moiety is coordinated to the  $N^4$  coordination site. The ring current effect of the adjacent bpy is experienced by  $H^{5'}$  when it is in such close vicinity.

The  $^{13}C$ -NMR of the complex shows that the presence of the asymmetric  $\Delta py$  ligand splits the carbons in 25 non equivalent signals: at around 124 ppm the five signals of the carbons in 5 position ( $C^5$ ) are visible, around 127 the five of  $C^3$ ,  $C^4$  are situated at 136 ppm and  $C^6$  about 153. The

four quaternary carbons on the bpy ligands appear around 157, instead the singlet of the quaternary carbon on the pyridine ring of the  $\Delta$ py ligand is upfielded to 150 and the one on the triazole is situated at a lower field of 162. The ternary carbon on the triazolate ring is situated at 154 ppm for the  $N^2$  isomer and 152 for the  $N^4$ . (Fig 4.6, 7, 8)

### 4.3.2 Redox Properties

The oxidation and reduction potentials are given in Table 2. All values have been corrected using the redox potential of ferrocene under the same experimental conditions as a secondary reference. Its potential is taken to be 0.38 V vs SCE.

The anodic region of the cyclic voltammogram features reversible metal centred oxidation, while the cathodic region has poorly defined waves resulting from the reduction of the coordinated polypyridyl ligands. The oxidation potentials are significantly lower than that of  $Ru(bpy)_3^{2+}$ , lower oxidation potentials indicating that the metal ion has more electron density, which could be caused by strong  $\sigma$  donating and  $\pi$  accepting ligands. When the triazole ligand is deprotonated ( $\Delta$ py<sup>-</sup>) the oxidation potentials are further lowered, which is induced by the strong  $\sigma$  donor capabilities of the triazolate ligand. On protonation of the complex it shows an anodic shift of between 200 and 300 mV compared to the deprotonated species, since in its protonated form the  $\Delta$ py is a better  $\pi$  acceptor and a weaker  $\sigma$  donor. This results in a



decrease in electron density at the metal centre, which then becomes more difficult to oxidise.

Comparing the oxidation potentials of the two pyrid-yl-triazole isomers shows that N<sup>2</sup> bound isomer, [Ru(bpy)<sub>2</sub>(HΔ<sup>2</sup>py)]<sup>2+</sup>, is oxidised more easily than the N<sup>4</sup> bound isomer, [Ru(bpy)<sub>2</sub>(HΔ<sup>4</sup>py)]<sup>2+</sup>. The same observation has been made for the analogous deprotonated species. This suggests that HΔpy is a better σ donor when the binding nitrogen to the Ru(bpy)<sub>2</sub> moiety is in the 4-position with respect to that of the 2-position. It should be noted that well defined reduction waves for the acidified species were not obtained, the problem is that even though the protonated species are formed by adding a 0.1 M HClO<sub>4</sub>/acetonitrile solution, they can readily be deprotonated when scanning to a negative potential.

The first two reductions of the isomers are very similar to those observed for [Ru(bpy)<sub>3</sub>]<sup>2+</sup>, which suggests bpy based reductions, the third being at a much more negative potential that will agree with the observation that (HΔpy) is a stronger σ donor but also a weaker π acceptor than the bpy moiety.

### 4.3.3 Electronic Spectroscopy

The absorption, emission and luminescent lifetime (room temperature) properties of the Ru(II) pyridine triazole complex are listed in Table 4.3. The electronic absorption spectra (Fig. 4.10, 11) of the Ru(II) complex is dominated in the visible region by  $d\pi-\pi^*$  metal to ligand charge transfer (MLCT) transitions (bpy based), which are typical of Ru(II) polypyridine complexes and in the UV region (280-310nm.) by intense  $\pi-\pi^*$  associated with the bipyridyl ligand blue shifted with respect to the  $[\text{Ru}(\text{bpy})_3]^{2+}$  as a result of strong  $\sigma$ -donation of the negatively charged triazole moiety. When the complex is protonated the coordination ligand becomes a weaker  $\sigma$ -donor and a stronger  $\pi$ -acceptor. As a consequence, the metal  $d\pi(t_{2g})$  orbitals are stabilised and the ground state-MLCT energy gap is increased, resulting in the observed blue shift in the emission and absorption spectra. As for the deprotonated species, the emission and absorption maxima occur at lower energy. This is because the metal  $t_{2g}$  orbitals are stabilised, decreasing the energy gap between the ground state and the MLCT.

The emission maxima (Fig 4.12, 13) for the complexes is in the region of 660 nm at room temperature. An important question is if the emitting state is localised on the bipyridyl ligands or located on the pyridyl moiety of the pyridyl triazole ligand. As discussed in the literature for other systems a relation is often present between the electrochemical potentials and the absorption and emission maxima. In a MLCT absorption process, one electron

is removed from the filled metal orbital ( $d\pi$ ) to an empty orbital of the ligand ( $\pi^*$ ).

Oxidation is also removal of one electron from the d orbitals and in the case of reduction one electron is transferred to the LUMO (bpy based) of the complex. A similar explanation is also valid for the MLCT emission process. By determining the nature of LUMO with electrochemical measurements it is possible to determine the nature of the emitting state. By comparison of the value in table 2, it is possible to assign the first two reduction potentials for the mixed ligand complex as bpy based. The  $\pi^*$ -levels of the bpy ligands are much lower than those of the pyridyl triazole.

	$E_{\text{ox}}^0$ (Volt)	$E_{\text{red}}^0$ (Volt)	$E_{\text{red}}^0$ (Volt)	$E_{\text{red}}^0$ (Volt)
$[\text{Ru}(\text{bpy})_3]^{2+}$	1.27	-1.31	-1.50	
$[\text{Ru}(\text{bpy})_2(\Delta^2\text{py})]^+$	0.83	-1.47	-1.72	
$[\text{Ru}(\text{bpy})_2(\Delta^4\text{py})]^+$	0.90	-1.44	-1.51	
$[\text{Ru}(\text{bpy})_2(\text{H}\Delta^2\text{py})]^{2+}$	1.14	(-1.49)	(-1.73)	(-2.25)
$[\text{Ru}(\text{bpy})_2(\text{H}\Delta^4\text{py})]^{2+}$	1.20	(-1.47)	(-1.72)	
$[\text{Ru}(\text{bpy})_2(\square\text{py})]^+$	1.02	-1.50	-1.72	(2.52)
$[\text{Ru}(\text{bpy})_2(\text{H}\square\text{py})]^{2+}$	1.12	(-1.50)		

**Table 4.2 Cyclic voltammetry data for the Ruthenium complexes (acetonitrile solution,  $[\text{nBu}_4\text{N}][\text{PF}_6]$  supporting electrolyte,  $\text{Fc}/\text{Fc}^+$  reference). All redox potentials are accurate to  $\pm 10$  mV. Redox potentials in brackets are for quasi-reversible processes.**

	Absorption		Emission				
	$\lambda$ (nm)	$\epsilon$ ( $M^{-1} \times cm^{-1}$ )	$\lambda_{(298\text{ K})}$ (nm)	$\phi$	$\tau_{(298\text{ K})}$ (nsec)	$\lambda_{(80\text{ K})}$ (nm)	$\tau_{(80\text{ K})}$ (nsec)
$[Ru(bpy)_3]^{2+}$	451	14600	608	$6.2 \times 10^{-2}$	946	582	6.2
$[Ru(bpy)_2(\Delta^2py)]^+$	465	10700	650	$3 \times 10^{-3}$	142	607	4.2
$[Ru(bpy)_2(\Delta^4py)]^+$	470	9000	660	$6.3 \times 10^{-3}$	146	607	4
$[Ru(bpy)_2(H\Delta^2py)]^{2+}$	437	8900	610	$4.3 \times 10^{-4}$	2	577	6.5
$[Ru(bpy)_2(H\Delta^4py)]^{2+}$	450	7700	615	$7.3 \times 10^{-4}$	5	580	6.0
$[Ru(bpy)_2(\square py)]^+$	466	10920	630	$6.3 \times 10^{-3}$	100	610	3.8
$[Ru(bpy)_2(H\square py)]^{2+}$	436	11600	610		-	577	7

**Table 4.3 Spectroscopic and photophysical data in de-gassed methanol.**

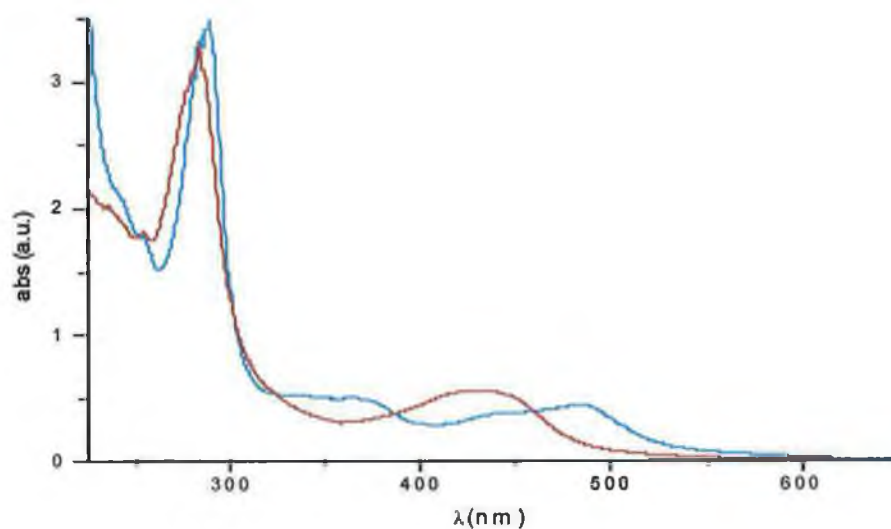


**Figure 4.10** Absorption spectra of  $[\text{Ru}(\text{bpy})_2(\text{H}\Delta^2\text{py})]^{2+}$  (red line) and  $[\text{Ru}(\text{bpy})_2(\Delta^2\text{py})]^+$  (blue line) in acetonitrile solution at room temperature.

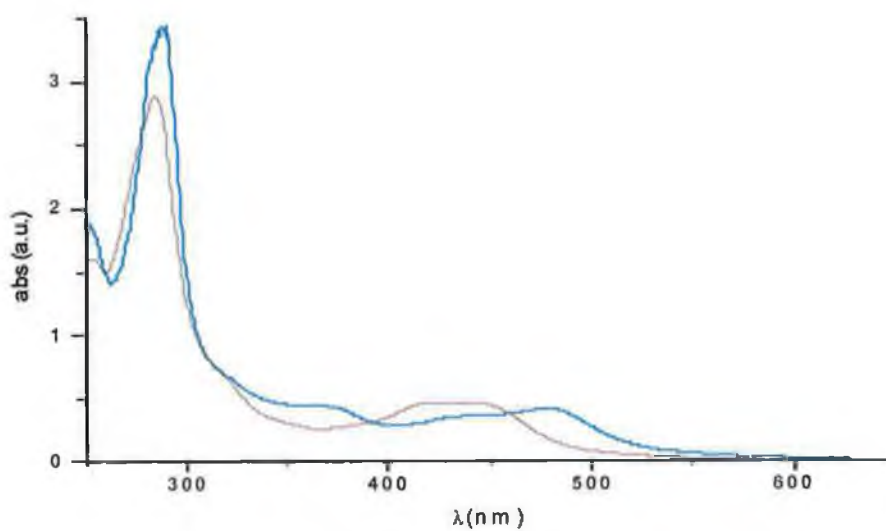


**Figure 4.11** Absorption spectra of  $[\text{Ru}(\text{bpy})_2(\text{H}\Delta^4\text{py})]^{2+}$  (red line) and  $[\text{Ru}(\text{bpy})_2(\Delta^4\text{py})]^+$  (blue line) in acetonitrile solution at room temperature.

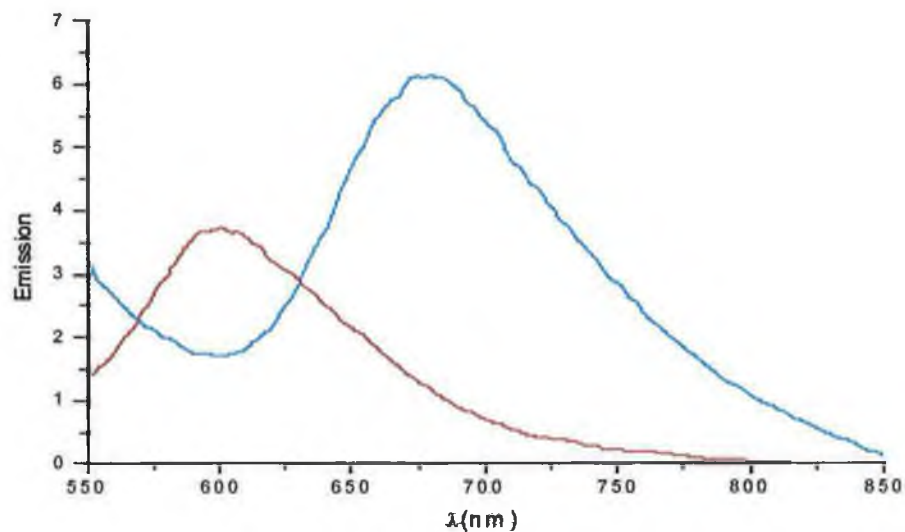


**Figure 4.12** Emission spectra of  $[\text{Ru}(\text{bpy})_2(\text{H}\Delta^2\text{py})]^{2+}$  and  $[\text{Ru}(\text{bpy})_2(\Delta^2\text{py})]^+$  in acetonitrile solution at room temperature.

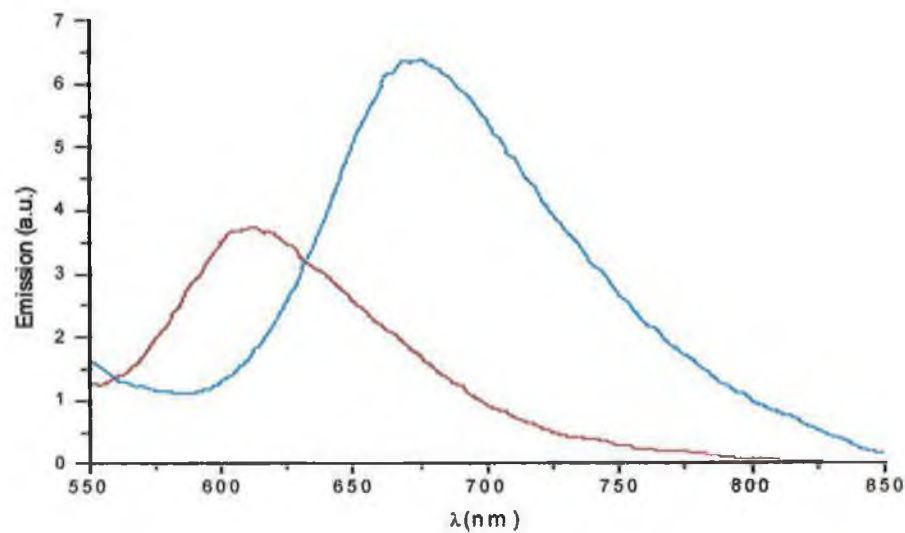


**Figure 4.13** Emission spectra of  $[\text{Ru}(\text{bpy})_2(\text{H}\Delta^4\text{py})]^{2+}$  and  $[\text{Ru}(\text{bpy})_2(\Delta^4\text{py})]^+$  in acetonitrile solution at room temperature.

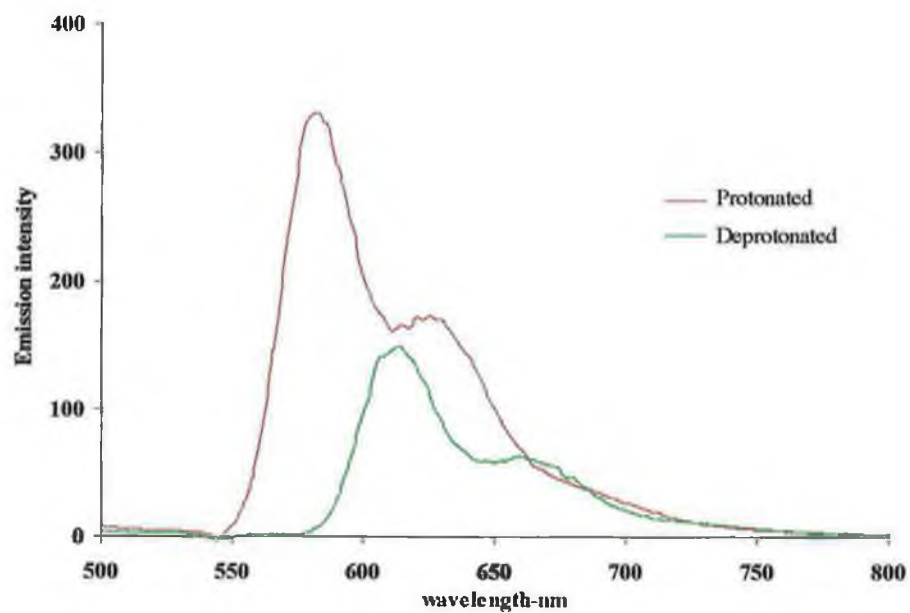


Figure 4.14 Emission spectra of  $[\text{Ru}(\text{bpy})_2(\text{H}\Delta^4\text{py})]^{2+}$  and  $[\text{Ru}(\text{bpy})_2(\Delta^4\text{py})]^+$  in ethanol-methanol (4:1) solution at 77 K

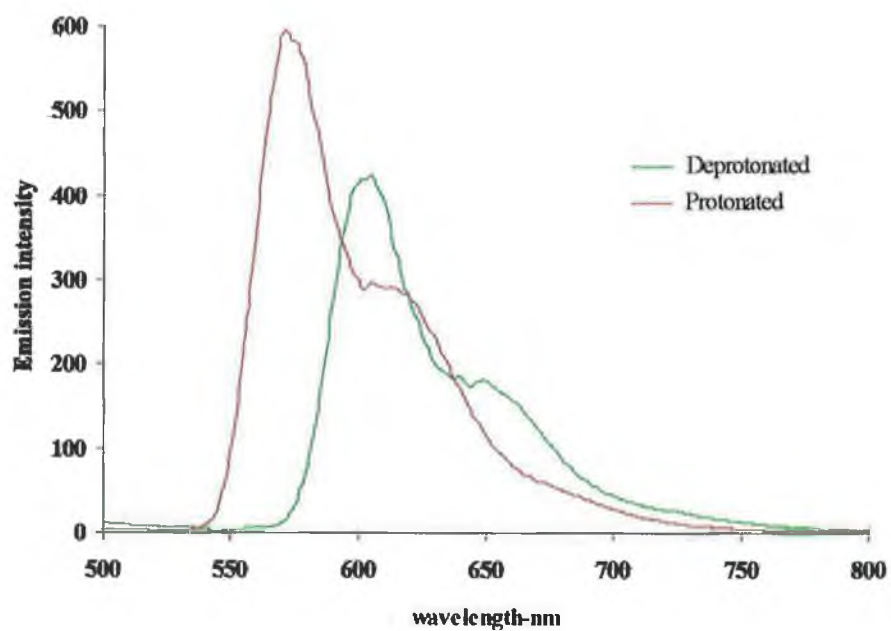


Figure 4.15 Emission spectra of  $[\text{Ru}(\text{bpy})_2(\text{H}\Delta^2\text{py})]^{2+}$  and  $[\text{Ru}(\text{bpy})_2(\Delta^2\text{py})]^+$  in ethanol-methanol (4:1) solution at 77 K.

At 77K the complex exhibit a strong emission with vibrational structure. This vibrational structure is due to relaxation via bipyridil based vibrations which is common in ruthenium polypyridyl complexes<sup>34</sup>. On cooling to 77K a blue shift is observed in the emission maxima for both : protonated and deprotonated species. This is associated with a phenomenon defined “rigidchromism” by Wrighton and co-workers<sup>35</sup>, who were the first to report on it. In the alcoholic glass formed at 77 K, the solvent dipoles are immobile on the time scale of the excited state and consequently they can not respond to the change in electronic configuration between the ground and excited state. The result is an increase in the emission energy, which is confirmed in a blue shift in the emission spectra. Another observation at low temperature is the increase in emission intensity and a longer lifetime of the excited state of the complex.

This is attributed to two factors:

- First factor, being solvent dependent, at low temperature, the complex and its environment are rigid, making it less susceptible to vibronic coupling to low frequency, high amplitude Ru-N vibrations, which contribute to radiationless decay,  $k_{nr}$ . Solvent interactions, which may contribute to  $k_{nr}$  are also considerably reduced in the frozen matrix, as too is quenching of the excited state by the presence of oxygen, since diffusion of oxygen is restricted.
- Second factor, it is related to the  $^3MLCT$ - $^3MC$  energy gap. Since this transition is thermally activated at 77K there will be



insufficient thermal energy to populate the  $^3MC$ , and as a consequence, the intensity of the emission increases.

#### 4.3.4 Acid-base Properties

The protonation and the deprotonation of the pyridine triazole ligand alter its  $\sigma$  donor and  $\pi$  acceptor properties. The emission properties of the complex are listed in table 4.3.

The acidity of the excited state has been investigated by a study of the pH dependence of the emitting properties of the compounds. The emission titrations were carried out by excitation into the appropriate isobestic point. By investigating the acid-base behaviour of this type of ruthenium compound important information about its electronic state properties can be obtained. The ground state behaviour tends to be a measure of the amount of electron donation from the ligand to the metal, while the excited state measurements can give information about the nature of the emitting state. Upon coordination to ruthenium, the acidity of the triazole proton in the ground state increases considerably, which is generally explained by  $\sigma$  donation from the ligand to the metal centre.

In Ru-polypyridyl complexes the nature of the Ru-N bond is mainly  $\sigma$  but it is also stabilised by backbonding between the  $t_{2g}$  and  $\pi^*$  orbitals of the metal and ligand respectively<sup>36,37,38</sup>. By manipulation of the acid-base properties of the pyridyltriazole unit in the complexes, the ground state pKa can yield information on the extent of backbonding from the metal and the  $\sigma$ -donor and  $\pi$ -acceptor properties of the ligand. Determination of the excited

state  $pK_a^*$  gives important information regarding the properties of the ligand and the nature of the emitting state. For these reasons the acid-base behaviour of the complexes is presented in this section. In most ruthenium complexes the  $pK_a$  value of the ligand decreases on coordination, which can be explained by strong  $\sigma$ -donation effects from the ligand to the metal centre. Less electron density is present on the triazole ring after coordination resulting in the increased acidity of the ligand. Figures 4.16 and 4.17 are typical examples of the acid-base chemistry of the ruthenium (II) complexes containing the  $\Delta py$  ligand. In the UV absorption spectra clean and clear isobestic points are observed in the bpy complexes at 460, 390 and 345 nm indicating that there are no intermediates formed in the pH range examined. All the spectroscopic changes of the complexes are reversible in the pH range 1-9. The absorption titrations are performed by adjusting the pH of a  $5 \times 10^{-5}$  M solution of the complex in Britton Robinson buffer. By monitoring the spectral changes, at a wavelength where there is considerable change as a function of pH, a graphical analysis was carried out by plotting percentage change in absorbance against pH. The  $pK_a$  was determined from the point of inflection of the curve. The  $pK_a$  obtained represents the  $pK_a$  of the triazole ring. In all titrations there is a blue shift of the MLCT band as the pH is lowered due to the stabilisation of the  $t_{2g}$  orbitals and the resultant increase in the  ${}^3MLCT-t_{2g}$  energy gap.

The excited state  $pK_a$  values ( $pK_{ae}$ ) can be evaluated in two different ways. The first method is one of the first and most important contributions to the excited state acid-base equilibria by Förster<sup>39</sup>. This thermodynamical treatment was based on the changes following protonation/deprotonation in the

excited state of an organic species and it leads to the Förster cycle equation (4.2). Using this equation the excited state  $pK_a^*$  of a species can be calculated from its ground state properties.

$$pK_a^* = pK_a + (0.625/T)(\nu_{B^-} - \nu_{HB}) \quad (4.2)$$

where  $\nu_{B^-}$  and  $\nu_{HB}$  are the  $E_{0-0}$  values (in  $\text{cm}^{-1}$ ) of the deprotonated and protonated complexes respectively. These values are taken from the  $\lambda_{\text{max}}$  of the emission spectra at 77 K as they are the most accurate means of obtaining an estimate for the energy difference involved in the 0-0 transition. An important point to remember in the use of the Forster equation (4.2) as a method for determining the  $pK_a^*$  is that small errors in the assessment of  $E_{0-0}$  for  $\nu_{B^-}$  and  $\nu_{HB}$  produce considerable errors in  $pK_a^*$ <sup>40</sup>.

The second method employed for the determination of  $pK_a^*$  is based on a kinetic model devised by Ireland and Wyatt<sup>39</sup> where the  $pK_a^*$  may be measured from the emission lifetimes of the protonated ( $\tau_{HB}$ ) and deprotonated ( $\tau_{B^-}$ ) complexes and the point of inflection of the emission titration curve,  $pH_i$ . The point of inflection of the luminescence intensity against pH titration curve is  $pH_i$ . Equation 4.3 describes the model.

$$pK_a^* = pH_i + \log(\tau_{HB} / \tau_{B^-}) \quad (4.3)$$

Although this method would be the preferred choice for the evaluation of  $pK_a^*$  it was not used due to the fact that it relies heavily on the establishment of the

value via  $pH_i$  and lifetimes. Thus the Forster cycle equation (4.2) was used for the evaluation of the  $pK_{ae}$  values shown in table 4.2. The trend for our  $pK_{ae}$  values is that they are more acidic than the ground-state  $pK_a$  values. These results suggest that as expected the excited state is not based on the triazole ligand which can then be referred to as the spectator ligand. These conclusions are in line with previous work on ruthenium(II) complexes of pyridyltriazole complexes.

	$pK_{ag}$	$pK_{ae}$	$pH_i$
$[Ru(bpy)_2(\Delta^2py)]^+$	4.07	2.2	2.8
$[Ru(bpy)_2(\Delta^4py)]^+$	5.7	4.2	5.1

**Table 4.4** Ground and excited state  $pK$  values of  $Ru(bpy)_2(\Delta^2py)^+$  and  $Ru(bpy)_2(\Delta^4py)^+$ ,  $pH_i$  is the inflection point of emission intensity titration,  $pK_{ae}$  is calculated using equation (4.3)

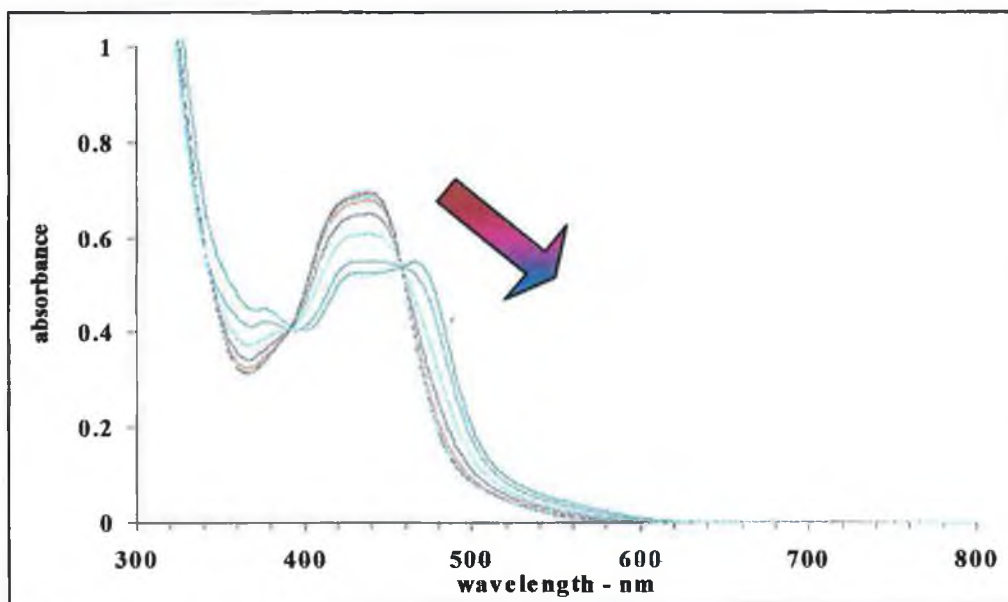


Figure 4.16 pH dependence of the absorption spectra of  $[\text{Ru}(\text{bpy})_2(\text{HA}^4\text{py})]^+$  ( $5 \times 10^{-5} \text{ M}$ ) in an aqueous Britton-Robinson buffer at pH 1.2, 1.6, 2.1, 2.5, 3.0, 3.5, 4, 4.5, 5.5 and 6.5

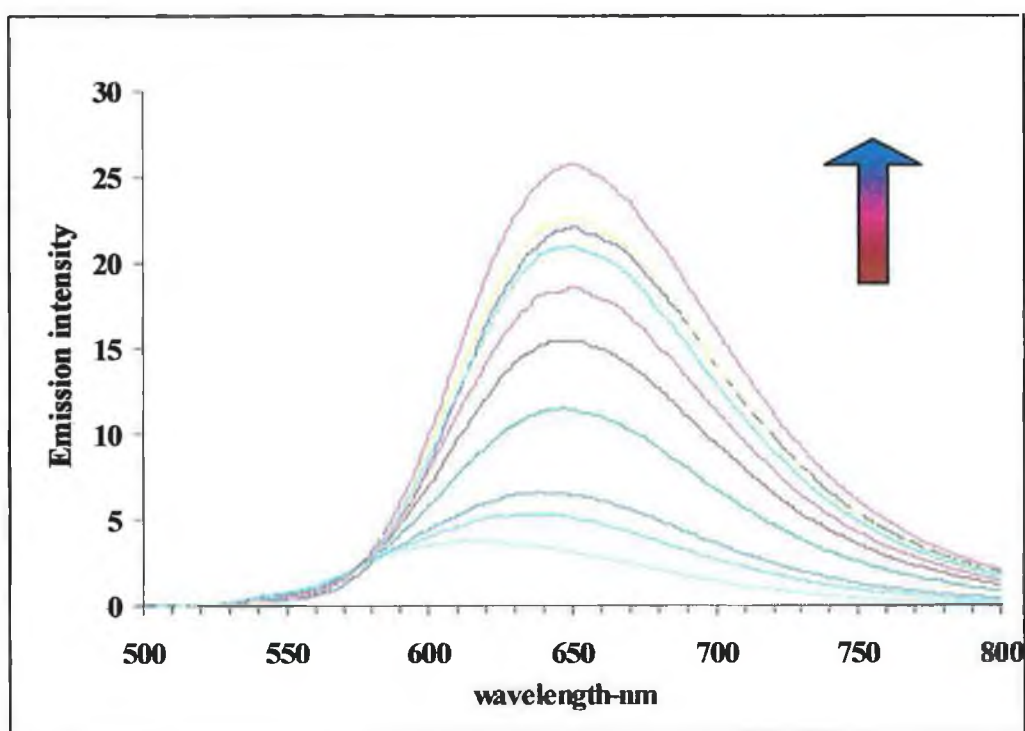


Figure 4.17 pH dependence of the emission spectra of  $[\text{Ru}(\text{bpy})_2(\text{HA}^4\text{py})]^+$  ( $5 \times 10^{-5} \text{ M}$ ) in an aqueous Britton-Robinson buffer at pH 1.2, 1.6, 2.1, 2.5, 3.0, 3.5, 4, 4.5, 5.5 and 6.5.

### 4.3.5 Lifetime temperature Dependence

The  $^3\text{MC}$ -state energies cannot be determined directly, but the gap between  $^3\text{MLCT}$  and  $^3\text{MC}$  states can be proximated from activation parameters obtained from temperature-dependent luminescence lifetimes, table 6. The activation parameters obtained for equation 4.1 for the  $^3\text{MLCT}$  emission of complexes usually fall into one of two categories:

- small activation energies, less than  $800\text{ cm}^{-1}$ , and low A factors, less than  $10^9\text{ sec}^{-1}$
- large activation energies, more than  $2000\text{ cm}^{-1}$ , and large A factors, more than  $10^{11}\text{ sec}^{-1}$

Complexes, for which both activation barrier and prefactor are small, are usually unreactive to photosubstitution since these values suggest that population of  $^3\text{MC}$  state does not occur<sup>41</sup>. Low prefactor also suggests that the process involves population of a state weakly coupled to the  $^3\text{MLCT}$ . On the basis of these observations and molecular calculation, Kober and Meyer have postulated that this activated process corresponds to population of a  $^3\text{MLCT}$  state

Another interesting effect noticed on the  $\Delta\text{py}$  complex was a small solvatochromic effect in the emission and absorption spectra, Table 4.4, which is due to the interaction between the external nitrogens and the solvent (table 4) and is stronger than that observed for  $[\text{Ru}(\text{bpy})_3]^{2+}$ .

	$[\text{Ru}(\text{bpy})_3]^{2+}$		$[\text{Ru}(\text{bpy})_2(\Delta^2\text{py})]^+$		$[\text{Ru}(\text{bpy})_2(\Delta^4\text{py})]^+$		$[\text{Ru}(\text{bpy})_2(\square\text{py})]^+$	
	Abs	Emi.	Abs	Emi.	Abs	Emi.	Abs	Emi.
	(kk)	(kk)	(kk)	(kk)	(kk)	(kk)	(kk)	(kk)
H <sub>2</sub> O	22.22	15.97	21.36	15.19	21.10	15.22	22.07	16.07
Methanol	22.22	15.95	21.36	15.15	21.03	15.17	22.01	16.05
Ethanol	22.22	19.94	21.27	14.88	20.90	14.92	21.95	16.02
CH <sub>2</sub> Cl <sub>2</sub>	22.17	15.91	20.90	14.70	20.56	14.75	21.60	15.95
DMSO	22.12	15.90	20.48	14.68	20.48	14.70	21.52	15.90
DMF	22.12	15.87	20.48	14.64	20.47	14.70	21.54	15.94
CH <sub>3</sub> CN	22.09	16.13	20.47	14.64	20.24	14.64	21.45	15.87
(CH <sub>3</sub> ) <sub>2</sub> CO	22.9	16.50	20.23	14.45	20.23	14.64	21.09	15.43

**Table 4.5 Spectroscopic, photophysical properties of the complexes in different solvents**

	$k^0$	$k_1$	$\Delta E_1$	$k_2$	$\Delta E_2$
$[\text{Ru}(\text{bpy})_3]^{2+}$	$5.2 \cdot 10^5$	$4.6 \cdot 10^5$	84	$2.6 \cdot 10^{14}$	3140
$[\text{Ru}(\text{bpy})_2(\Delta^2\text{py})]^+$	$1.7 \cdot 10^6$	$9.2 \cdot 10^7$	500	—	—
$[\text{Ru}(\text{bpy})_2(\Delta^4\text{py})]^+$	$1.6 \cdot 10^6$	$4.7 \cdot 10^7$	600	—	—
$[\text{Ru}(\text{bpy})_2(\square\text{py})]^+$	$3.7 \cdot 10^5$	$2.6 \cdot 10^7$	450	$1 \cdot 10^{11}$	2700

**Table 4.6 Activation parameters from temperature dependent luminescence lifetimes, in ethanol-methanol (4:1) solution.**

#### 4.4 The Tetrazolate Model: $[\text{Ru}(\text{bpy})_2(\text{tpt})]^+$

Tetrazole belongs to the class of aromatic azapyroles membered heterocycles with nitrogen atoms in the ring. Since the discovery, numerous tetrazoles and tetrazole derivatives have been reported.

The first tetrazole has been prepared by the Swedish chemist J.A. Bladin at the University of Uppsala in 1885.<sup>42</sup> He proposed the name Tetrazole for the new ring structure in 1886.

Tetrazole is the most acidic of the azoles ( $\text{pK}_a=4.89$ )<sup>43</sup> and readily deprotonates to form the tetrazolate ion. Surprisingly, the coordination chemistry of the tetrazole has received very little attention in the past. In 1977, a review of the chemistry of the tetrazoles discussed the metal complexes of the tetrazoles such as the parent compound 5-phenyltetrazole and its derivatives. Such ligands are only capable of monodentate coordination to a metal centre and, as such, the complex are less stable than the corresponding complexes of the chelate ligand discussed previously. In 1979 the first complex of chelating tetrazole containing ligand were described<sup>44</sup> and in 1988 a full review of the coordination chemistry of tetrazoles and tetrazolates was published<sup>45,46,47</sup>.

The ligand 5-(2-pyrid-yl) tetrazole ( $\text{Htpt}$ ) was prepared by reaction of pyridine-2-carbonitrile and hydrazoic acid. Its reaction with one equivalent of  $[\text{Ru}(\text{bpy})_2\text{Cl}_2]$  in methanol afforded the complex  $[\text{Ru}(\text{bpy})_2(\text{tpt})]^+$  in a good yield, which was isolated as the hexafluorophosphate salt and characterized by



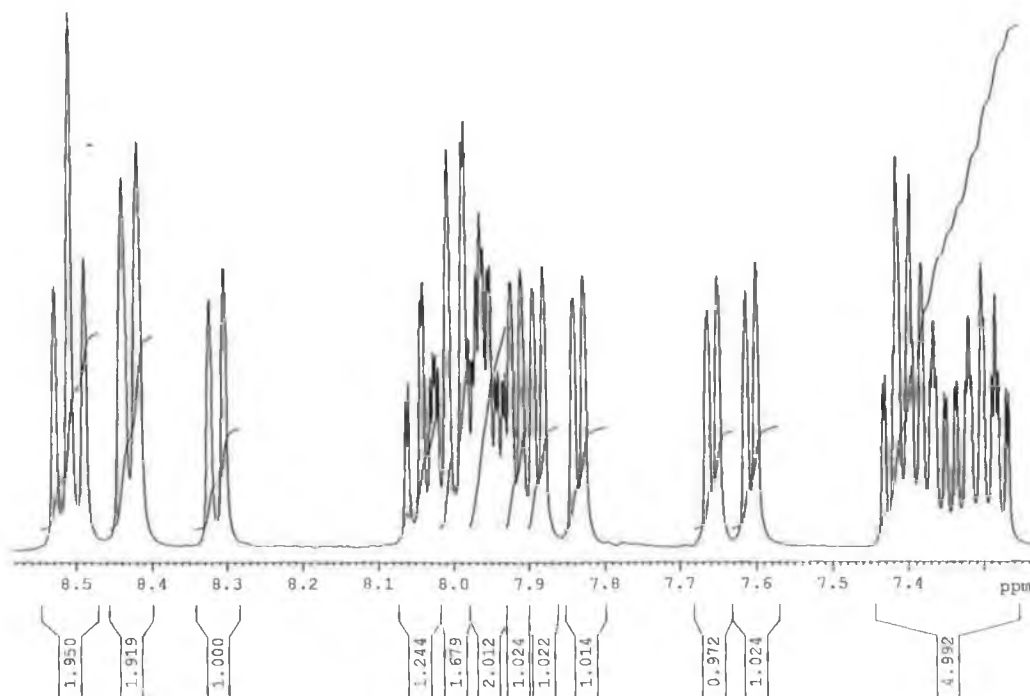
elemental analysis. Thus the H□py ligand formed complexes in the deprotonated tetrazolate form. This is consistent with the high acidity of the NH proton in tetrazoles.

#### 4.4.1 NMR Spectroscopy

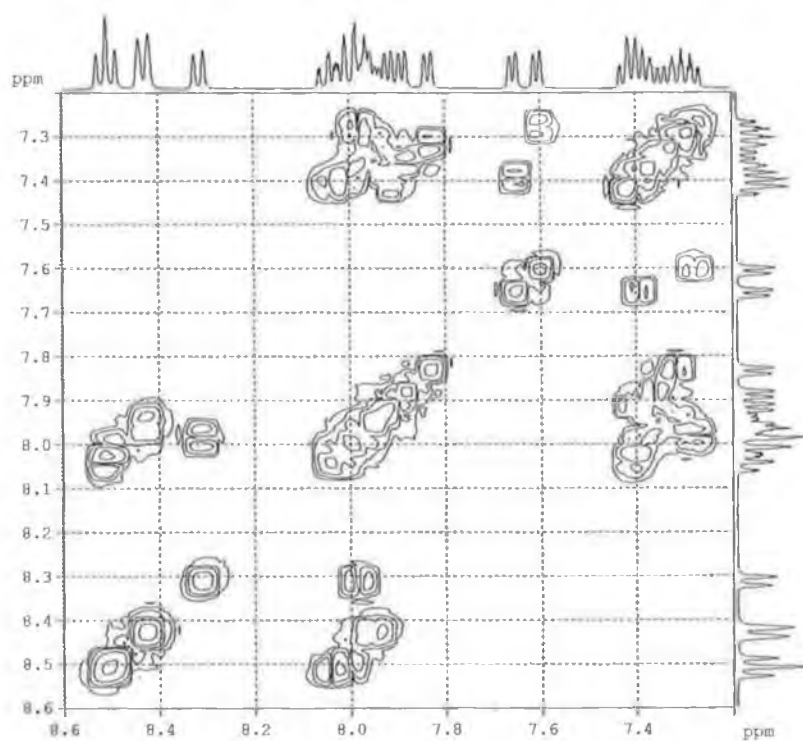
The  $^{13}\text{C}$ -NMR of the complex shows that the presence of the asymmetric □py ligand splits the carbons in 25 non equivalent signals: at around 125 ppm the five signals of the carbons in 5 position ( $\text{C}^5$ ) are visible, around 129 the five of  $\text{C}^3$ ,  $\text{C}^4$  are situated at 139 ppm and  $\text{C}^6$  about 153. The four quaternary carbons on the bpy ligands appear around 157, instead the singlet of the quaternary carbon on the pyridine ring of the □py ligand is observed at 150 and the one on the tetrazole is situated at a lower field of 162 ppm. The  $^1\text{H}$ -NMR shows 20 non-equivalent protons due to the non-symmetrical nature of the H□py. Despite considerable overlap of this signal, the five  $\text{H}^6$  protons are all resolved from each other in the region 7.5-8.0 ppm. A two-dimensional H-H (cosy) and C-H correlated spectra facilitated the assignment of the others.

Table 4.1 summarises the NMR for the complex and its CIS values. Some striking upfield shifts are noticed for the ligand proton signals on coordination to ruthenium. By far the prevalent upfield CIS (-1.17 ppm) is experienced by the  $\text{H}^6$  proton, this is certainly due to through space ring current anisotropy effects since the proton lies directly over the shielding plane of one of the bpy pyridine rings. The others protons experience smaller upfield shifts

(from -0.072 to -0.032 ppm) due to a combination of factors. Negative CIS values are usually ascribed to strong metal to ligand  $\pi$  back donation, however, in our case they may simply be a consequence of deprotonation of the tetrazole and resulting transfer of electron density from the negatively charged tetrazolate ring to the  $\pi$ -deficient pyridine ring.



**Figure 4.18**  $^1\text{H}$ -NMR spectrum of the complex  $[\text{Ru}(\text{bpy})_2(\square\text{py})]^+$  in D-acetonitrile



**Figure 4.19** H COSY-NMR spectrum of the complex  $[\text{Ru}(\text{bpy})_2(\square\text{py})]^+$  in D-acetonitrile

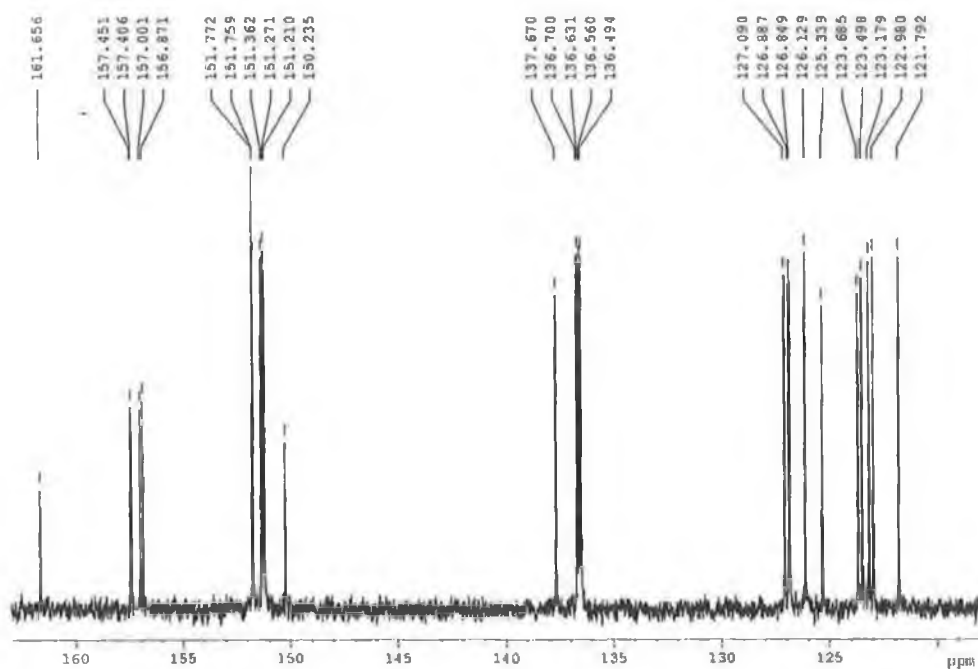


Figure 4.20  $^{13}\text{C}$ -NMR Spectrum of the complex  $[\text{Ru}(\text{bpy})_2(\square\text{py})][\text{PF}_6]$  in D-acetonitrile

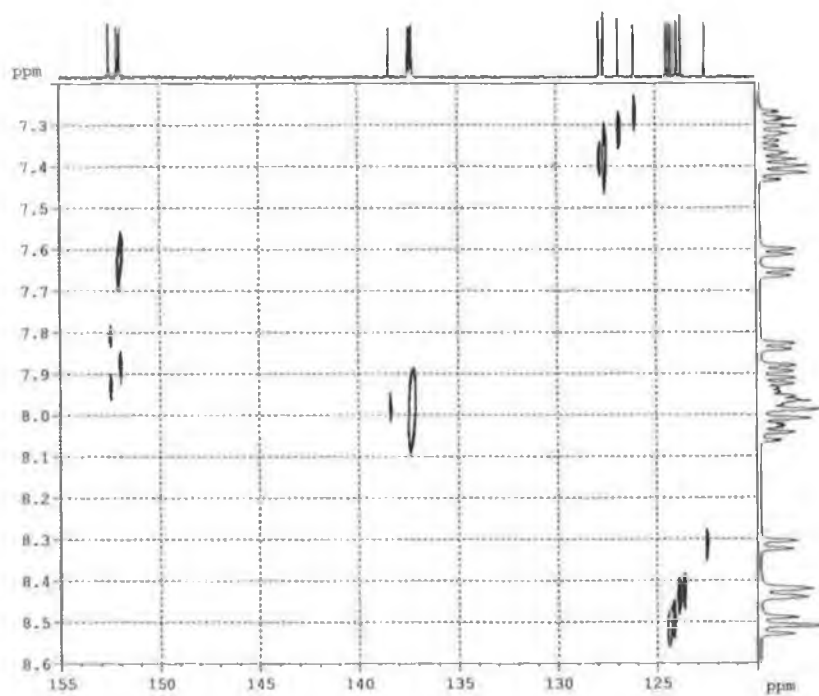
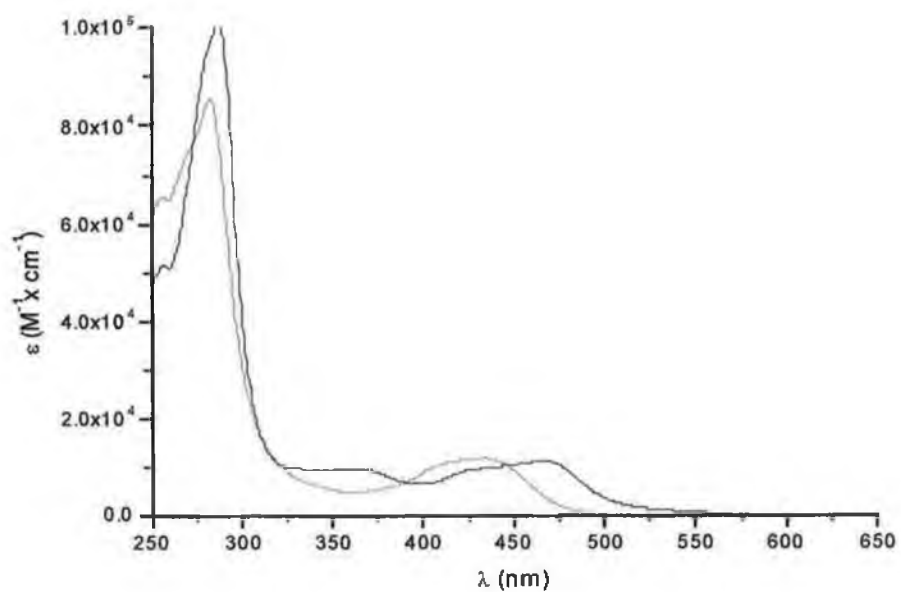
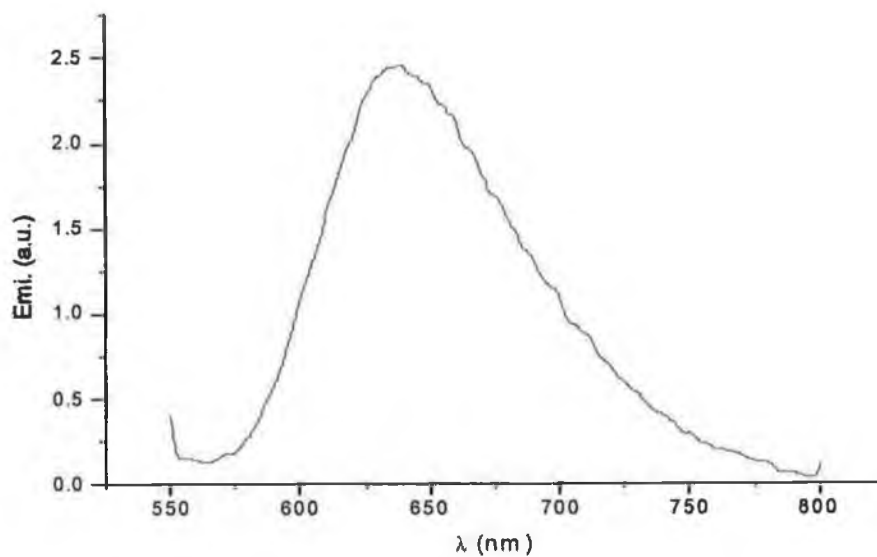


Figure 4.21 C-H correlation -NMR spectrum of the complex  $[\text{Ru}(\text{bpy})_2(\square\text{py})]^+$  in D-acetonitrile



**Figure 4.22** Absorption spectra of  $[\text{Ru}(\text{bpy})_2(\text{H}\square\text{py})]^{2+}$  (red line) and  $[\text{Ru}(\text{bpy})_2(\square\text{py})]^+$  (black line) in acetonitrile solution at room temperature.



**Figure 4.23** Emission spectrum of  $[\text{Ru}(\text{bpy})_2(\square\text{py})]^+$  in acetonitrile solution at room temperature

#### 4.4.2 Electronic Spectroscopy

The absorption emission and luminescent lifetime data of  $[\text{Ru}(\text{bpy})_2(\square\text{py})]^+$  are listed in Table 4.2. The electronic absorption spectra of the complex are dominated in the visible region by  $d\pi-\pi^*$  metal to ligand charge transfer (MLCT) with the maxima at 465 and 350 nm. In the UV region two intense  $\pi-\pi^*$  transition are visible at (280 and 310 nm), associated with the bipyridyl moiety, and are blue shifted with respect to  $[\text{Ru}(\text{bpy})_3]^{2+}$  as a result of stronger  $\sigma$  donation of the negatively charged tetrazole ring.

Addition of acid and consequentially formation of the protonated specie  $[\text{Ru}(\text{bpy})_2(\text{H}\square\text{py})]^{2+}$ , moves the MLCT absorption to higher energy (436 nm.) than that of  $[\text{Ru}(\text{bpy})_3]^{2+}$ . When the complex is protonated the coordinated ligand becomes a weaker  $\sigma$ -donor and a stronger  $\pi$ -acceptor, and as a consequence the  $t_{2g}(\text{M})$  and the  $\pi^*$  energy gap increases, which in turn increase the energy gap between the MLCT and the ground-state and a blue shift of the emission and absorption spectra occurs. The pH of the complex titration (Fig.4.25, 26) in its ground state revealed a pKa lower than 0, and it was not possible to measure the pKa of the excited state because in aqueous solution the protonated complex is not an emitting species.

The previous investigations have shown that the luminescence emission of the tetrazole complex originates from triplet ruthenium-bpy metal to ligand charge transfer (MLCT) excited states, the 5-(2-pyrid-yl) tetrazole playing, to a first approximation, the role of "spectator" ligands. Consideration of the molecular geometry shows that for the mono-charged, polar  $[\text{Ru}(\text{bpy})_2(\square\text{py})]^+$

complex the charge separation, with consequent generation of a dipole, caused by Ru-bpy CT excitation will reduce the molecular dipole in the excited state with respect to the ground state. In fluid solution rearrangement of the solvent molecules will occur afterward.

At 77K the complex exhibit a strong emission with vibrational structure. This vibrational structure is due to relaxation via bipyridil base vibrations, which is common in ruthenium polypyridyl complexes. On cooling to 77K a blue shift is observed in the emission maxima for both: the protonated and the deprotonated species. This is again associated with the “rigidchromism”.

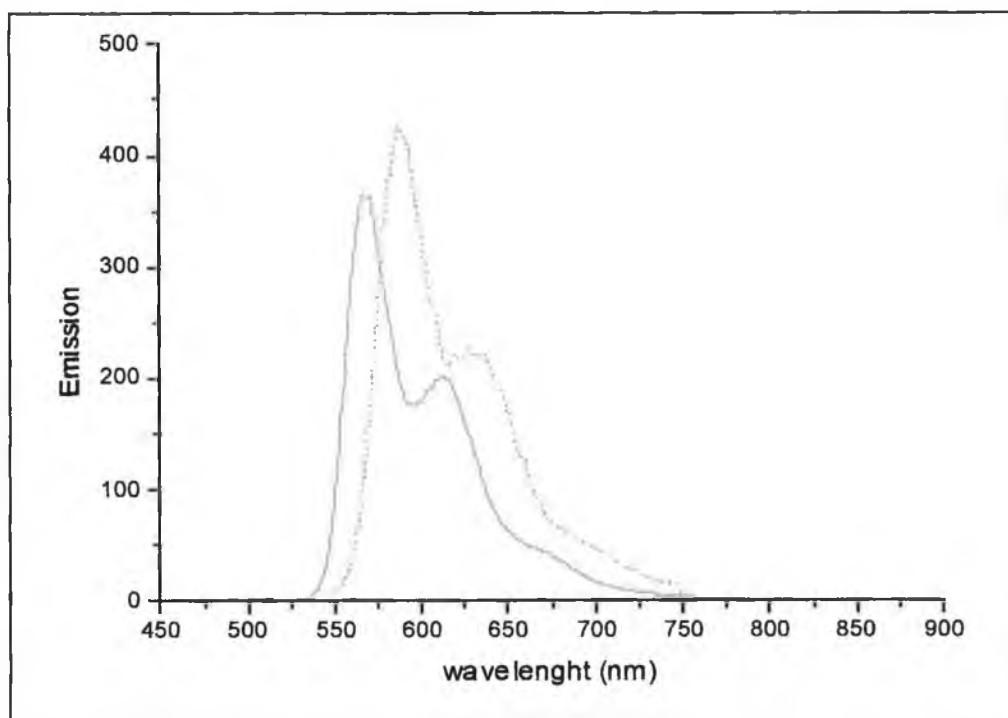


**Figure 4.24** Emission spectra of  $[\text{Ru}(\text{bpy})_2(\text{H}\square\text{py})]^{2+}$  (blue line) and  $[\text{Ru}(\text{bpy})_2(\square\text{py})]^+$  (red line) in acetonitrile solution at 77 K

### 4.4.3 Redox Properties

Further insight into these effects is provided by electrochemical data. The tetrazolate complex exhibits a reversible one-electron oxidation at 1.02 V and two reversible one electron reductions at -1.50 and -1.72 V, which are bpy based. There are no other reductions within the solvent limit. Thus relative to  $[\text{Ru}(\text{bpy})_3]^{2+}$ , the complex is more easily oxidised but more difficult to reduce. Clearly the negatively charged tetrazolate group is a powerful electron donor which significantly increases electron density of the Ruthenium centre. Furthermore, the  $\Delta E_{\text{ox-red}}$  value, 2.52 V, is less than that of  $[\text{Ru}(\text{bpy})_3]^{2+}$ , 2.58 V, which is consistent with the visible absorption spectra for which the same orbitals are involved. Addition of acid results in a significant increase in the oxidation potential for  $\text{Ru}(\text{bpy})_2(\text{H}\square\text{py})^{2+}$ , relative to  $\text{Ru}(\text{bpy})_2(\square\text{py})^{1+}$ , and this is consistent with the shift to higher energy of the MLCT absorption. Access to the reduction potentials was prevented by reduction of excess acid to hydrogen.



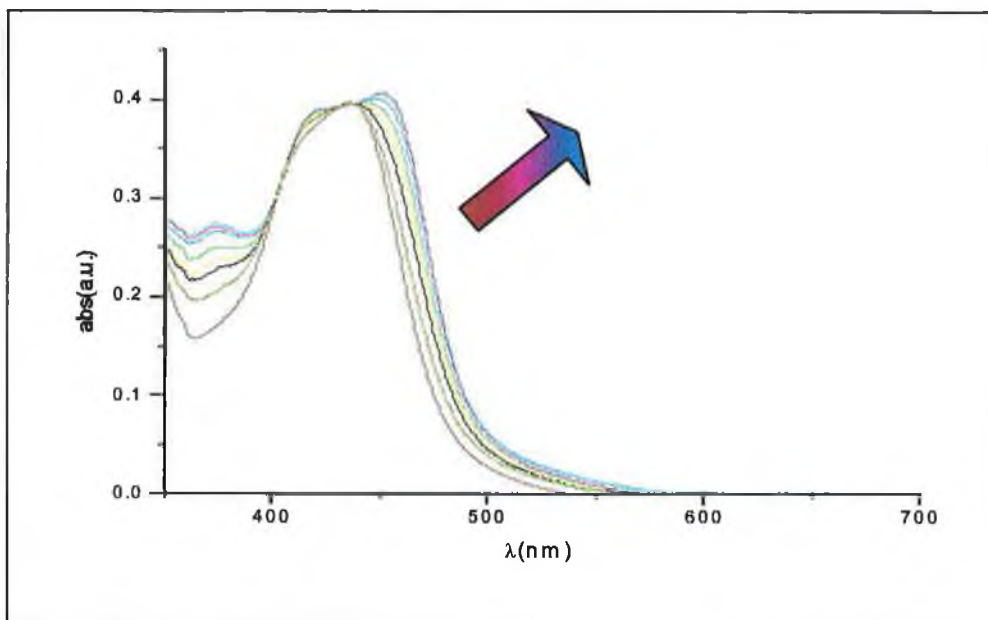


**Figure 4.25** 17 pH dependence of the absorption spectra of  $[\text{Ru}(\text{bpy})_2(\text{Hpy})]^+$  ( $5 \times 10^{-5} \text{ M}$ ) in an aqueous Britton-Robinson buffer at pH 0, 0.2, 0.4, 0.6, 0.9, 1.2, 1.4, 1.8, and 2.5.

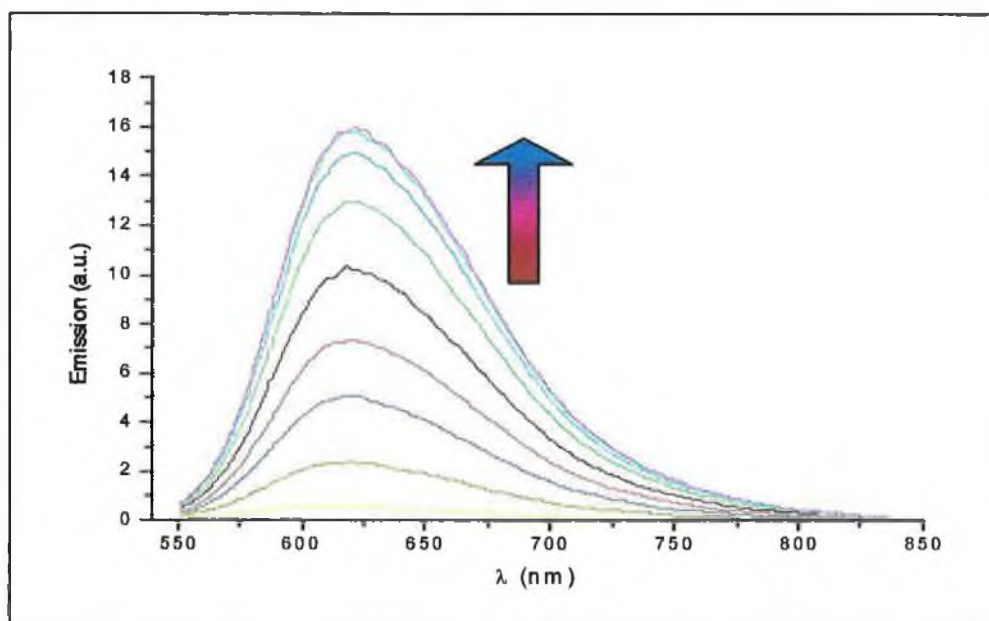


**Figure 4.26** 17 pH dependence of the emission spectra of  $[\text{Ru}(\text{bpy})_2(\text{Hpy})]^+$  ( $5 \times 10^{-5} \text{ M}$ ) in an aqueous Britton-Robinson buffer at pH 0, 0.2, 0.4, 0.6, 0.9, 1.2, 1.4, 1.8, and 2.5.

#### 4.4.4 Lifetime temperature Dependence

Equation 4.1 adequately describes the temperature dependent decay of the excited state of Ru(II) systems above the solvent melting temperature. As can be seen from Table 4.5, two Arrhenius terms are needed to explain the temperature dependence of the lifetimes. By analogy with  $[\text{Ru}(\text{bpy})_3]^{2+}$  the first Arrhenius term is thought to concern the thermal equilibration of MLCT levels spaced by  $450 \text{ cm}^{-1}$ . About the second term, there is a general agreement in the literature that the temperature dependence of the emission lifetime of Ru(II) polypyridine complexes is related to an activated surface crossing from the  $^3\text{MLCT}$  manifold to a  $^3\text{MC}$  level which undergoes photochemical or photophysical deactivation. The second term values ( $10^{11} \text{ sec}^{-1}$ ) for the  $[\text{Ru}(\text{bpy})_2(\square\text{py})]^+$  are too low to correspond to the frequency factor of a surface crossing process ( $10^{13}\text{-}10^{14} \text{ sec}^{-1}$ ), more reasonably  $A_2$  corresponds to the rate of the nonactivated  $^3\text{MC}$  decay, and the activation energy  $\Delta E_2$  corresponds to the  $^3\text{MC}$ - $^3\text{MLCT}$  energy gap.

## 4.5 Conclusions

The photophysical and electrochemical behaviours (Table 4.2, 3) of the azole complexes are quite similar, since both  $(\Delta\text{py})^-$  and  $(\square\text{py})^-$  ligands are charged strong  $\sigma$ -donor. The MLCT excitation involves a ruthenium to bpy electron transfer, in which both can be involved in non-specific interaction with the solvent (e.g. hydrogen bonding) because of the presence of free nitrogen on the ligands. We must highlight that in the  $(\Delta\text{py})^-$  case the interaction with the solvents are stronger (Table 4.5), probably because the lone pair on the non-coordinated nitrogens are more available than the  $(\square\text{py})^-$ , which is proved from the pH data (Table 4.4).

As for the electrochemical behaviour of the complexes, it is important to emphasise the following points:

- The metal centred oxidation potential become less positive moving from bpy to  $(\Delta\text{py})^-$ , passing through  $(\square\text{py})^-$ , which is expected because triazole is better  $\sigma$ -donor than tetrazole, and both are better  $\sigma$ -donor of bpy.
- The first and second reduction potentials of the complexes correlate well with the first and the second of  $[\text{Ru}(\text{bpy})_3]^{2+}$  and can they be assigned to reduction of coordinated bpy ligands.

A more complete discussion of the electrochemical properties of the  $(\Delta\text{py})^-$  and  $(\square\text{py})^-$  ligands can not be done because the reduction waves below  $-2.00$  V are irreversible under the experimental conditions. It would be certain worthwhile to extend the present investigation to low temperature ( $-54$  °C) conditions,

where higher number of reversible waves are usually observed for mononuclear ruthenium complexes<sup>48</sup>

The two heteroleptic complexes show a shorter lifetimes of the <sup>3</sup>MLCT if compared with [Ru(bpy)<sub>3</sub>]<sup>2+</sup>, for the (□py) complex it can be explain in term of the population of the population of the nearby <sup>3</sup>MC state, and consequentially fast deactivation from very efficient inter-system crossing between the <sup>3</sup>MC state and the ground state. In the case of [Ru(bpy)<sub>2</sub>(Δpy)]<sup>+</sup>, a possible factor, responsible of the shorter lifetime, could be the decrease in symmetry moving from tris bpy (D<sub>3</sub>) to a complex bearing only two bpy ( class of symmetry lower than C<sub>2v</sub>). Unfortunately, the influence that the low symmetry class has on the energies of the various excited states is difficult to assess even in a qualitative sense<sup>49</sup>. The symmetry problem will not be present in the tpy based complexes, that will be studied in this thesis, in fact all of them have the same symmetry.

## 4.6 Bibliography

- 
- <sup>1</sup> Reedijk, J, **Comprehensive Coordination Chemistry** Vol2, (1973)  
Pergamon, Oxford.
- <sup>2</sup> Balzani V, Moggi L, Ballardini R, Boletta F Gandolfi MT, Juris A, Maestri M  
Manfrin MF, Moggi L, Sabbattini N . **Coord. Chem Rew**, 1993, 125, 75..
- <sup>3</sup> Blau F, **Detsch. Chem. Ges.** 1888, 27, 1077.
- <sup>4</sup> Constable E C, **Adv. Inorg. Chem**, 1989, 34, 1.
- <sup>5</sup> Constable E C, Steel P J, **Coord. Chem. Rev.**, 1989, 93,205.
- <sup>6</sup> Juris A, Balzani V, Barigelletti F, Campagna S, Belser P, von Zelewsky  
**Coord. Chem. Rev.** 1988, 84, 85 and references there in
- <sup>7</sup> Steel P J, Lhousse F, **Inorg. Chem.**, 1983, 22, 1488.
- <sup>8</sup> Steel P J, Constable E C, **J. Chem. Soc. Dalton Trans.** 1990, 1399
- <sup>9</sup> Hage R, Prins R, Haasnoot J, Reedijk J, Vos J G, **J. Chem. Soc. Dalton  
Trans.** 1987, 1389
- <sup>10</sup> Buchanan B E, Degn P, Velasco J, Hughes H, Creaven B Long C, Vos J G,  
Hage R, van Ddiemen, Haasnoot J, Reedijk J, **J. Chem. Soc. Dalton Trans.**  
1992, 1177
- <sup>11</sup> Paris JP, Brandt WW, **J. Am. Chem. Soc.** 1958, 81, 5001.
- <sup>12</sup> Richard J W, **J. Chem. Ed.** 1983, 60, 797.
- <sup>13</sup> Adamson A W, **J. Chem. Ed.** 1983, 60, 797.
- <sup>14</sup> Orogel L E, **J. Chem. Soc.** 1961, 3683.
- <sup>15</sup> Brandt W W, Dwyer F P, **Chem. Rev.** 1954, 54, 954
- <sup>16</sup> Brandt W W, Smith G S, **Anal. Chem.** 1949, 21, 1313
- <sup>17</sup> Croosby GA, **Acc. Chem. Res.** 1975, 8, 231

- 
- <sup>18</sup> Harrigan R W, Crosby GA, **J. Phys. Chem** 1973, 59, 3468.
- <sup>19</sup> Hager G D, Watts R J, **J. Am. Chem. Soc.** 1975, 97, 7037.
- <sup>20</sup> Crosby G A, Elfring W H, **J. Phys. Chem.** 1976, 80, 2206.
- <sup>21</sup> Sprouse S, King KA, **J. Am. Chem. Soc.** 1984, 106, 6674
- <sup>22</sup> Hage.R **Ph. D. Thesis.** (1991) Leiden University. The Netherlands
- <sup>23</sup> Hughes H, **Ph. D. Thesis,** (1993) Dublin City University, Ireland
- <sup>24</sup> Buchanan B, Governon E N C Hughes H, Vos J G, Hage R, van Ddiemen, Haasnoot J, Reedijk J, **Inorg. Chim. Acta** 1998, 1674
- <sup>25</sup> Hage R, Lempers H, Haasnoot J, Reedijk J, Vos J G **Inorg Chem.** 1997, 36, 3139.
- <sup>26</sup> Bucharan B, Vos J G, Kaneko M, van der Putten W, Kelly J, Hage R, de Graaff, Prins R, Haasnoot J, Reedijk J, **J. Soc. Chem. Dalton Trans.** 1990, 2425
- <sup>27</sup> Nieuwenhuis H, Haasnoot J, Hage R, Reedijk J, Snoek T, Stufkens D, Vos J G, **Inorg. Chem.** 1991, 30, 48
- <sup>28</sup> Constable E C, Hemney R, **J. Soc. Chem. Dalton Trans.** 1990, 2425
- <sup>29</sup> Hage R, Prins R, **J. Soc. Chem. Dalton Trans.** 1987, 13889
- <sup>30</sup> Sullivan BP, Salmon DJ, Meyer TJ **Inorg. Chem.** 1978, 17, 3334
- <sup>31</sup> Stell PJ, Constable E C, **J. Soc. Chem. Dalton Trans.** 1990, 1389
- <sup>32</sup> Cathey C, Constable E C, Hannon M, Tocher D, Ward M, **J. Soc. Chem. Chem. Comm.** 1990, 621
- <sup>33</sup> Carraway C, Demas J, **Anal Chem** 1991, 63, 37
- <sup>34</sup> Lumpkin R S, Kober E M, Worl L, Murtaza Z, Meyer T J, **J. Phys. Chem.** 1990, 94, 239

- 
- <sup>35</sup> Wrihton M, Morse L, **J. Am. Chem. Soc.** 1974, 96, 996
- <sup>36</sup> Morris D E, Ohsawa Y, **Inorg. Chem.**, 1984, 23, 3010.
- <sup>37</sup> Giordano P.J., Bock C R, **J. Am. Chem. Soc.** 1977, 99, 3187.
- <sup>38</sup> Giordano P J, Bock C R, **J. Am. Chem. Soc.**, 1978, 100, 6960.
- <sup>39</sup> Ireland J F, Wyatt P A H, **Ad. Phys.Org.Chem.**, 1976, 12, 32.
- <sup>40</sup> Vos J G, **Polyhedron** 1992, 11, 25.
- <sup>41</sup> Barigelletti F, Juris F, Balzani V, Belser P, von Zelesky A, **Inorg. Chem.** 1983, 22, 3335
- <sup>42</sup> Bladin J A, **Ber.** 1885, 18, 2907
- <sup>43</sup> Katritsky A R, Handbok F, **Heterocyclic Chemistry** p 303 Pergamon Oxford
- <sup>44</sup> Haga M, Matsumura I, Yamabe S, **Inorg. Chem.** 1987, 26, 4148
- <sup>45</sup> Gill N S, Yang F Y, **Austr. J Chem.** 1979, 32, 1669
- <sup>46</sup> Erbe J, Beck W, **Chem Ber.** 1983, 116, 3867
- <sup>47</sup> Moore D S, Robinson S D, **Adv. Inor. Chem.** 1995, 48, 1625.
- <sup>48</sup> Ohsawa Y, Hanck K W, **J. Electroanal. Chem. Interfacial Electrochem.** 1984, 175, 229
- <sup>49</sup> Berger R M, McMillin D R, **Inorg. Chem**, 1988, 27, 4245.

## Chapter 5

### “The Prototype: [Ru(tpy)( $\Delta$ py $\Delta$ )]”

“Left to themselves, things tend to go from bad to worse.”  
Murphy



## 5.1 Introduction

Since the tridentate ligand 2, 2': 6', 2'' terpyridine, tpy (Fig. 5.1), was first prepared over 70 years ago<sup>1</sup>, its coordination chemistry, along with that of its substituent (X-tpy) analogues, has been widely studied<sup>2</sup>. They have been found highly sensitive reagents for the colorimetric determination of iron (II), with some finding potential applications in clinical chemistry. More recently tpy have found increasing favour as coordination chemistry has started to shift from the molecular to the supramolecular levels. Substituents on the ligand may be used to tailor the properties of the resulting coordination complexes. Appropriately functionalised tpy<sup>3</sup> have been anchored to oxide surfaces, permitting the build up of a monolayer or a thin film of coordination complexes. The ability of terpyridine to chelate to a wide range of metal ions has been led to its incorporation in macrocyclic ligands.

There has been considerable recent interest in metallosupramolecular species constructed from a number of metal ions linked by suitable ligands containing two or more sets of potential donor atoms. If such ligands are dinucleating, then linear oligomers and polymers may be formed. If, instead, the ligand contains three or more donor sets, then two- and three-dimensional metallo-supramolecular arrays can be created. Much of the interests derived from the possibility of photo-induced electron or energy transfer from one metal centre to the to the next if suitable energy gradient exists in the complex. Thus, suitably designed linear oligomers may act as molecular wires while two and three-dimensional species may be used for the harvesting of light energy.<sup>4</sup> The tpy-lanthanide complexes are attracting interest as luminescent agents.<sup>5</sup> Instead the tpy ruthenium complexes show weak luminescence from very short living

<sup>3</sup>MLCT excited state at room temperature (see Chapter 1).

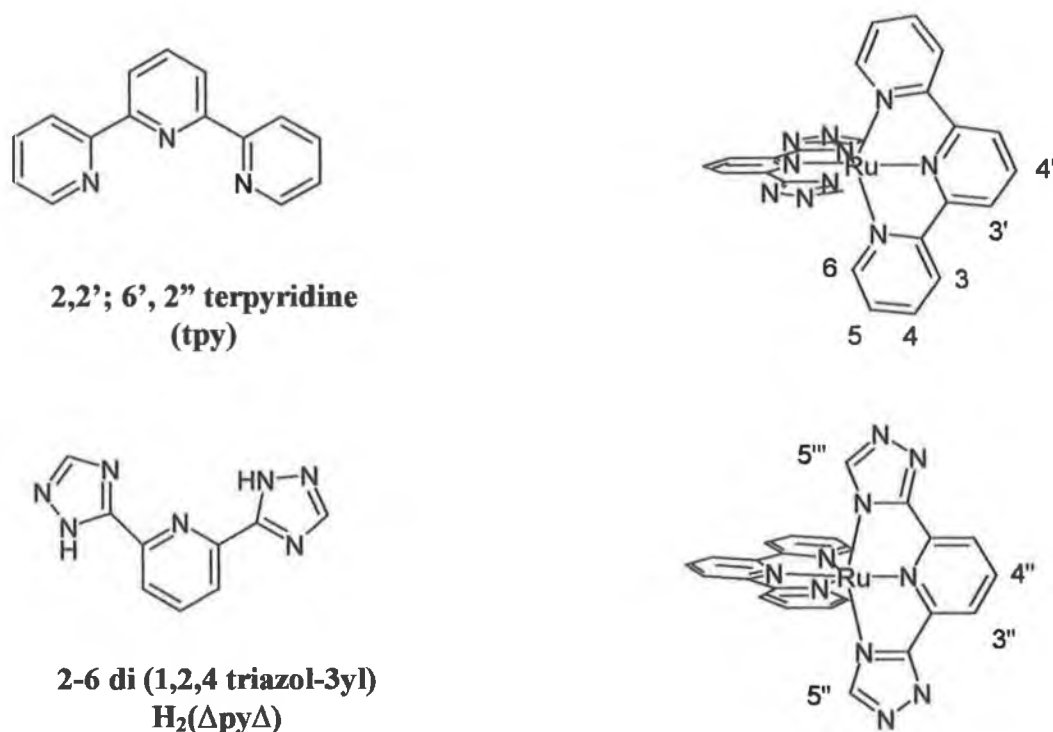


Figure 5.1 Ligands cited in the text, and <sup>1</sup>H-NMR proton assignments.

The aim of this chapter is to study comprehensively a method to increase the emission quantum yield and increase the lifetime of the excited state.

The tridentate ligand H<sub>2</sub>(ΔpyΔ), 2-6 di (1,2,4 triazol-3yl) pyridine (Fig. 5.1) was synthesised according to the literature for similar ligands<sup>6</sup>, using little modifications, and used for its σ donor and π acceptor properties and it is hoped that due to these properties the excited states of the Ru(II) complexes would substantially alter their photophysical properties.

The H<sub>2</sub>(ΔpyΔ) ligand contains a pyridine ring which is a good π acceptor and two triazolate moieties which are strong σ donors, its coordination to ruthenium

complexes is tridentate, in a pseudo-octahedral coordination. Due to the ruthenium complexes building block potential in supramolecular systems, it is necessary to know their properties as individual units.

## 5.2 Synthesis and Purification

Different synthetic pathways were followed for the synthesis of complex [Ru(tpy)( $\Delta$ py $\Delta$ )], first approach was based on the formation of [H<sub>2</sub>( $\Delta$ py $\Delta$ )RuCl<sub>3</sub>] precursor. RuCl<sub>3</sub> and H<sub>2</sub>( $\Delta$ py $\Delta$ ) ligand were reacted in ethanol, under the same conditions used in the synthesis of the analogous Ru(tpy)Cl<sub>3</sub>, this reaction produced a brown-yellowish complex with a yield of 90%. The elemental analysis yielded the correct ratio of nitrogen, hydrogen and carbon; a <sup>1</sup>H-NMR analysis of the complex in DMSO showed the presence of the ligand in a symmetrical coordination. However unfortunately NMR analysis revealed that the oxidation state of the ruthenium was three instead of two. After a period of 10 minutes in solution, the complex changed its colour from brown to green. In contrast to the behaviour of the other [Ru(tpy)Cl<sub>3</sub>], this complex did not undergo any reaction upon boiling with a solution of one equivalent of tpy in methanol, in presence of a reducing agent, even after prolonged reaction times. Those observation may be indicative that the new ruthenium species is polymeric, with adjacent ruthenium centres being bridged by the ( $\Delta$ py $\Delta$ )<sup>2-</sup> free nitrogens. All the attempts of using this complex as a precursor in other reactions was unsuccessful

The next method investigation was the reaction between Ru(tpy)Cl<sub>3</sub> and

the  $H_2(\Delta py\Delta)$  ligand. This method proved to be somewhat problematic. The major problem encountered involved the solubility of the ligand. The  $H_2(\Delta py\Delta)$  ligand is soluble in hot DMF, DMSO or in aqueous solution in presence of base as anionic form.

In the course of preparation of the target complex two solvents scheme were used:

- A DMF-ethylen glycol (1:1) boiling solution
- A basic aqueous solution in presence of N-ethyl morpholine as a reducing agent

Both were found to give the desired complex, in the same quantities, 30% of yield. However, the later was the favourite method in terms of ease of preparation. Purification by column chromatography on alumina (acetonitrile-methanol 1-1) produced the stated yield. The complex was recrystallised from 1:1 water-methanol solution and obtained as an analytically pure intensely dark coloured powder. The elemental analysis suggests that a mixture of mono protonated-deprotonated (80/20) species be formed after recrystallisation, as it has been seen for the model bpy based complex,  $[Ru(bpy)_2(\Delta py)]^+$ , triazoles facilitate the formation of hydrogen bonds<sup>7</sup>.

At the end of the purification, HPLC (Fig.5.3) and  $H^1$ -NMR (Fig. 5.4) investigations, due to the different coordination sites of the triazolate moieties detected three configurational isomers (Fig. 5.2). The major isomer (about 60%) is the complex with  $N^2$  and  $N^4$  bounded triazolate rings,  $[Ru(\Delta^2 py\Delta^4)(tpy)]$ , with a retention time of 7.3 minutes. The second isomer with an abundance around 30% is assigned to the double  $N^4$  coordination,  $[Ru(II)(\Delta^4 py\Delta^4)(tpy)]$ , (very broad peak

with retention time approximately of 20.2 minutes). The third isomer (about 10%) is all N<sup>2</sup> bound with a retention time of 3.3 minutes. The isomer ratios were estimated by integrating the H<sup>6</sup>, <sup>1</sup>H-NMR signals, where the three isomers show distinctly different positions, and it was confirmed using the integration of the HPLC peaks.

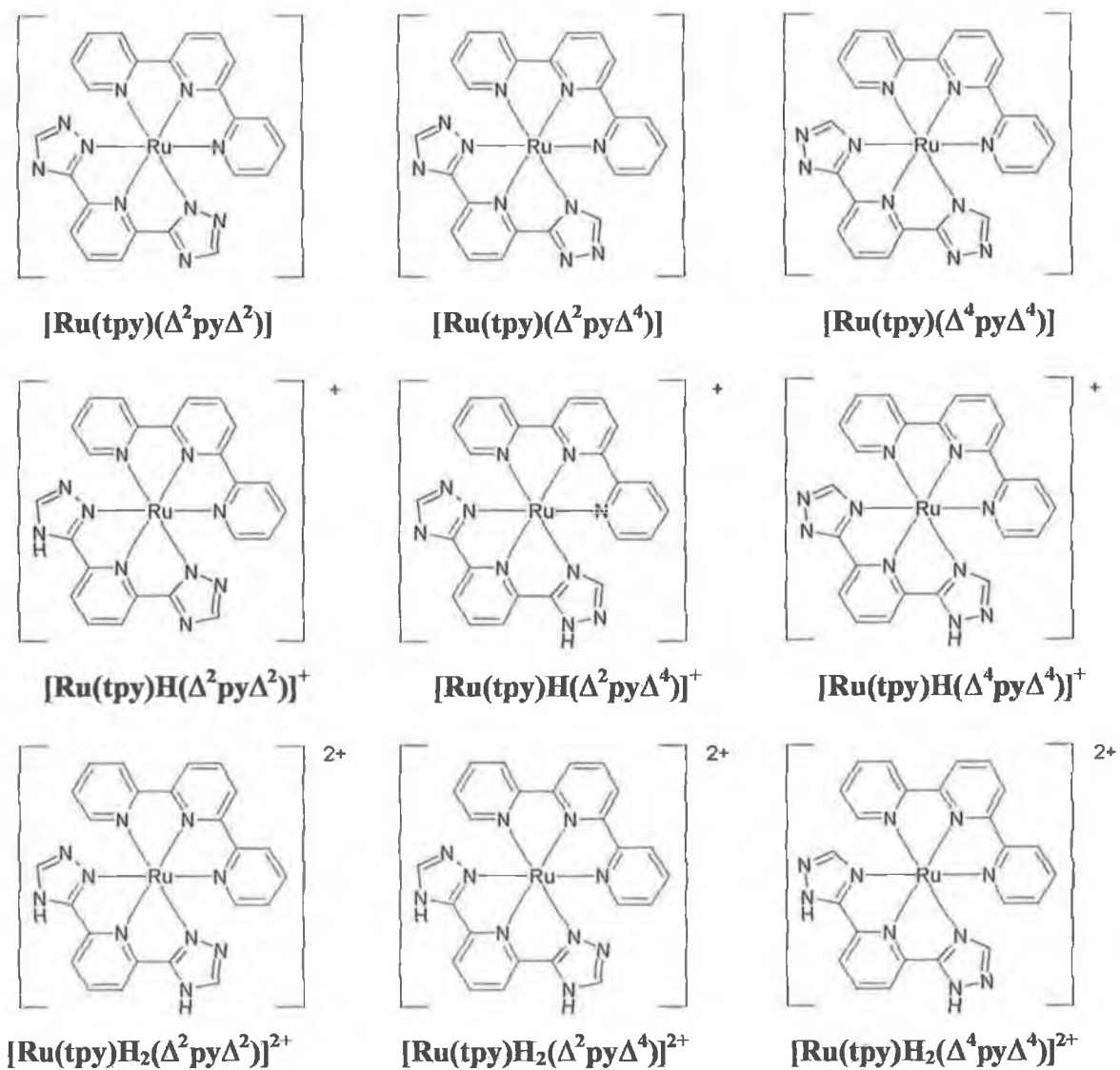


Figure 5.2. Possible isomers for  $[\text{Ru}(\text{tpy})(\Delta\text{py}\Delta)]$  complex in various protonation states.

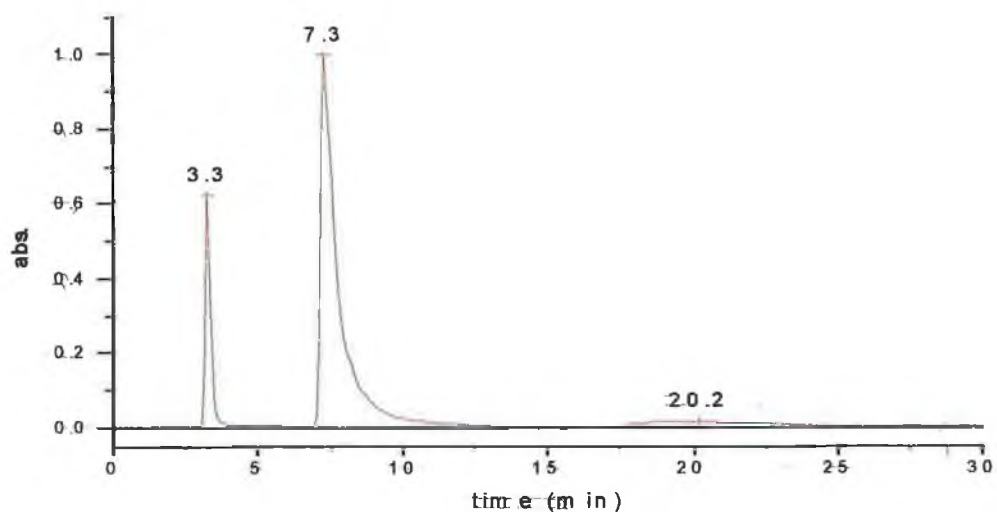


Figure 5.3 HPLC Chromatogram of  $[\text{Ru}(\text{tpy})(\Delta\text{py}\Delta)]$  isomers in a phase solution a solution of  $\text{LiClO}_4$  (0.08 M) in acetonitrile/water (80/20)

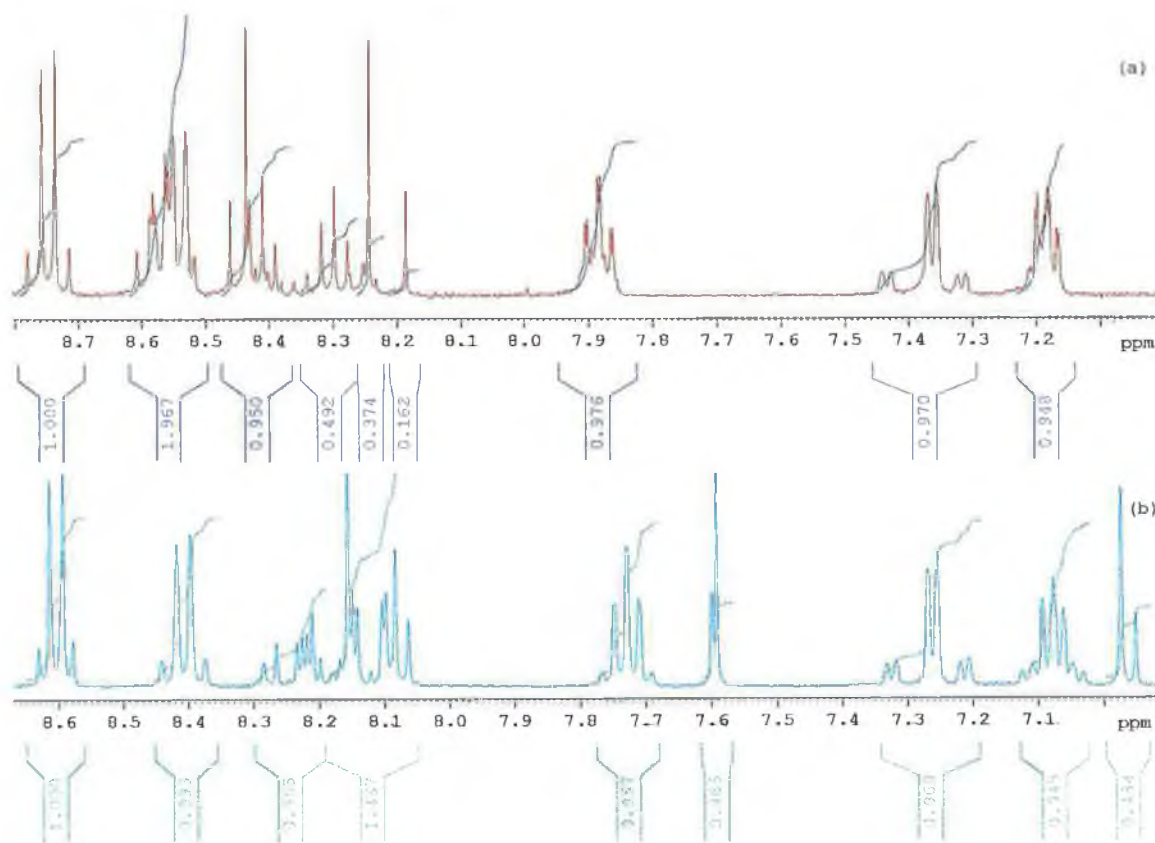


Figure 5.4  $^1\text{H}$ -NMR spectra of the isomers of the  $[\text{Ru}(\text{tpy})(\Delta\text{py}\Delta)]$  complex in (a) acidic (red) and (b) basic (blue)  $\text{d}^4$ -methanol

Acid-base ground and excited state studies of the isomers showed peculiar differences, which portrayed the non-equivalence of the triazole coordination sites. Initially the mononuclear complexes were investigated on an analytical HPLC using a CSX cation exchange column and a 0.08 LiClO<sub>4</sub>, 80:20 acetonitrile-water mobile phase with a flowrate of 1.8 cm<sup>3</sup>/min and a detector wavelength of 280 nm. The chromatogram in Figure 5.3 is an example of the mononuclear complex containing the three isomers at their different retention times. The UV-visible spectra of the three different isomers, obtained from the photodiode array detector of the HPLC Varian ProStar system, appear similar. It's thought that the isomer separation is due to the difference in acid-base properties based on their binding sites as shown in Chapter 4 for the analogous bpy complexes.

The separation of a mixture of isomers: ([Ru(II)( $\Delta^2$ py $\Delta^2$ )(tpy)], [Ru(II)( $\Delta^2$ py $\Delta^4$ )(tpy)]; [Ru(II)( $\Delta^4$ py $\Delta^4$ )(tpy)], was achieved on neutral alumina columns 100% acetonitrile to isolate the first fraction and 100% methanol in the isolation of the second fraction containing the third isomer. Semi-preparative HPLC was utilised in the isolation of the other two isomers with a mobile phase 0.1 M tetrabutylammonium acetate in methanol. Semi-preparative HPLC is a useful technique for the isolation of isomers<sup>8</sup>, and high percentage purity (95 %) of the isolated isomers was achieved. However some drawbacks do occur, for example when dealing with a large quantity of salt and a small quantity of complex, a considerable part of the complex is lost through a process of irreversible adsorption on the HPLC column.



### 5.3 NMR Spectroscopy

All three isomers were diamagnetic, and the  $^1\text{H-NMR}$  properties were investigated in order to probe the ligand to ligand and metal-ligand interactions in these systems; in all cases, the  $^1\text{H-NMR}$  spectra were recorded in  $d^4$ -methanol. (Fig. 5.4, 5.5 and Table 5.1)

In general in  $\text{tpy-Ru(II)}$  complexes<sup>9</sup>, the lowest field resonance is  $\text{H}^3$ , followed by  $\text{H}^4$ ,  $\text{H}^6$  and  $\text{H}^5$ . The upfield shifting of  $\text{H}^6$  with respect to  $\text{H}^3$  is explained by the fact that it lies in the shielding region above a pyridine ring of the other ligand. (protons numbering are shown in Fig. 5.1)

The CIS coordination shifts are relative to the free ligand in DMSO solution (Table 8.1). A number of general patterns are observed, which provide information about the conformational and electronic charges upon coordination. In the diprotonated complex  $\text{H}^3$  experiences a small downfield shift upon coordination, which is usually attributed to Van der Waals deshielding by  $\text{H}^{3'}$ . It has been suggested that this is a direct consequence of the change from transoid to cisoid configuration about the intramolecular C-C bonds upon coordination, however, charge and  $\pi$ -cloud perturbation with the ligands as a consequence of coordination are equally important. In general,  $\text{H}^5$  undergoes very minor coordination shifts. Large upfield coordination shifts are associated with  $\text{H}^6$ . This represents a balance between the expected downfield shield shifts resulting from positive charge building up upon coordination and the upfield shifts from the proton or the nitrogen of the  $\text{H}_2(\Delta\text{py}\Delta)$  ligand lying over a nearby triazole ring, together with the uncertain anisotropic effects associated with the ruthenium (II)

centre. The shift of H<sup>3</sup>, on the central tpy ring, is associated in part with Van der Waals interaction, in part it may be attributed to the metal interaction with the central pyridine ring, this shift is greater than that with the terminal rings. It is generally observed that the shorter Ru-N bond distances are associated with the central rings of the terpyridine moiety<sup>10</sup>.

It is of interest to note that the H<sup>6</sup> proton is the most sensitive to differences in coordination of the ligand H<sub>2</sub>(ΔpyΔ). In the case of the H<sub>2</sub>(ΔpyΔ) ligand, the observed shift of the H<sup>3''</sup> and H<sup>4''</sup> protons may be attributed to the same reasons referred to those for the terpyridine ligand. That is that the H<sup>5'''</sup> and H<sup>6'''</sup> proton shifts are strongly dependent on the N-bonding of the (ΔpyΔ)<sup>2-</sup> ligand and the acidity-basicity and polarity of the solution is of great importance. This has already been shown for the bpy based analogue in Chapter 4.

In the case of the deprotonated isomers, the negative CIS values become greater, this is simply a consequence of deprotonation of the triazole rings and the resulting transfer of electron density from the negatively charged triazolate to the Ruthenium centre. In direct comparison of the [Ru(tpy)<sub>2</sub>]<sup>2+</sup> and the [H<sub>2</sub>(ΔpyΔ)Ru(tpy)]<sup>2+</sup> complexes, it is important to note that the three protons, H<sup>6</sup> and H<sup>3'</sup> and H<sup>4'</sup>, are the tpy protons more sensitive to the presence of the new ligand. The H<sup>3'</sup> and H<sup>4'</sup> shifts are an evidence of a strong interaction between the two pyridine rings lying on the C<sub>2</sub> axes of symmetry of the complexes

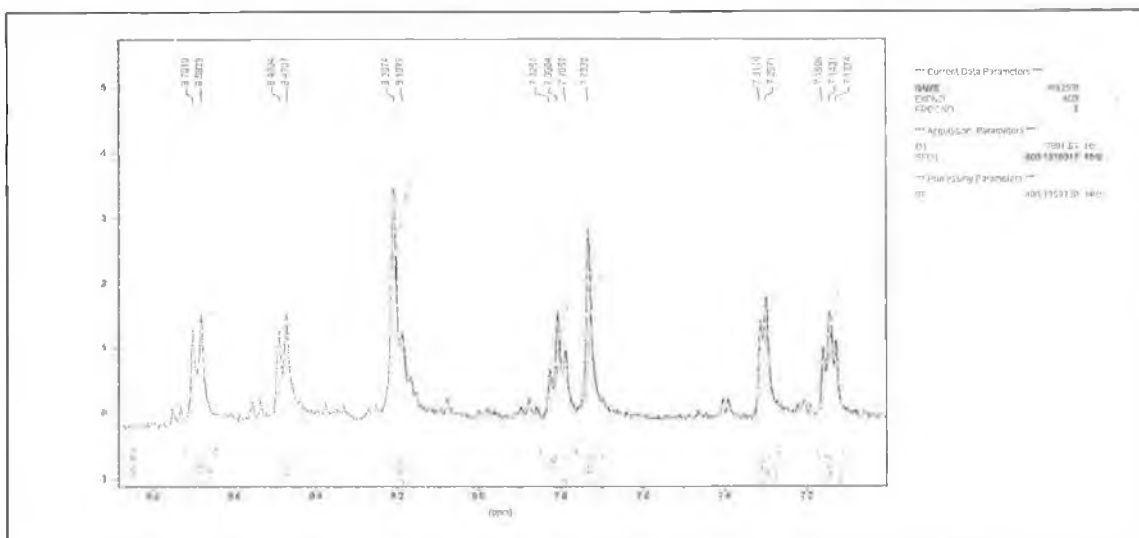


Figure 5.5  $^1\text{H-NMR}$  of  $[\text{Ru}(\text{tpy})\text{H}(\Delta^4\text{py}\Delta^4)]^+$  in  $\text{d}^4$ -methanol.

(ppm)	$\text{H}^3$	$\text{H}^4$	$\text{H}^5$	$\text{H}^6$	$\text{H}^{3'}$	$\text{H}^{4'}$	$\text{H}^{3''}$	$\text{H}^{4''}$	$\text{H}^{5''}$	$\text{H}^{6''}$
	(d)	(dd)	(dd)	(d)	(d)	(t)	(d)	(t)	(s)	(s)
<b>Tpy</b>	8.7	8.00	7.50	8.70	8.55	8.10				
$\text{H}_2(\Delta\text{py}\Delta)^a$							8	8	8	8
$[\text{Ru}(\Delta^2\text{py}\Delta^2)(\text{tpy})]$	8.43	7.75	7.10	7.33	8.63	8.08	8.30	8.27	7.60	
$[\text{Ru}(\Delta^2\text{py}\Delta^4)(\text{tpy})]$	8.40	7.73	7.07	7.26	8.60	8.08	8.22	8.17	7.59	6.80
$[\text{Ru}(\Delta^4\text{py}\Delta^4)(\text{tpy})]$	8.30	7.69	7.05	7.21	8.57	8.08	8.10	8.10		6.96
$[\text{Ru}(\text{H}_2\Delta^2\text{py}\Delta^2)(\text{tpy})]^{2+}$	8.69	7.98	7.31	7.55	8.8	8.35	8.42	8.54	8.48	
$[\text{Ru}(\text{H}_2\Delta^2\text{py}\Delta^4)(\text{tpy})]^{2+}$	8.68	7.98	7.30	7.48	8.84	8.40	8.42	8.54	8.45	8.25
$[\text{Ru}(\text{H}_2\Delta^4\text{py}\Delta^4)(\text{tpy})]^{2+}$	8.67	7.97	7.29	7.43	8.82	8.35	8.42	8.54		8.19
$[\text{Ru}(\text{tpy})_2]^{2+}$	8.82	8.08	7.34	7.72	9.09	8.59				

Table 5.1  $^1\text{H-NMR}$  spectroscopic data for  $\text{d}^4$ -methanol solutions of ligands and their ruthenium complexes (see Fig. 5.1), a)  $\text{d}^6$ -DMSO.

## 5.4 Electronic Spectroscopy

The UV-vis. absorption spectra of the complexes (tab. 5.2 and Fig. 5.7, 5.8, 5.9), in basic ethanol show intense metal-to-ligand charge transfer bands around 390 nm and 480nm, with a molar extinction coefficient of  $7900 \text{ M}^{-1} \times \text{cm}^{-1}$ . The bands around 275 and 309 are assigned to the intra ligand  $\pi$ - $\pi^*$  transitions of the ligand. The small shoulders at 626, 579 nm have not yet been assigned, however one possible explanation is that they arise due to a rare example of a phenomenon involving Ru(II) complexes in which absorption from the excited triplet state<sup>11,12</sup>, which is usual observed for Os(II) complexes. Alternatively, they may be explained in terms of low-energy shoulders in the absorption which can be explained in terms of the qualitative orbital splitting diagram for  $[\text{Ru}(\text{tpy})_2]^{2+}$  as described in figure 5.6. As we have seen for  $[\text{Ru}(\text{bpy})_3]^{2+}$ , the relative energies of the molecular orbitals can be inferred from the zero order energies of the ligand orbitals. The two lowest lying  $\pi^*$  orbitals of the tpy ligand are labelled in light of their symmetry, which is perpendicular to the ligand and passes through the central nitrogen. An AM1 calculation<sup>13,14</sup> reveals that the lowest energy unoccupied orbital, termed  $\chi$ , is antisymmetric with respect to this operation. It lies 0.543 eV below the next lowest energy  $\pi^*$  orbital, termed  $\psi$ , which is symmetric with respect to this operator. Under the assumption of  $D_{2d}$  symmetry, the  $\chi$  orbitals from the tpy ligand split in  $a_2$  and  $b_1$  representations while the higher energy  $\psi$  orbitals span the e representation. Simple perturbation theory arguments lead to the orbital splitting scheme in figure 5.6. In accordance with the theory developed by Mulliken<sup>15,16,17</sup> the transitions with significant oscillator

strength should be those that are z polarised, and they are indicated with arrows in picture 5.9. The lowest in energy transition, namely the e-a<sub>2</sub> orbital excitation, is allowed. However, it occurs with xy polarisation and should be comparatively weak since it does not benefit from the charge transfer term (we must highlight that in our case the symmetry group of the complex is C<sub>2v</sub>, which will slightly change the orbital energy levels).

	Abs 298 K <sup>a</sup>		Emi. 298 K <sup>a</sup>			Emi. 77 K <sup>a</sup>		Electrochem. <sup>c</sup>	
	λ (nm) <sup>a</sup>	ε (M <sup>-1</sup> cm <sup>-1</sup> )	λ (nm) <sup>c</sup>	τ (nsec) <sup>f</sup>	φ <sub>em</sub> <sup>h</sup>	λ (nm) <sup>e</sup>	τ (μsec)	E <sub>red</sub> (Volt)	E <sub>ox</sub> (Volt)
[Ru(tpy) <sub>2</sub> ] <sup>2+</sup>	474	10400	629	0.25	5*10 <sup>-6</sup>	598	8.9	1.67	0.92
[Ru(Δ <sup>2</sup> pyΔ <sup>2</sup> )(tpy)]	479.5	9800	701.5	77	5*10 <sup>-4</sup>	670	4.1	(1.38)	0.50
[Ru(Δ <sup>2</sup> pyΔ <sup>4</sup> )(tpy)]	480.5	8700	697.5	62	5*10 <sup>-4</sup>	662	4.2	(1.38)	0.49
[Ru(Δ <sup>4</sup> pyΔ <sup>4</sup> )(tpy)]	479	9900	692	70	5*10 <sup>-4</sup>	660	4.2	(1.35)	0.47
[Ru(H <sub>2</sub> (Δ <sup>2</sup> pyΔ <sup>2</sup> )(tpy)] <sup>2+</sup>	443	11450	—	—	—	620	—	—	0.80
[Ru(H <sub>2</sub> Δ <sup>2</sup> pyΔ <sup>4</sup> )(tpy)] <sup>2+</sup>	444	11250	—	—	—	620	7.5	(1.40)	0.75
[Ru(H <sub>2</sub> Δ <sup>4</sup> pyΔ <sup>4</sup> )(tpy)] <sup>2+</sup>	439	11300	—	—	—	610	—	—	0.75

**Table 2** a) Ethanol, b) Methanol, ethanol (1, 4), c) DMF vs. Fc/ Fc<sup>+</sup>, in briquette not reversible reductions d) Wavelength of the lowest energy absorption maximum e) Wavelength of highest energy emission feature f) Luminescence emission lifetime (± 10%) h) Luminescence quantum yield

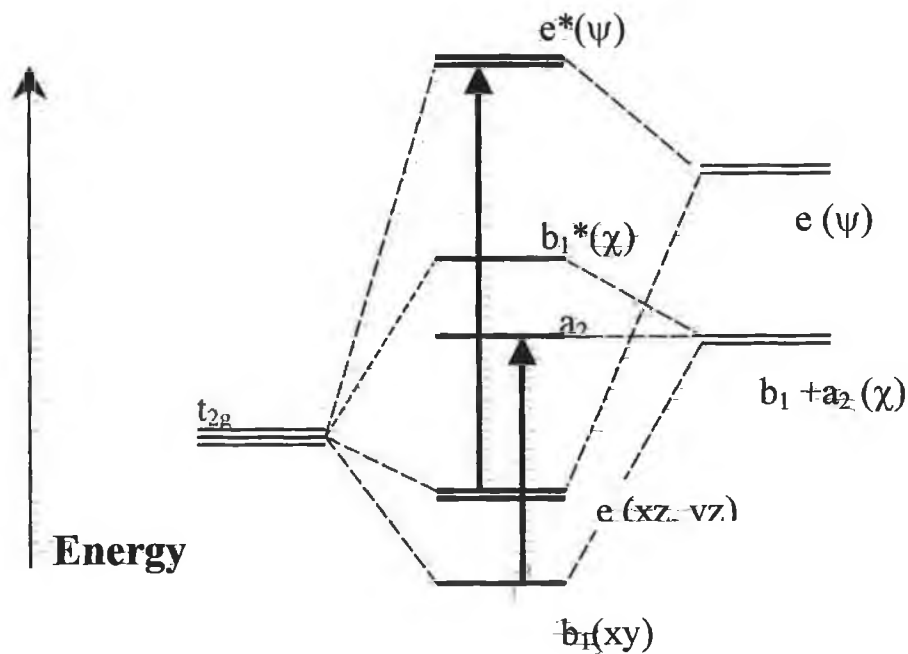


Figure 5.6 Schematic one-electron energy level diagram for  $[\text{Ru}(\text{tpy})_3]^{2+}$  symmetry  $D_{2d}$ . The  $x, y, z$  axis are chosen to lie along the  $C_2$  symmetry elements aligned so that the  $z$  axis passes through each ligand. Arrows indicate the  $z$ -polarised transition.

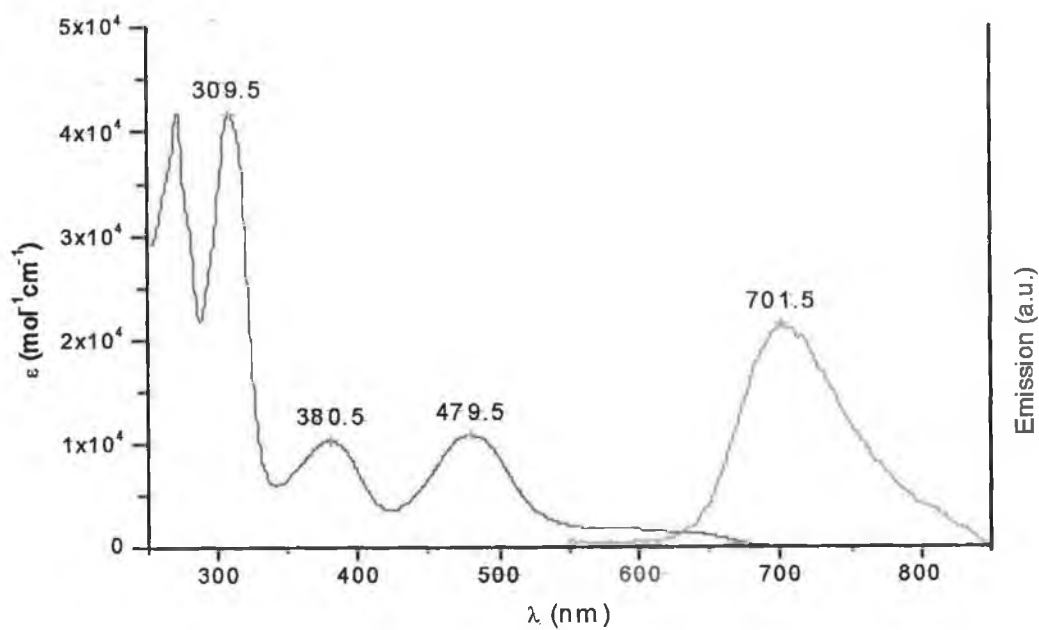


Figure 5.7 Absorption (black) and emission (red) spectra of  $[\text{Ru}(\Delta^2\text{py}\Delta^2)(\text{tpy})]$ , in ethanol.

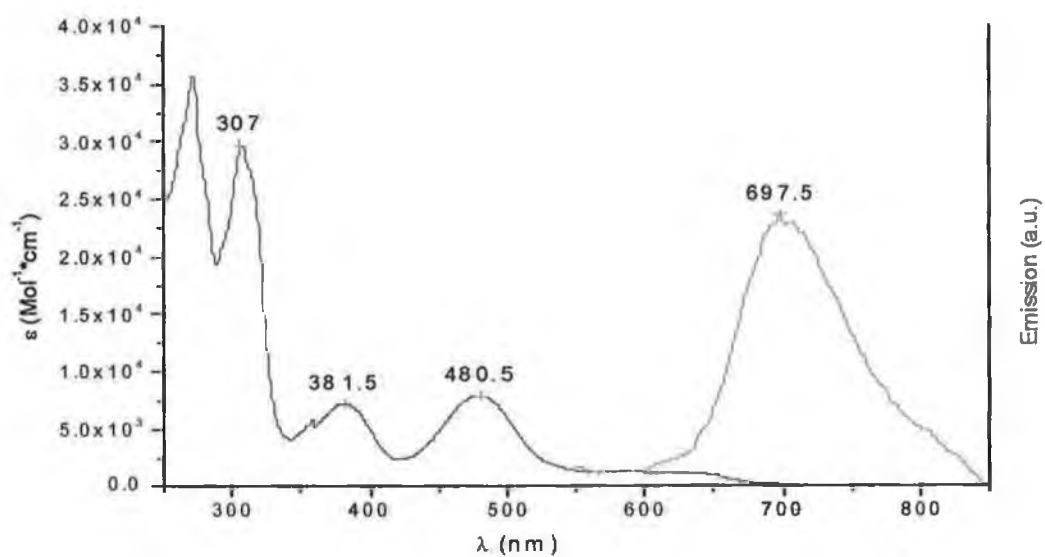


Figure 5.8 Absorption (black) and emission (red) spectra of  $[\text{Ru}(\Delta^2\text{py}\Delta^4)(\text{tpy})]$ , in ethanol solution.

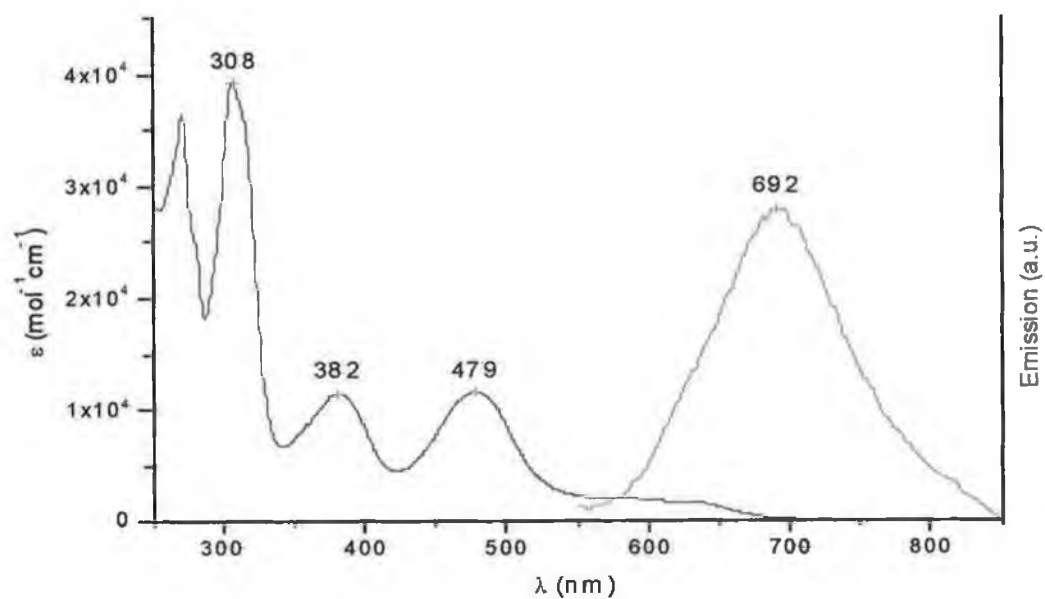


Figure 5.9 Absorption (black) and emission (red) spectra of  $[\text{Ru}(\Delta^4\text{py}\Delta^4)(\text{tpy})]$ , in ethanol.

When excited within the MLCT absorption bands at 298 K in a basic deaerated ethanol solution, the complexes exhibit quite a strong phosphorescence with a single band centred around 700 nm (table 2) and a lifetime around 60 nsec. The decrease in energy of the  $^3\text{MLCT}$  state, reflected by the red shifted emission in comparison with the emission of  $[\text{Ru}(\text{tpy})_2]^{2+}$  is probably due to the destabilisation of the  $t_{2g}$  metal orbital by the negative charges present on the ligand. This effect can be understood by considering the removal of one electron from the metal results in the formation of Ru(III) which withdraws electronic charge from the negative charged  $(\Delta\text{py}\Delta)^{2-}$  ligand destabilising the  $t_{2g}$  metal orbitals, similar results are obtained from the electrochemistry.

The protonation of one or both triazole rings results in a total quenching of the emission. The origin of the quenching of the luminescence of the protonated complexes is not clear. In many Ru(II) diimine complexes, a competing path for nonradiative relaxation is the thermally activated population of a  $^3\text{MC}$  energy to the  $^3\text{MLCT}$  state. In studies of the effects of protonation on the excited-state behaviour of  $[(\text{bpy})_2\text{Ru}(\text{CN})_2]$ , Scandola and co-worker postulated that protonation of the complex results in a decrease in the  $^3\text{MLCT}$ - $^3\text{MC}$  gap and a subsequent increase in the nonradiative relaxation rate. In the case of the  $(\Delta\text{py}\Delta)^{2-}$  complex, protonation results in an increase in the emission energy. The  $^3\text{MLCT}$  transition results from a Ru – tpy transition, while the  $^3\text{MC}$  state has its origin as a Ru( $t_{2g}$ ) – Ru( $e_g$ ) transition. Protonation of the complex results in a stabilisation of the ground state since  $\text{H}_2(\Delta\text{py}\Delta)$  is a weaker  $\sigma$ -donating ligand than  $(\Delta\text{py}\Delta)^{2-}$  and, assuming an averaged ligand field environment for both species, the Ru( $t_{2g}$ ) – Ru( $e_g$ ) energy should be larger for the deprotonated species. Thus both



changes in metal-ligand interaction which occurs upon protonation should serve to decrease the energy gap between the  $^3\text{MLCT}$  and  $^3\text{MC}$  states. It is reasonable that the decrease in the luminescence lifetime upon protonation of the ligand, complexes may result from facile internal conversion to  $^3\text{MC}$  state which rapidly relaxes to the ground state.

As we have seen in the previous chapter, the excited state acid base properties can differ significantly from those in the ground state. These acidity changes can be explained by the differences in electron distribution between the ground state and the excited state. The theoretical principles of the excited state acid base process have been described many times in the literature. In general protonation<sup>18,19,20</sup> will change the electronic levels in a particular molecule and this will naturally lead to changes electronic transitions. The excited state acid base properties of the compounds are therefore, most easily probed by absorption or emission spectroscopy. The excited state acidity of a compound can be evaluated using Forster cycle which is based exclusively on thermodynamic principles.

$$pk^*_a = pk_a + (0.625/RT) (\nu_{HB} - \nu_B) \quad (5.1.a)$$

Where  $k^*_a$  and  $k_a$  are the excited and ground state equilibrium constant,  $R$  the gas constant and  $T$  the absolute temperature, and  $\nu$  values are express in  $\text{cm}^{-1}$ . With this approach excited state  $pK_a$  values,  $pK_a^*$ , can be obtained from the ground state and spectroscopic parameters. Apart from the thermodynamics of the acid-base system, the kinetic aspects must also be considered. In the Forster

only thermodynamic and kinetic aspects are not included. However, if the species involved in the proton transfer does not emit then its excited state will be very short lived and an equilibrium between the species will not be established. Detailed kinetic analyses have been given elsewhere<sup>19</sup>.

When proton exchange is much faster than the excited state decay of both protonated and deprotonated species, non-equilibrium can be established in the excited state. Under those conditions meaningful results can be obtained from the Forster cycle.

$$pk^*_a = pH_i + (0.625/RT) (\tau_{HB} - \tau_B) \quad (5.1.b)$$

By monitoring the spectral changes as a function of pH in Robison & Britton buffer solution, titration curves were obtained (Fig. 5.10, 11,12) from which the ground state pKa values were obtained. The complex shows reversible behaviour in the pH range 2-9. Lowering the pH results in a blue shift of the MLCT band, which is probably due to stabilisation of the  $t_{2g}$  orbitals. Observed inflection points of the different species are listed in Table 5.3, they are obtained from a sigmoidal fit of the spectroscopic data.

In order to investigate the excited state acidity (Fig. 5.13, 5.14), emission titrations were carried out by excitation at the isobestic point taken from the ground state pKa titration. Unfortunately the pKa values obtained from the fit of the emission data were the same as the ground state and it was preferred report them as inflection point of the sigmoidal curve. The value obtained for absorption and emission titration were the same is because the lifetime of the mono or

diprotonated species excited states is too short and there was no equilibrium between the species in their excited states, as it has seen previously.

	<b>pKa(1)</b>	<b>pKa(2)</b>
<b>[Ru(<math>\Delta^2</math>py<math>\Delta^2</math>)(tpy)]</b>	2.2	5.2
<b>[Ru(<math>\Delta^2</math>py<math>\Delta^4</math>)(tpy)]</b>	2.7	5.2
<b>[Ru(<math>\Delta^4</math>py<math>\Delta^4</math>)(tpy)]</b>	2.8	5.8

**Table 5.3 Ground state pKa values of [Ru(tpy)( $\Delta$ py $\Delta$ )] isomers**

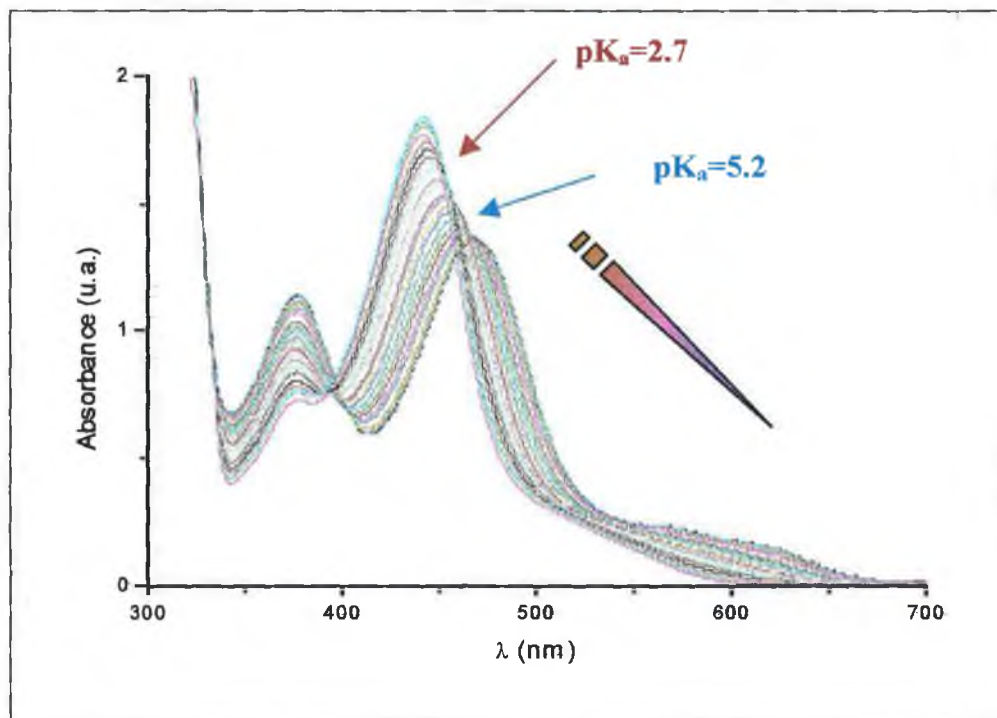


Figure 5.10 Absorption/pH dependence of  $[\text{Ru}(\text{tpy})(\Delta^2\text{py}\Delta^4)]$ , 2 to 9 pH.

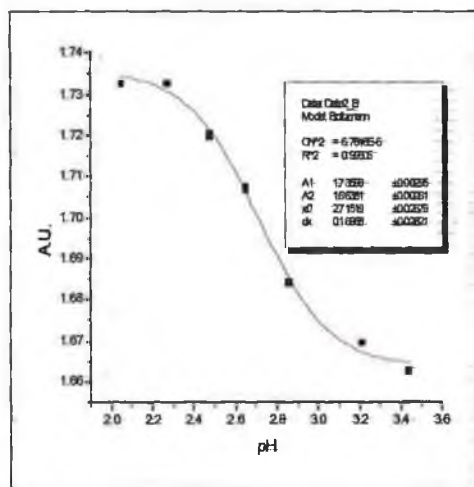


Figure 5.11 Sigmoidal fit of absorption/pH titration, wavelength 472 nm.

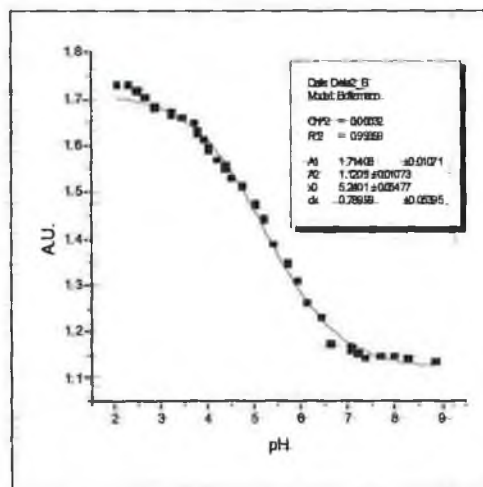


Figure 5.12 Sigmoidal fit of absorption/pH titration, wavelength 472 nm.

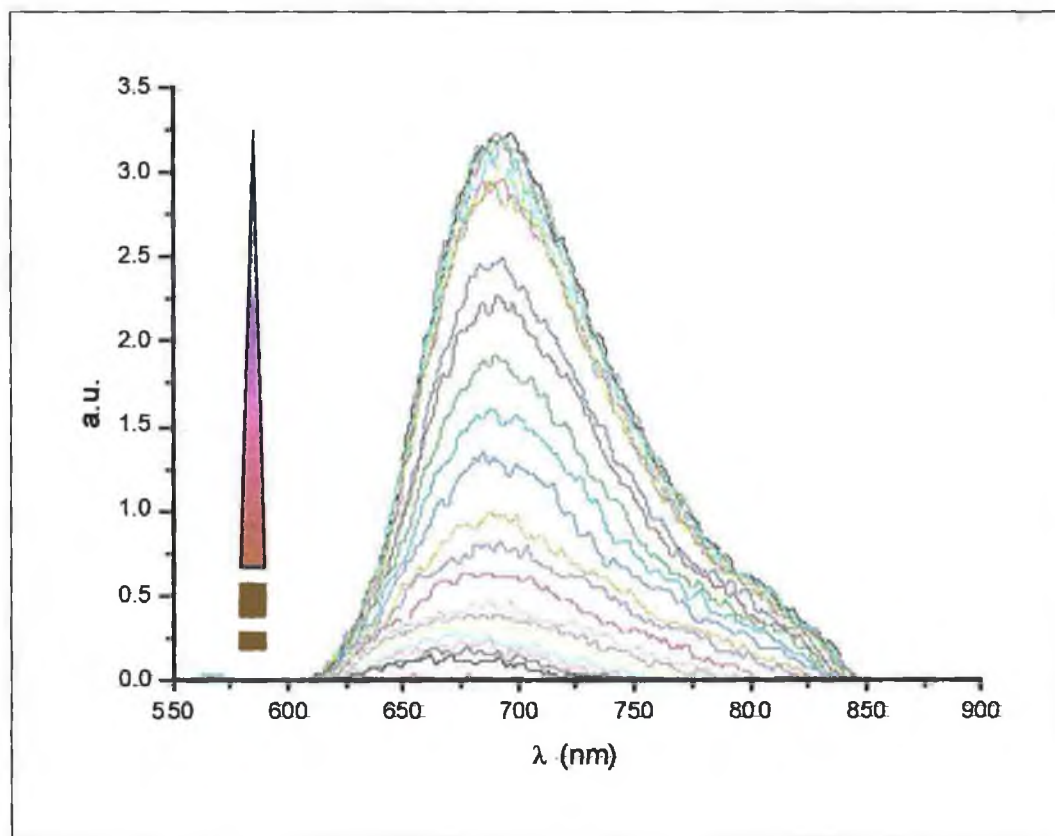


Figure 5.13 Emission/pH dependence of  $[\text{Ru}(\text{tpy})(\Delta^2\text{py}\Delta^4)]^+$ , from 2 to 9 pH units.

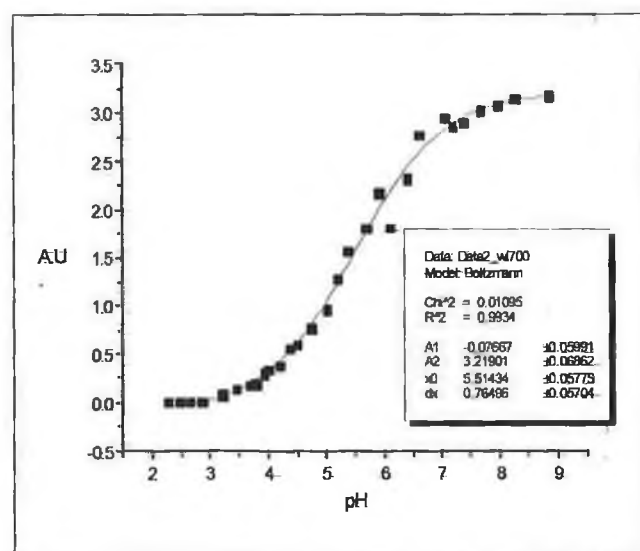


Figure 5.14 Sigmoidal fit of the fluorimetric titration, wavelength 700 nm.

## 5.5 Redox Properties and Spectroelectrochemistry

The oxidation and reduction potentials of the complexes are given in table 5.4. As discussed in the literature for the previous systems, a relationship is often present between the electrochemical potentials and the absorption and emission maxima. In a MLCT absorption process, an electron is removed from the d orbital ( $d\pi$ ) to an empty orbital of the ligand ( $\pi^*$ ). Oxidation is also removal of an electron from the d orbitals and in the case of reductions, the electron is transferred to the LUMO (tpy) of the complex. By determining the nature of the LUMO with the electrochemical measurements, it is possible to assign on which ligand is the emitting state based. By comparison of (tpy) based Ru(II) complexes<sup>21,22,23</sup> the first not reversible reduction potential for these mixed ligand complexes are terpyridine based, the  $\pi^*$  levels of the terpyridine are expected to be much lower than those of the  $(\Delta\text{py}\Delta)^{2-}$  ligand.

The oxidation potentials of the neutral isomers are significantly lower than that of  $[\text{Ru}(\text{tpy})_2]^{2+}$ , which indicates that the  $[(\Delta\text{py}\Delta)]^{2-}$  ligand is a much stronger  $\sigma$  donor ligand than tpy, in the diprotonated species the potentials become slightly lower than the tpy complex. Oxidation and reduction potentials have shown to be solvent dependent. (Table 5.2 and 5.5)

The utility of spectroelectrochemistry in the study of the electrochemically generated reduction products of the  $d^6$  polypyridyl complexes has previously been demonstrated.<sup>24,25</sup> Usually the UV-visible spectrum of the reduced form of the appropriate homoleptic complex provides a model spectrum for a particular ligand anion in a mixed ligand complex. In the case of  $[\text{Ru}(\text{tpy})_2]^{2+}$ , it was found that two

strong absorption bands grow in when an electron is added. One has a maximum at around 340 nm. and has been assigned as a  $\pi$ - $\pi^*$  transition from the highest completely filled LUMO( $\pi_6$ ) to the half filled HOMO( $\pi_7$ ) of the tpy anion.<sup>26,27</sup>

Another more structured absorption appears near 525 nm. and has been assigned as a  $\pi^*$ - $\pi^*$  transition ( $\pi_7$ - $\pi_{10}$ ) of tpy<sup>-</sup>. Two other less intense bands are resolved. One appears as pronounced shoulder at 625 nm. In the spectrum of [Ru(tpy)<sub>2</sub>]<sup>+</sup>, and it shift to 665 nm on further reduction. A second barely resolved band is observed between 420 and 450 nm. in the [Ru(tpy)<sub>2</sub>]<sup>+</sup> and [Ru(tpy)<sub>2</sub>] spectra. Two similar features are observed in the spectrum of singly and doubly reduced [Os(tpy)<sub>2</sub>]<sup>2+</sup>.

The spectroelectrochemistry data are shown in figure 5.15 and 5.16. Electrogeneration of one electron oxidised form is possible with more than 95% regeneration of the original oxidation state. In the oxidative spectroelectrochemistry of [Ru(tpy)( $\Delta$ py $\Delta$ )] the ruthenium to tpy <sup>3</sup>MLCT transitions are completely lost upon the one oxidation of the Ru(II) centre, as observed for other Ru-tpy complexes.<sup>28</sup>

Electrogeneration of one electron reduced form is irreversible, the spectrum is not easy to interpret since it virtually tracks the spectrum of the [Ru H( $\Delta$ py $\Delta$ )(tpy)]<sup>+</sup>. Therefore it is evidence that the tpy ligand reduction is followed by reaction of the negatively charged molecule with the solvent, through an irreversible process.

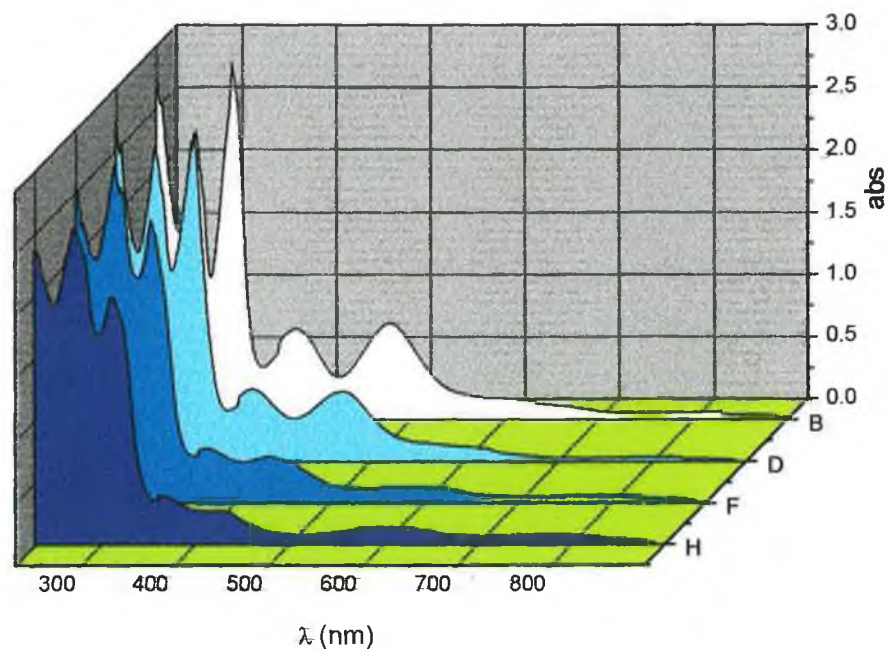


Figure 5.15 Near-UV-visible spectra of [Ru(tpy)(ΔpyΔ)] (B) and [Ru(tpy)(ΔpyΔ)]<sup>+</sup> (H) recorded at 0 (B), 0.7 (D), 1 (F), 1 Volt (H), in acetonitrile containing 0.5 M TBAH.

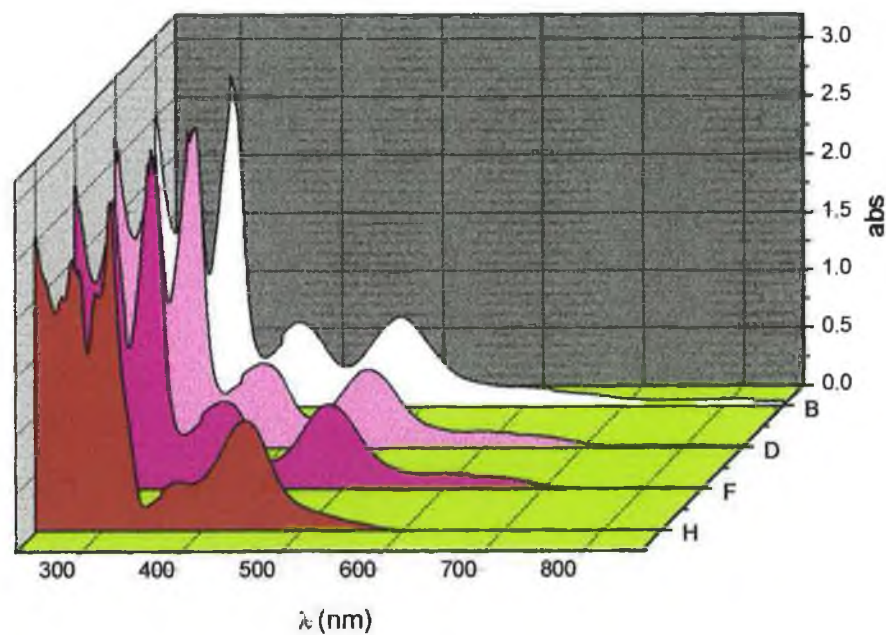


Figure 5.16 Near-UV-visible spectra of [Ru(tpy)(ΔpyΔ)] (B) and [Ru(tpy)(ΔpyΔ)]<sup>-</sup> (H) recorded at 0 (B), -1 (D), -1.4 (F), 1.5 Volt (H), in acetonitrile containing 0.5 M TBAH.



## 5.6 Lifetime temperature dependence

The emission lifetime of the excited state obtained for the [Ru( $\Delta$ py $\Delta$ )(tpy)] species represents an increase by 2 order of magnitude with respect to [Ru(terpy)<sub>2</sub>]<sup>2+</sup> (Tab. 5.2). It is, therefore, clear that the use of the ligand dramatically extends the lifetime of the <sup>3</sup>MLCT excited states of the Ru(II)(tpy) complex. This is likely to originate from the raising of the <sup>3</sup>MC states following the replacement of the weak field terpyridine ligand by a strong field ligand.

In order to investigate the increase of the ligand field, low temperature excited state lifetime measurements were made. As we have seen in the introduction, the decay of an excited state takes place by competitive radiative and not radiative processes.

In general, the changes in the (1/ $\tau$ ) vs. 1/T plot (Fig. 5.18) over a large temperature range can be accounted for by the coming into play of additional contributions to the radiationless decay process of the emitting excited states as the temperature increases:

$$1/\tau = k_0 + \sum_i k_i \quad (5.2)$$

In equation 5.2,  $k_0$  is a temperature independent term and  $k_i$  is the rate constant of the step which contributes to the decay process. Previous studies have shown that the  $k_i$  terms can be either in the form of an Arrhenius equation (5.3)<sup>29,30,31,32,33</sup>:

$$k_i = A_i \exp(-\Delta E_i/RT) \quad (5.3)$$

where  $A_i$  is a frequency factor and  $\Delta E_i$  an activation energy, or an empirical equation(5.4)<sup>34,35,36,37</sup>:

$$k_i = B_i / \{1 + \exp[C_i(1/T - 1/T_{Bi})]\} \quad (5.4)$$

This describes a stepwise behaviour centred around a certain temperature  $T_{Bi}$ . In equation 5.4  $C_i$  is temperature related to the step smoothness, and  $B_i$  is the value assigned  $k_i$  when  $T \gg T_{Bi}$ . The method by which eq. 5.4 may be derived is given in the reference<sup>38</sup>.

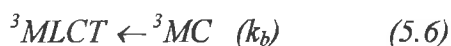
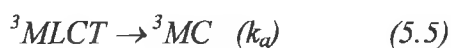
The temperature dependence of the emission lifetime of  $[\text{Ru}(\Delta\text{py}\Delta)(\text{tpy})]$  in a mixture of deareted butyrronitrile-ethanol (5:4) solution can be accounted for by two Arrhenius terms (equation 5.3) and one stepwise term (equation 5.4). The kinetic parameters derived from the fitting of equation 5.2 to the experimental results of figure 5.18 are shown in table 5.5. The stepwise term o,  $T_{Bi}=137.5$  K,  $A_i=8.7 * 10^4 \text{ sec}^{-1}$ , corresponds to the red shift observed in the emission spectra of the complex in the range 120-150 K (Figure 5.19, 20) and is thought to be associated with a relaxation of the Ru-N co-ordinates or small solvent molecule rearrangements (table 3). The second little red shift observed for the emission spectra in the range of 150-170 K, (Fig. 5.19) is thought to be associated with the reorientation of the solvent molecules<sup>40</sup>, which can only take place when the solvent has acquired the properties of nonviscous fluid.

Hence, two Arrhenius terms are needed to fit the temperature dependence. The equivalent Arrhenius terms have been obtained by fitting the value under 120

K and above 140 K separately, these values lie in the vicinity of the melting point of the solvent matrix, and this ensures that the term has an intramolecular origin.

By analogy with previous studies on ruthenium polypyridine complexes, which term is thought to concern the thermal equilibration of different  $^3\text{MLCT}$  levels, spaced by  $500\text{ cm}^{-1}$ , this occurs since, under the  $C_{2v}$  symmetry of the  $\text{Ru}(\text{tpy})(\Delta\text{py}\Delta)$  complex, the  $\pi_m(\text{t}_2\text{g})$  octahedral orbitals split into  $a_1$ ,  $b_1$  and  $b_2$  and the  $\pi^*$  tpy orbital belongs to the  $b_1$  symmetry. From the overlap between the  $b_1$  metal and ligand orbitals, first order bonding and antibonding orbitals are obtained. The low energy  $^3\text{MLCT}$  excited states are obtained by promoting an electron from the  $b_1$  bonding and  $a_1$  and  $b_2$  non-bonded metal orbitals to the  $b_1$  antibonding ligand orbital. Their symmetry is hence  $A_1$ ,  $B_1$  and  $A_2$  respectively with triplet multiplicity. The  $^3A_1$  state deriving from the transition between bonding and antibonding orbitals will lie at higher energy than the others.

As the temperature increases ( $T > 250$ ) a second Arrhenius term is needed. There is a general agreement in the literature that the temperature dependence (at high temperature) of the emission lifetime in ruthenium polypyridine complexes (Figure 5.17), on a activated surface, is related to energy crossing from a  $^3\text{MLCT}$  manifold to a  $^3\text{MC}$ (metal centred) level.



The MC level undergoes photochemical and a photophysical deactivation (eq 5.7).



$k_c$  is the sum of all the rate constants of the possible deactivation processes that can deactivate the  ${}^3\text{MC}$  states. As pointed out by Meyer and co-workers<sup>39</sup>, the experimental deactivation rate constant that comes into play at high temperatures can be expressed as follows,

$$k_2 = A_2 \exp(-\Delta E_2/RT) \quad (5.8)$$

or kinetically as

$$k_2 = k_a [k_c / (k_b + k_c)] \quad (5.9)$$

the equation can describe two limiting cases, as described by Balzani et al<sup>34</sup>.

(i) when  $k_c \gg k_b$  the decay of the  ${}^3\text{MC}$  is rapid  $k_2 = k_a$ . It follows that:

$$A_2 \exp(-\Delta E_2/RT) = A_a \exp(-\Delta E_a/RT) \quad (5.10)$$

In this limit,  $A_2$  and  $\Delta E_2$  are parameters obtained from the fit corresponding to the pre-exponential factor and the activation energy for the  ${}^3\text{MLCT}$  to  ${}^3\text{MC}$  surface crossing, Fig. 5.18

(ii) When  $k_b \gg k_c$ , the decay of  ${}^3\text{MC}$  is slow compared to the back surface crossing to  ${}^3\text{MLCT}$ . In such a case, the two states are in equilibrium and the equation becomes:

$k_2 = (k_a / k_b) k_c$ . Since :

$$k_a / k_b = k_c \exp(-\Delta E/RT) \exp(-\Delta S/R) \quad (5.11)$$

Where  $\Delta E$  and  $\Delta S$  are the internal energy and entropy differences between the  $^3\text{MLCT}$  and  $^3\text{MC}$ . Neglecting the expected small entropic term, it becomes possible to write the following equation:

$$A_2 \exp(-\Delta E_2/RT) = k_c \exp(-\Delta E/RT) \quad (5.12)$$

The meaning of the experimental quantities  $A_2$  and  $\Delta E_2$  depends on the nature of the processes that contribute to  $k_c$ . The following limiting cases are of interest

(ii-1)

When the major contribution to  $k_c$  comes from a chemical reaction or the deactivation processes of the  $^3\text{MC}$  an Arrhenius type equation is employed.

$$A_2 \exp(-\Delta E_2/RT) = A_c \exp(-\Delta E_c + \Delta E/RT) \quad (5.13)$$

The  $A_2$  and  $\Delta E_2$  parameters obtained will correspond to the pre-exponential factor of the decay processes of the  $^3\text{MC}$  and to the sum of the MC-MLCT energy gap and the activation energy.

(ii-2)

When the main contribution to  $k_c$  comes from a non-activated process,  $A_2$  will correspond to the rate of the non-activated process ( $k'_c$ ), and the activation energy

$\Delta E_2$  may correspond either to the energy gap between  $^3\text{MLCT}$  and  $^3\text{MC}$  or the distance between the  $^3\text{MLCT}$  level and the crossing point of the two surfaces. For complexes of the same family the  $\Delta E_2$  data have probably the same meaning and the energy gap between the minimum energy of the  $^3\text{MLCT}$  level and the  $^3\text{MC}$  level is most likely related to the distance between the  $^3\text{MLCT}$  level and the crossing point of the two surfaces.

In principle it can be expected that  $A_2$  in the first and second cases are high frequency ( $10^{13}$ - $10^{14}$   $\text{sec}^{-1}$ ) vibrations whose activation leads to the  $^3\text{MLCT}$ - $^3\text{MC}$  surface crossing region ( Fig 5.17 i and ii-1). By contrast, in the third case,  $A_2$  can be much smaller because it represents the rate constant of a radiationless transition having a poor Frank-Condon Factor.

The  $A_2$  and  $\Delta E_2$  values for the  $\text{Ru}(\Delta\text{py}\Delta)(\text{tpy})$  isomers, Table 5.4, could suggest that they are borderline cases between the type (ii-b) and the type (i), in fact the  $A_2$  factors are quite small to correspond to a frequency factors of a surface crossing process. Other examples of such limiting are reported in the literature<sup>37</sup>. It is interesting to notice how the parameters obtained from the different isomers result quite close, even closer than the ones obtained for the analogous bpy complexes,  $[\text{Ru}(\text{bpy})_2(\Delta^2\text{py})]^+$  and  $[\text{Ru}(\text{bpy})_2(\Delta^4\text{py})]^+$ .

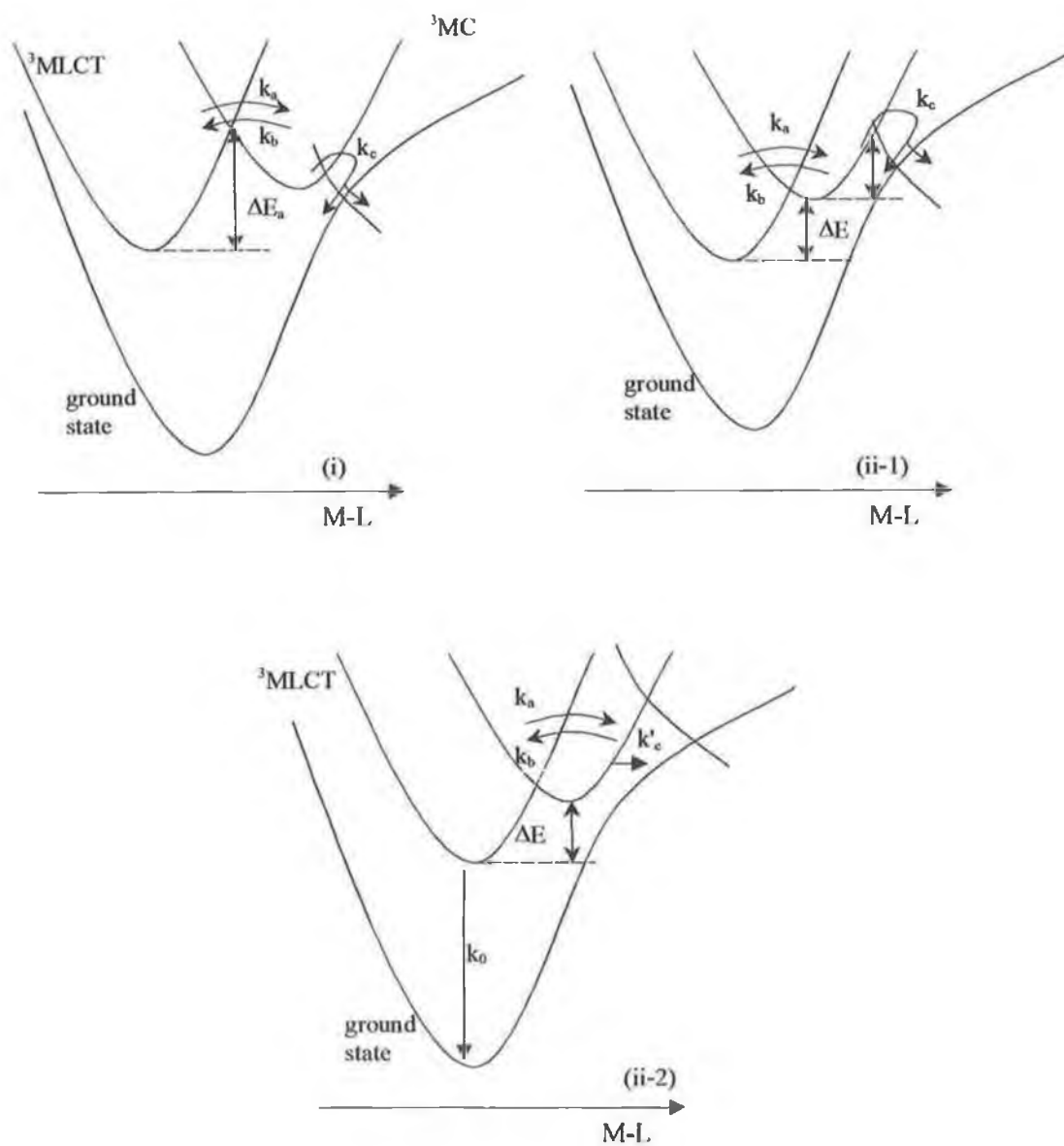
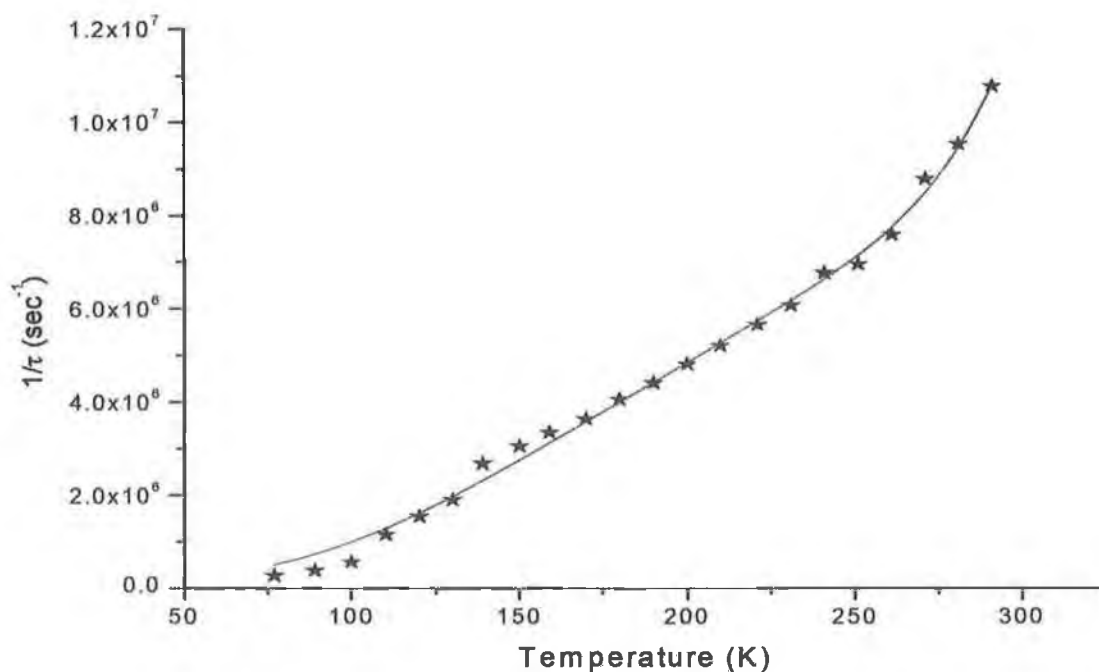


Figure 5.17 Schematic representation of the situation of the potential energy surfaces for the three limiting cases described in the text.

	$k_0$ ( $\text{sec}^{-1}$ )	$k_1$ ( $\text{sec}^{-1}$ )	$\Delta E_1$ ( $\text{cm}^{-1}$ )	$k_2$ ( $\text{sec}^{-1}$ )	$\Delta E_2$ ( $\text{cm}^{-1}$ )
$[\text{Ru}(\Delta^2\text{py}\Delta^2)(\text{tpy})]$	$2.2 \times 10^5$	$2.6 \times 10^7$	520	$2 \times 10^{12}$	2730
$[\text{Ru}(\Delta^2\text{py}\Delta^4)(\text{tpy})]$	$2.1 \times 10^5$	$2.2 \times 10^7$	439	$2 \times 10^{12}$	2700
$[\text{Ru}(\Delta^4\text{py}\Delta^4)(\text{tpy})]$	$2.2 \times 10^5$	$2.6 \times 10^7$	540	$1.9 \times 10^{12}$	2750

**Table 5.4 Kinetic parameters for excited state decay obtained from the fitting of equation (5.2) to the experimental results**



**Figure 5.18 Plot of  $1/\tau$  vs T of  $[\text{Ru}(\text{tpy})(\Delta^2\text{py}\Delta^4)]$ . Curve fit in according to equation 5.2.**



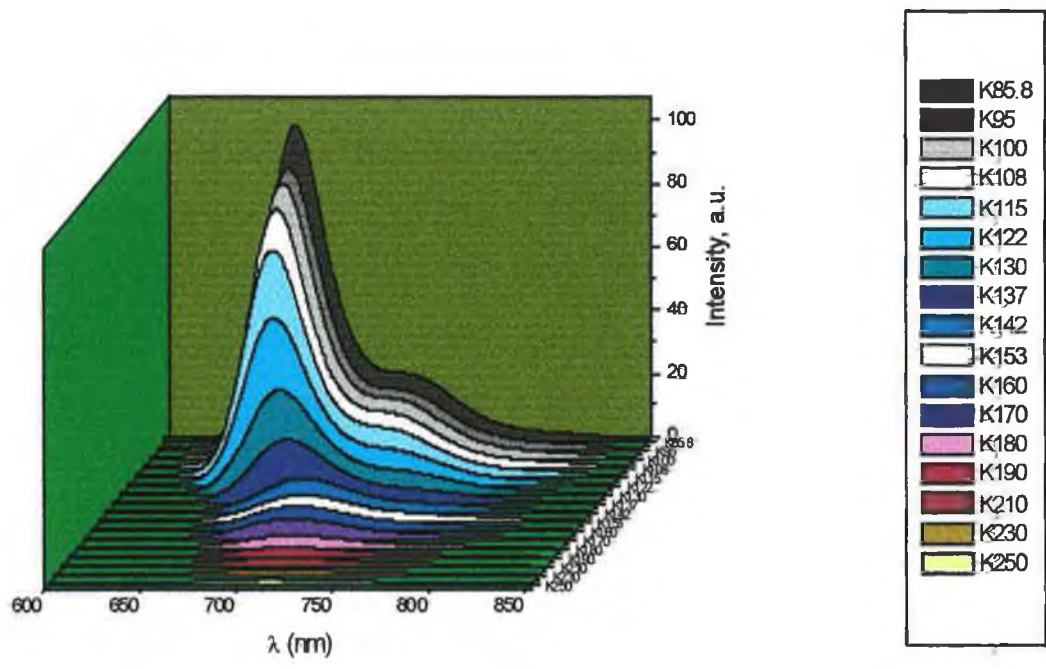


Figure 5.19 Shift of the emission band maximum as a function of the temperature for  $[\text{Ru}(\text{tpy})(\Delta^2\text{py}\Delta^4)]$

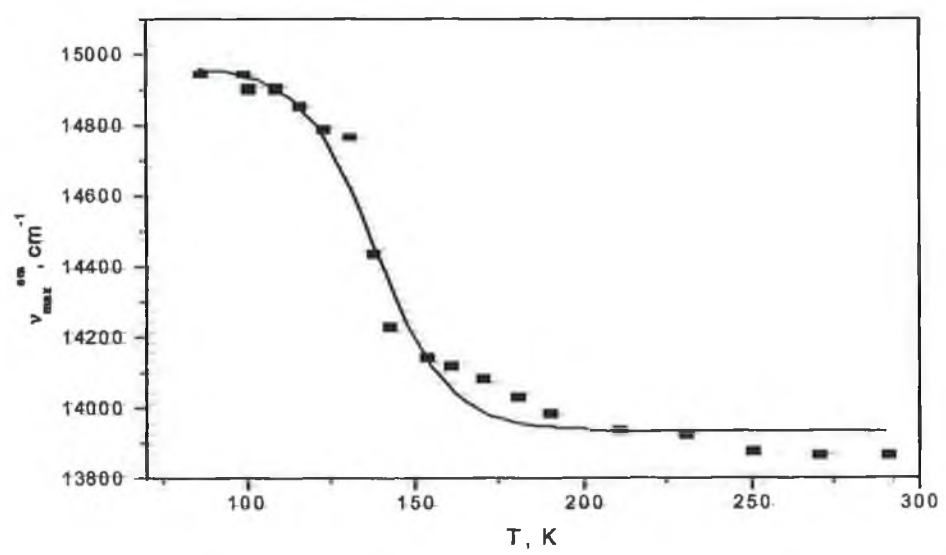


Figure 5.20 Schematic diagram showing the shift of the emission band maximum as a function of the temperature for  $[\text{Ru}(\text{tpy})(\Delta^2\text{py}\Delta^4)]$

## 5.7 Solute Solvent Interaction

[Ru(tpy)( $\Delta$ py $\Delta$ )] exhibits a pronounced solvatochromic behaviour. The absorption spectra in water, ethanol, DMF and acetonitrile are shown in picture 5.22. For these and other solvents, the energies of the lowest energy absorption band maximum  $\lambda_{\max}^{\text{abs}}$  (298 K), are collated in table 5.5. This behaviour is similar, but not as compelling as, what is observed for [Ru(tpy)CN<sub>3</sub>]<sup>-</sup>.<sup>40</sup>

Solvent (Acceptor number)	$\nu_{\max}^{\text{abs}}$ cm <sup>-1</sup>	$\nu_{\max}^{\text{em}}$ cm <sup>-1</sup>	$\tau$ ns	$\tau^{\text{a}}$ $\mu$ s	$E^{0-0}$ cm <sup>-1</sup> (eV)	$E_{1/2}$ V	$*E_{1/2}$ (eV)
	(298 K)	(298 K)	(298 K)	(84 K)			
<b>Water</b> (54.8)	21186	14450	55	4	15150		
<b>Methanol</b> (41.3)	21119	14415	60		15083 (1.87)	0.60	-1.28
<b>Ethanol</b> (37.1)	20812	14267	63	3.8	15080	0.58	
<b>Dichloromethane</b> (20.4)	20661	13531	70		14947		
<b>Acetonitrile</b> (19.3)	20492	13453	75		14947		
<b>DMSO</b> (19.3)	20243	13480	75		14903		
<b>DMF</b> (16.0)	20202	13292	82	2.5	14771 (1.83)	0.49	-1.31
<b>Pyridine</b> (14.2)	20202	13271	88		14749		
<b>Acetone</b> (12.5)	20202	13239	70		14620		
<b>THF</b> ( 8.0)	20202	13192	63		14450		

Table 5.5 Spectroscopic, photophysical and redox properties of [Ru(tpy)( $\Delta$ py $\Delta$ )] in different solvents. a) the data are collected from the frozen matrix referred in picture 5.24.

Specific solute-solvent interactions are known to play an important role in optical and thermal electron transfer involving transition metal complexes. These interactions can influence both spectroscopic energies, because of the relative abundance of the isomer [Ru(tpy)( $\Delta^2$ py $\Delta^4$ )] on comparison with the other two isomers, the following measurements were made only on it.

Dielectric continuum theory provides a starting point for analysis of this data. It has been successfully applied to solvent shifts or MLCT absorption bands in polypyridyl complexes<sup>41</sup>. This theory predicts that correlation should exist between band energies and solvent dielectric functions whose forms depend upon the assumption made in modelling the charge transfer process.<sup>42</sup> In the classical limit, the energies of absorption ( $E_{abs}$ ) and Emission ( $E_{em}$ ) are related to the internal energy charge,  $\Delta E^0$ , and re-organisational energies ( $\chi$ ) as shown in eqs 5.14 and 5.15.

$$E_{abs} = \Delta E^0 + \chi = \Delta E^0 + \chi_i + \chi_0 \quad (5.14)$$

$$E_{em} = \Delta E^0 - \chi = \Delta E^0 - \chi_i - \chi_0 \quad (5.15)$$

$\chi_i$  and  $\chi_0$  are intramolecular and solvent reorganisational energies, respectively. These simple relationships are exact only for Gaussian band shapes. They also assume equal force constants (quantum spacing) in the initial and final states for the vibrations and solvent vibrations coupled to transitions. With unequal quantum spacing the re-organisational energy of the excited state above the ground state ( $\chi_{es}$ ) and of the ground state below the excited state ( $\chi_{gs}$ ) are unequal.



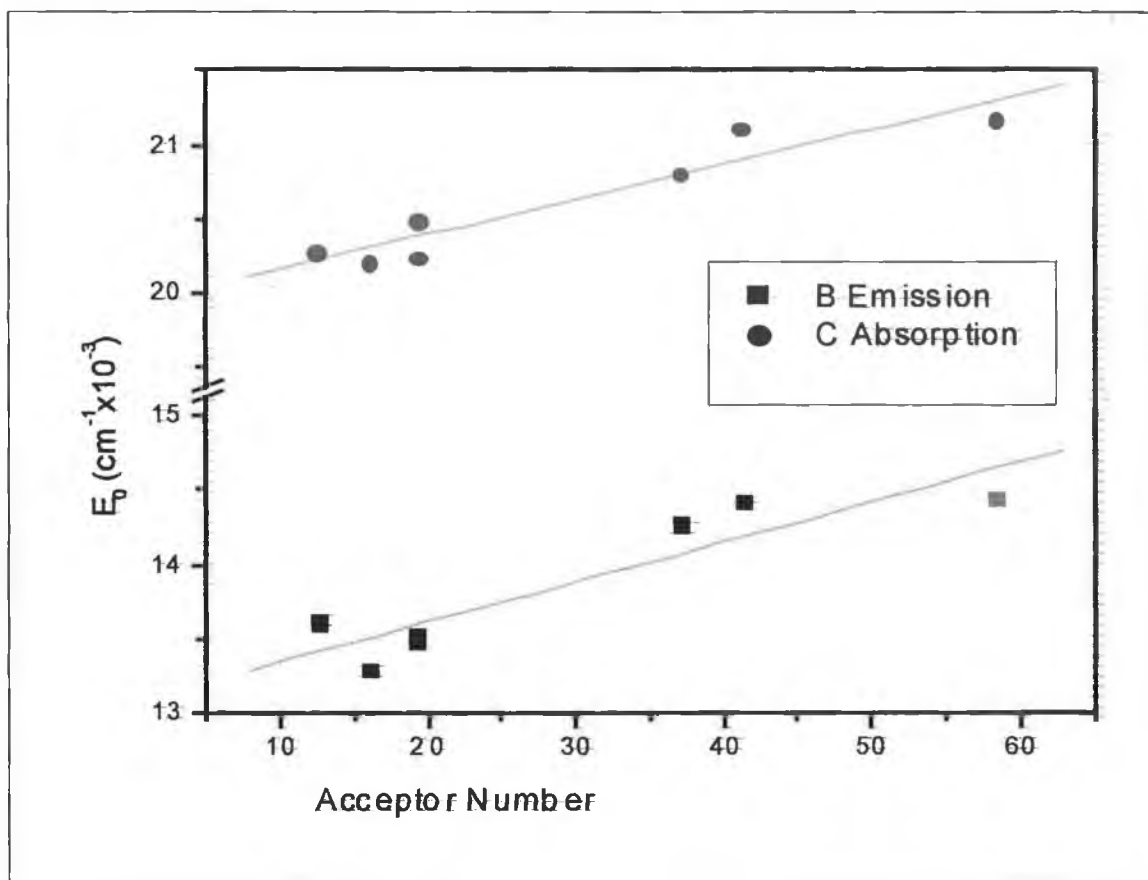


Figure 5.21 Variations in  $E_{\text{abs}}$  (red dots) and  $E_{\text{em}}$  (black squares) with acceptor number for the complex. Slopes, intercepts and correlation coefficients are listed in Table 5.6.

$\text{Ru}(\text{tpy})(\Delta^2\text{py}\Delta^4)$		
$E_{\text{abs}}(\text{MLCT})$	slope	$23.52 \pm 0.00354$
	intercept	$19.93473 \pm 0.11701$
	$R^2$	0.94776
$E_{\text{em}}$	slope	$26.93 \pm 0.00521$
	intercept	$13.07708 \pm 0.17228$
	$R^2$	0.91774

Table 5.6 Fitting parameters from correlation with acceptor number, slopes, intercepts and correlation coefficients were calculated from linear regression between the quantities indicated and the acceptor number. The slopes are in  $\text{cm}^{-1}/\text{acceptor number}$  unit.

In the classical limit with  $\hbar\omega \neq \hbar\omega'$  and  $\Delta\omega = |\omega - \omega'| \ll \omega, \omega'$ , the energy quantities in the equations 5.17, 18 are the free energies of the excited state above the ground state,  $\Delta G_{es}^0$ , giving eqs(5.18, 20);  $\Delta G_{es}^0$  is equal to the 0-0 energy,  $E_{0-0}$ , in this limit. If the excited and ground states are approximated as dipoles in a sphere and the solvent as a dielectric continuum, the solvent dependent parts of  $E_{abs}$  ( $E_{abs,s}$ ) and  $E_{em}$  ( $E_{em,s}$ ) are given by equations 5.19, 20.<sup>43,44</sup>

$$E_{abs,s} = \frac{1}{a^3} \left[ 2\vec{\mu}_g (\vec{\mu}_g - \vec{\mu}_e) \left( \frac{D_s - 1}{2D_s + 1} \right) - 2\vec{\mu}_g (\vec{\mu}_g - \vec{\mu}_e)^2 \left( \frac{D_{op} - 1}{2D_{op} + 1} \right) \right] \quad (5.19)$$

$$E_{em,s} = \frac{1}{a^3} \left[ 2\vec{\mu}_g (\vec{\mu}_g - \vec{\mu}_e) \left( \frac{D_s - 1}{2D_s + 1} \right) + 2\vec{\mu}_g (\vec{\mu}_g - \vec{\mu}_e)^2 \left( \frac{D_{op} - 1}{2D_{op} + 1} \right) \right] \quad (5.20)$$

$E_{abs}$  is the sum of the solvent-dependent part of  $\Delta G_{es}^0$  ( $\Delta G_{es,s}^0$ ) and  $\chi_{0,es}$ .  $E_{em,s}$  is the difference between  $\Delta G_{es,s}^0$  and  $\chi_{0,gs}$ . In these expressions,  $\vec{\mu}_g$  and  $\vec{\mu}_e$  are the vector dipole moments of the ground and excited states,  $a$  is the radius of the effective spherical cavity enclosing the dipoles, and  $D_{op}$ , equal to the square of the medium refractive index, and  $D_s$  are the optical and static dielectric constants of the solvent. The internal dielectric constants of the solute and reference medium are taken to be one. A more elaborate treatment has been developed by McRae which includes repolarisation solvent, solute, dipole solvent induced dipole, and solute dipole solvent dipole interactions as well as mixing with the other electronic transitions within the solute. Because of the difficulty in calculating individual terms, McRae presented the empirical function in equation (5.21)<sup>45</sup> in

which A, B and C are constants characteristic of the solute and  $L_0$  is the characteristic constant of the solvent

$$E_{abs,s} = (AL_0 + B) \left( \frac{D_{op} - 1}{2D_{op} + 1} \right) + C \left( \frac{D_s - 1}{D_s + 2} + \frac{D_{op} - 1}{D_{op} + 2} \right) \quad (5.21)$$

Attempts to find reasonable correlations between  $E_{abs}$  and any of these dielectric functions were unsuccessful, instead statistically reasonable correlations ( $R^2 > 0.90$ ) were found to exist with Gutmann's acceptor number (AN)<sup>46</sup>, Fig. . The slopes and the intercepts derived from the correlation are listed in tab 5.6.

The universal dependence of the various experimental and derived quantities on acceptor number is striking. The acceptor number dependence can be explained by invoking simple bonding arguments. They assume that specific donor acceptor electronic interaction exists between individual solvent molecules and that the lone pair of electrons centred primarily on nitrogen atoms of the triazole rings. Electron pair donation to the solvent makes the ligand a better  $\pi$  acceptor increasingly so as the acceptor number increases.

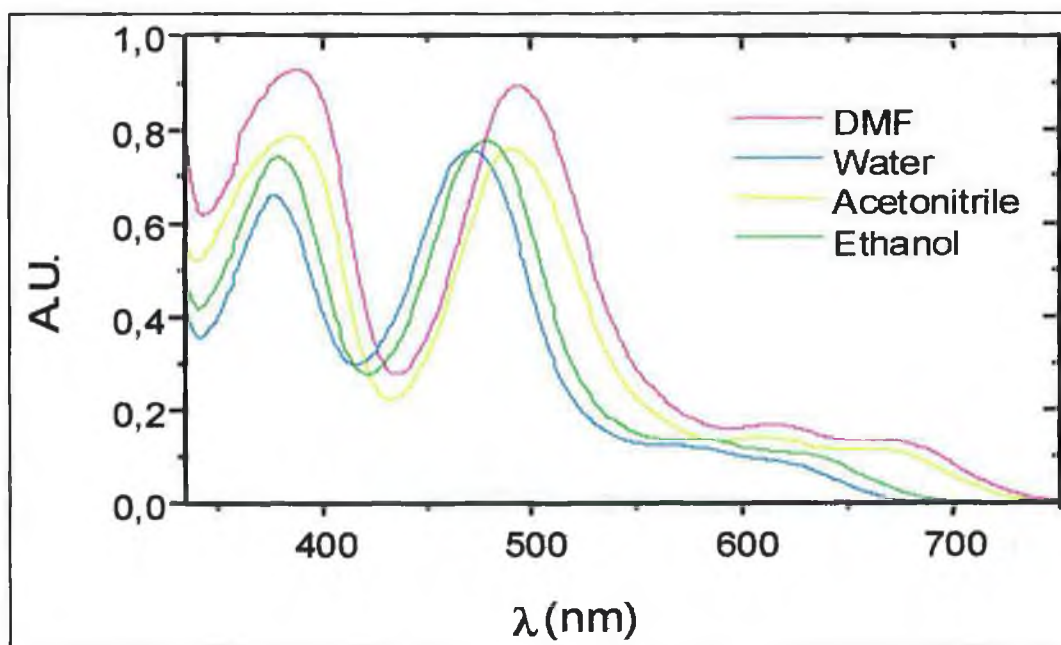


Figure 5.22 Solvent dependency of the  $[\text{Ru}(\text{tpy})(\Delta^2\text{py}\Delta^4)]$  absorption spectra at 298 K.

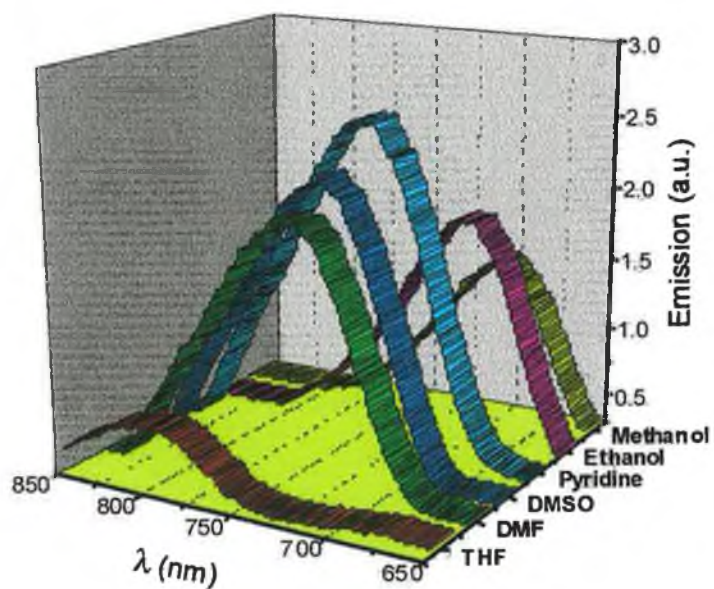
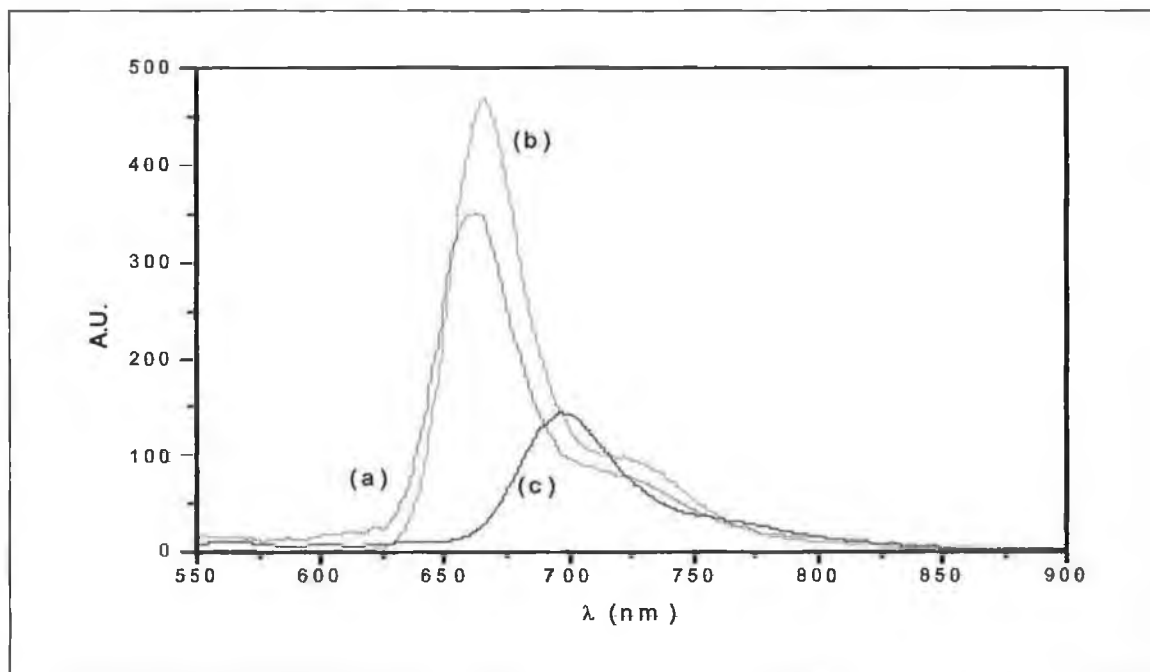


Figure 5.23 Solvent dependency of the  $[\text{Ru}(\text{tpy})(\Delta^2\text{py}\Delta^4)]$  emission spectra at 298 K.





**Figure 5.24** Solvent dependence of the emission spectra of  $[\text{Ru}(\text{tpy})(\Delta^2\text{py}\Delta^4)]$  at 77 K; <sup>a</sup> 9 M LiCl glass. <sup>b</sup> EtOH:MeOH (4:1) glass. <sup>c</sup> DMF:CH<sub>2</sub>Cl<sub>2</sub> (9:1) glass

The plot of lifetimes of  $[\text{Ru}(\Delta^2\text{py}\Delta^4)(\text{tpy})]$  emission in various solvents, at room temperature against the solvent acceptor number or the related excited state energy, has a rather bi-phasic shape (Fig. 5.25, 26): the longer lifetime is found (86 ns) in pyridine, and the lifetime of the excited state drops increasing or decreasing the acceptor number of the solvent or the relative emission energies. This behaviour can be interpreted using the previously outlined energy scheme (Figure 5.17, (ii-2)). The emitting <sup>3</sup>MLCT state deactivates along two main competing channels: (1) direct radiationless transition to the ground state ( $k_r, kn_r$ ) and (2) conversion to the lowest metal centred <sup>3</sup>MC excited state and from there, to the ground state ( $k_d$ ).

$$\frac{1}{\tau} = (k'_0 + k''_0) + k' e^{-\frac{\Delta E_a}{RT}} \quad (5.22)$$

$k'_0$  is not expected to be sensitive to  $^3\text{MLCT}$  energy change, see table 5.8. The other two channels are expected to be sensitive to changes in the energy of the  $^3\text{MLCT}$ . The term  $k^{nr}_0$  in equation 4.22 represents *the energy gap law*, which predicts an exponential decrease in deactivation rate with corresponding increase of the MLCT energy.

$$k_0^{nr} = k_{0,0}^{nr} e^{-\alpha E_{\text{MLCT}}} \quad (5.23)$$

In the third term  $\Delta E_a$  represents the energy gap between the MLCT and the MC states, and the value of  $k'$  depends on the situations which we have previously explored. As we have seen for the thermally activated pathway the decay rate is expected to increase, while the energy of the  $^3\text{MLCT}$  state growth, results in a decrease of the  $^3\text{MLCT}$  to  $^3\text{MC}$  energy separation.

$$\frac{1}{\tau} = (k'_0 + k_{0,0}^{nr} e^{-\alpha E_{\text{MLCT}}}) + k' e^{\frac{\Delta E_a}{RT}} \quad (5.24)$$

These opposing effects provide a simple basis for the rationalisation of the biphasic behaviour of the lifetimes.

Finally, considering the equilibrium kinetic limit, which we postulated previously in the temperature dependence measures, and assuming that the energy of the  $^3\text{MC}$  state is not solvent dependent, or at least much more solvent-independent than the  $^3\text{MLCT}$  energies, it becomes possible to fit the  $^3\text{MLCT}$  state

lifetimes using equation 5.24. This results in a surprisingly acceptable model when a reasonable set of parameters are used (Table 5.8). The ascending arc of the calculated curve occurs as a result of direct deactivation. In contrast the descending arc is due to deactivation from the near MC energy states. In low-temperature glass, the population of the MC states is completely deactivated and the solvent dependence follows the energy-gap law, that is that the lifetime increases with increasing acceptor number. It is interesting to note the fact that the  $k'$  obtained from equation 5.2 (temperature-lifetime dependence) has the same value as that obtained from equation 5.24 (lifetime-solvent dependence). Also the value of the MC energy, achieved from equation 5.24, is equal to the sum of the  $\Delta E$  procured from the previous calculation (equation 5.2) and the  $E^{0-0}$  from the emission of the complex at 77K in the ethanol/butyronitrile mixture.

[Ru( $\Delta^2$ py $\Delta^4$ )(tpy)]	Emi. (kk) (b)	$\tau$ (nsec) (a)	$\Phi_{em}$ ( $1 \times 10^{-5}$ ) (a)	$k^0$ ( $\text{sec}^{-1}$ ) $\times 10^5$ (b)	$k^r_0$ ( $\text{sec}^{-1}$ ) $\times 10^4$ (a)	$k^{nr}_0$ ( $\text{sec}^{-1}$ ) $\times 10^5$ (b)
H <sub>2</sub> O, 9 M LiCl	15.15	50	3.90	1.86	7.81	1.09
EtOH:MeOH (4:1)	15.01	60	4.86	2.08	8.10	1.20
EtOH:Butyronitrile (4:5)	14.95	92	8.20	2.2	8.90	1.30
DMF:CH <sub>2</sub> Cl <sub>2</sub> (9:1)	14.60	82	7.40	2.5	9.00	1.60

**Table 5.7 Solvent dependence of decay properties and excited state decay parameters for [Ru(tpy)( $\Delta^2$ py $\Delta^4$ )] in a variety of solvents at 298 K (a) and their glasses at 80 K(b). The values were obtained by fitting the observed temperature dependence of the luminescence lifetimes.**

Equation	$A_1$ ( $s^{-1}$ )	$\Delta E_1$ ( $cm^{-1}$ )	$A_2$ ( $s^{-1}$ )	$\Delta E_2$ ( $cm^{-1}$ )	$B_1$ ( $s^{-1}$ )	$T_{B1}$ (K)
(5.2)	$2.6 \times 10^7$	439	$2 \times 10^{12}$	2700	$8.7 \times 10^{-4}$	137.5
	$k^0$ ( $s^{-1}$ )	$\alpha$ ( $cm^{-1}$ )	$k'$ ( $s^{-1}$ )	$E_{MC}$ ( $cm^{-1}$ )	${}^a\Delta E_a = E_{MC} - E_{MLCT}$ ( $cm^{-1}$ )	
(5.24)	$5.6 \times 10^{13}$	0.00103	$2 \times 10^{12}$	17815	2820	

**Table 5.8: Kinetic parameters for excited obtained from the fitting of the experimental results. <sup>a</sup> The  $E_{MLCT}$ , used in this calculation, is obtained from the emission at 80K in the mixture Ethanol/Butyronitrile (4/5)**

## 5.8 Conclusions

In this chapter, the use of  $(\Delta\text{py}\Delta)$  ligand to extend the lifetime of the  $^3\text{MLCT}$  excited states of Ru(II) terpyridine complexes has been explored. With respect to  $[\text{Ru}(\text{tpy})]^{2+}$  a gain of two order of magnitude in the  $^3\text{MLCT}$  state is obtained. With lifetimes in this range, interesting perspectives arise for the use of structurally attractive Ru(II) terpyridine units as photosensitiser molecular components in supramolecular devices. The presence of the  $(\Delta\text{py}\Delta)^{2-}$  ligand introduces solvatochromic behaviour in the complexes. Emission energy correlates linearly with solvent acceptor number, while a clearly biphasic dependence is observed for emission lifetimes as a function of emission energy. The lifetime solvent dependence can be readily explained in terms of a standard model involving competition between direct radiationless decay to the ground state and a thermally activated pathway through upper metal centred states.

The general question as to the effect of replacing a tpy ligand with a  $(\Delta\text{py}\Delta)^{2-}$  ligand on the lifetime of Ru(II) complexes does not allow a simple answer. The prediction is complicated by the solvent dependence of lifetimes, their sensitivity to the energy of both  $^3\text{MC}$  and  $^3\text{MLCT}$  states, and the occurrence of intrinsic vibronic effects of triazoles on  $^3\text{MLCT}$  decay. In the case of Ru(II) terpyridine complexes, however, the effect is certainly one of lifetime enhancement, and its main reason is the lifting of the MC states accompanying the substitution of strong-field  $(\Delta\text{py}\Delta)^{2-}$  ligand for the weak-field tpy ligand.

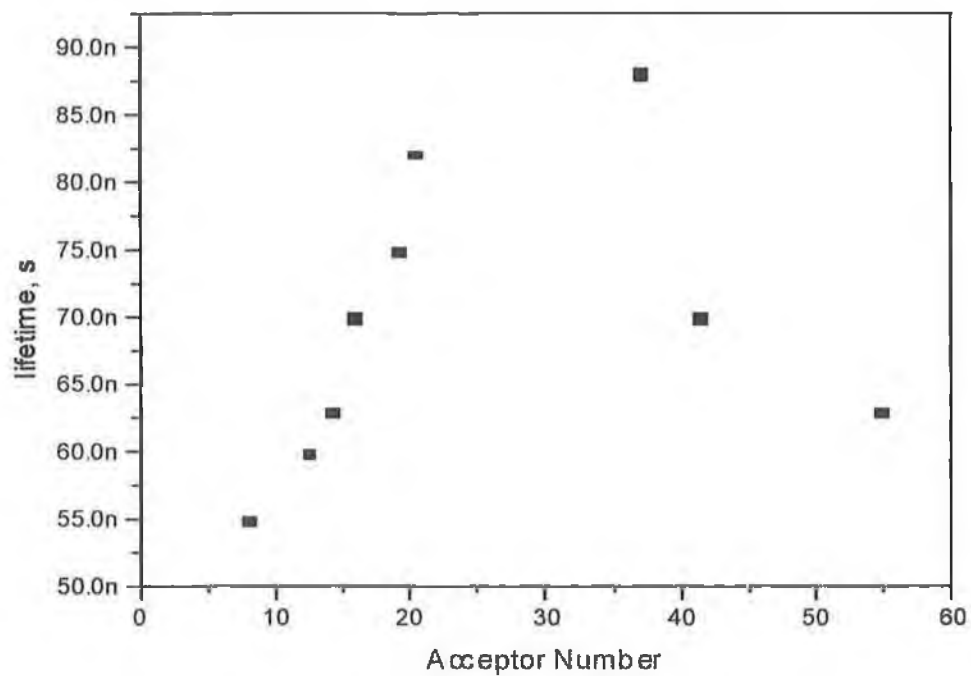


**Figure 5.25** Correlation of the emission lifetime with the Gutmann acceptor number for  $[\text{Ru}(\text{tpy})(\Delta^2\text{py}\Delta^4)]$

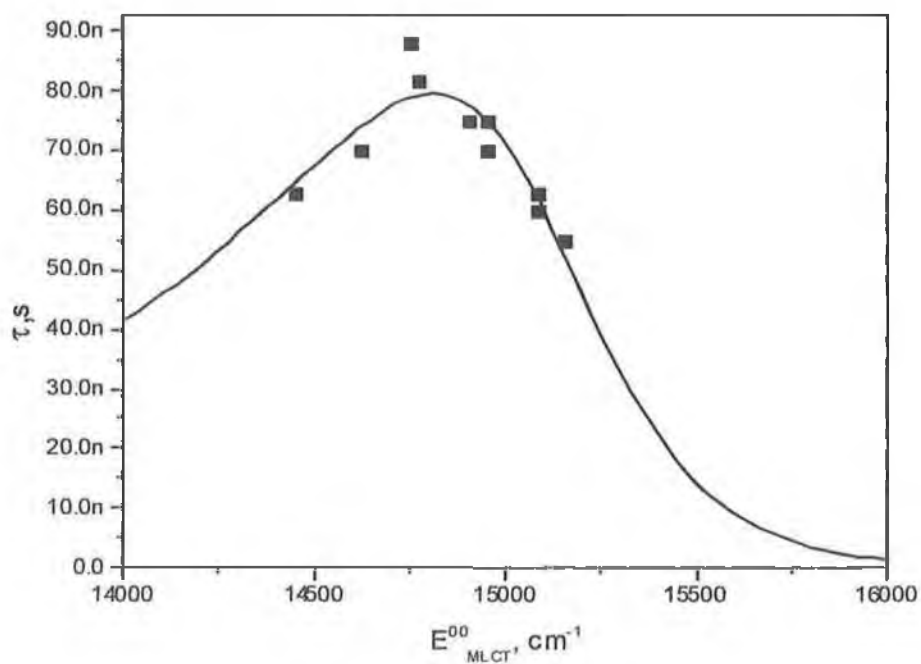


**Figure 5.26** Plot of the emission lifetime vs solvent-dependent emission energy with for  $[\text{Ru}(\text{tpy})(\Delta^2\text{py}\Delta^4)]$ , the full line is calculated using equation 5.24.

## 5.9 Bibliography

- 
- <sup>1</sup> Morgan G T, Burstall F H, **J. Chem. Soc.** 1932, 20.
- <sup>2</sup> Cargill Thompson A M W, **Coord Chem. Rev.** 1997, 160, 1
- <sup>3</sup> Pechy P, Rotzinger F P, Nazeeruddin MK, Kohle O, Zakeeruddin S M, Humprhry-Baker R, Grätzel M, **J. Chem Soc. Chem. Commun.** 1995, 65.
- <sup>4</sup> Ward M D, **Chem. Soc. Rev.** 1995, 121
- <sup>5</sup> Mukkala M, Helenius M., **Helv. Chim. Acta**, 1992, 76, 1361.
- <sup>6</sup> Sugiyarto K H, Craig D C, Rae A D, Goodwin H A, **Aust. J. Chem.** 1993, 46, 1269
- <sup>7</sup> O'Connor C, **PhD Thesis**, 1999, Dublin City University, Ireland
- <sup>8</sup> Hughes H, **PhD Thesis**, 1993 Dublin City University, Ireland
- <sup>9</sup> Constable E C, Cargill Thompson A M W, **New J. Chem.** 1992, 16,855
- <sup>10</sup> Constable E C, **Adv. Inorg. Chem. Radiochem.** 1986, 30, 69 and references there in
- <sup>11</sup> Kober E M, Meyer T J, **Inorg. Chem** 1982, 21, 3967
- <sup>12</sup> Yersin H, Braun D. In **Vibronic Processes in Inorganic Chemistry**, Ed. Kluwer, (1989) Boston, MA.
- <sup>13</sup> Dewar M J S, Stewart J J P, **J. Am. Chem. Soc.** 1985,107, 3902
- <sup>14</sup> Hecker C R, Fanwick P E, McMillin D R, **Inorg. Chem.** 1991, 30,659
- <sup>15</sup> Mulliken R S, **J. Am. Chem. Soc.** 1952, 74, 811
- <sup>16</sup> Day P, Sanders N **J. Chem. Soc.** 1967, A 1356
- <sup>17</sup> Ceulemans A, Vanquickenborne LG, **J. Am. Chem. Soc** 1981, 103, 2238
- <sup>18</sup> Ireland J F, Wyatt P A H, **Adv. Phys. Org. Chem.** 1976, 12,131.

- 
- <sup>19</sup> Brand L, Laws W R, in **Time Resolved Fluorescence spectroscopy in Biochemistry and Biology**, Nato Asi, Series A, Vol. 61
- <sup>20</sup> Vos J G, **Polyhedron** 1992, 18, 2285
- <sup>21</sup> Maestri M, Armaroli N, Balzani V, Constable E C, Cargill Thopson A M W, **Inorg. Chem.** 1995, 34, 2759
- <sup>22</sup> Wolfbauer G, Bond A M, Deacon GB, Howitt J, MacFarlane D R, Spiccia L **J. Electrochem. Soc.** 2001, E97, 148
- <sup>23</sup> Wolfbauer G, Bond A M, Deacon GB, Howitt J, MacFarlane D R, Spiccia L J. **Electroanal. Chem** 2000, 7, 490.
- <sup>24</sup> Ruminski R, Underwood S, Valley K, Smith S J. **Inorg. Chem.** 1998, 37, 6528
- <sup>25</sup> Tait C D, Vess T M, **J. Chem. Soc. Chem. Commun.** 1981, 287.
- <sup>26</sup> Konig E, Kremer S, **Chem. Phys. Lett.** 1970, 5, 87.
- <sup>27</sup> Berger R M, Mc Millin D R, **Inorg Chem** 1988, 27, 4245.
- <sup>28</sup> Hecker C R, Fanwick P E, Mc Millin D R, **Inorg Chem.** 1991, 30, 659
- <sup>29</sup> Van Housten J, Watt R J, **J. Am. Chem. Soc.** 1976, 98, 4853.
- <sup>30</sup> Durhan B, Caspar J V, Meyer T J, **J. Am. Chem. Soc.** 1982, 104, 4803.
- <sup>31</sup> Caspar J V, Meyer T J, **J. Am. Chem. Soc.** 1983, 105, 5583.
- <sup>32</sup> Caspar J V, Meyer T J, **Inorg. Chem.** 1983, 22, 2444.
- <sup>33</sup> Belser P, Balzani V, Juris A, von Zelewsky A **Gazz. Chim. Italiana** 1985, 115, 723
- <sup>34</sup> Barigelletti F, Belser P, Von Zelewsky A, Juris A, Balzani V, **J. Phys. Chem** 1985, 89, 3680.
- <sup>35</sup> Juris A, Barigelletti F, Balzani V, Belser P Von Zelewsky, **Inorg. Chem.** 1985, 24, 202



- 
- <sup>36</sup> Hammarström L, Barigelletti F, Flamigni L, Indelli MT, Armaroli N, Calogero G, Guardigli M, Sour A, Collin J P, Sauvage J P, **J. Phys. Chem A** 1997, 101, 9061
- <sup>37</sup> Hammarström L, Barigelletti F, Flamigni L, Armaroli N, M, Sour A, Collin J P, Sauvage J P, **J. Am. Chem. Soc.** 1996, 118, 11972
- <sup>38</sup> Barigelletti F, Juris A, Balzani V, , Belser P Von Zelewsky **J. Phys. Chem.** 1987, 91,1095.
- <sup>39</sup> Allen GH, White RP, Meyer T J, **J Am Chem. Soc.** 1984, 106, 2163.
- <sup>40</sup> Timpson C J, Meyer T J, **J. Phys. Chem.** 1996, 100, 2915.
- <sup>41</sup> Kober E M, Meyer T J, **Inorg Chem.** 1984, 23, 2089.
- <sup>42</sup> Kolling OW, **J. Phys. Chem.** 1991, 95, 3950.
- <sup>43</sup> Kober E M, Meyer T J, **Inorg Chem** 1984, 22, 2098.
- <sup>44</sup> Brunschwig B S, Sutin S, **J. Phys. Chem** 1984, 91, 4714.
- <sup>45</sup> MC Rae E G, **J. Phys. Chem** 1957, 61, 562.
- <sup>46</sup> Gutmann V, **The acceptor-donor Approach to molecular interaction**, (1980), Plenum, New York

## **Chapter 6:**

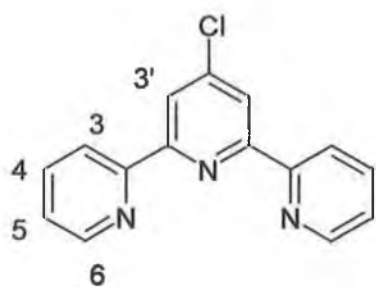
### **“The Triazolate Family”**

“If everything seems to be going well, you have obviously overlooked something”

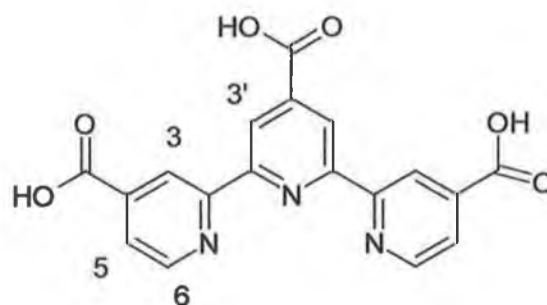
**Murphy**

## 6.1 Introduction

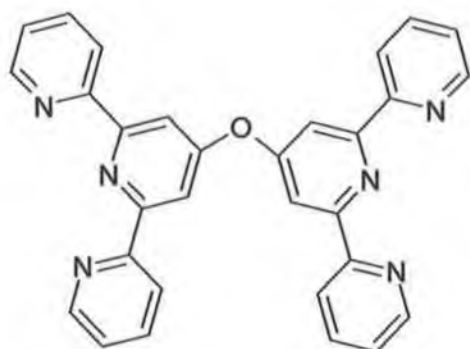
In Chapters 5 the synthesis, characterisation and properties of tpy complex with the ligand  $H_2(\Delta py\Delta)$  have been reported. In this chapter the preparation and characterisation of some related compounds are discussed. These investigations are aimed at widening the scope of the application of the triazole ligands. Therefore the  $H_2(\Delta py\Delta)$  ligand is complexed to the metal centre with two different substituted tpy ligands (Fig 6.1). The photophysical and electrochemical properties of these complexes are compared with those of the unsubstituted tpy ligand. It was hoped that by varying the nature of the tpy ligands more information on the nature of the excited state could be obtained. The chosen ligands were Cl-tpy and  $H_3(tctpy)$ . The introduction of the chlorine and the carboxylic groups is expected to effect the  $\pi^*$  level of the tpy ligand. In addition these are several possible applications of substituted tpy complex. The second problem that this chapter aims to address is that of the coordination isomers observed for the  $H_2(\Delta py\Delta)$  ligand. The new ligand  $H_2(\Phi\Delta py\Delta\Phi)$  has been prepared aimed at reducing the number of isomer formed.



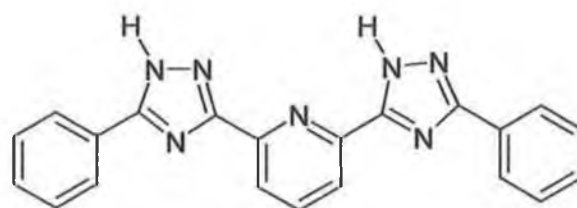
**4' chloro-2,2':6',2'' terpyridine  
(Cl-tpy)**



**4',4'',4''' tri carboxyl -2,2':6',2'' terpyridine  
H<sub>3</sub>(tctpy)**



**bis{4'-(2,2':6',2'' terpyridyl)} ether  
(ypt<sup>t</sup>tpy)**



**di-2,5 [3' phen-yl (1',2',4', triazol-yl)] pyridine  
H<sub>2</sub>(ΦΔpyΔΦ)**

**Figure 6.1. Ligands cited in the text**

## 6.2 [Ru(Cl-tpy)( $\Delta$ py $\Delta$ )]

Metallodendrimers, dendrimers incorporating metal sites, are an important emerging motif in supramolecular chemistry. They offer the advantage of multiple reaction sites within a chemically well-defined and discrete macromolecular systems.<sup>1</sup> Four main strategies may be identified for the inclusion of metal centres in metallodendrimers:

- Use of a metal-containing core which is then structurally developed using a divergent dendrimer synthesis or the convergent attachment of dendritic wedges,
- Decoration of the surface of inner generations of a conventionally prepared and functionalised dendrimers
- Incorporation of the metal centres as part of the backbone connectivity of the dendrimer
- The use of the metal as the branching point within the dendrimer.

Critical concepts in dendrimers and metallodendrimer chemistry are those of successive generations and building blocks that are used in divergent iterative synthesis or in the preparation of dendritic wedges for convergent synthesis. These concepts may be transferred to metallostars, which are expected to be closer to monodispersed and exhibit fewer or no failure sequences. Constable et al.<sup>2</sup> considered methodology leading to topologically linear heteromultinuclear complexes, which will subsequently be adapted for the attachments, as equivalents of dendritic wedges. The strategy adopted is the formation of the bis{4'-(2,2':6',2'' terpyridyl)} ether (Fig.

6.1), which contains two tpy metal-binding domains. A 4' chloro-2,2':6',2'' terpyridine Ruthenium complex is the precursor, the presence of the metal enhances the Cl-tpy electrophilicity, allowing the in situ synthesis of the ether ligand under mild conditions by reaction with the nucleophilic 4'-hydroxy-(2,2':6',2'' terpyridine)

3

### 6.2.1 Synthesis and purification

[Ru(Cl-tpy)( $\Delta$ py $\Delta$ )] was prepared, in order to be used as possible precursor, in a basic DMF solution in presence of N-ethyl morpholine as a reducing agent. The complex was precipitated as a PF<sub>6</sub> salt, by adding an aqueous NaPF<sub>6</sub> solution to the reaction mixture. Purification by column chromatography on alumina (acetonitrile) produced an overall yield of around 30%. The complex was recrystallised from 1:1 water-acetone solution and obtained as an analytically pure Cayenna red coloured powder. The elemental analysis indicates the presence of the di-protonated complex.

Following purification, HPLC and <sup>1</sup>H-NMR (Fig. 6.2) investigations were carried out and it was concluded that, due to the presence of different coordination sites of the triazolite moieties, three configurational isomers were produced. The isomer ratios were estimated by integrating the H<sup>6</sup> resonance (because of the impossibility of separation, the proton <sup>1</sup>H-NMR signal assignment was obtained by comparison with the [Ru(tpy)( $\Delta$ py $\Delta$ )], Fig. 6.2), which is at different position for

each of the isomers. The ratio obtained from the  $^1\text{H-NMR}$  signal integrals was confirmed by HPLC.

Based on this NMR evidence it is proposed that here the major isomer (about 50%) is presumably the complex with  $\text{N}^2$  and  $\text{N}^4$  bounded triazolate rings,  $[\text{Ru}(\Delta^2\text{py}\Delta^4)(\text{Cl-tpy})]$ , the second isomer with an abundance around 35% is assigned to the double  $\text{N}^4$  coordination,  $[\text{Ru}(\text{II})(\Delta^4\text{py}\Delta^4)(\text{Cl-tpy})]$ . The third isomer (about 5%) is probably all  $\text{N}^2$  bound.

Unfortunately all the attempts of isomer separation were unsuccessful, all the measure reported in this section are on the isomer mixture.

The cyclic voltammogram of the complex in acetonitrile presents one very broad and not well-defined oxidation peak around 0.60 Volt.

The absorption spectrum of the mixture is shown in Figure 6.3. The bands at 218 nm and 376 nm have been assigned to LC  $\pi\text{-}\pi^*$  transitions by comparison with the spectrum  $[\text{Ru}(\text{tpy})(\Delta\text{py}\Delta)]$  (see Chapter 5, section 5.3 and references therein). The two remaining intense bands at 379 and 489 nm have been assigned to singlet MLCT  $\text{d-}\pi^*$ transitions. In the long wavelength of the absorption spectrum two shoulders are present at about 612 and 660 nm. Those absorption features are thought to correspond to the lowest  $^1\text{MLCT}$ , see Chapter 5.

Excitation of the complex in any of its absorption bands leads to a broad luminescence (Fig. 6.3) around 770 nm. with a lifetime of 45 nsec., in deaerated acetonitrile, whose intensity, lifetime and energy positions are temperature and solvent dependent. The presence of the electron-accepting group, chlorine, in 4'

position of the tpy moiety will stabilise the LUMO ( $\pi^*$  orbital located on the tpy), decreasing consequentially the distance in energy between ground-state and  $^3\text{MLCT}$ , that will correspond to a red shift for absorption and emission spectra<sup>4,5</sup> compared with the unsubstituted analogous complex. This is an additional piece of evidence of the tpy based  $^3\text{MLCT}$  assignation.

Once again<sup>6</sup> the presence of the structural isomers proved to be a major problem for the investigation of the products in the successive steps of the supramolecular system synthesis, because of the impossibility of separate the isomers no further investigation or synthesis were made.





### 6.3 [Ru( $\Delta$ py $\Delta$ )(tctpy)]

Dye-sensitised solar cell (Fig. 6.4) technology is an interesting and promising inexpensive alternative to the solid state photovoltaic cells. In recent years, many groups<sup>7, 8, 9, 10, 11</sup>, have been focusing their attention on fundamental aspect of dye sensitised solar cell components.

Dye derivatised mesoporous TiO<sub>2</sub> film is one of the components. The electrochemical, photophysical and ground/ excited state properties of the dye play an important role in the charge-transfer dynamics at the semiconductor interface.

The optimal sensitiser for the dye sensitised solar cell should be panchromatic, that is, absorbs light of all colours. Ideally, all photons, below a threshold wavelength of about 920 nm., should be harvested and converted to electric current.

In addition the sensitiser should fulfil several demanding conditions:

- It must be firmly grafted to the semiconductor oxide surface and inject electrons into the conduction band with a quantum yield of unity.
- Its redox potential should be sufficiently high so that it can be regenerated rapidly via electron donation from the electrolyte as a hole conductor
- It should be stable enough to sustain at least 20 years of exposure to natural sunlight.

Molecular engineering of ruthenium complexes that can act as panchromatic charge transfer sensitisers for TiO<sub>2</sub> based solar cells presents quite a challenge, as several requirements have to be contemporaneously fulfilled by the dye.

Firstly, the LUMO and HOMO need to be at levels where photoinduced electron transfer in the TiO<sub>2</sub> conduction band and regeneration of the dye by iodide can take place at practically 100% off yield. This restricts greatly the option available to accomplish the desire red shift of the metal to ligand charge transfer transitions (MLCT) to about 900 nm.

The spectral and red-ox properties of ruthenium can be tuned in two ways:

- First by introducing a ligand with low-lying  $\pi^*$  molecular orbital
- Second by destabilisation of the metal  $t_{2g}$  orbital through the introduction of a strong  $\sigma$ -donor ligand.

Meyer et al<sup>12</sup> have used these strategies to tune the MLCT in ruthenium complexes. However, the extension of the spectral response into the near IR was gained at expense of shifting the LUMO orbital to lower levels from where charge injection in the TiO<sub>2</sub> conduction can no longer occur, especially in tpy complexes.

A near infrared response can also be gained by increasing the energy of the ruthenium  $t_{2g}$  (HOMO) levels. However, it turns out that the introduction of the strong  $\sigma$ -donor ligands into the complex often does not lead to the desired spectral result as both the HOMO and the LUMO are displaced in the same direction. Furthermore, the HOMO position cannot be displaced on freely as the redox potential to insure rapid regeneration of the dye by electron donation from iodide following charge injection into the TiO<sub>2</sub>. The use of terpyridine incorporating carboxylate functions because:

- It increases the molar coefficient of the complex

- It facilitates the grafting of the dye on the semiconductor surface
- It ensures intimate electronic coupling between its excited state and the conduction band of the titanium dioxide.

The role of the  $H_2(\Delta py\Delta)$  ligand is to tune the metal  $t_{2g}$  orbitals of ruthenium and possibly stabilise the positive hole, generated on the metal, after having injected an electron into the conduction band.



### 6.3.1 Synthesis and purification

[RuH<sub>3</sub>(tctpy)(ΔpyΔ)] has been prepared using a modified version of a literature method (see Chapter 3). The synthesis of the tctpy ligand precursor was carried out utilising 4-ethylpyridine rather than 4-methylpyridine which has allowed the dehydrogenation catalysed by Pd/C to be carried out at a higher temperature and hence doubling the yield of 4,4',4''-triethyl-2,2',6',2''-terpyridine. This ligand was then converted to the corresponding acid by oxidation with dichromate and then esterified with diazomethane. These modifications have proved extremely useful for obtaining pure esterified ligand. Moreover the complexes have been purified by size exclusion chromatography, the presence of carboxylate groups and free nitrogens which prevent the use of any other kind of chromatography purification.

Three isomers were found by <sup>1</sup>H-NMR investigations however just one of them was isolated by precipitation from an acidic water solution, presumably the isomer [RuH<sub>3</sub>(tctpy)H<sub>2</sub>(Δ<sup>2</sup>pyΔ<sup>2</sup>)]<sup>2+</sup>, which is expected to be more hydrophobic, by comparison with the homologous [Ru(tpy)(Δ<sup>2</sup>pyΔ<sup>2</sup>)], which showed to be less interactive with the polar solid phase of the HPLC chromatographic column than with the less polar liquid phase.

The complex was characterised by elemental analysis, <sup>1</sup>H NMR and UV spectroscopy. The electronically excited states of the complexes were characterised by emission spectroscopy and lifetime measurements. The <sup>1</sup>H-NMR (Fig. 6.5) spectrum of the isolated isomer is in agreement with a C<sub>2v</sub> symmetry, showing the presence of a single symmetric isomer.

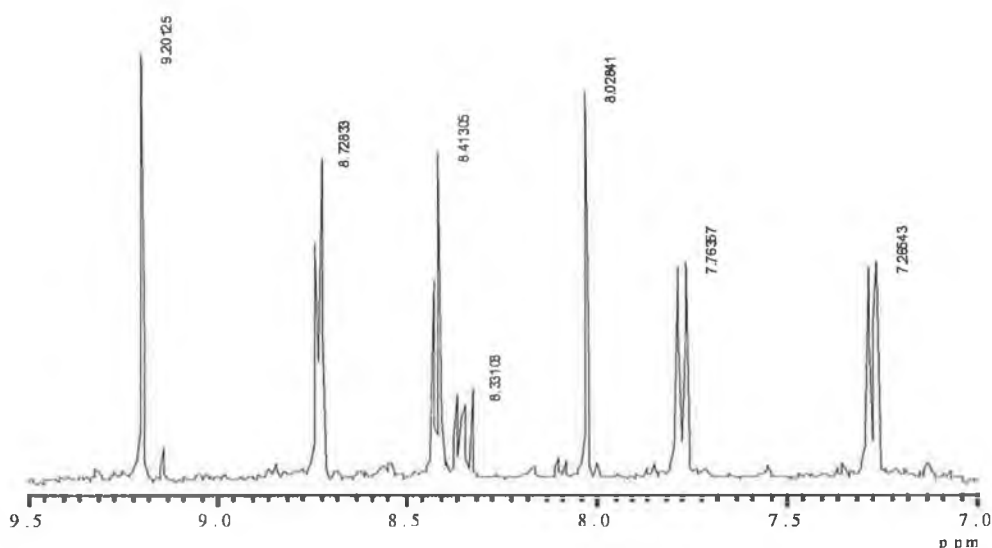


**Figure 6.5**  $^1\text{H-NMR}$  spectra of the isomers of the  $[\text{Ru}(\text{tctpy})(\Delta^2\text{py}\Delta^2)]$  complex in  $d^4$ -methanol.

The  $^1\text{H-NMR}$  spectrum of the complex, Fig 6.5, shows seven sharp and well resolved signals in the aromatic region, four of them correspond to the terpyridyl protons in which the two peripheral rings are magnetically equivalent. In the pseudo octahedral geometry, a tridentate ligand like tpy coordinates to a metal centre in a meridional fashion, and the  $\Delta\text{py}\Delta$  lies in the orthogonal plane. Using arguments similar to those used in Chapter 5, for the tpy ligand, the lowest field signals centred at 9.2 and 8.8 ppm are assigned to  $\text{H}^{3'}$  and  $\text{H}^3$  protons respectively. These two singlets are downfield shifted compared to the  $\text{H}^6$  proton that appears as a doublet centred at 7.70 ppm. The  $\text{H}^5$  proton signal shows a doublet centred at 7.5 ppm. In the case of the  $\text{H}_2(\Delta\text{py}\Delta)$  ligand, the observed shift of the  $\text{H}^{3''}$  (triplet) and  $\text{H}^{4''}$  (doublet) are 8.33 and 8.41 ppm, respectively. That is that the  $\text{H}^{5''}$  proton shift, knew to be strongly

dependent on the N-bonding of the  $(\Delta\text{py}\Delta)^{2-}$  ligand and the acidity-basicity and polarity of the solution, as it was seen in chapter 5, section 5.3, in the present solution shows a singlet signal at 8.02 ppm, this is a evidence of a totally symmetric complex, in agreement with the  $[\text{RuH}_3(\text{tctpy})\text{H}_2(\Delta^2\text{py}\Delta^2)]^{5+}$  isomer assignment.

The electronic spectra of the complexes  $\{\text{Ru}[\text{H}_3(\text{tctpy})][\text{H}_2(\Delta^2\text{py}\Delta^2)]\}^{5+}$  shows metal to ligand charge transfer bands (MLCT) that dominate the visible region and  $\pi$ - $\pi^*$  transitions in the UV region (Fig 6.6). The spectra are very sensitive to variation in solvent and pH because of the presence of the  $\Delta\text{py}\Delta$  ligand and the carboxylic functionality. Upon changing from a solvent of high to one of low polarity, the MLCT band moved to lower wavelength. This solvatochromism, previously reported for the  $\Delta\text{py}\Delta$ -Ru complexes, is associated with the interactions of polar solvents with coordinated  $\Delta\text{py}\Delta$  moiety and the carboxyl tpy functionalities, which reduce the electron density on the metal. The effect of protonation on the spectra of these complexes, shown in Fig 6.6 and 6.7, are not so easily interpreted. The ruthenium-tctpy moiety complexed to the  $\Delta\text{py}\Delta$  ligand forms a meridional configuration, in which the two peripheral pyridyl groups are trans to each other and electronically equivalent<sup>13</sup>. The central pyridine is different to the two peripheral pyridines. The tctpy ligand symmetry, which is preserved after coordination suggests that the pKa of the carboxylate group on the central pyridine is different from those that are attached to the peripheral pyridines. Four different pKa values were detected, respectively 5.8, 4.8, 2.8, 1.8 pH units (Fig. 6.5). The first protonation, (value of pKa 5.8, associated with a small blue shift in the absorption maximum), is assigned to one of the



triazolate moieties of  $(\Delta\text{py}\Delta)^{2-}$  ligand (associated with a quenching of the emission), while the second arises due to protonation on the carboxylate functional group on the central pyridine of the tpy ligand (little red shift). The third and the fourth pKa values are related to protonation of the second triazolate ring (blue shift of the absorption maximum) and the double protonation of the peripheral equivalent  $\text{CO}_2^-$  functionality on the tpy (associated with an increase of the quantum emission and a red shift of the absorption maximum) respectively. The last protonation, on the carboxylate functions on the tpy ligand, causes a lowering of the LUMO energy associated with this ligand and consequently both the  $\pi-\pi^*$  and MLCT bands undergo a blue shift. A similar explanation can be used to explain the emission spectra in Fig. 6.6. Which is consistent with a stabilisation of the triplet state in the last protonated form.

The electrochemical behaviour of these species is in general non-reversible and so it is not possible to make a meaningful comparison of the relative energies of the  $\pi^*$  antibonding orbitals for the terpyridine carboxylate ligand and the analogous terpyridine ligand. Nevertheless it is noted that the tpy carboxylate complexes show less cathodic reduction waves than the bpy ones indicating the greater electron-acceptor capacity of the tpy ligand. Clearly this is reflected in the substantial shift in the MLCT to higher wavelength in the visible spectrum. The oxidation potentials indicated in Table 6.2 show that the new complex of the tpy ligand is more easily oxidised than the corresponding complexes with tpy ligands. This effect must arise from the negative charges on the  $\Delta\text{py}\Delta$  ligand that, through  $\sigma$ -donation, in low polarity solvents, increase the electron density on the metal centre.

The photophysical properties of the complex show that the new tctpy complex emits at lower energy than the corresponding tpy complexes. The reduction/oxidation data reported in Table 6.2 are therefore to be considered purely qualitative (not reversible reductions and quite poor resolution in oxidation), but useful for comparisons of spectroscopic energies and the oxidation/reduction properties of the excited states of the complex. One can therefore assume that the reduction capacity of the excited states of these complexes are well represented by calculating the values of  $E_{ox}^*$  (Excited-state redox potential obtained as a difference of ground state oxidation potential and excited state energies,  $E_{ox} - E^{0-0}$ ). These values suggest that the excited states of the studied complex can act as moderately strong reductants with potentials around -1.3 eV, a value suitable for  $TiO_2$  photovoltaic cells.

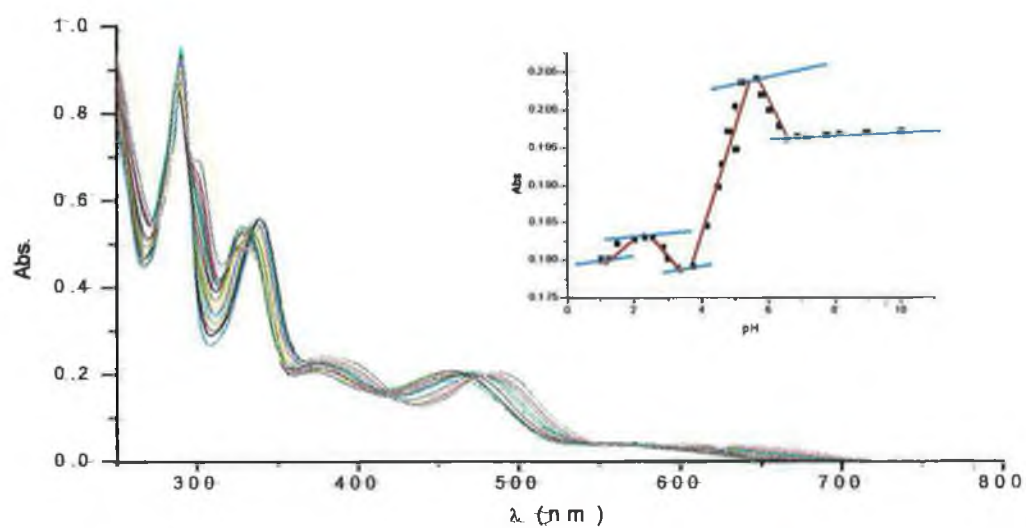


**Figure 6.6** Absorption/pH dependence of  $[\text{Ru}(\text{tctpy})(\Delta^2\text{py}\Delta^2)]^{5-}$ , 1 to 8 pH, in Britton Robson Buffer.

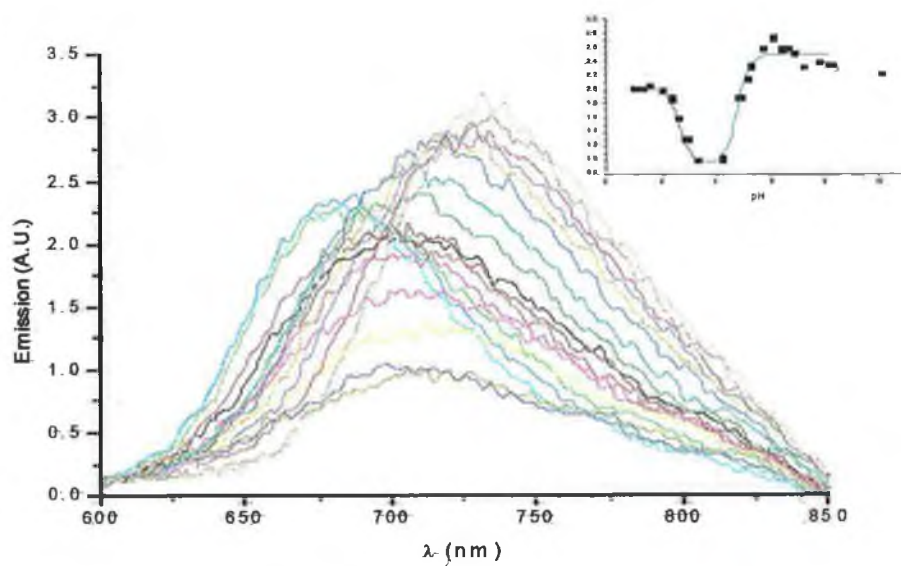


**Figure 6.7** Emission/pH dependence of  $[\text{Ru}(\text{tctpy})(\Delta^2\text{py}\Delta^2)]^{5-}$ , 1 to 8 pH, in Britton Robson Buffer.

A monolayer of the complex was absorbed from a warm  $2 \times 10^{-4}$  M solution of the complex in ethanol containing 40 mM of sodium taurodeoxycholate as a co adsorbent<sup>14</sup> onto a 7 nm thick nanocrystalline TiO<sub>2</sub> film (see Chapter 3) prepared on conducting glass.

The photoaction spectra of the dark orange-green coloured film measured on TiO<sub>2</sub> in a photovoltaic cell in conjunction with a redox electrolyte such as 0.9M LiI and 0.1 M LiI<sub>3</sub> in propylene carbonate reveal a lower efficiency of light conversion for complexes containing the tpy ligand than that observed for bpy. This is apparently in contrast with what has been reported for the complex [Ru(tctH<sub>3</sub>)(NCS)<sub>3</sub>] by Graetzel et al.<sup>15</sup> For this species, a photoaction spectrum has been reported with IPCE values of the order of 80%, as observed with the complex [Ru(dcbH<sub>2</sub>)<sub>2</sub>(NCS)<sub>2</sub>]<sup>16</sup>. The reasons for the different behaviour observed is most likely related to the difference in optical density between the photoanodes used. In the two experiments the IPCE is related to differences in transmittance or absorbance between the electrodes used, according to the equation

$$\text{LHE} = 1 - 10^{-A}$$

where A is the absorbance. The thickness of 7 μm was used in our experiments, this resulted in values of maximum absorbance, which were of the order of 70%. While in the laboratories in Lausanne, the optical density of the electrode used were almost double because of the greater thickness of the colloidal TiO<sub>2</sub> film (114 μm). If this difference is taken into account, the LHE term in our experiment should be 20% lower than the value obtained by Grätzel & al.<sup>18</sup> and the maximum photocurrent

obtained for the complex  $[\text{Ru}(\text{tctH}_3)(\text{NCS})_3]\text{TBA}$  should show a conversion efficiency of about 60%. The fact that the IPCE (Fig 6.7) in our measurement in the 400-500 nm interval varies from 70 to 60 % validates this hypothesis.

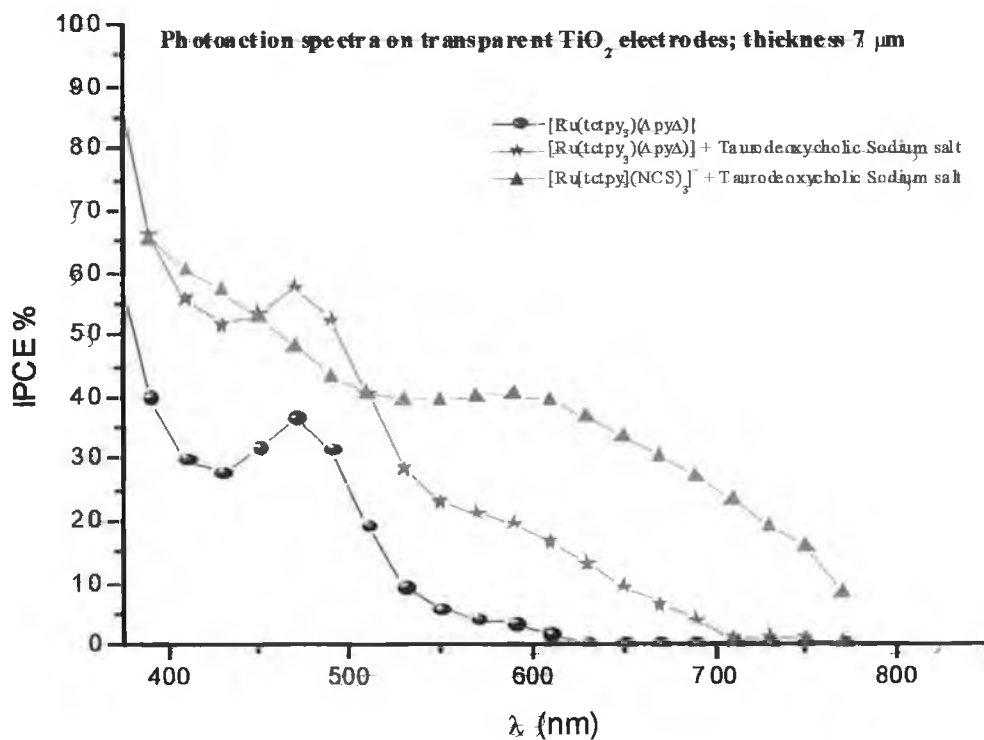


Figure 6.8 Photocurrent action spectra obtained with nanocrystalline  $\text{TiO}_2$  film supported onto a conducting glass sheet and derivatised with  $[\text{Ru}(\text{tctpy})(\Delta\text{py}\Delta)]$  (red and black lines) and  $\text{Ru}(\text{tctpy})(\text{SCN})_3$  (green line). The IPCE is plotted as a function of wavelength. A sandwich type cell configuration was used to measure this spectrum.

## 6.4 Synthesis and Characterisation of [Ru(tpy)( $\Phi\Delta\text{py}\Delta\Phi$ )]

As pointed out in the introduction of Chapter 5 the reason for the preparation of  $\text{H}_2(\Phi\Delta\text{py}\Delta\Phi)$  is aimed to the number of structural isomers. This goal can be obtained of the steric hindrance between the terpyridine and the extended ( $\Phi\Delta\text{py}\Delta\Phi$ ) ligand during the formation of the complex, this should result in the formation of solely the [Ru(tpy)( $\Phi\Delta^2\text{py}\Delta^2\Phi$ )] isomer (Fig 6.4). It has already been shown that for triazolate bidentate ligands<sup>17,18</sup> containing bulking groups at the 5 position, such as phenyl, phenol or bromine moieties, differentiation of the two coordinating nitrogens occurs leading almost exclusively to complexation at  $\text{N}^2$  atom. Molecular model of the possible configurational isomers, using the Hyperchem Software, supports the importance of steric hindrance for the ligand, in fact just as in the case of the [Ru(tpy)( $\Phi\Delta^2\text{py}\Delta^2\Phi$ )] isomer the two phenyl groups, lying in an orthogonal plane to the tpy ligand in the energetic configurational minimum, have the possibility of free rotation. However in the other two isomers, one or two of the phenyl groups are constricted in an almost frozen position from the interaction of the tpy lying on the parallel plane (Fig. 6.9).

The new  $\text{H}_2(\Phi\Delta\text{py}\Delta\Phi)$  ligand was prepared in a similar way to the  $\text{H}_2(\Delta\text{py}\Delta)$  ligand (chapter 3). For the synthesis of the [Ru(tpy)( $\Phi\Delta\text{py}\Delta\Phi$ )] complex, two solvent schemes were used, a DMF solution and a 1,2-ethandiol solution. Both solvents gave the desired complex in the same quantity of a 23% yield. More recently, DMF has been used for the reaction, because of the easier work up of the product.

The purity of the complexes was verified with HPLC-measurements (Fig. 6.5). In the chromatogram of the solid before purification, three bands were observed. Two peaks were located between two and three minutes and a third around four minutes. The last peak was an  $[\text{Ru}(\text{tpy}_2)]^{2+}$  impurity, which was eliminated by column chromatography onto alumina, using acetonitrile as solvent. From the purified solids obtained from both reactions, surprisingly two isomers were obtained, which could be separated using silica chromatographic column and methanol as eluent. The ratio of the isomer fractions resulted 45%: 55% of isomer  $[\text{Ru}(\text{tpy})(\Phi\Delta^2\text{py}\Delta^4\Phi)]$  : Isomer  $[\text{Ru}(\text{tpy})(\Phi\Delta^2\text{py}\Delta^2\Phi)]$ .

The formation of an intermediate with formula  $\{\text{Ru}[\text{tpy}][(\eta^2)\Phi\Delta\text{py}\Delta\Phi]\text{X}\}$  (X = solvent molecule) (Fig.6.9), where, initially, the  $(\Phi\Delta\text{py}\Delta\Phi)$  ligand bonds to the Ru-tpy complex as a bidentate ligand, may explain the formation of the two isomers instead of the expected three or the anticipated  $[\text{Ru}(\text{tpy})(\Phi\Delta^2\text{py}\Delta^2\Phi)]$ . It is envisaged that the first coordination will be via the nitrogen of the central pyridine ring and subsequently indifferently via  $\text{N}^2$  or  $\text{N}^4$  of one of the triazole moieties. The second triazole ring will always bind through the  $\text{N}^4$  atom. This is expected because of the steric hindrance between the phenyl ring and the tpy ligand already complexed. Synthesis or photochemical formations of a  $\eta^2$ -tpy complex have precedents in literature.<sup>19, 20</sup>

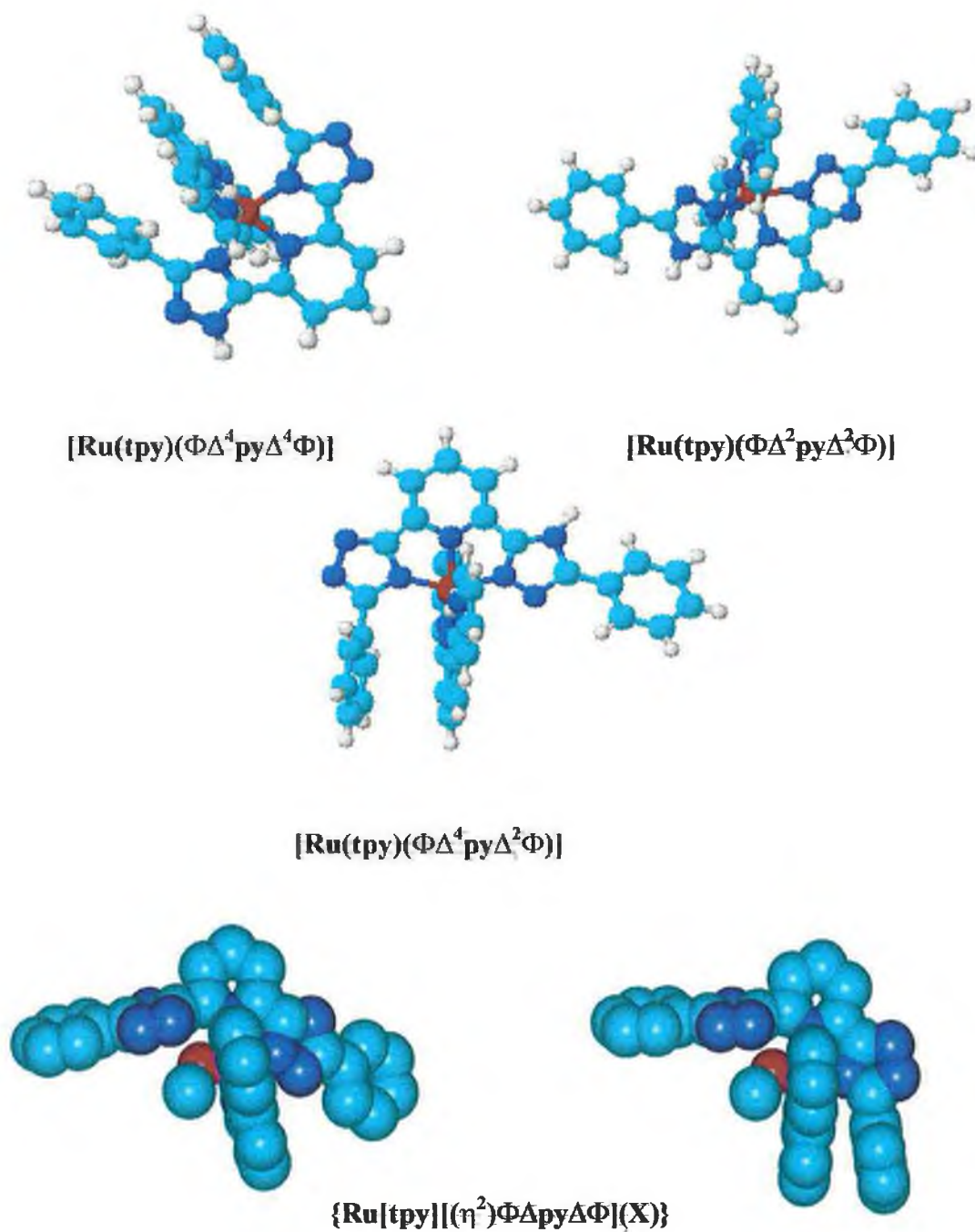


**Figure 6.9 Possible isomers for [Ru(tpy)(ΦΔpyΔΦ)] complex, and space filling molecular models for the possible intermediates {Ru[tpy]((η<sup>2</sup>)ΦΔpyΔΦ)(X)}, where X is a solvent molecule.**



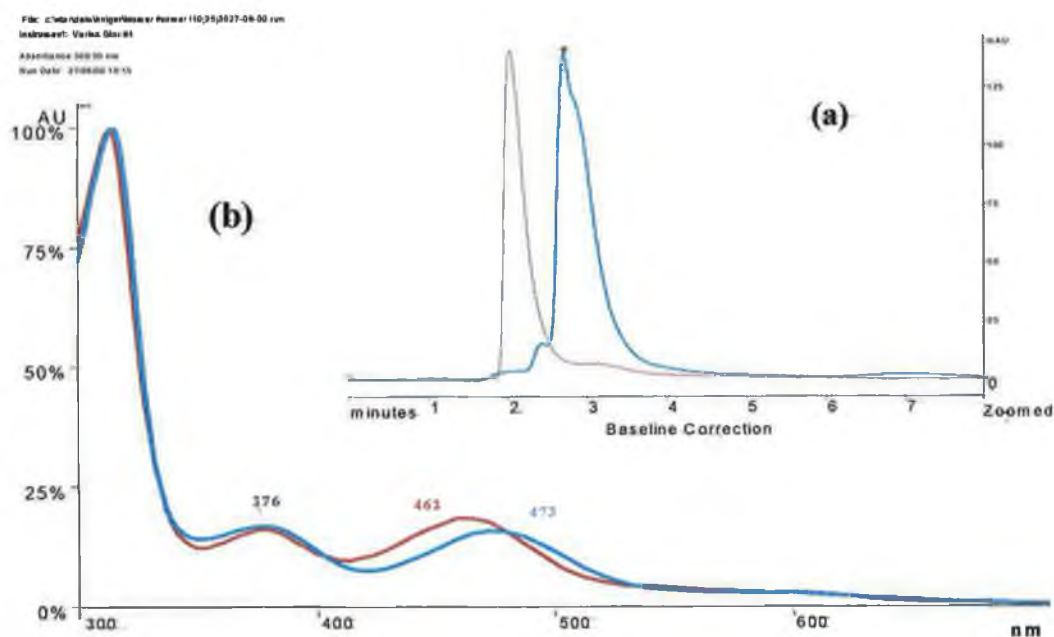


Figure 6.10 Chromatograms (a) and absorption spectra (b) in 0.01 LiClO<sub>4</sub> M acetonitrile: water (4:1) solution of [Ru(tpy)(ΦΔ<sup>2</sup>pyΔ<sup>2</sup>Φ)] (red line) and [Ru(tpy)(ΦΔ<sup>2</sup>pyΔ<sup>4</sup>Φ)] (blue line)

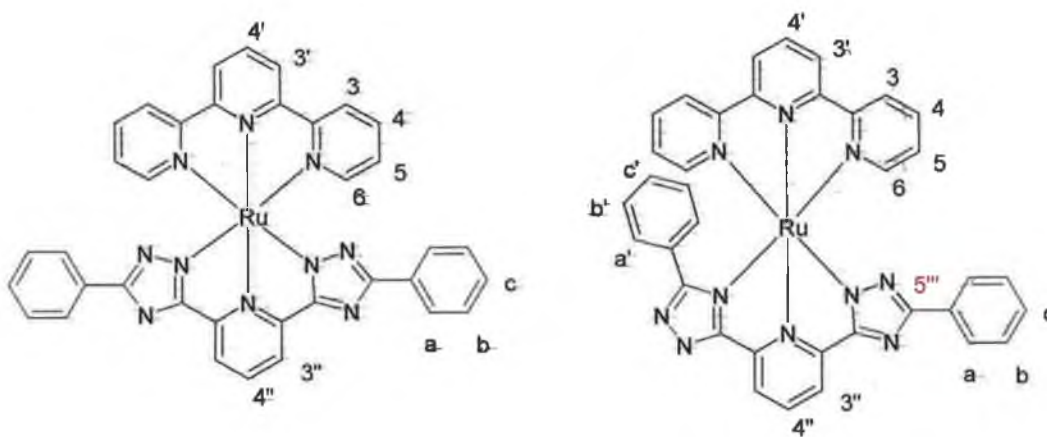


Figure 6.11 [Ru(tpy)(ΦΔ pyΔ Φ)] isomers and their <sup>1</sup>H-NMR assignments.

The chromatograms of the two pure isomers are shown in Figure 6.10, the retention times are a three minutes for  $[\text{Ru}(\text{tpy})(\Phi\Delta^2\text{py}\Delta^4\Phi)]$  and around 2 minutes for  $[\text{Ru}(\text{tpy})(\Phi\Delta^2\text{py}\Delta^2\Phi)]$ .

The  $^1\text{H}$ -NMR spectra (Fig. 6.12, 6.13, 6.14) of a methanol solution of the two isomers are qualitatively quite similar to that of the analogous  $[\text{Ru}(\text{tpy})(\Delta\text{py}\Delta)]$  isomers, assignments were made on the basis of coupling constants and by analogy with  $[\text{Ru}(\text{tpy})(\Delta\text{py}\Delta)]$ .

As expected one of the two  $^1\text{H}$ -NMR spectra exhibits eleven resonances (Fig. 6.13 and 6.14), six from the tpy ligand and five from the  $(\Phi\Delta\text{py}\Delta\Phi)$  ligand. The observation of the eleven resonances confirms the symmetrical structure of one of the isomer on the NMR time scale. The other  $^1\text{H}$ -NMR (Fig. 6.12) spectrum instead showed the presence of 14 signals, evidence of non-symmetrical coordination by the  $(\Phi\Delta\text{py}\Delta\Phi)$  ligand. The assignments of the tpy ligand proton signals were made on the basis of the coupling constants. The tpy terminal pyridyl ring resulted in 4 resonances at 8.37, 7.75, 7.17, 7.44 ppm, in the sequence  $\text{H}^3$ ,  $\text{H}^4$ ,  $\text{H}^5$  and  $\text{H}^6$  respectively, made on the basis of the differing coupling constants  $J(\text{H}^5 \text{H}^6)$  and  $J(\text{H}^3 \text{H}^4)$ . The two remaining tpy resonances, assigned to  $\text{H}^{3'}$  and  $\text{H}^{4'}$  of the central pyridine ring of the tpy, are sensitive to the different coordination of the  $(\Phi\Delta\text{py}\Delta\Phi)$  ligand, or better, sensitive to interaction with the pendent phenyl groups (Fig. 6.9 and Table 6.1).

The assignment of the proton signals of the  $(\Phi\Delta\text{py}\Delta\Phi)$  ligand was also made on the basis of the coupling constants. The two resonances, assigned to  $\text{H}^{3'}$  and  $\text{H}^{4'}$  of the central pyridine ring of  $(\Phi\Delta\text{py}\Delta\Phi)$ , data in Table 6.1, are slightly sensitive to the

$N^2/N^4$  coordination. The presence of two sets of signals for the each proton on the phenyl rings,  $[H^a, H^b, H^c]$  and  $[H^{a'}, H^{b'}, H^{c'}]$  (Fig. 6.11), in one of the  $^1H$ -NMR spectra, that is the asymmetric one (Fig.6.12), is in agreement with the presence of one asymmetric complex  $[Ru(tpy)(\Phi\Delta^2py\Delta^4\Phi)]$ . In the asymmetric complex, the upfield shift of the tpy  $H^{4'}$  and  $H^{3'}$  protons and the upfield shifts of  $(\Phi\Delta py\Delta\Phi)$   $H^{a'}$ ,  $H^{b'}$  and  $H^{c'}$  protons, in comparison with  $H^a$ ,  $H^b$ ,  $H^c$ , are indicative of a strong interaction between one of the phenyl moieties and the central ring of the tpy. That presumably means that the triazole moiety, with the phenyl group in the 5''' position (Fig. 6.11 and 6.9), must be bound to the triazole ring coordinating via  $N^4$  nitrogen. In the symmetric  $^1H$ -NMR spectrum (Fig.6.7, 6.8), the phenyl protons are all shifted down field, which will prelude to a fully complexed  $N^2$  bonded,  $[Ru(tpy)(\Phi\Delta^2py\Delta^2\Phi)]$  isomer.

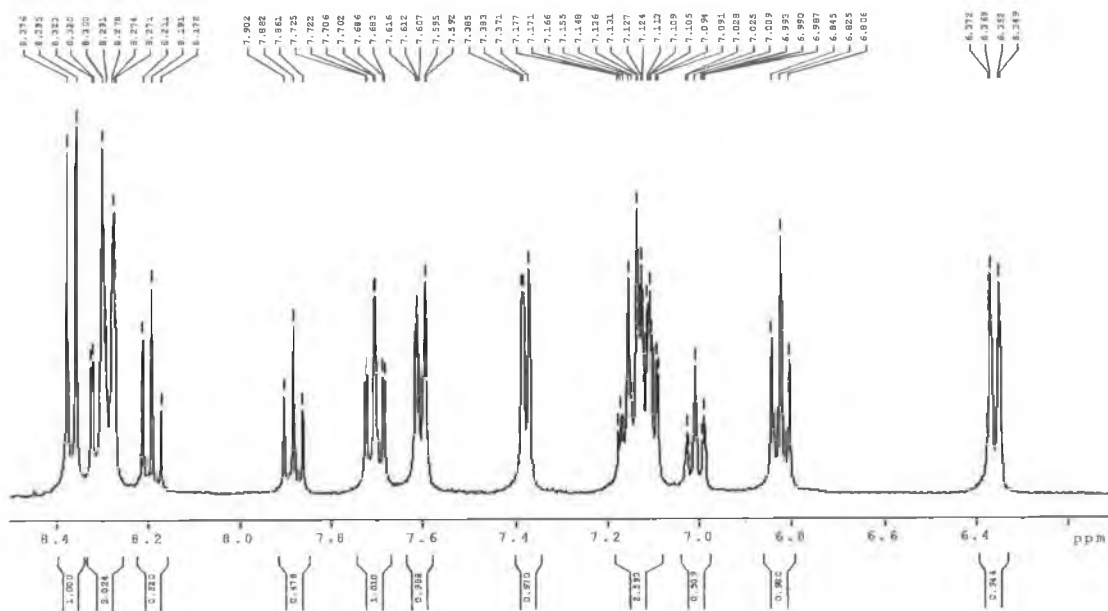


Figure 6.12  $^1\text{H-NMR}$  spectrum of the  $[\text{Ru}(\text{tpy})(\Phi\Delta^2\text{py}\Delta^4\Phi)]$  complex in  $d^4$ -methanol.

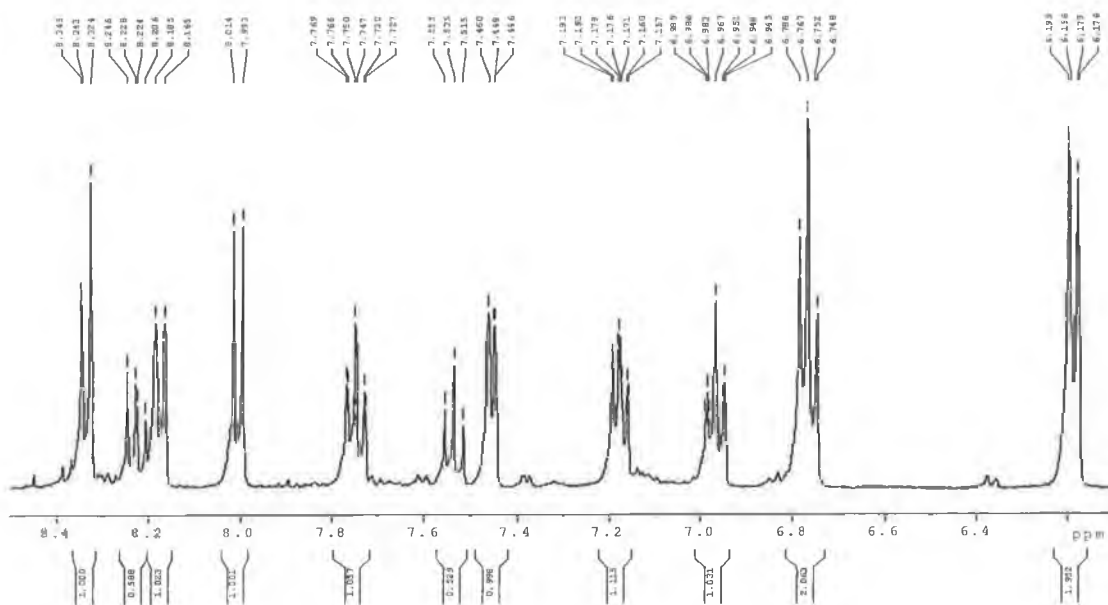
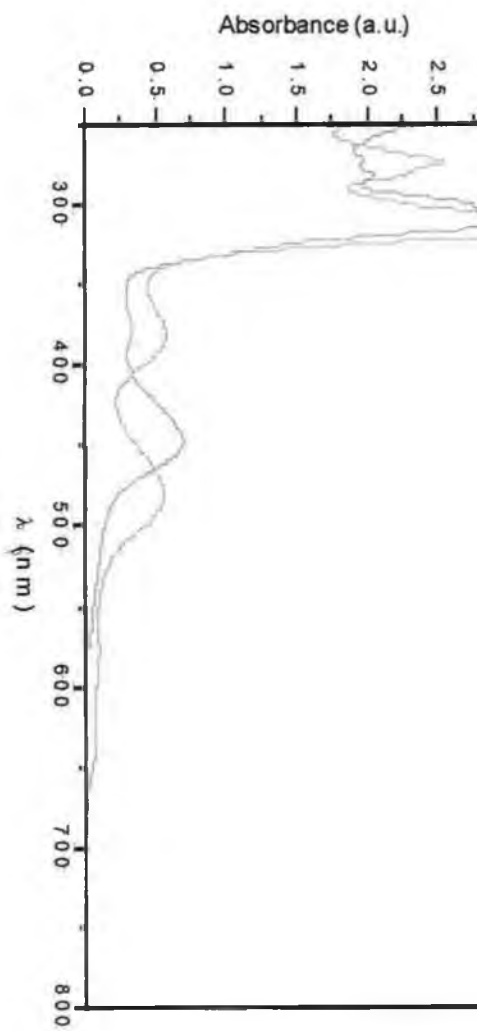


Figure 6.13  $^1\text{H-NMR}$  spectrum of the  $[\text{Ru}(\text{tpy})(\Phi\Delta^2\text{py}\Delta^2\Phi)]$  complex in  $d^4$ -methanol.



**Figure 6.9** Absorption spectra of the [Ru(tpy)( $\Phi\Delta^2$ py $\Delta^2\Phi$ )] complex in basic (blue line) or acidic (red line) ethanol.

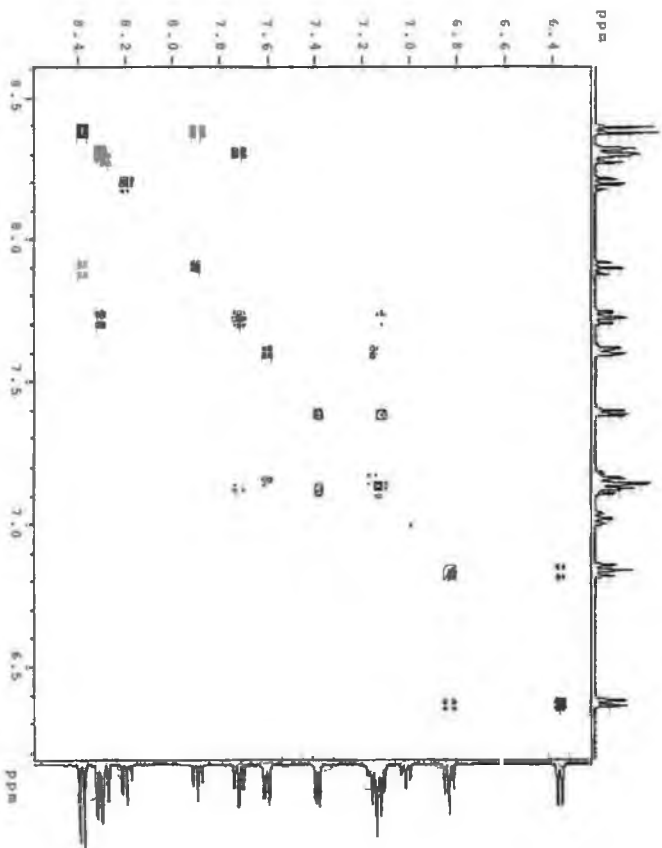


Figure 6.14  $^1\text{H}$ -Cosy-NMR spectrum of the  $[\text{Ru}(\text{tpy})](\text{D}\Delta^2\text{py}\Delta^2\Phi)$  complex in  $d^4$ -methanol.



As previously observed for [Ru(tpy)( $\Delta$ py $\Delta$ )], the UV/VIS absorption spectra of the isomers show, in a basic ethanol solution, a strong metal to ligand tpy based charge transfer band, for the [Ru(tpy)( $\Phi\Delta^2$ py $\Delta^4\Phi$ )] isomer at 475 nm and for [Ru(tpy)( $\Phi\Delta^2$ py $\Delta^2\Phi$ )] at 477 nm. The bands at 272, 315 of both isomers are assigned to the intra ligand  $\pi-\pi^*$  transition (Table 6.2, Fig. 6.9 and 6.12). Two small shoulders were detected at around 620 and 650 nm.(for the assignments see Chapter 5, section 5.3)

In the same solvent at room temperature, the complex shows a strong phosphorescence band at 701 nm for [Ru(tpy)( $\Phi\Delta^2$ py $\Delta^2\Phi$ )] and at 694 nm for [Ru(tpy)( $\Phi\Delta^2$ py $\Delta^2\Phi$ )], the emission maxima and the lifetimes of the excited states, as seen for the analogous [Ru(tpy)( $\Delta$ py $\Delta$ )], show a strong temperature (Table 6.2) and solvent ( Table 6.3 and Fig. 6.12 and 6.13) dependency, but the [Ru(tpy)( $\Phi\Delta$ py $\Delta\Phi$ )] isomers showed more significant differences than the corresponding [Ru(tpy)( $\Delta$ py $\Delta$ )] species.

In comparison with [Ru(tpy) $_2$ ] $^{2+}$  complex, the [Ru(tpy)( $\Phi\Delta$ py $\Delta\Phi$ )] also shows a decrease in the energy of the  $^3$ MLCT state, the emission maxima are red shifted.

In the pH-titration of the isomers, two different patterns were found. Both isomers display a reversible behaviour in the pH range between 1.5-9. For the emission titrations the wavelength of 475 nm was chosen for excitation, which does not vary greatly from the wavelength of the isobestic points of the pKa values of both

titrations. A quenching of the emission was observed in the acid pH-range of the pH-titration.

The  $[\text{Ru}(\text{tpy})(\Phi\Delta^2\text{py}\Delta^2\Phi)]$  isomer shows a blue shift of the MLCT band upon lowering of the pH. Two isobestic points at 470 nm and 405 nm. were observed. A double sigmoidal fitting of the data procured two pKa values of 2.1 and 5.3. For the emission titration curve only one inflexion point was observed at 5.6 which is due to the total quenching of the emission after the first protonation. In contrast the pH-titration of the isomer  $[\text{Ru}(\text{tpy})(\Phi\Delta^2\text{py}\Delta^4\Phi)]$  contained two shifts, first a blue-shift which was then followed by a red-shift. There were also two isobestic points at around 474 nm and 400 nm. The data, when sigmoidally fitted, yield two ground-state pKa values for the absorption, occurring at 2.6 and 6.7 and two inflexion points for the emission at 3.5 and 6.3.

The oxidation potential, E/V vs SCE in methanol solution, observed is 0.60 V for the isomer  $[\text{Ru}(\text{tpy})(\Phi\Delta^2\text{py}\Delta^4\Phi)]$  and 0.50 V for  $[\text{Ru}(\text{tpy})(\Phi\Delta^2\text{py}\Delta^2\Phi)]$ . These shifts, compared to the potential of  $[\text{Ru}(\text{tpy})_2]^{2+}$  (Table 6.2), result from the higher charge density on the metal centre, caused by the strong  $\sigma$ -donor ligand  $(\Phi\Delta\text{py}\Delta\Phi)$ . The values show that  $(\Phi\Delta^2\text{py}\Delta^2\Phi)$  coordinated ligand is a slightly stronger  $\sigma$ -donor than  $(\Phi\Delta^2\text{py}\Delta^4\Phi)^{2-}$  or than the  $(\Delta\text{py}\Delta)^{2-}$  isomers. Both isomers displayed an irreversible reduction around -1.35 V.

For the two isomers the tpy based luminescence lifetimes and spectra in temperature interval from 300 to 80K were measured. As shown by the previous investigations, it was possible to analyse the temperature dependence of the



luminescence lifetime using an Arrhenius –type approach (Equation 5.2). In equation 5.2,  $A_1$  and  $\Delta E_1$  are parameters concerned with the fact that the luminescent level is actually composed of cluster of  $^3\text{MLCT}$  states, and  $\Delta E_1$  can be viewed as the energy width of the clustered levels.  $A_2$  and  $\Delta E_2$  are the pre-exponential factor and the energy barrier, for thermal population of a higher-lying metal-centred state of d-d orbital origin, which is involved in the deactivation of the MLCT state luminescence.

The kinetic parameters, for the excited state decay of the complexes examined, are collected in Table 6.4, they show that:

- The photophysical behaviour is strongly affected by temperature
- In the high temperature region, deactivation of the MLCT excited state is governed by a deactivation process.

According with the lifetime temperature dependency treatment used in chapter 5 this implies population of a higher-lying  $^3\text{MC}$  state which is in turn so strongly coupled to the ground state that this rate constant is much higher than that for the backward  $^3\text{MC}$ - $^3\text{MLCT}$  step. This represents the limiting kinetic case whereby the pre-exponential factors  $A_2$  is in the range of  $10^{11}$ - $10^{12}$   $\text{sec}^{-1}$  and the energy differences ( $\Delta E_2$ ) is the energy between the  $^3\text{MLCT}$  and  $^3\text{MC}$  curves, see picture 5.16.

It is of particular interest to note how the two isomers displayed quite different  $\Delta E_2$  values and how this relates to the difference in the energy gap between the  $^3\text{MLCT}$  and  $^3\text{MC}$  states. As seen for the oxidation potentials, the  $[\text{Ru}(\text{tpy})(\Phi\Delta^2\text{py}\Delta^2\Phi)]$  isomer proved to be a stronger  $\sigma$ -donor than the other isomer, increasing the ligand

field strength and consequentially the distance in energy between the  $^3\text{MC}$  and  $^3\text{MLCT}$  curves .

A similar outcome was also expected as a result of the different solvent behaviour illustrated by the two isomers in polar solvents (Table 6.3), in fact, the lifetimes of the MLCT excited state was to be much longer for  $[\text{Ru}(\text{tpy})(\Phi\Delta^2\text{py}\Delta^2\Phi)]$  than for the other isomer, due to the increase in energies between  $^3\text{MLCT}$  and  $^3\text{MC}$  states. However the general solvent acceptor number- $^3\text{MLCT}$  energy dependency and  $^3\text{MLCT}$  lifetime-energy dependency trends, as seen in Chapter 5 for the archetypal  $[\text{Ru}(\text{tpy})(\Delta^2\text{py}\Delta^4)]$  complex, were also followed by the  $[\text{Ru}(\text{tpy})(\Phi\Delta\text{py}\Delta\Phi)]$  isomers (Table 6.3).

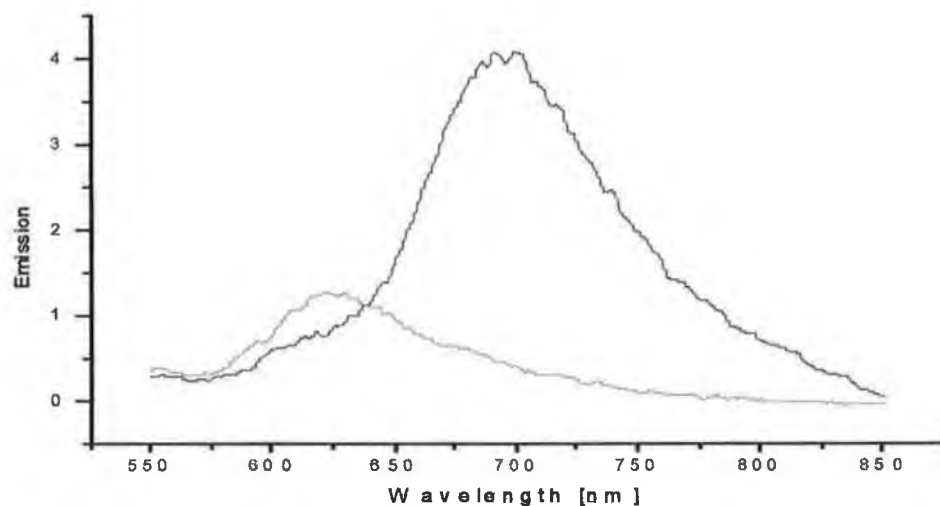


Figure 6.10 Emission spectra of the  $[Ru(tpy)(\Phi\Delta^2py\Delta^4\Phi)]$  complex in basic (black line) or acidic (red line) ethanol, registered at r.t.

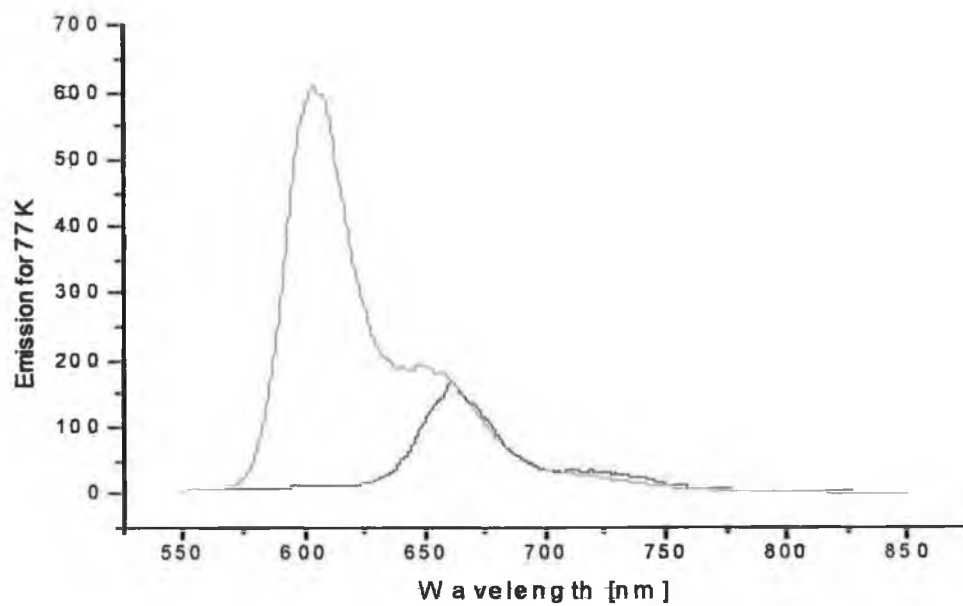


Figure 6.11 Emission spectra of the  $[Ru(tpy)(\Phi\Delta^2py\Delta^4\Phi)]$  complex in basic (black line) or acidic (red line) ethanol, registered at 77K.

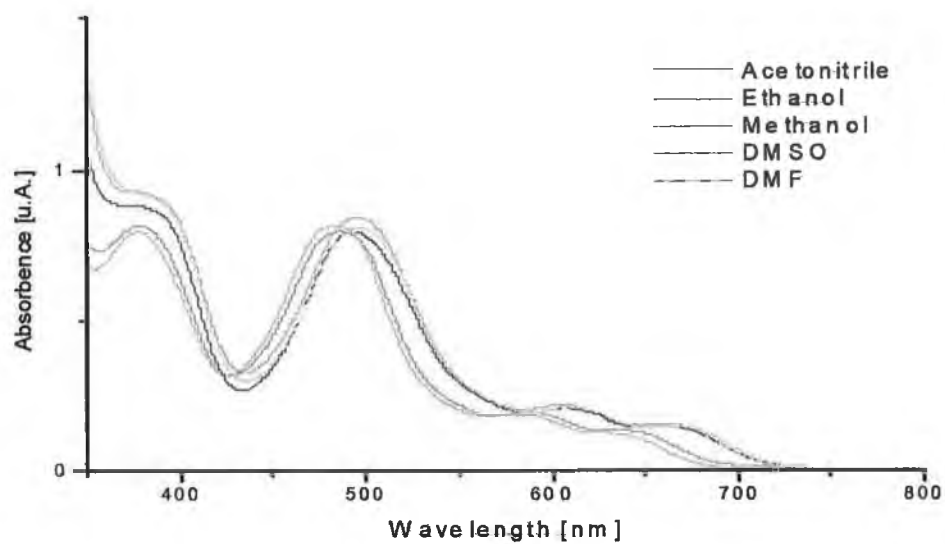


Figure 6.12 Solvent dependency of the  $[\text{Ru}(\text{tpy})(\Phi\Delta^2\text{py}\Delta^2\Phi)]$  absorption spectra at 298 K

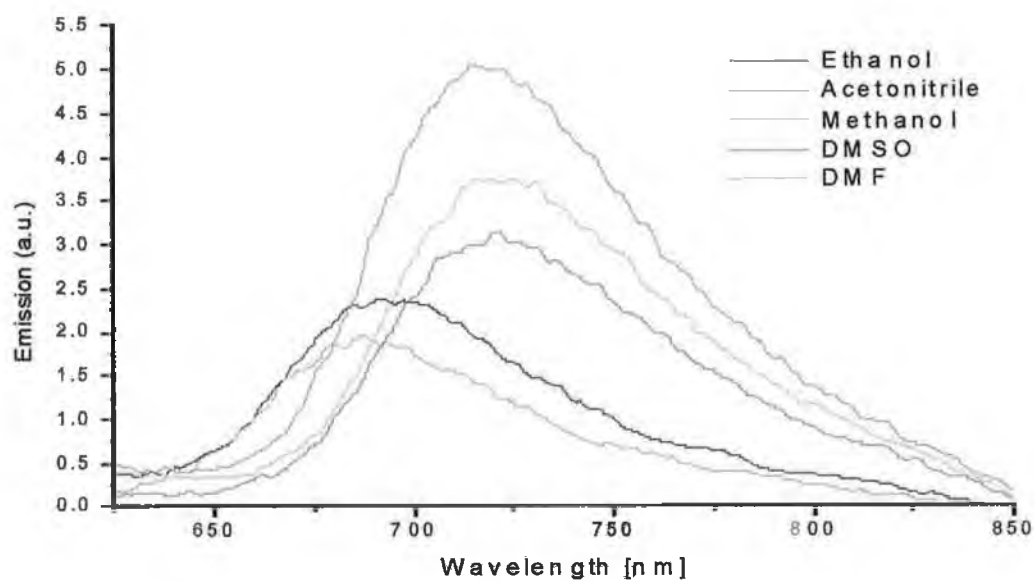


Figure 6.13 Solvent dependency of the  $[\text{Ru}(\text{tpy})(\Phi\Delta^2\text{py}\Delta^2\Phi)]$  emission spectra at 298 K

(ppm)	H <sup>3</sup>	H <sup>4</sup>	H <sup>5</sup>	H <sup>6</sup>	H <sup>3'</sup>	H <sup>4'</sup>	H <sup>3''</sup>	H <sup>4''</sup>	H <sup>a/a'</sup>	H <sup>b/b'</sup>	H <sup>c/c'</sup>
	(d)	(dd)	(dd)	(d)	(d)	(t)	(d)	(t)	(d)	(t)	(t)
Tpy	8.7	8.00	7.50	8.70	8.55	8.10					
H <sub>2</sub> (ΦΔpyΔΦ) <sup>*</sup>							8.1	8.2	8.1	8.2	7.54
[Ru(tpy) <sub>2</sub> ] <sup>2+</sup>	8.82	8.08	7.34	7.72	9.09	8.59					
[Ru(ΦΔ <sup>2</sup> pyΔ <sup>2</sup> Φ)(tpy)]	8.37	7.75	7.17	7.44	8.34	7.55	8.20	8.29	6.19	6.76	6.98
[Ru(ΦΔ <sup>2</sup> pyΔ <sup>4</sup> Φ)(tpy)]	8.34	7.70	7.12	7.38	8.01	7.90	8.22	8.19	6.36/ 7.61	6.86 /7.12	6.98/ 7.17

Table 6.1 <sup>1</sup>H-NMR spectroscopic data for d<sup>4</sup>-methanol solutions of ligands and their ruthenium complexes (see Fig. 6.5), a) d<sup>6</sup>-DMSO.

	Abs 298 K <sup>a</sup>		Emi. 298 K <sup>a</sup>			Emi. 77 K <sup>a</sup>		Electrochem <sup>c</sup>	
	λ (nm) <sup>a</sup>	ε (M <sup>-1</sup> cm <sup>-1</sup> )	λ (nm) <sup>c</sup>	τ (nsec) <sup>f</sup>	φ <sub>em</sub> <sup>h</sup>	λ (nm) <sup>c</sup>	τ (μsec)	E <sub>red</sub> (Volt)	E <sub>ox</sub> (Volt)
[Ru(tpy) <sub>2</sub> ] <sup>2+</sup>	474	10400	629	0.25	5.0*10 <sup>-6</sup>	598	8.9	1.67	0.92
[Ru(ΔpyΔ)(Cl-tpy)] <sup>i</sup>	489	13250	770	45				1.30	0.60
[Ru(ΦΔ <sup>2</sup> pyΔ <sup>2</sup> Φ)(tpy)]	486	13500	694	51	2.5*10 <sup>-4</sup>	648	7	(1.36)	[0.50] <sup>m</sup>
[Ru(ΦΔ <sup>2</sup> pyΔ <sup>4</sup> Φ)(tpy)]	485	12800	701	24	1.0*10 <sup>-4</sup>	660	5.5	(1.35)	[0.60] <sup>m</sup>
[Ru(Δ <sup>2</sup> pyΔ <sup>2</sup> )(tctpy)] <sup>-5 i</sup>	490	10500	770	100		670		(1.31)	0.40

Table 6.2 a) Ethanol, b) Methanol, ethanol (1, 4), c) DMF vs. Fc/ Fc<sup>+</sup>, in round braquette not reversible reductions. d) Wavelength of the lowest energy absorption maximum. e) Wavelength of highest energy emission feature. f) Luminescence emission lifetime (± 10%). h) Luminescence quantum yield. i) photophysical measurements in deaerated DMF solution. m) Measured in methanol solution where the complex presented the higher solubility

Solvent (Acceptor number)	$V_{\max}^{\text{abs}}$ nm.	$V_{\max}^{\text{abs}}$ nm.	$V_{\max}^{\text{em}}$ nm.	$\tau$ ns
	(298 K)	(298 K)	(298 K)	(298 K)
<b>[Ru(<math>\Phi\Delta^2\text{py}\Delta^2\Phi</math>)(tpy)]</b>				
Methanol (41.3)	483	374	687	50
Ethanol (37.1)	486	378	694	51
Acetonitrile (19.3)	492	382	721	72
DMSO (19.3)	495	388	718	94
DMF (16.0)	495	391	723	80
<b>[Ru(<math>\Phi\Delta^2\text{py}\Delta^4\Phi</math>)(tpy)]</b>				
Methanol (41.3)	483	378	700	20
Ethanol (37.1)	485	380	701	24
Acetonitrile (19.3)	493	384	729	65
DMSO (19.3)	498	387	734	92
DMF (16.0)	498	390	738	62

**Table 6.3 Spectroscopic and photophysical properties of [Ru(tpy)( $\Phi\Delta\text{py}\Delta\Phi$ )] isomers in different solvents.**

	$k_0$ ( $\text{sec}^{-1}$ )	$k_1$ ( $\text{sec}^{-1}$ )	$\Delta E_1$ ( $\text{cm}^{-1}$ )	$k_2$ ( $\text{sec}^{-1}$ )	$\Delta E_2$ ( $\text{cm}^{-1}$ )
[Ru( $\Phi\Delta^2\text{py}\Delta^2\Phi$ )(tpy)]	$1.5 \cdot 10^5$	$9 \cdot 10^8$	700	$5 \cdot 10^{12}$	2850
[Ru( $\Phi\Delta^2\text{py}\Delta^4\Phi$ )(tpy)]	$2.00 \cdot 10^5$	$1 \cdot 10^9$	350	$2 \cdot 10^{12}$	2650

**Table 6.4 Kinetic parameters for excited state decay obtained from the fitting of equation (5.2) to the experimental results**

## 6.5 Bibliography

---

- <sup>1</sup> Newkome G R, He E., Moorefield C N, **Chem. Rev.**, 1999, 99, 1689.
- <sup>2</sup> Constable E C, Harverson P, **Chem Commun.** 1996, 1821.
- <sup>3</sup> Constable E C, Harverson P, Housecroft C E, **J. Chem. Soc Dalton Trans**, 1999, 3693.
- <sup>4</sup> Constable E C, Cargill Thompson A M W, Tocher D A, Daniels M A M, **New J. Chem**, 1992, 16, 855.
- <sup>5</sup> Maestri M, Armaroli N, Balzani V, Constable E C, Cargill Thompson A M W, **Inorg. Chem.** 1995, 34, 2759.
- <sup>6</sup> Duati M, Fanni S, Vos JG, **Inorg Chem Comm** 2000, 3, 68.
- <sup>7</sup> Nazeerudin M K, Pechy P, Renouard T, Zakkerudin S M, Baker R H, Comte P, Liska P, Cevey L, Costa E, Shklover V, Spiccia L, Deacon G B, Bignozzi C A, Grätzel M. **J. Am. Chem. Soc.**, 2001, 123, 1613
- <sup>8</sup> Lemon B I, Hupp J. T. **J. Phys. Chem B** 1999, 103, 3797
- <sup>9</sup> Ferrere S, Gregg B A **J. Am. Chem. Soc.** 1998, 120, 843.
- <sup>10</sup> Kelly C A, Farzard F, Thompson D W, Stipkala J M, Meyer G J, **Langmuir** 1999, 15, 650.
- <sup>11</sup> Argazzi R, Bignozzi C A, Heimer T A, Meyer G J, **Inorg Chem.** 1997, 36, 2
- <sup>12</sup> Anderson P A, Strouse G F, Treadway J A, Keene F R, Meyer T J **Inorg Chem.** 1994, 33, 3863
- <sup>13</sup> Perez, W.J., Lake C. H. **J. Chem. Soc. Dal Trans.** 1999, 2281.
- <sup>14</sup> Nazeeruddin M. K, Pechy P, Grätzel M, **Chem Commun** 1997, 1705

- 
- <sup>15</sup> Nazeeruddin M K, Pechy P, Renouard T, Zakeeruddin S M, Humpr-Baker R, Comte, Liska P, Costa E, Shklover V, Spiccia L, Deacon G, Bignozzi C A, Grätzel M. **J. Am. Chem. Soc.** 2001, 123, 1613
- <sup>16</sup> Nazeeruddin M K, Kalyanasundaram K, Grätzel M, **Inorg. Synth.** 1998, 32, 181
- <sup>17</sup> Hage R, Turkenburg J P, de Graaff R A G, Haasnoot J G, Reedijk J, Vos J G **Acta Crystallgraph. Sect C**, 1989, 45, 381.
- <sup>18</sup> Hage R, Haasnoot J G, Reedijk J, Wang R, Ryan E M, Vos J G Spek A L, Duisenberg A J M, **Inorg. Chim Acta**, 1990, 174, 77
- <sup>19</sup> Fletcher N C, Keene F, **J. Chem. Soc., Dalton Trans.** 1998, 2293
- <sup>20</sup> Hecker C R, Fanwick PE, McMillin D R **Inorg. Chem**, 1991, 30, 659



## **Chapter 7**

### **“The Tetrazolate Family”**

“Nature always sides with the hidden flaw. ”

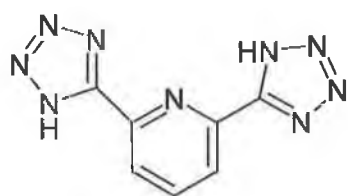
**Murpy**

## 7.1 Introduction

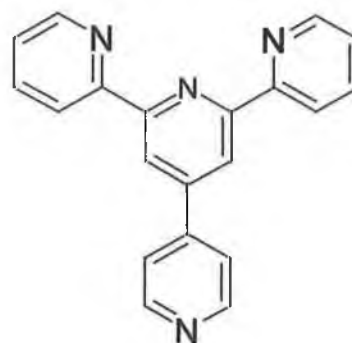
Tetrazole and substituted tetrazoles, although sometimes capable of violent decomposition reactions, have been used in coordination chemistry to prepare a number of coordination compounds during the last decades<sup>1,2,3</sup>. Nevertheless they are not widely known as common ligands and little is known about the nature and strength of the coordination behaviour of the tetrazole ring. This encouraged the investigation into some unknown fields of the tetrazole coordination chemistry.

In Section 4.4 the ( $\square$ py) ligand and its bis (bipyridyl) ruthenium complex have been discussed. The nature of the metal-to-ligand interaction in this complex was studied by <sup>1</sup>H-NMR, electronic spectroscopies and cyclic voltammetry. It was shown that the negatively charged tetrazole group is a strong electron donor whereas the protonated tetrazoles demonstrated a significant lowering in the energy of the metal based HOMOs and raising in the energy of the ligand base LUMOs.

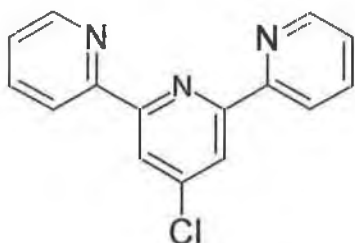
The H<sub>2</sub>( $\square$ py $\square$ ) ligand (Fig. 7.1) was synthesised for its electronic,  $\sigma$ -donor and  $\pi$ -acceptor, and structural, tpy type ligand, properties. Like the H<sub>2</sub>( $\Delta$ py $\Delta$ ) ligand, it contains a central pyridine ring which is a good  $\pi$ -acceptor and instead of the two triazolate moieties, two tetrazolate rings are present. They also are good  $\sigma$ -donor, as shown in Chapter 4, but because of the high symmetry of the nitrogens in the tetrazole moiety, the presence of structural isomers is avoided. The H<sub>2</sub>( $\square$ py $\square$ ) ligand coordination to ruthenium complexes is tridentate, in a pseudo-octahedral coordination, the class of symmetry of its tpy complexes is C<sub>2v</sub>.



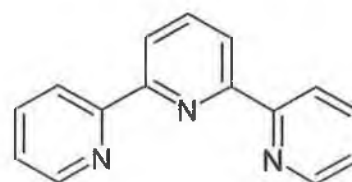
**2-6 di (tetraz-5-yl) pyridine**  
 $H_2(\square py \square)$



**4 (pyrid-4-yl) 2,2'; 6', 2'' terpyridine**  
 (py-tpy)



**4 chloro 2,2'; 6', 2'' terpyridine**  
 (Cl-tpy)



**2,2'; 6', 2'' terpyridine**  
 (tpy)

**Figure 5.1 Ligands cited in the text .**

The aim of this chapter is to study comprehensively a method to increase the emission quantum yield and increase the lifetime of the excited state, avoiding the formation of structural isomers.

The tridentate ligand  $H_2(\square py \square)$ , (Fig.7.1) was synthesised (see Chapter 3) according to the literature for similar ligands<sup>4</sup>, using little modifications, and used for its  $\sigma$  donor and  $\pi$  acceptor properties and it is hoped that due to these properties the excited states of the Ru(II) complexes would substantially alter their photophysical properties.

The  $H_2(\text{py})$  ligand contains a pyridine ring which is a good  $\pi$  acceptor and two tetrazolate moieties which are strong  $\sigma$  donors but they do not have different sites of coordination. The coordination to ruthenium complexes is tridentate, in a pseudo-octahedral coordination. Due to the ruthenium complexes building block potential in supramolecular systems, it is necessary to know their properties as individual units

## 7.2 Synthesis and Purification

The ligand di 2,6-(tetraz-5-yl) pyridine,  $H_2(\square py \square)$ , was prepared by reaction of pyridine-2,6, carbonitrile and sodium azide, as shown in section 3. The preparation of the complexes involved its reaction with one equivalent of  $[Ru(X-tpy)Cl_3]$ , where  $X = H, Cl$  or  $py$ . Once again the method proved to be somewhat problematic. The major problem was again the solubility of the ligand and the solubility of the resulting complex. The  $H_2(\square py \square)$  ligand is soluble in hot DMF or in basified polar solvents in its anionic form.

In the course of preparation of the mononuclear complex a boiling DMF solution, in presence of N-ethyl morpholine as a reducing agent, was used.

The reaction was found to give the desired complex with an average yield of 30%. Purification was achieved by recrystallisation from 1:1 water-DMF solution and producing an analytically pure, curry-brown coloured powder. The protonated species is very poorly soluble in all solvent systems tried. The  $[Ru(py-tpy)(\square py \square)]$  was the only exception, it was isolated as  $[Ru(Hpy-tpy)(\square py \square)][PF_6]$  and  $[Ru(Hpy-tpy)H_2(\square py \square)][ClO_4]_3$  salts. These complexes showed good solubility in acetone, acetonitrile and DMF.

### 7.3 NMR Spectroscopy

The complexes obtained were diamagnetic, and the  $^1\text{H-NMR}$  properties were investigated to probe the inter ligand and metal-ligand interactions in these systems. The  $^1\text{H-NMR}$  spectra (Fig.7.3, 7.4, 7.5, 7.6, 7.7 and Table 7.1) were recorded in  $d_6$ -DMSO.

As discussed in Chapters 5 and 6, in  $\text{tpy-Ru(II)}$  complexes, the lowest field resonance is  $\text{H}^3$ , followed by  $\text{H}^4$ ,  $\text{H}^6$  and  $\text{H}^5$ . The upfield shifting of  $\text{H}^6$  with respect to  $\text{H}^3$  is explained by the fact that it lies in the shielding region above the tetrazolate ring of the other ligand.

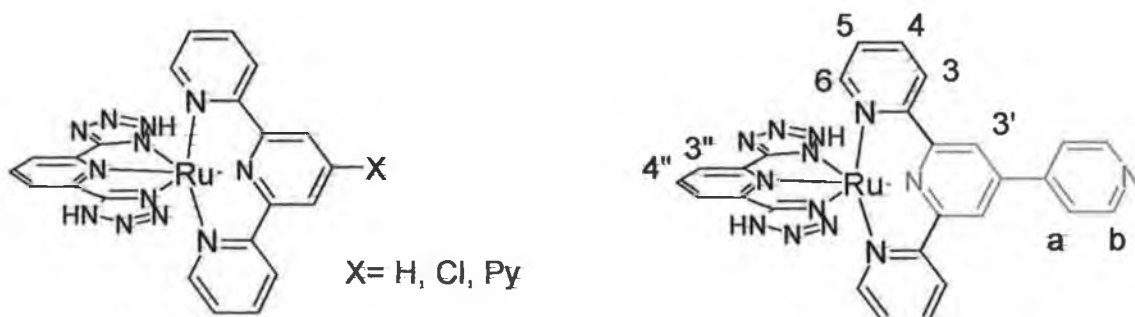


Figure 7.2. Ruthenium complexes, and  $^1\text{H-NMR}$  proton assignments.

From the CIS coordination shift,  $\text{CIS} (= \delta_{\text{complex}} - \delta_{\text{ligand}})$ , a number of general patterns are observed, which provide information about the conformational and electronic charges upon coordination. In the deprotonated complexes  $\text{H}^3$  experiences a small downfield shift upon coordination, which is usually attributed to Van der Waals deshielding by  $\text{H}^{3'}$ . In general,  $\text{H}^5$  undergoes very minor coordination shifts. The shift of  $\text{H}^{3'}$  is related in part to the Van der

Waals interaction, in part it may be attributed to the metal interaction with the central pyridine ring, which is greater than that with the terminal rings.

In the case of the  $H_2(\square py \square)$  ligand, the  $H^{3''}$  and  $H^{4''}$  proton shifts observed may be explained in similar terms as those referred to for the  $H^{3'}$  and  $H^{4'}$  protons of the terpyridine ligand.

The negative CIS values appear greater than for the analogous tpy complexes, this is simply a consequence of deprotonation of the tetrazole rings and the resulting transfer of electron density from the negatively charged tetrazole to the metal.

The  $^1H$ -NMR spectral data (Fig. 7.3, 7.4, 7.5, 7.6, 7.7) of a  $d^8$ -DMF solution of  $[Ru(py-tpy)(\square py \square)]$  are collected in Table 7.1. The spectrum is relatively clear and well resolved, and illustrates the symmetry of the ruthenium complex. The spectrum was unambiguously assigned on the basis of H-cosy and by comparison with the spectrum of  $[Ru(tpy)(\square py \square)]$  and  $[Ru(py-tpy)_2]^{2+}$ . It is of particular interests that, in the tetrazolate compounds  $[Ru(tpy)(\square py \square)]$  and  $[Ru(py-tpy)(\square py \square)]$ , the coordination shifts associated with  $H^{3'}$  (CIS<sub>tpy</sub> +0.46, CIS<sub>py-tpy</sub> 0.38 ppm) are similar. This strongly suggests that the electronic changes occurring within the ligand upon coordination to the metal are similar to the two ligands, which indicates that there are no significant changes in the configuration of the non-coordinated pyridine ring upon adoption of the tridentate mode.

Although it was not possible to have solid state structural data for the complex, analogous studies on 4'-phenyl substituted ligands suggest that the interplanar angles between the central ring of the tpy and the 4-pyridyl substituent will be in the range 5-20°.<sup>5</sup>

The mono protonated species, in which the coordinated (py-tpy) ligand is protonated at the free 4-pyridyl group, is shown in Figure 7.2. Looking at the protonation shifts  $\Delta\delta$  ( $=\delta_{\text{protonated complex}} - \delta_{\text{parent complex}}$ ) and the CIS ( $=\delta_{\text{complex}} - \delta_{\text{ligand}}$ ), a number of features are immediately noted. The terminal pyridine rings are essentially unperturbed by protonation and all of the changes in charge density are associated with the central '4, 4' bipyridine functionality (Fig. 7.2). Most surprisingly, the major shift (0.63 ppm) is associated with H<sup>a</sup> and not with H<sup>b</sup>, the proton adjacent to the site of protonation. This is in accord with the known protonation behaviour of pyridine, and 4, 4' bipyridine in D<sub>2</sub>O.<sup>6</sup> The down field shift of H<sup>a</sup> is much larger than that for H<sup>3'</sup>. Two possible factors are involved in these shifts. The first is a purely electronic one, which results in charge build-up on the non-coordinated pyridyl ring. The second effect involves rotation about the inter-annular bond between the two rings of the '4, 4' bipyridine unit. This will result in changes in the anisotropic shielding and deshielding of H<sup>a</sup> and H<sup>3'</sup>, but cannot easily be quantified.



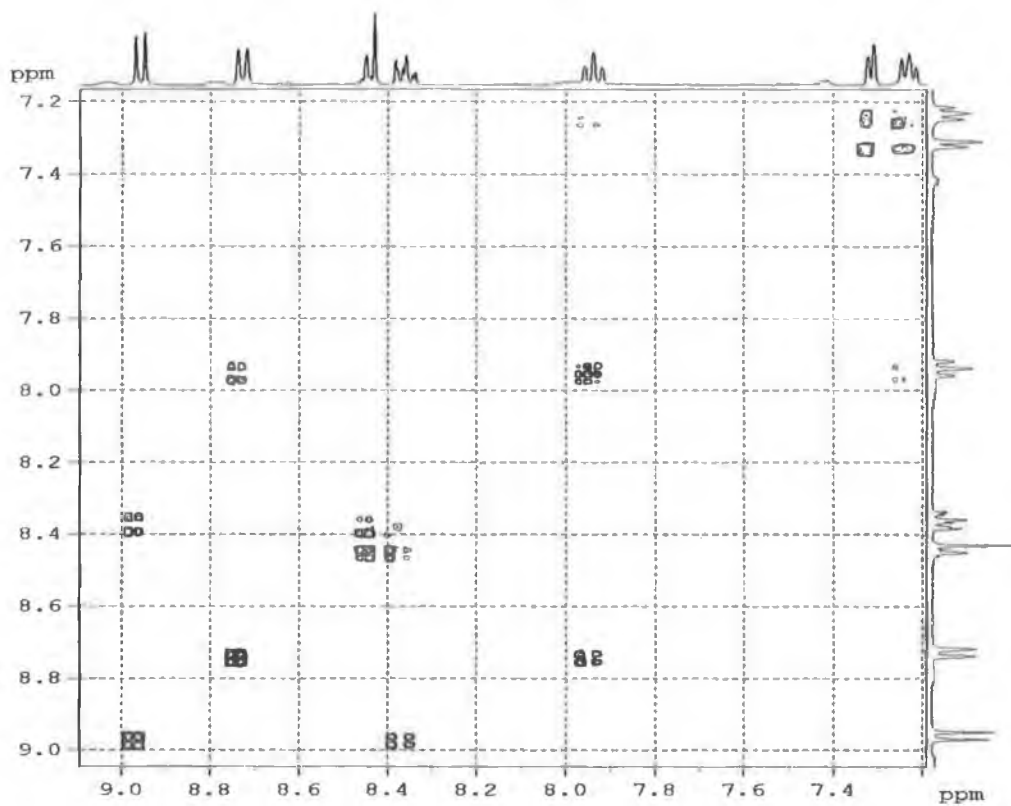


Figure 7.3  $^1\text{H}$ -Cosy-NMR spectra of the  $[\text{Ru}(\text{tpy})(\text{py})]$  complex in  $\text{d}^6$ -DMSO

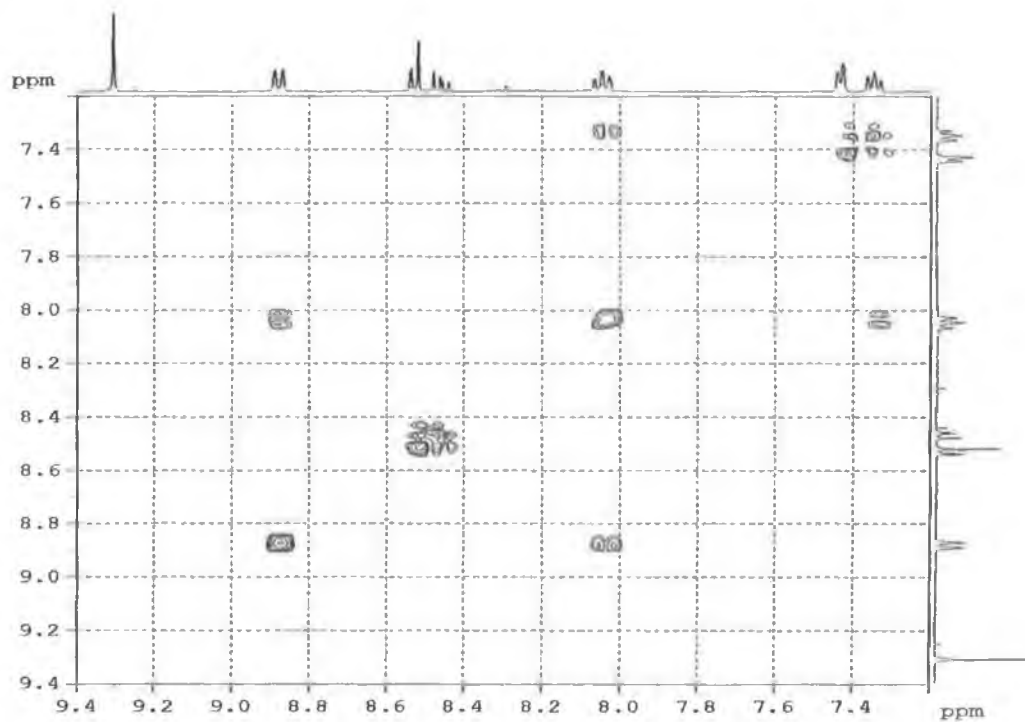


Figure 7.4  $^1\text{H}$ -Cosy-NMR spectra of the  $[\text{Ru}(\text{Cl-tpy})(\text{py})]$  complex in  $\text{d}^6$ -DMSO

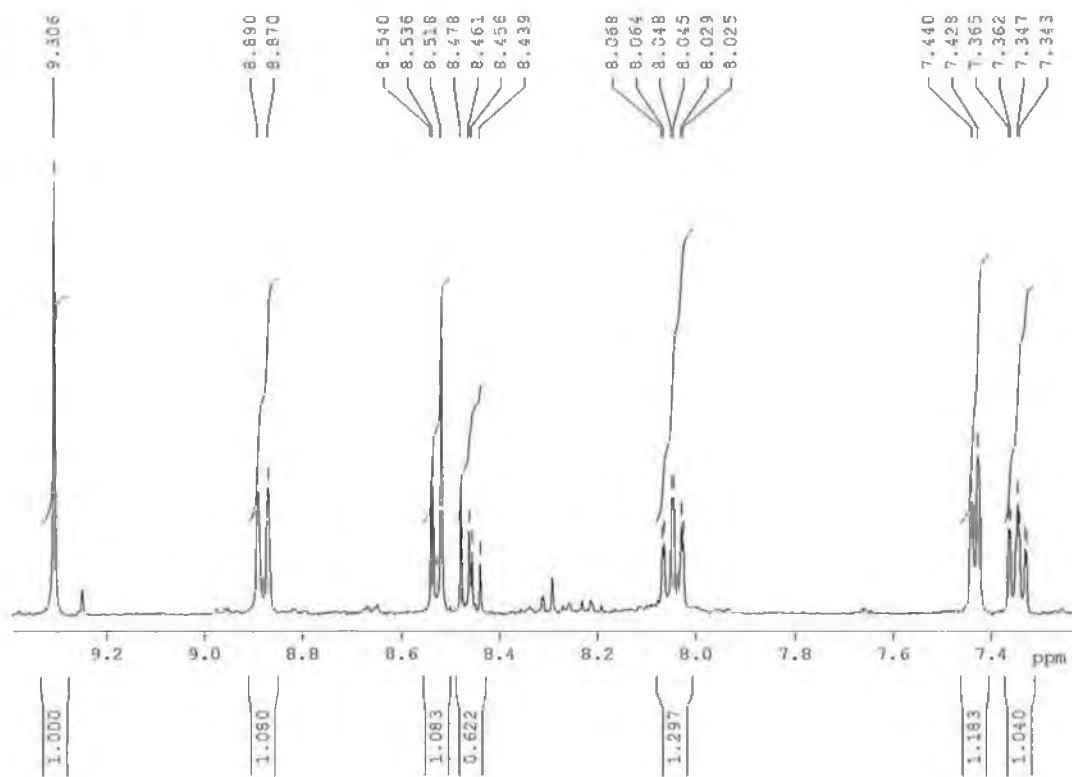


Figure 7.5  $^1\text{H-NMR}$  spectra of the  $[\text{Ru}(\text{Cl-tpy})(\text{py})]$  complex in  $d^6\text{-DMSO}$ .

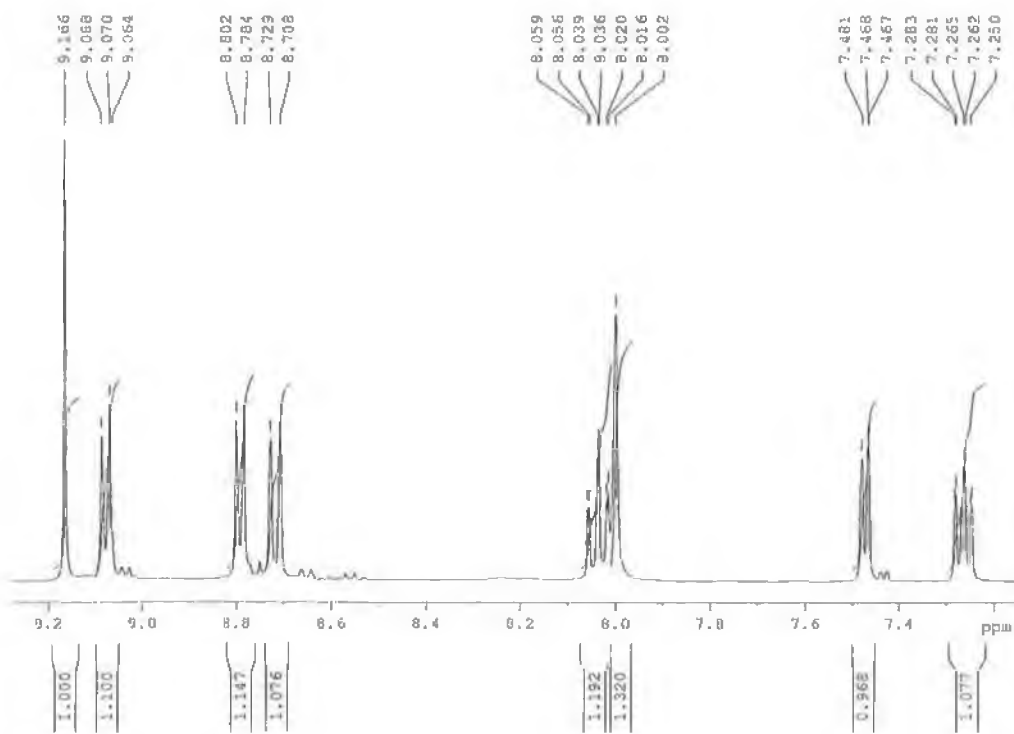


Figure 7.6  $^1\text{H-NMR}$  spectra of the  $[\text{Ru}(\text{HPy-tpy})(\text{py})]^+$  complex in  $d^6\text{-DMSO}$ .

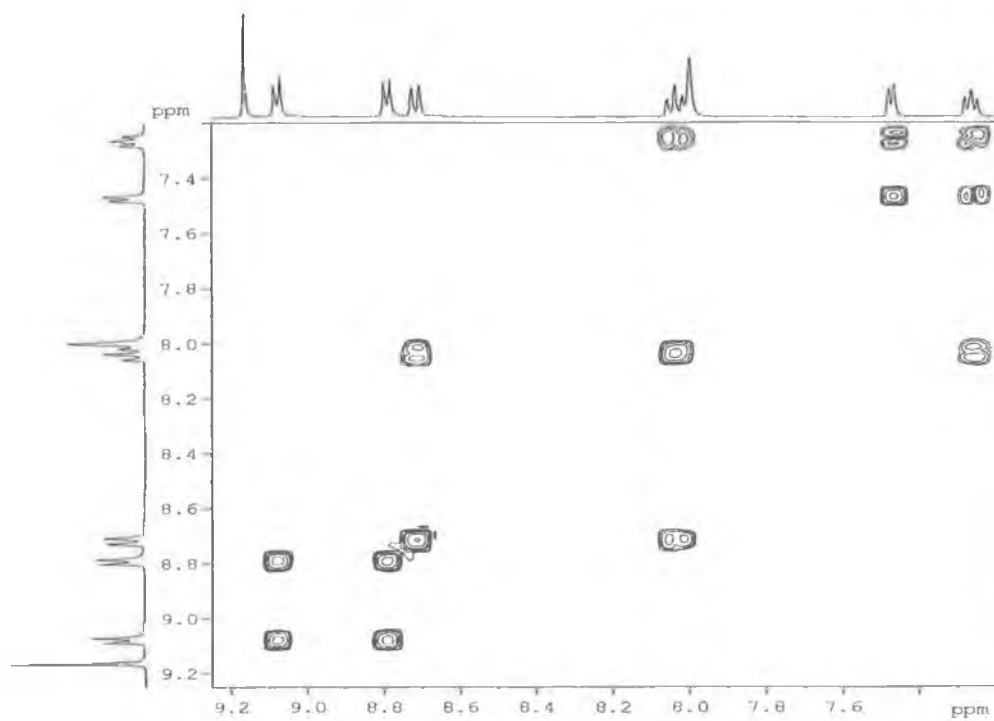


Figure 7.7 <sup>1</sup>H-Cosy-NMR spectra of the [Ru(py-tpy)(py)] complex in d<sup>6</sup>-DMSO

(ppm)	H <sup>3</sup>	H <sup>4</sup>	H <sup>5</sup>	H <sup>6</sup>	H <sup>3'</sup>	H <sup>3''</sup>	H <sup>4''</sup>	H <sup>X1</sup>	H <sup>X2</sup>
	(d)	(dd)	(dd)	(d)	(d)	(d)	(t)		
tpy	8.66	7.95	7.42	8.69	8.54			8.02	
Cl-tpy	8.59	7.84	7.36	8.70	8.48				
Py-tpy	8.72	7.99	7.47	8.74	8.78			7.83	8.77
H <sub>2</sub> (□py□)						8	8		
[Ru(tpy)(□py□)]	8.80	8.00	7.30	7.38	9.00	8.55	8.45	8.45	
[Ru(□py□)(Cl-tpy)]	8.91	7.73	7.37	7.46	9.34	8.56	8.49		
[Ru(□py□)(Hpy-tpy)]	8.30	8.06	7.47	7.46	9.16	8.01	8.01	8.78	9.07
[Ru(□py□)(py-tpy)]	8.96	8.00	7.37	7.34	9.37	8.45	8.39	8.85	9.07
[Ru(tpy) <sub>2</sub> ] <sup>2+</sup>	8.48	7.91	7.15	7.33	8.74			7.92	
[Ru(Cl-tpy) <sub>2</sub> ] <sup>2+</sup>	8.90	8.12	7.38	7.86	9.23				
[Ru(py-tpy) <sub>2</sub> ] <sup>2+</sup>	8.66	7.97	7.20	7.43	9.07			8.14	8.97
[Ru(Hpy-tpy) <sub>2</sub> ] <sup>4+</sup>	8.69	8.01	7.24	7.44	9.13			8.74	9.05

Table 7.1 <sup>1</sup>H-NMR spectroscopic data for d<sup>6</sup>-DMSO solutions of ligands and their Ruthenium complexes (see Fig. 7.2), when in X-tpy, the substituent X= py then H<sup>X1</sup>= H<sup>a</sup> and H<sup>X2</sup>= H<sup>b</sup>, instead when X= H then H<sup>X1</sup>= H<sup>d</sup>.

## 7.4 Electronic Spectroscopy

The UV-vis. absorption spectra of the complexes (tab. 7.2 and Fig. 7.6, 7.7), in DMF show two intense metal to ligand charge transfer bands around 390 nm and 480nm, the bands around 275, 309 are assigned to the intra ligand  $\pi$ - $\pi^*$  transitions of the ligand.

$H_2(\square py \square)$ , after coordination with the Ru-tpy moiety, is found to be a much stronger acid, pKa values of less than 0 were found upon titration in Britton Robinson, than  $H_2(\Delta py \Delta)$  (pKa values 2.4 and 4.5), the species studied in solution are normally the fully deprotonated.

The  $(\square py \square)^{2-}$  is expected to be, as will be shown in section 7.4, easier to reduce than  $(\Delta py \Delta)^{2-}$  but much less than tpy. On this basis, it is possible to hypothesise that, in coordination compounds,  $(\square py \square)^{2-}$  ligand is a poorer  $\sigma$ -donor than  $(\Delta py \Delta)^{2-}$ , but a better  $\sigma$ -donor and a poorer  $\pi$ -acceptor than terpyridine. In agreement with this hypothesis, all the emission spectra were blue shifted in respect with the analogous  $(\Delta py \Delta)$  complexes. However replacement of one X-tpy (X= H, Cl, py) ligand of  $[Ru(X-Tpy)_2]^{2+}$  with  $(\square py \square)^{2-}$  ligand causes an increase in the electronic charge on the metal, with a consequent red shift of the metal to ligand (tpy based) charge transfer absorption and emission bands (Fig. 7.8, 7.9, 7.10, 7.11).

Upon adding acid to the acetonitrile solution of  $[Ru(py-tpy)(\square py \square)]$  a colour change from crab brown to lobster pink occurred. This corresponds to the formation of a complex in which the coordinated ligand is protonated at the free 4-pyridyl group,  $[Ru(Hpy-tpy)(\square py \square)]^+$ , and the colour change is associated with

a shift in the MLCT band from 490 to 506 nm. Shifts also occur within the free pendant pyridine based  $\pi$ - $\pi^*$  transitions which are observed at 340 nm. The shift of the MLCT band to lower energy is compatible with the lowering in energy of  $\pi^*$  levels of the protonated ligand. Systematic shifts in the electronic spectrum occurred upon titration of buffer solutions of  $[\text{Ru}(\text{py-tpy})(\square\text{py}\square)]$  complex. A single protonation process with an approximate pKa of 2.8 is observed, in agreement with the analogous  $[\text{Ru}(\text{py-tpy})_2]^{2+}$ , a large excess of acid must be added to observe the protonation on the  $(\square\text{py}\square)^{2-}$  ligand, (pKa less than 0). The fully protonated species shows, in fact, a lemon-the yellow colour with a maximum around 460 nm.

	abs 298 K <sup>a</sup>		emi 298 K <sup>a</sup>			emi 77 K <sup>a</sup>	
	$\lambda$ (nm) <sup>a</sup>	$\epsilon$ (M <sup>-1</sup> cm <sup>-1</sup> )	$\lambda$ (nm) <sup>e</sup>	$\tau$ (nsec) <sup>f</sup>	$\phi_{\text{em}}$ <sup>h</sup>	$\lambda$ (nm) <sup>e</sup>	$\tau$ ( $\mu$ sec)
$[\text{Ru}(\text{tpy})_2]^{2+}$	475	11600	629	0.25	$5 \cdot 10^{-6}$	598	11.3
$[\text{Ru}(\square\text{py}\square)(\text{tpy})]$	474	9500	680	42	$7 \cdot 10^{-4}$	615	8.4
$[\text{RuH}_2(\square\text{py}\square)(\text{tpy})]^{2+}$	461	10800	—	—	—	595	
$[\text{Ru}(\square\text{py}\square)(\text{Cl-tpy})]$	474	10500	695	107	$8 \cdot 10^{-4}$	625	6.5
$[\text{RuH}_2(\square\text{py}\square)(\text{Cl-tpy})]^{2+}$	463	11700	—	—	—	607	
$[\text{Ru}(\square\text{py}\square)(\text{Hpy-tpy})]^+$	506	11500	700	8	$2 \cdot 10^{-4}$		
$[\text{Ru}(\square\text{py}\square)(\text{py-tpy})]$	490	10300	671	110	$2 \cdot 10^{-4}$	615	

Table 7.2 a) DMF, b) Methanol, ethanol (1, 4), c) DMF vs.  $\text{Fc}/\text{Fc}^+$ , in braquette not reversible reductions d) Wavelength of the lowest energy absorption maximum e) Wavelength of highest energy emission feature f) Luminescence emission lifetime ( $\pm 10\%$ ) h) Luminescence quantum yield

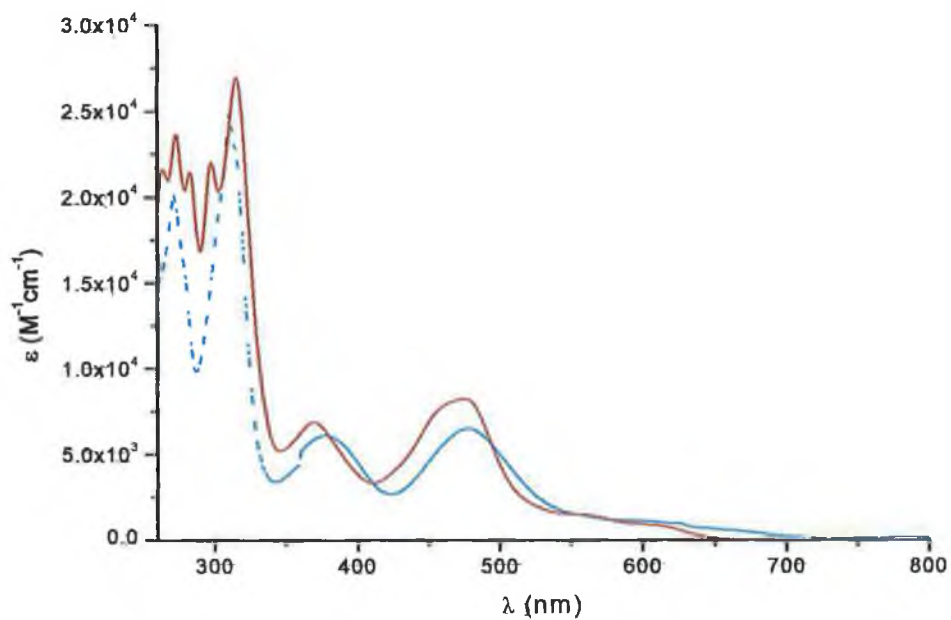


**Figure 7.8** Absorption spectra of  $[\text{Ru}(\text{tpy})(\text{py})]$  (red line) and  $[\text{Ru}(\text{tpy})(\Delta^2\text{py}\Delta^4)]$  (blue dashed line) in ethanol solution.

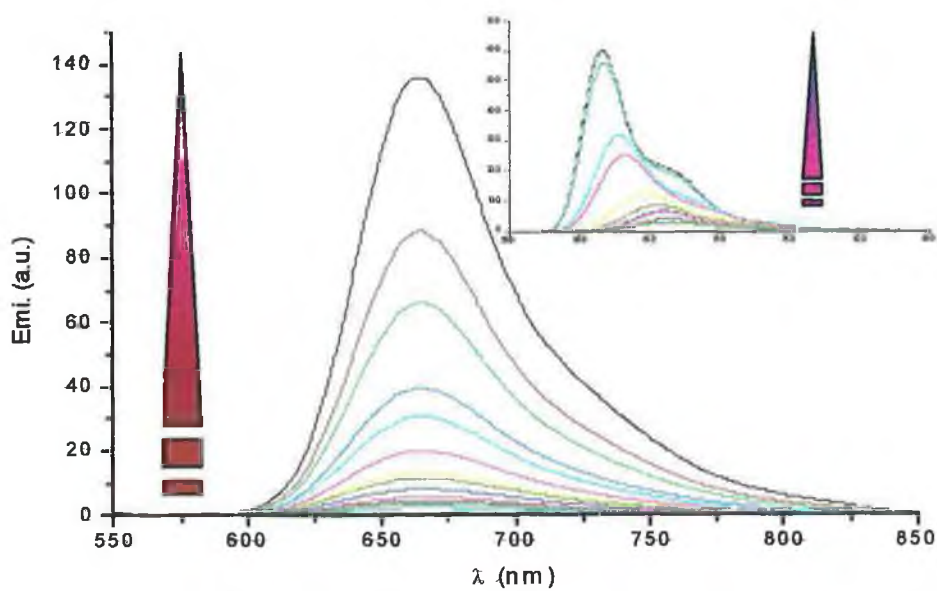


**Figure 7.9** Emission spectra temperature dependence of the  $[\text{Ru}(\text{tpy})(\text{py})]$  from 298 to 80 K in ethanol: butyronitrile (4,5) solution.

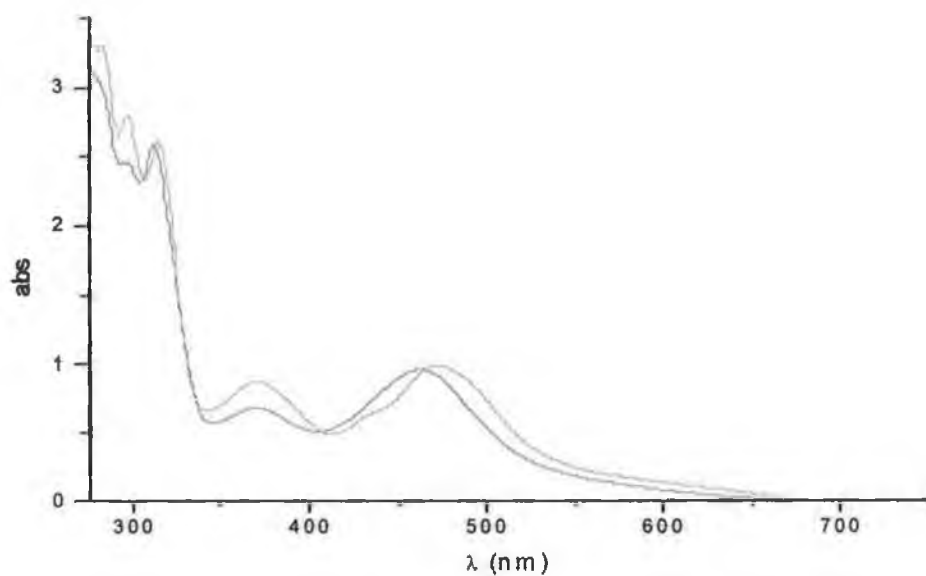


**Figure 7.10** Absorption spectra of  $[\text{Ru}(\square\text{py})(\text{Cl-tpy})]$  in acidic (red line) or basic (green line) DMF solution.

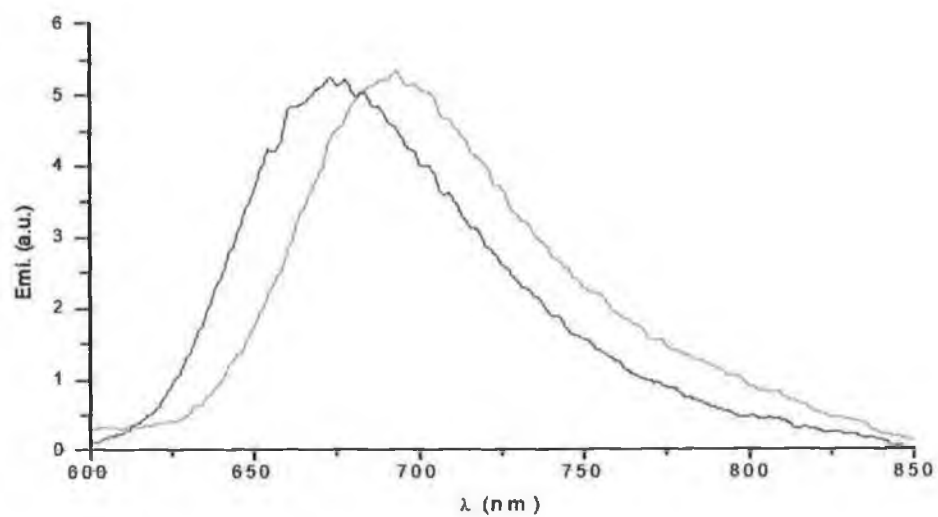


**Figure 7.11** Emission spectra of  $[\text{Ru}(\text{tpy})(\square\text{py})]$  (black line) and  $[\text{Ru}(\text{Cl-tpy})(\square\text{py})]$  (red line) in acetonitrile.



When excited within the MLCT absorption bands at 298 K in a deaerated DMF solution, the complexes exhibit a visible phosphorescence with single bands. Emission lifetimes and wavelength maxima are reported in table 7.2. The protonation of one or both tetrazole rings results in a total quenching of the emission.

The origins of the quenching of the luminescence of the protonated complexes are:

- protonation of the complex results in a stabilisation of the ground state since  $\text{H}_2(\text{py})$  is a weaker  $\sigma$ -donating ligand than  $(\text{py})^{2-}$ .
- Assuming an averaged ligand field environment for both species, the  $\text{Ru}(t_{2g})\text{--Ru}(e_g)$  energy gap should be larger for the deprotonated species.

Those changes, which occur upon protonation, should serve to decrease the energy gap between the  $^3\text{MLCT}$  and  $^3\text{MC}$  states. As we have seen in chapter 5 for  $(\Delta\text{py}\Delta)^{2-}$ , it is expected that also for  $\text{py}$  complexes quenching of the luminescence lifetime upon protonation of the ligand may result from facile internal conversion to a lower energy  $^3\text{MC}$  state which rapidly relaxes to the ground state.

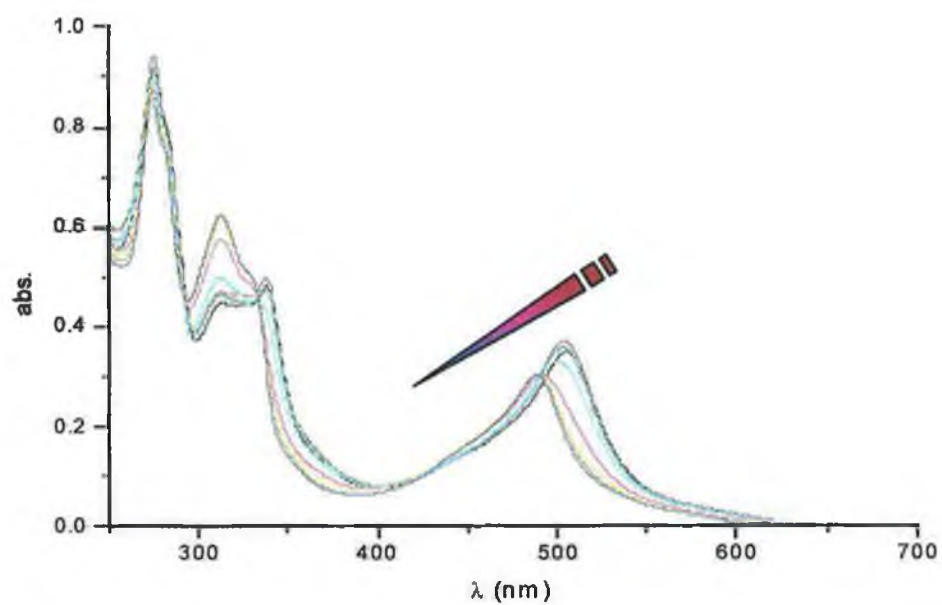


**Figure 7.12** Absorption spectra pKa dependency of  $[\text{Ru}(\text{phen})(\text{py-tpy})]^+$  in Britton Robinson buffer solution, from pH 1 to pH 5

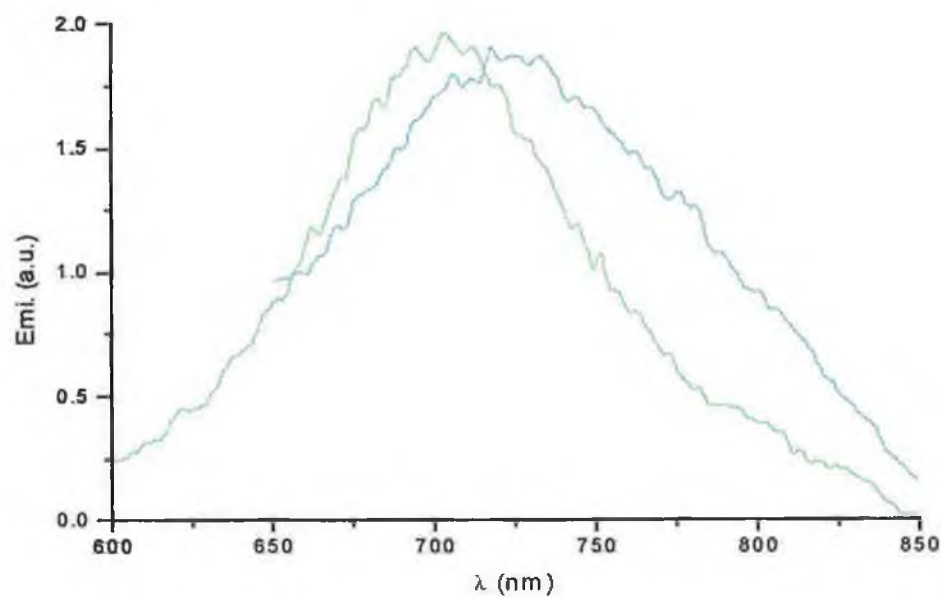


**Figure 7.13** Emission spectra of  $[\text{Ru}(\text{phen})(\text{py-tpy})]^+$  in Britton Robinson buffer solution (pH 6 green, pH 1 blue line).

## 7.5 Redox Properties and Spectroelectrochemistry

The oxidation and reduction potentials of the complexes are given in Table 7.3. By comparison of (tpy) based Ru(II) complexes the first (not reversible) reduction potential for these mixed ligand complexes are terpyridine based, the  $\pi^*$  levels of the terpyridine are slightly lower than those of the  $(\square\text{py}\square)^{2-}$  ligand. The oxidation potentials of the neutral complexes are lower than that of  $[\text{Ru}(\text{X-tpy})_2]^{2+}$ , which indicates that the  $(\square\text{py}\square)^{2-}$  ligand is a stronger  $\sigma$  donor ligand than tpy, they are higher than that of  $[\text{Ru}(\text{tpy})(\Delta\text{py}\Delta)]$ , which confirms that  $(\square\text{py}\square)^{2-}$  is a less stronger  $\sigma$ -donor ligand than  $(\Delta\text{py}\Delta)$ .

The potential of spectroelectrochemistry in the study of the electrochemically generated reduction products of the  $d^6$  polypyridyl complexes has previously been demonstrated.<sup>7,8</sup> Usually the UV-visible spectrum of the reduced form of the appropriate homoleptic complex provides a model spectrum for the ligand anion, in a mixed ligand complex, upon excitation. (See chapter 5)

Spectroelectrochemistry data of  $[\text{Ru}(\text{tpy})(\square\text{py}\square)]$  are shown in figure 7.14 and 7.15. Electrogenation of the one electron oxidised and reduced forms are possible with more than 95% regeneration of the original oxidation state.

In the oxidative spectroelectrochemistry for  $[\text{Ru}(\text{tpy})(\Delta\text{py}\Delta)]$  the ruthenium to tpy MLCT transitions are completely lost upon the one oxidation of the Ru(II) centre, as observed for other Ru-tpy complexes.<sup>9</sup>

Electrogenation of one electron reduced form is reversible, the spectrum obtained virtually tracks the spectrum of the  $[\text{Ru}(\text{tpy})_2]^+$ . In the case of  $[\text{Ru}(\text{tpy})_2]^{2+}$ , two strong absorption bands grow in when an electron is added. One

has a maximum at around 340 nm. and has been assigned as a  $\pi$ - $\pi^*$  transition from the highest completely filled LUMO( $\pi_6$ ) to the half filled HOMO( $\pi_7$ ) of the tpy anion.<sup>10,11</sup> Another more structured absorption appears near 525 nm. and it has been assigned as a  $\pi^*$ - $\pi^*$  transition ( $\pi_7$ - $\pi_{10}$ ) of tpy<sup>-</sup>. Two further, less intense bands, are also observed. One appears as a pronounced shoulder at 625 nm. In [Ru(tpy)<sub>2</sub>]<sup>+</sup> this band shifts to 665 nm on further reduction. A second barely resolved band is observed between 420 and 450 nm. in both the [Ru(tpy)<sub>2</sub>]<sup>+</sup> and [Ru(tpy)<sub>2</sub>] spectra. Two similar features are observed in the spectrum of singly and doubly reduced [Os(tpy)<sub>2</sub>]<sup>2+</sup>. The [Ru(tpy)([py])]<sup>-</sup> has maxima near 420 and 660 nm. Therefore it is more evidence that the tpy ligand is reduced first. However a third band grows 850, which is assigned to a ligand to metal charge transfer, from the electron rich ([py])<sup>2-</sup> ligand to the electron deficient metal centre.

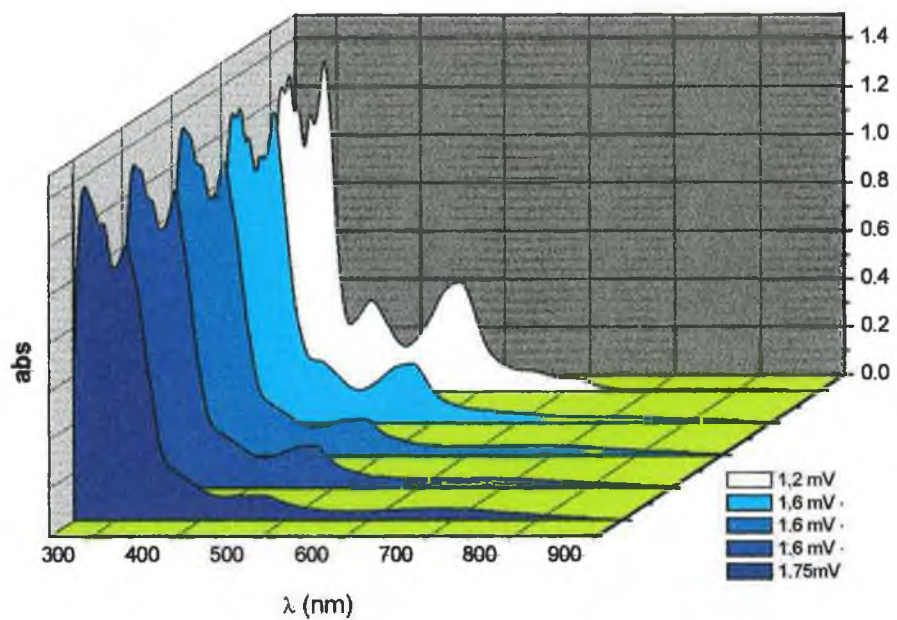


Figure 7.14 Near-UV-visible spectra of  $[\text{Ru}(\text{tpy})(\Delta\text{py}\Delta)]$  (white) and  $[\text{Ru}(\text{tpy})(\Delta\text{py}\Delta)]^+$  (navy) recorded in acetonitrile containing 0.5 M TBAH.

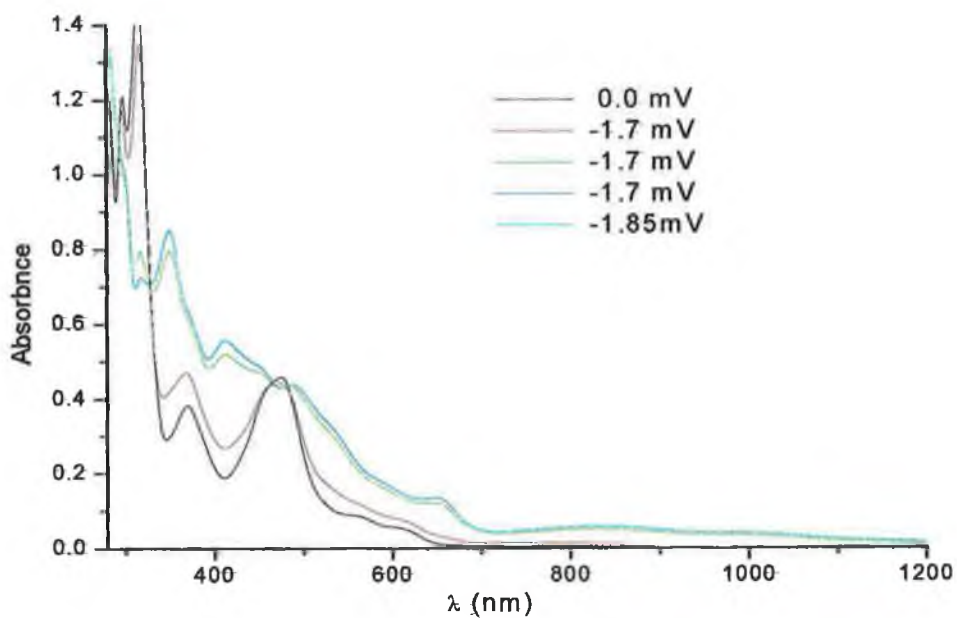


Figure 7.15 Near-UV-visible spectra of  $[\text{Ru}(\text{tpy})(\Delta\text{py}\Delta)]$  (black) and  $[\text{Ru}(\text{tpy})(\Delta\text{py}\Delta)]^-$  (blue) in acetonitrile containing 0.5 M TBAH.

## 7.6 Temperature Dependence of the MLCT Energy and Lifetime

The temperature dependence of the  $^3\text{MLCT}$  excited state emission lifetime of the  $[\text{Ru}(\text{X-tpy})(\text{py})]$  species still represents an increase of magnitude with respect to  $[\text{Ru}(\text{X-tpy})_2]^{2+}$  complexes (Tab. 7.2). Using arguments put forwards in Chapter 5 it is likely that this increase can be explained by the increase of the energy gap between  $^3\text{MC}$  and  $^3\text{MLCT}$  states following the replacement of the weak field terpyridine ligand by a strong field ligand.

To determinate the increase of the ligand field, low temperature excited state lifetime measurements of  $[\text{Ru}(\text{tpy})(\text{py})]$  were made in butyronitrile-ethanol (5:4) solution.

As discussed in Chapter 5 and 6, the decay of an excited state takes place by competitive radiative and not radiative processes. The  $(1/\tau)$  vs.  $1/T$  plot (Fig. 7.16) have been obtained, with equation 5.2 fitted to the experimental points. The  $k_0$ ,  $A_i$ , and  $\Delta E_i$  are collected in Table 7.4.

The temperature dependence behaviour of the  $[\text{Ru}(\text{tpy})(\text{py})]$  emission lifetime and emission energy maxima (Fig 7.8) are consistent with that measured for the analogous  $[\text{Ru}(\text{tpy})(\Delta\text{py}\Delta)]$  complexes. The most important features are the presence of two closely spaced states,  $\Delta E$  of  $450\text{ cm}^{-1}$ , whose have similar decay properties and an excited state lying  $2450\text{ cm}^{-1}$ , which undergoes fast radiationless deactivation.

As it was seen in Chapter 5, section 5.6 and Fig. 5.17, when the main contribution to  $k_c$  ( $k_c$  is the sum of all the rate constants of the possible deactivation processes that can deactivate the  $^3\text{MC}$  states), comes from a non-

activated process,  $A_2$  will correspond to the rate of the non-activated process ( $k'_c$ ). The activation energy  $\Delta E_2$  may correspond either to the energy gap between  $^3\text{MLCT}$  and  $^3\text{MC}$  or the distance between the  $^3\text{MLCT}$  level and the crossing point of the two surfaces. For complexes of the same family the  $\Delta E_2$  data have probably the same meaning and the energy gap between the minimum energy of the  $^3\text{MLCT}$  level and the  $^3\text{MC}$  level is most likely related to the distance between the  $^3\text{MLCT}$  level and the crossing point of the two surfaces. This will be discussed in Chapter 8.

	Electrochemistry		
	$E_{\text{ox}}$ (Volt)	$E_{\text{red}}$ (Volt)	$E_{\text{red}}$ (Volt)
$[\text{Ru}(\text{tpy})_2]^{2+}$	0.92	-1.67	-1.82
$[\text{Ru}(\text{Cl-tpy})_2]^{2+}$	1	-1.53	-1.78
$[\text{Ru}(\text{Py-tpy})_2]^{2+}$	0.895	-1.66	-1.92
$[\text{Ru}(\text{HPy-tpy})_2]^{4+}$	1.045	a	a
$[\text{Ru}(\square\text{py}\square)(\text{tpy})]^{2+}$	0.89	-1.53	
$[\text{Ru}(\square\text{py}\square)(\text{Cl-tpy})]^{2+}$	0.95	-1.45	-1.98
$[\text{Ru}(\square\text{py}\square)(\text{Hpy-tpy})]^+$	0.95	a	a
$[\text{Ru}(\square\text{py}\square)(\text{py-tpy})]$	0.87	(1.53)a	

Table 7.3 Red-ox potentials in DMF solutions vs.  $\text{Fc}/\text{Fc}^+$ , in braquette not reversible reductions. a) reductive processes poorly resolved.

	$k_0$ (sec <sup>-1</sup> )	$k_1$ (sec <sup>-1</sup> )	$\Delta E_1$ (cm <sup>-1</sup> )	$k_2$ (sec <sup>-1</sup> )	$\Delta E_2$ (cm <sup>-1</sup> )
[Ru( $\square$ py $\square$ )(tpy)]	$1.2 \times 10^6$	$6.5 \times 10^7$	450	$1.4 \times 10^{13}$	2450

**Table 7.4 Kinetic parameters for excited state decay obtained from the fitting of equation (5.2) to the experimental results.**

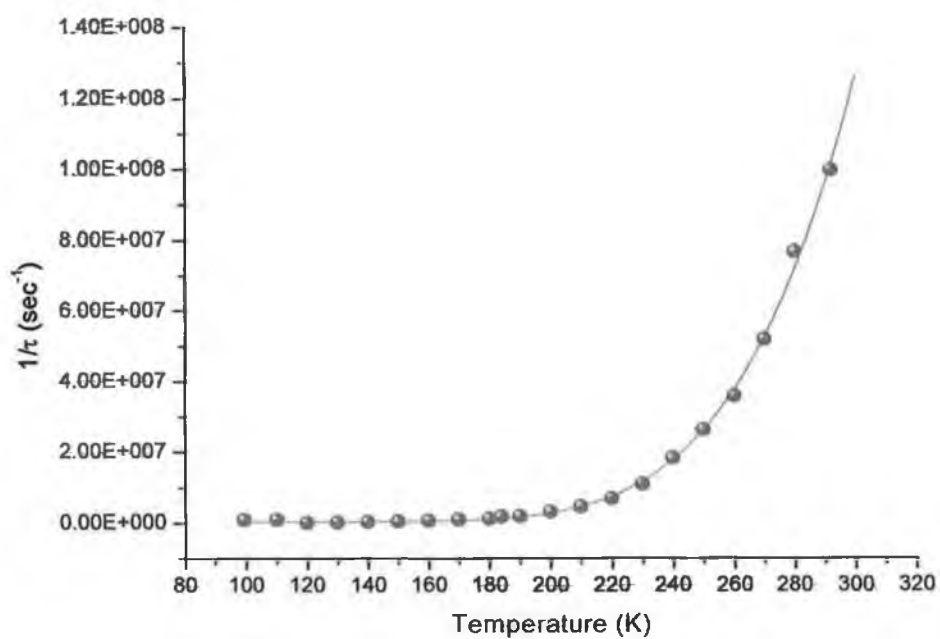


**Figure 7.16 Plot of  $1/\tau$  vs T of [Ru(tpy)( $\square$ py)]. Curve fit in according to equation 5.2.**



## 7.7 Solute Solvent Interaction

The  $[\text{Ru}(\text{tpy})(\text{tpy})]$  exhibits pronounced solvatochromic behaviour, the emission spectra in different solvents are shown in picture 7.18. The energies of the lowest absorption and emission band maxima are collated in table 7.5. Table 7.5 clearly shows that both absorption and emission spectra of  $[\text{Ru}(\text{tpy})(\text{tpy})]$  depend on the nature of the solvent. As for the analogous  $[\text{Ru}(\text{tpy})(\Delta\text{py}\Delta)]$  no statistic correlation of both absorption and emission energies with dielectric constants or refractive index of the solvent (See Chapter 5).

Previously different research groups<sup>12, 13</sup> explained the solvent dependence of the  $[\text{RuL}_2(\text{CN})_2]$  and  $[\text{Ru}(\text{tpy})(\text{CN})_3]^-$  absorption and emission energies based on the Gutmann's acceptor number<sup>14</sup>, and the  $[\text{Ru}(\text{tpy})(\Delta\text{py}\Delta)]$  complex showed a similar dependence as discussed in Chapter 5.

Figure 7.17 shows that there is a linear correlation of  $[\text{Ru}(\text{tpy})(\text{tpy})]$  absorption and emission energies with the solvent acceptor number.

However the  $[\text{Ru}(\text{tpy})(\text{tpy})]$  solvatochromic behaviour is less pronounced when compared with the analogous  $[\text{Ru}(\text{tpy})(\Delta\text{py}\Delta)]$ , showing that the tetrazole nitrogen lone pairs are less available for coordination than the triazole ones.

It is interesting highlight how the emission curve area of the complex in different solvents increases (Fig 7.18), increasing the acceptor number of the solvent, while the lifetimes of the complex do not have noticeable increase.

This could be explained in two different ways:

1. Supposing that to the increase of the emission curve areas correspond a increase of the quantum yield in different solvents,

increase of the  $k_{em}$  and the generation of different species (polinuclear cluster united by hydrogen bonds) must be admitted

The presence of an equilibrium between a non-emitting species (hydrogen bonded with the solvent) and the emitting one. The latter hypothesis would explain why the emission intensity is almost 100 times higher in less protic solvent than in water, but instead the lifetimes are not substantially changing.

In order to prove the formation of hydrogen bond a titration of the complex was made in THF, adding water, the result was a gradual quenching of the emission. The titration result cannot be considered the final prove of the formation of hydrogen bonds, but it can be considered an evidence of the interaction of the water with the complex.

Solvent (Acceptor number)	$\nu_{\max}^{\text{abs}}$ kk	$\nu_{\max}^{\text{abs}}$ kk	$\nu_{\max}^{\text{em}}$ kk	$\tau$ ns
	(298 K)	(298 K)	(298 K)	(298 K)
<b>Water (54.8)</b>	22.57	27.24	14.92	45
<b>Methanol (41.3)</b>	22.22	27.17	14.88	
<b>Ethanol (37.1)</b>	21.83	27.10	14.88	45
<b>Dichloromethane (20.4)</b>	20.96	26.88	14.83	
<b>Acetonitrile (19.3)</b>	21.27	27.17	14.61	48
<b>DMSO (19.3)</b>	21.14	26.95	14.85	54
<b>DMF (16.0)</b>	21.14	27.02	14.61	54
<b>THF ( 8.0)</b>	20.92	26.70	14.57	

**Table 7.5 Solvent dependence of absorption and emission spectra of [Ru(tpy)(py<sup>2</sup>)] at 298 K.**

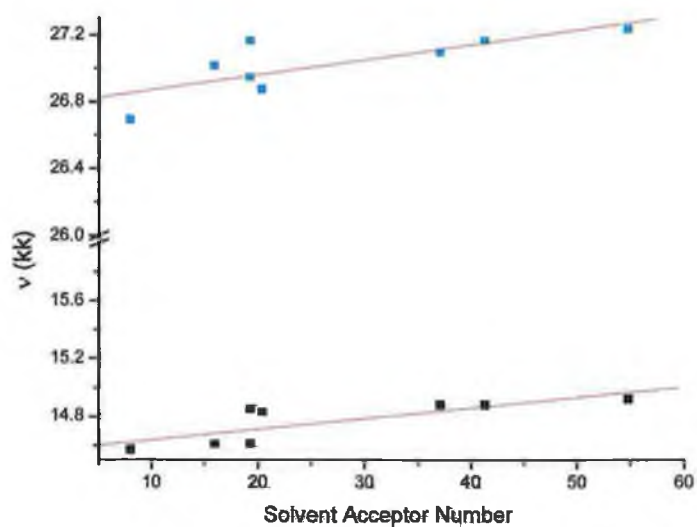


**Figure 7.17** Variations in  $E_{abs}$  (black squares) and  $E_{em}$  (blue squares) with solvent acceptor number for the  $[Ru(tpy)(\square py)]$  complex.

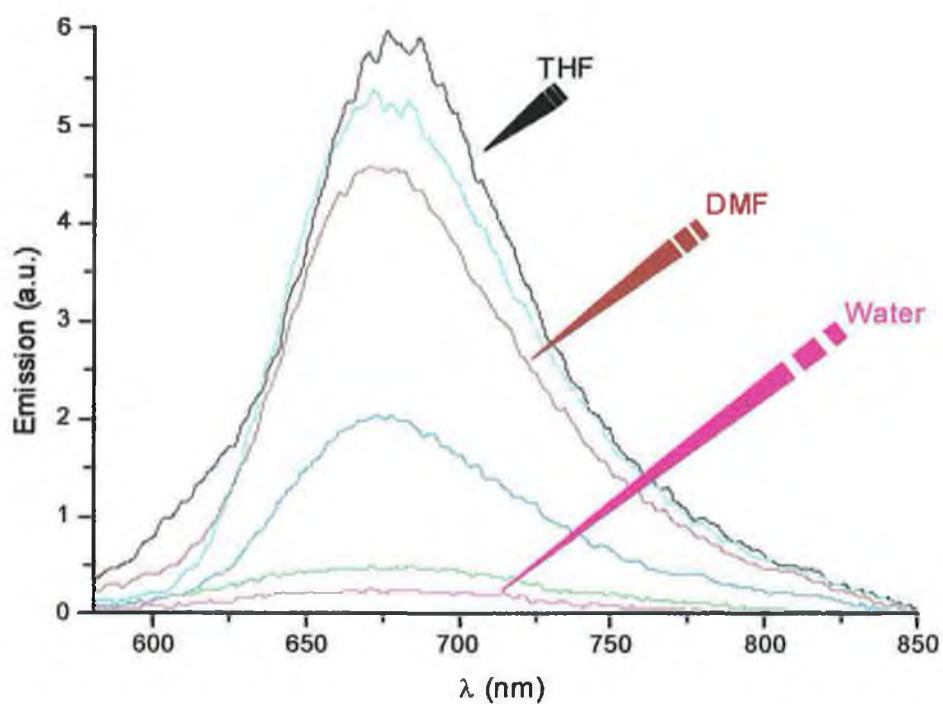


**Figure 7.18** Solvent dependency of the  $[Ru(tpy)(\square py)]$  emission spectra at 298 K, the different solutions had the same optical density.

## 7.8 Conclusions

In this chapter, the use of ( $\square$ py $\square$ ) ligand, as alternative to ( $\Delta$ py $\Delta$ ), ligand to extend the lifetime of the  $^3$ MLCT excited states of Ru(II) terpyridine complexes has been explored. Photophysical and electrochemical data were analysed in order to give a well defined picture of {Ru(tpy)( $\square$ py $\square$ )} properties,.

In comparison with [Ru(tpy)( $\Delta$ py $\Delta$ )], [Ru(X-tpy)( $\square$ py $\square$ )] has a shorter  $^3$ MLCT excited state lifetime due to the decrease of the energy gap between the  $^3$ MC and  $^3$ MLCT states. However these complexes display an advantageous lack of structural isomers, which will be an agreeable factor in any further investigation on their ultimate supramolecular systems. In fact, the lifetimes of the tetrazolate complexes is still in an acceptable range, interesting perspectives arise for the use of structurally attractive Ru(II) terpyridine units as photosensitiser molecular components in supramolecular devices.

## 7.9 Bibliography

---

- <sup>1</sup> Franke P N, Ph.D. Thesis "Tetrazoles in coordination Chemistry" (1982),  
Leiden, NL
- <sup>2</sup> Finnegan W A, Henry R A, Lofquist R J, *J. Am. Chem. Soc.* 1958, 80, 3908.
- <sup>3</sup> Buttler R N, " **Comprehensive Heterocyclic Chemistry II**", (1996) Storr. Ed.  
Tetrazoles. Pergamon Press Oxford
- <sup>4</sup> Sugiyarto K H, Craig D C, Rae A D, Goodwin H A, *Aust. J. Chem.* 1993, 46,  
1269
- <sup>5</sup> Constable E C, Lewis J, *Inorg Chim. Acta* 1980, 41, 21
- <sup>6</sup> Constable E C, Cargill Thopson A M W *J. Chem. Soc. Dalton Trans.* 1992  
2947.
- <sup>7</sup> Vogler L M, Scott B, Brewer J K, *Inorg. Chem.* 1993, 32, 898
- <sup>8</sup> Brewer J K, Lumpkin R S, Otvos J W, Spreer L O, Calvin M, *Inorg. Chem.*  
1993, 32, 898.
- <sup>9</sup> Thummel R P, Chirayil S, *Inorg. Chim. Acta* 1988, 154, 77.
- <sup>10</sup> Konig E, Kremer S, *Chem. Phys. Lett.* 1970, 5, 87.
- <sup>11</sup> Berger RM, Mc Millin D R, *Inorg Chem* 1988, 27, 4245.
- <sup>12</sup> Kitamura N, Sato Masami, Kim H B, Obata R, Tazuke S. *Inorg. Chem.* 1988,  
27, 651
- <sup>13</sup> Burgess J, Chambers J G, Haines R I, *Trans. Met. Chem.*, 1981, 6, 145.

---

<sup>14</sup> Gutmann, V. **The Donor-Acceptor Number Approach to Molecular Interactions**, Plenum New York, 1978,

**Chapter 8**  
**Final Discussion, Conclusions and**  
**Future Work**

“Mother nature is a bitch.....”

**Murphy**



## 8.1 Introduction

The design of supramolecular systems with appropriate electronic properties is an area of intense activity. Metal polypyridine complexes are often used as building blocks in supramolecular species performing complex light induced functions (photochemical molecular devices). Particularly important in this context are the polypyridine complexes of  $d^6$  metals. With their strong metal to ligand charge transfer (MLCT) absorption and long lived emitting  $^3\text{MLCT}$  excited states, such complexes are ideal candidates as photosensitisers.

In the studied ligand, bidentate ligands such as 2,2' bipyridine or 1,10 phenanthroline type and tridentate ligands such as terpyridine (tpy) are commonly used.

Although the coordination chemistry of substituted bidentate pyridine based ligands has been intensively utilised over the past thirty years, there have been few systematic studies of the analogous tridentate systems. Substituted 2,2' 6',2'' terpyridines have been evaluated as colorimetric reagents for the detection of iron (II), but it is only recently that there has been any interest in their coordination chemistry with ruthenium (II), (more than 250 papers in the last ten years, see Appendix 2). In part this is due to the differences in the photochemical and photophysical properties of the ruthenium of the bidentate and tridentate ligands. In terms of the symmetry and topology of molecular arrays, the bidentate and tridentate ligands have strongly different properties. At a given octahedral metal centre, three bipyridines are arranged in a mutually orthogonal fashion, whereas only two tpy types occupy two of the

orthogonal planes, creating the possibility to design well defined supramolecular systems.

Along with these structural advantages observed for tpy complexes, there is, however, a serious draw back of a photophysical nature. The lifetime of the  $^3\text{MLCT}$  excited states is known to be strongly dependent on:

- The energy of the state (energy gap law)
- The proximity of higher energy metal-centred ( $^3\text{MC}$ ) excited states, which can provide an additional, thermally activated decay path.

In contrast to bischelating bpy-type ligands, the bite angles of a tris-chelating ligand such as tpy are not ideally suited for octahedral coordination. A recent crystal structure of a bis (tpy) complex of Ru(II) with a derivative of tpy has shown that the coordination about the metal centre deviates substantially from the octahedral such that the N-Ru-N' bite angle is only about  $160^\circ$ .<sup>1</sup> The distortion results in a relatively weak ligand field at the metal, low energy  $^3\text{MC}$  states, and efficient thermally activated decay pathway.

As a consequence, terpyridine complexes tend to have relatively short-lived  $^3\text{MLCT}$  states and are weak emitters, if compared to the analogous bpy complexes.

While the  $^3\text{MLCT}$  state of the  $[\text{Ru}(\text{bpy})_3]^{2+}$  is long lived, 960 nsec in deaerated acetonitrile, and highly luminescent  $\Phi_{\text{em}} = 0.059$ ,  $[\text{Ru}(\text{tpy})_2]^{2+}$  has an extremely short lifetime,  $\tau = 250$  psec in deaerated acetonitrile, and displays little luminescence ( $\Phi_{\text{em}} \approx 5 \times 10^{-6}$ ) at room temperature. This is a severe drawback for the use of Ru(II) terpyridine complexes as photosensitiser units. All but very fast

intercomponent processes are inefficient in supramolecular systems containing these units, and pico or femtosecond spectroscopy is required for those investigations. Alternatively, low temperatures can be used to reach convenient excited-state lifetimes, but this introduces other experimental problems and may rule out the occurrence of thermally activated intercomponent processes.

In this thesis more than ten new ruthenium-tpy complexes were synthesised (Chapter 3) and their photophysical and electrochemical properties were investigated (Chapters 5-7). All the complexes examined displayed a strong luminescence at room temperature with lifetimes of the excited states in the order of one hundred nanoseconds.

## 8.2 Discussion

Rational strategies can be devised to increase the excited state lifetime of ruthenium-tpy type complexes. Since one of the main origins of the short lifetime of the  $^3\text{MLCT}$  excited state is the small energy gap between the emitting state and the upper lying  $^3\text{MC}$  state, increasing this energy gap is expected to be beneficial. In bis-tpy complexes, substitution of the 4' positions of the ligands has been used for this purpose. Investigations carried out on  $[\text{Ru}(\text{X-tpy})(\text{Y-tpy})]$  complexes<sup>2,3</sup>, (where X and Y are substituents in the 4' position of the 2,2',6',2''-terpyridine) have shown that electron-donating (D) or electron-accepting (A) substituents can cause changes in the luminescence and electrochemical properties. Electrochemical studies indicate:

- The electron accepting groups stabilise the LUMO  $\pi^*$  ligand orbitals more than the HOMO  $\pi(t_{2g})$  metal orbitals.
- The electron-donor groups destabilise the HOMO  $\pi(t_{2g})$  metal orbitals more than the LUMO  $\pi^*$  ligand orbitals.

Where luminescence properties are concerned, two general trends were found<sup>3</sup>:

- The energy of the emission maximum decreases regardless of the electron accepting and donating nature of the substituent.
- At high temperature, electron accepting substituents have the opposite effect.

These conclusions can be explained on the basis of the correlation between the electrochemical potentials and emission energies, the two processes involve electron transfer between the same molecule orbitals. It was concluded that when the substituents are electron acceptors, the  $\pi^*$  ligand centred orbital is more stabilised than the  $\pi(t_{2g})$  metal centred orbital because of proximity reasons. In addition the oxidised metal, in the excited state, does not receive any charge compensation from the A-ty ligand not involved in the electronic transition. When the substituents are electron donating groups, the MLCT excited state energy decreases as a consequence of the destabilisation of the metal centred  $\pi(t_{2g})$  orbital. Heteroleptic complexes carrying an electron accepting and a electron donating group always show lower emission energies when compared to the parent homoleptic complexes because the  $\pi^*$  orbital of the A-ty ligand is stabilised and the D-ty destabilises the metal centred  $\pi(t_{2g})$  orbitals.

These effects can also explain why the room temperature luminescence quantum yield and lifetime increase upon replacing H<sup>4'</sup> with an electron accepting substituents and its decrease with electron-donating moieties.

When the tpy are connected through their 4' position with  $\pi$ -delocalising<sup>4</sup> moieties, remarkable lifetime enhancements are observed. Again this can be rationalised in terms of stabilisation of the <sup>3</sup>MLCT upon delocalisation. However the concomitant decrease of the excited state distortion and, thus, of the Frank-Condon factors for radiationless decay probably add to the effects.

An alternative strategy to the design of long-lived Ru(II) terpyridine complexes is the use of ancillary ligands, to change the relative <sup>3</sup>MLCT and <sup>3</sup>MC energy states. To increase the energy <sup>3</sup>MC states and decrease the energy of the <sup>3</sup>MLCT, an ideal ancillary ligand should simultaneously:

- Increase the strength of the ligand field.
- Provide high charge density on the metal.

In the past ten years just two examples can be found in literature<sup>5, 6, 7</sup>, [Ru(tpy)(NCS)<sub>3</sub>]<sup>-</sup> and [Ru(tpy)(CN)<sub>3</sub>]<sup>-</sup>. It should be pointed out that the properties of these two complexes are found to be strongly solvent dependent, through second sphere donor-acceptor interaction with free nitrogen or sulphur atoms.

The complexes synthesised and studied in this thesis give the possibility to investigate the last cited strategy.

In an attempt to rationalise the results obtained, in the present Chapter it will be examined the correlation between spectroscopic, photophysical and electrochemical data.

From the data discussed in the earlier chapters a number of conclusions can be achieved:

- the oxidation is centred on the  $\pi(t_{2g})$  ruthenium orbitals and the reduction is centred on the  $\pi^*$  orbitals of the x-tpy
- the lowest energy absorption and emission bands have a MLCT orbital origin,

On the basis of these conclusions a linear correlation between the electrochemical and spectroscopic energy values is expected.

In Figure 8.1, the general trend observed is a linear correlation, with a mutual increase of the spectrochemical and electrochemical energies, which confirms the MLCT nature of the absorbing and emitting states. It is of importance to note that a linear regression coefficient of the emission correlation ( $R_{em}$ ) of over 0.94 indicates a good statistical correlation. The data points for the absorption are quite scattered around the linear fit,  $R_{abs}$  less than 0.7. A explanation for this behaviour is the presence of an overlap between several MLCT bands in the absorption spectra, in this case the selected maxima do not always correspond to the lowest energy  $^1MLCT$  transition. In fact we noted, in almost all the complexes examined, the presence of two small shoulders around 650 nm and in Chapter 5 it has been shown that the

molecular orbitals of the Ru(tpy) complexes split under  $C_{2V}$  symmetry, generating many different MLCT transitions.

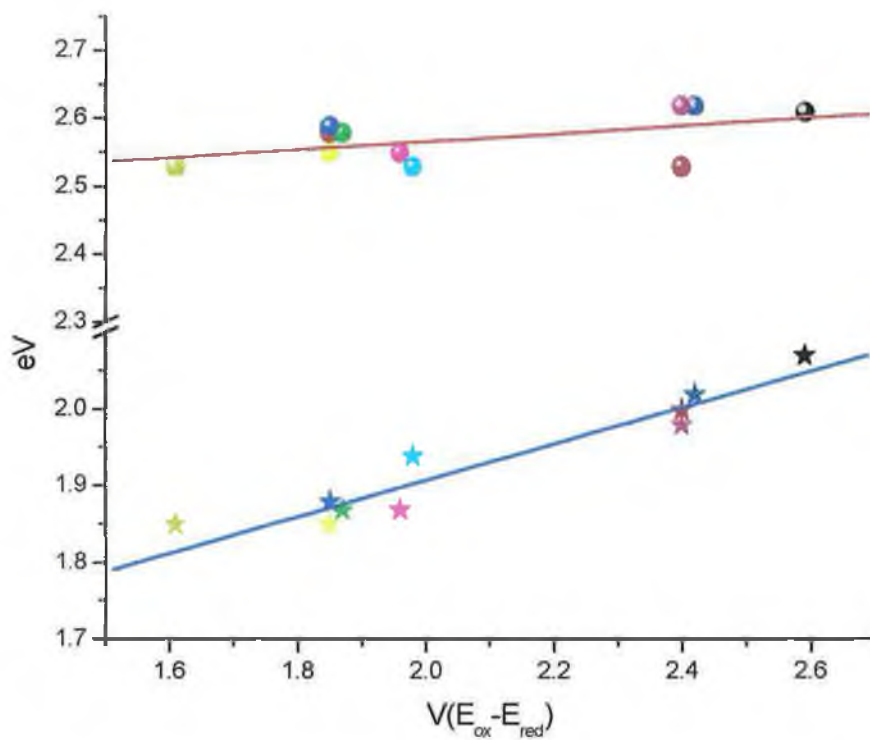


**Figure 8.1** Correlation between the energy of the absorption maximum (planets) and emission maximum at 80 K (stars) and the redox energy.

In the following discussion only complexes bearing an unsubstituted tpy moiety and an ancillary ligand will be considered (Tab 8.1), hence it is possible to make the assumption that the oxidation is on the metal centre and the reduction on the  $\pi^*$  orbital of the tpy moiety.

According to Lever<sup>8</sup>, the stronger  $\sigma$ -donor capacity of the ancillary ligand gives rise to a smaller effective nuclear charge on the ruthenium, destabilising the  $\pi(t_{2g})$  orbital on the metal, this can be understood by considering that removal of one electron from the metal centre causes the formation of Ru(III), which withdraws electronic charge from the electron rich ancillary ligand, thereby destabilising the HOMO  $\pi(t_{2g})$  metal orbitals. As previously seen, oxidation of the studied complexes is metal centred, the increase in oxidation potentials is related to the  $\sigma$ -donation capacity, the order of increasing capacity of  $\sigma$ -donation is  $\text{tpy} < (\text{Cpy})^{2-} < (\Delta\text{py}\Delta)^{2-} \cong \Phi\Delta\text{py}\Delta\Phi \leq \text{CN}^-$ .

Figures 8.2 and 8.3, respectively, show how the decrease of the MLCT energies depend on mutual decreases of reduction and oxidation potentials, following the  $\sigma$ -donation capacity of the ancillary ligand.



Complex	$E_{Abs}$ (eV)	$E_{Em1\ 80K}$ (eV)	$E_{Red}$ (V)	$E_{ox}$ (eV)	$\ln(1/\tau_{80K})$
(1) [Ru(tpy)(CN) <sub>3</sub> ]	2.60	1.78	-1.35	0.49	10.28915
(2) [Ru(tpy)( $\Delta^4$ py $\Delta^4$ )]	2.58	1.85	-1.35	0.50	10.10194
(3) [Ru(tpy)( $\Phi\Delta^2$ py $\Delta^2\Phi$ )]	2.55	1.85	-1.35	0.50	9.80818
(4) [Ru(tpy)( $\Delta^4$ py $\Delta^2$ )]	2.58	1.87	-1.38	0.49	10.07784
(5) [Ru(tpy)( $\Phi\Delta^2$ py $\Delta^4\Phi$ )]	2.55	1.87	-1.36	0.60	9.56702
(6) [Ru(tpy)( $\Delta^2$ py $\Delta^2$ )]	2.59	1.88	-1.38	0.47	10.07784
(7) [Ru(tpy)(□py□)]	2.62	2.00	-1.53	0.89	9.38469
(8) [Ru(tpy) <sub>2</sub> ] <sup>2+</sup>	2.61	2.07	-1.67	0.92	9.08812

Tabella 8.1 Spectroscopical and electrochemical data of the complexes containing a tpy moiety

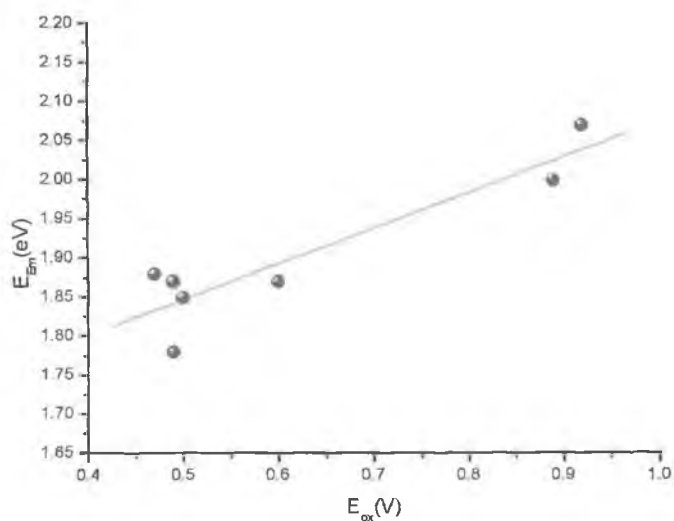
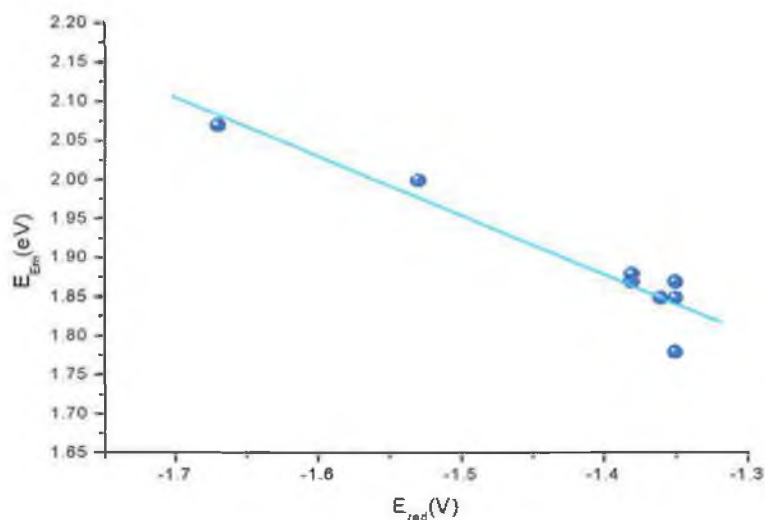


Figura 8.2 Plot of the emission energy (80K) vs the potential of oxidation.



**Figura 8.3** Plot of the emission energy (80K) vs the potential of reduction.

As discussed in Chapter 5, it is possible to find a correlation between energy and lifetime of the luminescent excited state. In fact, the decay of excited states takes place by competitive radiative and radiationless transition. For all the complexes the temperature dependence of the excited state lifetime can be fitted using the equation 5.2, in the study of the present complexes the equation was used in the form:

$$1/\tau = k_0 + A_1 e^{-\frac{\Delta E_1}{RT}} + A_2 e^{-\frac{\Delta E_2}{RT}} \quad (8.1)$$

Here,  $k_0$  is the sum of radiative and radiationless rate constant at 80K, the second term of equation 8.1 is related to different MLCT state clusters (see Chapter 5), the third term can be associated with an activated surface crossing to an upper lying level.

As the temperature increases the term  $A_2 \exp(-\Delta E_2/RT)$  becomes more important, at room temperature it usually represents the predominant radiationless decay path. This process is interpreted as an activated surface crossing to an upper lying, shorter lived  $^3\text{MC}$  level, which is derived from a  $\sigma(t_{2g})-\sigma^*(e_g)$ , d-d, transition.

Referring to Chapter 5 and Figure 5.28, in principle it can be expected for the cases i and ii-1 that  $A_2$  is high frequency vibrations ( $10^{13}$ - $10^{14}$   $\text{sec}^{-1}$ ) whose activation leads to the  $^3\text{MLCT}$ - $^3\text{MC}$  surface crossing region. For the case ii-2,  $A_2$  will be much smaller because it represents the rate constant of a radiationless transition having a poor Frank-Condon factor.  $[\text{Ru}(\text{bpy})_3]^{2+}$  ( $A_2 \approx 10^{14}$   $\text{sec}^{-1}$   $\Delta E_2 \approx 4000$   $\text{cm}^{-1}$ ) and several other Ru polypyridine complexes<sup>9,10,11</sup> are thought to belong to case i, The  $A_2$  ( $10^{-10}$ - $10^{-12}$ , solvent dependency) and  $\Delta E_2$  values for  $[\text{Ru}(\text{bpy})_2\text{CN}_2]$ , however are quite different, in particular the value for  $A_2$  is far too low to correspond to the frequency factor of a surface crossing process. The behaviour observed for this compound is therefore described by the case ii-2.

The complexes considered here have  $A_2$  values ( $10^{-12}$ - $10^{-13}$ ) on the borderline between the case ii-2 and the case i and they could be assigned more to i case than to ii-2. Controversial assignation were also done for  $[\text{Ru}(\text{tpy})_2]^{2+}$ ,<sup>12,13,3</sup> but as discussed in the previous Chapters, for similar complexes the  $\Delta E_2$  values probably have the same meaning, we will consider all our complexes a limit case i.

The data, Table 8.1, show that the energy gap between the luminescent  $^3\text{MLCT}$  state and the crossing point with the upper lying  $^3\text{MC}$  state, is increasing following the  $\sigma$ -donating capacity of the ancillary ligands ( $\text{tpy} < (\text{py})_2 < \text{CN}^- \leq$

$(\Delta\rho\Delta)^2 \cong \Phi\Delta\rho\Delta\Phi$ ), it is important to note that the cyanide complex would be expected to have a larger gap, but the  $^3\text{MC}$  energy value, taken from reference 6, was evaluated, in less accurate way, by means of the solvent dependency. It should be highlighted that because of the increasing energy gap between the two states, a strong luminescence is observed for the complexes.

The low temperature radiationless lifetimes vs. the emission maxima are plotted in Fig. 8.4. At 80 K, where the internal conversion process between  $^3\text{MLCT}$  and  $^3\text{MC}$  states is blocked, the data behave according to the energy gap law (linear correlation). The rate constant of radiationless decay of the  $^3\text{MLCT}$  excited state to the ground state increases as the energy gap between ground and excited state decreases. Because of this effect, complexes with low energy absorption bands, and consequentially low energy emission, typically are weak emitters, with short-lived excited states.

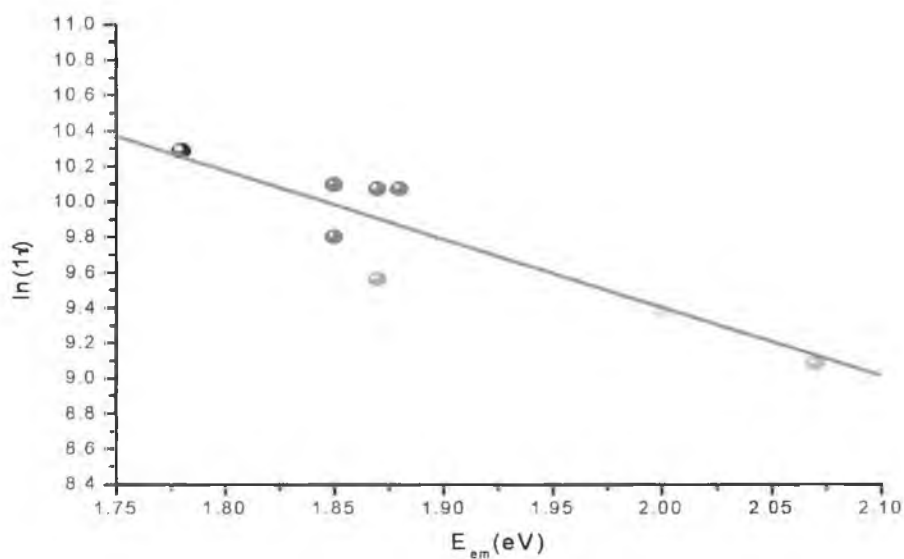


**Figure 8.4** Plot of  $\ln(1/\tau_{80K})$  against the excited state energy.

A schematic diagram outlining the energy levels involved is shown in Fig 8.5, the 80 K emission wavelength represents the energy of the  $^3\text{MLCT}$  and the  $^3\text{MC}$  state energies are estimated from the  $^3\text{MLCT}$ - $^3\text{MC}$  energy gap obtained from the excited state lifetime temperature dependence.

Quite surprisingly the energy scheme obtained shows that the increase of the excited state lifetimes obtained from the new set of Ru-tpy complexes is not dependent, as believed, on an increase of the energy difference between the  $d(t_{2g})$  and  $d(e_g)$  ruthenium orbitals, due to the increase of the strength of the ligand field obtained by moving from tpy to cyanide, as ancillary ligands. The  $^3\text{MC}$  state energies are, in fact, decreasing moving through the  $\sigma$ -donating series, that is because what we are considering it is not the really MC level but the crossing point of the two energy

surfaces. The presence of the electron rich ancillary ligands lowered the  $^3\text{MLCT}$  states and the crossing points between the  $^3\text{MC}$  and the  $^3\text{MLCT}$  states increasing the lifetime of the excited state, but the decrease in energy of the  $^3\text{MLCT}$  is larger than that of the crossing point, consequentially the energy gap between the two states becomes bigger moving through the ligand series.

The  $^3\text{MLCT}$  energy decrease is related to:

- The destabilisation of the  $t_{2g}$  orbitals on the ruthenium, moving all the way through the ligand series from tpy to  $\text{CN}^-$ , as it was discussed previously (decrease of the oxidation potential).
- The energy stabilisation of the  $\pi^*$  orbital of the tpy, moving from tpy to  $\text{CN}^-$  (increase of the reduction potential, that was not expected, being the MLCT energy always tpy-based). This behaviour needs to be more thoroughly investigated. The  $[\text{Ru}(\text{tpy})(\text{SCN})_3]^-$  complex, ( $E_{\text{ox}} = 0.60\text{V}$ ;  $E_{\text{red}} = -1.40\text{V}$  data from reference 7), follows this general comportment.

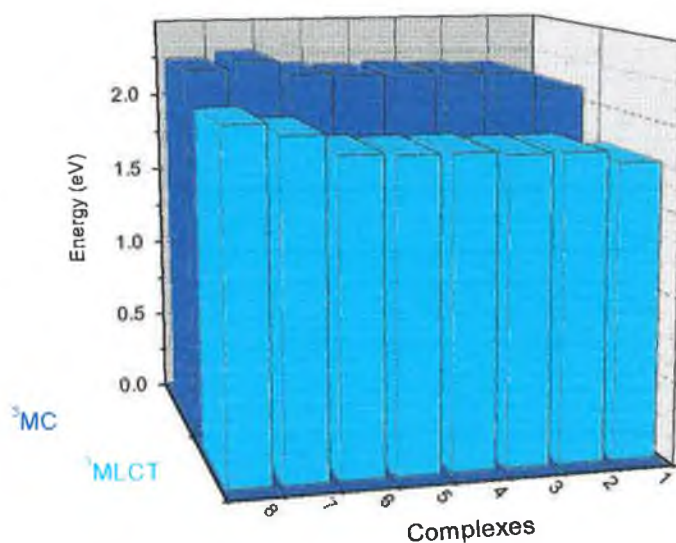


**Figure 8.5 Schematic representation of the energy levels moving through the  $\sigma$ -donating ligand series (See table 8.1).**

### 8.3 Future Work

The new series of ligands and the luminescent properties of their complexes, tpy based, discussed in this thesis, combine the luminescent properties of bpy based Ru complexes to the advantageous structural properties of tpy based.

The long lived excited state of these complexes makes them suitable building blocks for the introduction in PMDs or in solar cell, as shown in Chapter 6. They also have the advantageous property to be pH sensitive, the eventual supramolecular system, incorporating these molecules, can be “switched off” or “on” simply changing the solution pH.

The future work of this thesis will involve the incorporation of the molecules in simple linear arrays as diads (Fig 8.5, 8.6) and triads.

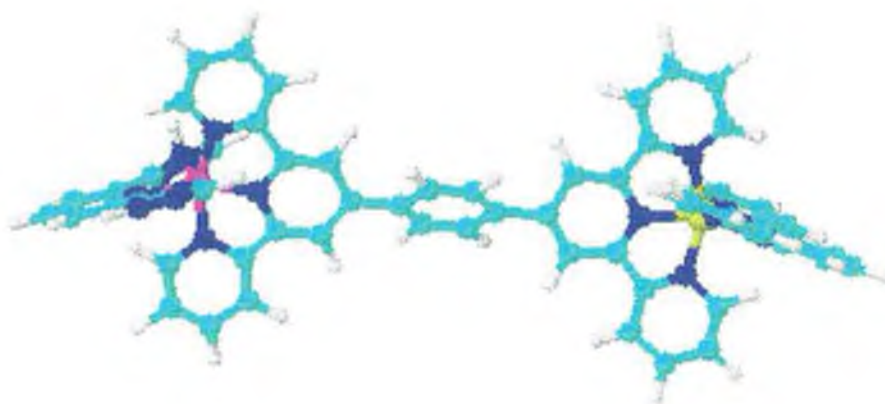


**Fig. 8.5 Possible linear hetero-nuclear diad incorporating a phenyl spacer.**

Covalently-linked donor acceptor systems are a class of supramolecular systems of great photochemical interest. The simplest system of this type, two components, “dyads”, are suited for the study of photoinduced electron or energy transfer processes. From a fundamental standpoint, such unimolecular processes are free from many of the kinetic complications inherent to bimolecular analogues. Indeed, studies on dyads have greatly contributed to shaping our understanding of the effect of basic physical factors (energy gradient, distance, intervening bonds, medium, etc.) on the kinetics of electron and energy transfer processes. In multicomponent systems such as “triads”, “tetrads”, etc., light absorption can trigger sequences of electron transfer processes which, under appropriate kinetic control, yield vectorial transport of electronic charge. Also, energy transfer can be used, upon appropriate organisation in space and energy, to channel the excitation energy from



many chromophoric components to a common acceptor component. On this basis, important functions such as antenna effect and photo-induced charge separation can be obtained with relatively simple systems, and sensible approaches toward more complex supramolecular system for artificial photosynthesis can be devised.

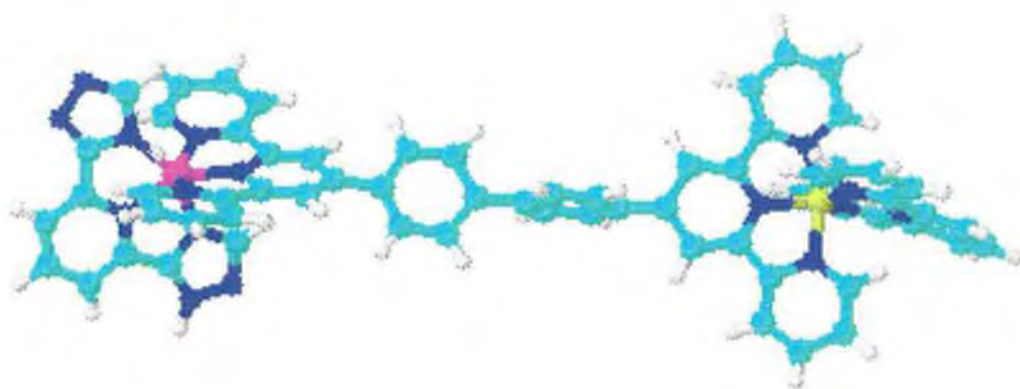


**Fig. 8.6 Possible linear hetero-nuclear diad incorporating two phenyl spacer.**

Taking advantage of the structural properties of  $M(\text{tpy})$  type complexes the syntheses of rigid, rod-like compounds, where  $\text{Ru}(\text{II})(\Delta\text{py}\Delta)$  or  $(\square\text{py}\square)$  based and  $\text{Os}(\text{II})$ ,  $\text{Rh}(\text{III})$ ,  $\text{Ir}(\text{III})$ - $(\text{tpy})$  based building blocks are either directly linked or connected by one or two phenyl, or thiophene spacers.

These kind of systems will give the possibility to study processes such as energy ( $\text{Ru}(\text{II})$ - $\text{Os}(\text{II})$ ) (Fig 8.5, 8.6) or electron transfer ( $\text{Ru}(\text{II})$ - $\text{Ir}(\text{III})$ ) or  $\text{Ru}(\text{II})$ - $\text{Rh}(\text{III})$ ) in the nanosecond range scale.

## 8.4 Bibliography

- <sup>1</sup> Thummel R P, Jahng Y. **Inorg Chem.** 1986, 25, 2527
- <sup>2</sup> Constable E C, Cargill Thompson A M W, Toecher D A, Daniels M A, **New J. Chem.**, 1992, 16, 855.
- <sup>3</sup> Maestri M, Armaroli N, Balzani V, Constable E C, Cargill Thompson A M W, **Inorg. Chem.**, 1995, 34, 2759.
- <sup>4</sup> Ceroni P, Credi A, Balzani V, Campagna S, Hanan G S, Arana C R, Lehn J M **Eur. J. Inorg. Chem.** 1999, 9, 1409.
- <sup>5</sup> Timpson C J, Bignozzi C A, Sullivan P B, Kober E M, Meyer T J, **J. Phys. Chem.** 1996, 100, 2915.
- <sup>6</sup> Indelli M T, Bignozzi C A, Scandola F, Collin J P, **Inorg. Chem.** 1988, 37, 6084
- <sup>7</sup> Nazeeruddin M K, Pechy P, Renouard T, Zakeeruddin S M, Humpry Baker R, Comte P, Liska P, Cevey L, Costa E, Shklover V, Spiccia L, Deacon G B, Bignozzi C A, Grätzel M. **J. Am. Chem. Soc.** 2001, 123, 1613
- <sup>8</sup> Crutchley, R J, Lever A B P, **J. Am. Chem. Soc.** 1980, 102, 7128
- <sup>9</sup> Caspar J V, Meyer T J, **Inorg Chem.** 1983, 22, 2444.
- <sup>10</sup> Allen G H, White R P, Rillema, D P, Meyer T J, **J. Am. Chem. Soc.** 1984, 106, 2613.
- <sup>11</sup> Durhan B, Caspar T J, Nagle J K, Meyer T J, **J. Am. Chem Soc.** 1982, 104, 4803.
- <sup>12</sup> Hecker C R, Gushurst A K I, McMillin D R **Inorg. Chem** 1991, 30, 538.
- <sup>13</sup> Hecker C R, Fanwick P E, McMillin D R **Inorg. Chem** 1991, 30, 659.

**Appendix I**

**“Literature Survey 1991-2001”**

1. Hansongnorn K, Saeteaw U, Cheng J, et al.  
(Nitro-kappa N)[2-(phenyldiazenyl-kappa N-2)-pyridine-kappa N](2,2':6',2"-terpyridine-kappa N-3)ruthenium(II) tetrafluoroborate  
ACTA CRYSTALLOGR C 57: 895-896 Part 8 AUG 2001
2. Wolfbauer G, Bond AM, Deacon GB, et al.  
The voltammetric reduction, deprotonation and surface activity of ruthenium photovoltaic sensitizers in acetone  
ELECTROCHEM COMMUN 3: (8) 400-405 AUG 2001
3. Haider JM, Chavarot M, Weidner S, et al.  
Metallocyclodextrins as building blocks in noncovalent assemblies of photoactive units for the study of photoinduced intercomponent processes  
INORG CHEM 40: (16) 3912-3921 JUL 30 2001
4. Teixidor F, Angles P, Vinas C, et al.  
Comparative study of NS2(S-aryl) pyridine-based dithia-containing ligands with different substituent groups. Reactivity toward Cu(II) and Ru(II)  
INORG CHEM 40: (16) 4010-4015 JUL 30 2001
5. Sun SS, Lees AJ  
Self-assembly organometallic squares with terpyridyl metal complexes as bridging ligands  
INORG CHEM 40: (13) 3154-3160 JUN 18 2001
6. Dixon IM, Collin JP  
Synthesis and properties of diads based on tetra-aryl porphyrins and ruthenium bis-terpyridine-type complexes  
J PORPHYR PHTHALOCYA 5: (7) 600-607 JUL 2001
7. Padilla-Tosta ME, Lloris JM, Martinez-Manez R, et al.  
Fluorescent chemosensors for heavy metal ions based on bis(terpyridyl) ruthenium(II) complexes containing aza-oxa and polyaza macrocycles  
EUR J INORG CHEM (6) 1475-1482 JUN 2001
8. Silva ML, Burrows HD, Formosinho SJ, et al.  
Room temperature and low-temperature absorption and emission spectra of some polypyridylruthenium(II) 3.2.1 complexes  
J MOL STRUCT 565: 79-82 Sp. Iss. SI MAY 30 2001
9. Gallagher LA, Meyer TJ  
Surface control of oxidation by an adsorbed Ru-IV-oxo complex  
J AM CHEM SOC 123: (22) 5308-5312 JUN 6 2001
10. Amatore C, Bouret Y, Maisonhaute E, et al.  
Precise adjustment of nanometric-scale diffusion layers within a redox dendrimer molecule by ultrafast cyclic voltammetry: An electrochemical nanometric microtome  
CHEM-EUR J 7: (10) 2206-2226 MAY 18 2001
11. Kelson EP, Phengsy PP, Arif AM  
A chloro(2-pyridinecarboxaldehyde)(2,2':6',2"-terpyridine)ruthenium(II) complex  
ACTA CRYSTALLOGR C 57: 517-519 Part 5 MAY 2001
12. Sondaz E, Gourdon A, Launay JP, et al.  
(Bipyridine)(terpyridine)(4-iodophenylcyanamide)ruthenium(II) complex: crystallography, electronic absorption spectroscopy, cyclic voltammetry and EPR measurements  
INORG CHIM ACTA 316: (1-2) 79-88 MAY 7 2001
13. Schubert US, Eschbaumer C, Andres P, et al.  
2,2':6',2"-Terpyridine metal complexes as building blocks for extended functional metallo-supramolecular assemblies and polymers  
SYNTHETIC MET 121: (1-3) 1249-1252 Sp. Iss. SI MAR 15 2001
14. Padilla-Tosta ME, Lloris JM, Martinez-Manez R, et al.  
ATP recognition through a fluorescence change in a multicomponent dinuclear system containing a Ru(Tpy)(2)(2+) fluorescent core and a cyclam-Cu2+ complex  
EUR J INORG CHEM (5) 1221-1226 MAY 2001
15. Chao H, Yang G, Xue GQ, et al.  
Ruthenium(II) complexes containing novel asymmetric tridentate ligands: synthesis, structure, electrochemical and spectroscopic properties  
J CHEM SOC DALTON (8) 1326-1331 2001
16. Constable EC, Housecroft CE, Johnston LA, et al.  
Dicobalt cluster functionalized 2,2':6',2"-terpyridine ligands and their ruthenium(II) complexes  
POLYHEDRON 20: (6) 483-492 MAR 30 2001
17. Abe T, Kaneko M  
pH-dependent electrocatalysis for proton reduction by bis(2,2':6',2"-terpyridine) cobalt(II) complex embedded in Nafion (R) membrane  
J MOL CATAL A-CHEM 169: (1-2) 177-183 MAR 28 2001
18. Sugimoto H, Tanaka K  
Syntheses of new ruthenium carbonyl terpyridine o-phenylene complexes: strong interaction between carbonyl and o-phenylene ligands  
J ORGANOMET CHEM 622: (1-2) 280-285 MAR 15 2001
19. Yang IV, Thorp HH  
Oxidation of 7-deazaguanine by one-electron and oxo-transfer oxidants: Mismatch-dependent electrochemistry and selective strand scission  
INORG CHEM 40: (7) 1690-1697 MAR 26 2001
20. Mosher PJ, Yap GPA, Crutchley RJ  
A donor-acceptor-donor bridging ligand in a class III mixed-valence complex  
INORG CHEM 40: (6) 1189-1195 MAR 12 2001
21. Santos JP, Zaniquelli MED, Batalini C, et al.  
Modified electrodes using mixed Langmuir-Blodgett films containing a ruthenium complex: Features of the monolayers at air-liquid interface  
J PHYS CHEM B 105: (9) 1780-1785 MAR 8 2001
22. Nazeeruddin MK, Pechy P, Renouard T, et al.  
Engineering of efficient panchromatic sensitizers for nanocrystalline TiO<sub>2</sub>-based solar cells  
J AM CHEM SOC 123: (8) 1613-1624 FEB 28 2001
23. Wolfbauer G, Bond AM, Deacon GB, et al.  
Dependence of the voltammetric oxidation of the photovoltaic sensitizer [(H<sub>3</sub>-tctpy)Ru-II(NCS)<sub>3</sub>] on the electrode material, solvent, and isomeric purity  
J ELECTROCHEM SOC 148: (2) E97-E104 FEB 2001

24. Abe T, Hirano K, Shiraishi Y, et al.  
Electrocatalysis for proton reduction by polypyridyl platinum complexes dispersed in a polymer membrane  
EUR POLYM J 37: (4) 753-761 APR 2001
25. Hartshorn CM, Maxwell KA, White PS, et al.  
Separation of positional isomers of oxidation catalyst precursors  
INORG CHEM 40: (4) 601-606 FEB 12 2001
26. Mondal B, Paul H, Puranik VG, et al.  
Ruthenium mononitro and mononitroso terpyridine complexes incorporating azoimine based ancillary ligands. Synthesis, crystal structure, spectroelectrochemical properties and kinetic aspects  
J CHEM SOC DALTON (4) 481-487 2001
27. Mosher PJ, Yap GPA, Crutchley RJ  
Influence of the inner coordination sphere on the Ru(III)-cyanamido ligand-to-metal charge transfer chromophore  
INORG CHEM 40: (3) 550-+ JAN 29 2001
28. Sugimoto H, Tsuge K, Tanaka K  
Ruthenium terpyridine complexes with mono- and bi-dentate dithiolene ligands  
J CHEM SOC DALTON (1) 57-63 2001
29. Wolfbauer G, Bond AM, Deacon GB, et al.  
Electrochemical, spectroelectrochemical and theoretical studies on the reduction and deprotonation of the photovoltaic sensitizer  $[(\text{I}_3\text{tcpy})\text{Ru}-\text{II}(\text{NCS})_3]$  ( $\text{H}_3\text{tcpy}=2,2':6',2''\text{-terpyridine-4,4',4''-tricarboxylic acid}$ )  
J ELECTROANAL CHEM 490: (1-2) 7-16 AUG 18 2000
30. Murfee HJ, Thoms TPS, Greaves J, et al.  
New metallodendrimers containing an octakis(diphenylphosphino)-functionalized silsesquioxane core and ruthenium(II)-based chromophores  
INORG CHEM 39: (23) 5209-5217 NOV 13 2000
31. Mondal B, Walawalkar MG, Lahiri GK  
Ruthenium terpyridine complexes incorporating azo-imine based ancillary ligands. Synthesis, crystal structure, spectroelectrochemical properties and solution reactivities  
J CHEM SOC DALTON (22) 4209-4217 2000
32. Kelson EP, Phengsy PP  
Kinetic study of 2-propanol and benzyl alcohol oxidation by alkaline hexacyanoferrate(III) catalyzed by a terpyridyl ruthenium complex  
INT J CHEM KINET 32: (12) 760-770 DEC 2000
33. Nazeeruddin MK, Zakeeruddin SM, Humphry-Baker R, et al.  
Determination of pKa values of 4-phosphonato-2,2':6',2''-terpyridine and its ruthenium(II)-based photosensitizer by NMR, potentiometric, and spectrophotometric methods  
INORG CHEM 39: (20) 4542-4547 OCT 2 2000
34. Rice CR, Ward MD, Nazeeruddin MK, et al.  
Catechol as an efficient anchoring group for attachment of ruthenium-polypyridine photosensitizers to solar cells based on nanocrystalline  $\text{TiO}_2$  films  
NEW J CHEM 24: (9) 651-652 2000
35. Ponce A, Gray HB, Winkler JR  
Electron tunneling through water: Oxidative quenching of electronically excited  $\text{Ru}(\text{tpy})_2^{2+}$  ( $\text{tpy}=2,2':6',2''\text{-terpyridine}$ ) by ferric ions in aqueous glasses at 77 K  
J AM CHEM SOC 122: (34) 8187-8191 AUG 30 2000
36. Yutaka T, Kurihara M, Nishihara H  
Synthesis and physical properties of a pi-conjugated ruthenium(II) dinuclear complex involving an azobenzene-bridged bis(terpyridine) ligand  
MOL CRYST LIQ CRYST 343: 511-516 2000
37. Wada T, Tsuge K, Tanaka K  
Oxidation of hydrocarbons by mono- and dinuclear ruthenium quinone complexes via hydrogen atom abstraction  
CHEM LETT (8) 910-911 AUG 5 2000
38. Mondal B, Chakraborty S, Munshi P, et al.  
Ruthenium-(II)/-(III) terpyridine complexes incorporating imine functionalities. Synthesis, structure, spectroscopic and electrochemical properties  
J CHEM SOC DALTON (14) 2327-2335 2000
39. Holmstrom SD, Cox JA  
Electrocatalysis at a conducting composite electrode doped with a ruthenium(II) metallodendrimer  
ANAL CHEM 72: (14) 3191-3195 JUL 15 2000
40. Franco M, Araki K, Rocha RC, et al.  
Molecular association and solvent effects in the electronic and NMR spectra of the tricyanoterpyridineruthenate(II) complex  
J SOLUTION CHEM 29: (7) 667-684 JUL 2000
41. Seok WK, Yim SB, Lee HN, et al.  
Synthesis, spectroscopic investigation, and theoretical study of the ruthenium diazide complex  $[\text{Ru}(\text{tpy})(\text{PPh}_3)(\text{N}_3)_2]$   
Z NATURFORSCH B 55: (6) 462-466 JUN 2000
42. Michalec JF, Bejune SA, McMillin DR  
Multiple ligand-based emissions from a platinum(II) terpyridine complex attached to pyrene  
INORG CHEM 39: (13) 2708-+ JUN 26 2000
43. Catalano VJ, Heck RA, Ohman A, et al.  
Synthesis, characterization, and electrocatalytic oxidation of benzyl alcohol by a pair of geometric isomers of  $[\text{Ru}(\text{trpy})(4,4'\text{-Me}_2\text{dppi})(\text{OH}_2)]^{2+}$  where 4,4'-dppi is 3,6-di-(4-methylpyrid-2-yl)pyridazine  
POLYHEDRON 19: (9) 1049-1055 MAY 15 2000
44. Constable EC, Housecroft CE, Neuburger M, et al.  
Programmed assembly of heteromultinuclear complexes using 4'-diphenylphosphino-2,2':6',2''-terpyridine  
INORG CHIM ACTA 300: 49-55 APR 30 2000
45. Khatyr A, Ziesse R  
Synthesis of soluble bis-terpyridine ligands bearing ethynylene-phenylene spacers  
J ORG CHEM 65: (10) 3126-3134 MAY 19 2000
46. Laemmel AC, Collin JP, Sauvage JP  
Photosubstitution of ancillary ligands in octahedral mono-terpyridine ruthenium (II) complexes  
CR ACAD SCI II C 3: (1) 43-49 JAN 2000
47. Sun SS, Silva AS, Brinn IM, et al.  
Self-assembly molecular squares with metal complexes as bridging ligands  
INORG CHEM 39: (7) 1344-+ APR 3 2000
48. Tsuge K, Kurihara M, Tanaka K  
Energy conversion from proton gradient to electricity based on characteristic redox behavior of an aqua ruthenium complex with a quinone ligand  
B CHEM SOC JPN 73: (3) 607-614 MAR 2000

49. Padilla-Tosta ME, Lloris JM, Martinez-Manez R, et al.  
Bis(terpyridyl)-ruthenium(II) units attached to polyazacycloalkanes as sensing fluorescent receptors for transition metal ions  
EUR J INORG CHEM (4) 741-748 APR 2000
50. Konno H, Kobayashi A, Sakamoto K, et al.  
Synthesis and properties of  $[\text{Ru}(\text{tpy})(4,4\text{-X}_2\text{bpy})\text{H}](+)$  ( $\text{tpy}=2,2':6',2''\text{-terpyridine}$ ,  $\text{bpy}=2,2'\text{-bipyridine}$ ,  $\text{X} = \text{H}$  and  $\text{MeO}$ ), and their reactions with  $\text{CO}_2$   
INORG CHIM ACTA 299: (2) 155-163 MAR 15 2000
51. El-ghayoury A, Harriman A, Khatyr A, et al.  
Intramolecular triplet energy transfer in metal polypyridine complexes bearing ethynylated aromatic groups  
J PHYS CHEM A 104: (7) 1512-1523 FEB 24 2000
52. Duati M, Fanni S, Vos JG  
A new luminescent Ru(terpy) complex incorporating a 1,2,4-triazole based sigma-donor ligand  
INORG CHEM COMMUN 3: (2) 68-70 FEB 2000
53. Brewer KJ  
Tridentate-bridged polyazine complexes of ruthenium(II) and osmium(II) and their application to the development of photochemical molecular devices  
COMMENT INORG CHEM 21: (4-6) 201-224 Part A 1999
54. Farrer BT, Pickett JS, Thorp HH  
Hydride transfer in oxidation of nucleic acid sugars: Electronic effects of 2'-substituents on activation of the 1'-C-H bond by oxoruthenium(IV)  
J AM CHEM SOC 122: (4) 549-553 FEB 2 2000
55. Barigelletti F, Ventura B, Collin JP, et al.  
Electrochemical and spectroscopic properties of cyclometallated and non-cyclometallated ruthenium(II) complexes containing sterically hindering ligands of the phenanthroline and terpyridine families  
EUR J INORG CHEM (1) 113-119 JAN 2000
56. Farrer BT, Thorp HH  
Redox pathways in DNA oxidation: Kinetic studies of guanine and sugar oxidation by para-substituted derivatives of oxoruthenium(IV)  
INORG CHEM 39: (1) 44-49 JAN 10 2000
57. Hossain MD, Ueno R, Haga M  
Synthesis and tuning of chemical properties by protonation/deprotonation of novel dinuclear ruthenium complexes containing 2,6,2',6'-tetra(4,5-dimethylbenzimidazol-2-yl)-4,4'-bipyridine  
INORG CHEM COMMUN 3: (1) 35-38 JAN 2000
58. Padilla-Tosta VE, Lloris JM, Martinez-Manez R, et al.  
A fluorescent chemosensor based on a ruthenium (II)-terpyridine core containing peripheral amino groups that selectively sense ATP in an aqueous environment  
INORG CHEM COMMUN 3: (1) 45-48 JAN 2000
59. Laurent F, Plantalech E, Donnadiou B, et al.  
Synthesis, structure and redox properties of ruthenium complexes containing the tpm facial and the trpy meridional tridentate ligands - Crystal structures of  $[\text{RuCl}_2(\text{trpy})]$  and  $[\text{Ru}(\text{tpm})(\text{py})_3](\text{PF}_6)_2$   
POLYHEDRON 18: (25) 3321-3331 1999
60. Jahng YD, Park JG  
Reaction of  $\text{Ru}(\text{tpy})\text{Cl}_2$  with N,N,C-terdentates, 3,2'-annulated-6-(2''-pyridyl)-2-phenylpyridines  
B KOR CHEM SOC 20: (10) 1200-1204 OCT 20 1999
61. Hugot-Le Goff A, Joiret S, Falaras P  
Raman resonance effect in a monolayer of polypyridyl ruthenium(II) complex adsorbed on nanocrystalline  $\text{TiO}_2$  via phosphonated terpyridyl ligands  
J PHYS CHEM B 103: (44) 9569-9575 NOV 4 1999
62. Ceroni P, Credi A, Balzani V, et al.  
Absorption and emission properties of di- and trinuclear ruthenium(II) rack-type complexes  
EUR J INORG CHEM (9) 1409-1414 SEP 1999
63. Constable EC, Harverson P, Housecroft CE  
Convergent syntheses of topologically linear heterotri- and heteropenta-nuclear complexes based upon bis(4'-(2,2':6',2''-terpyridinyl)) ether  
J CHEM SOC DALTON (21) 3693-3700 1999
64. Flamigni L, Barigelletti F, Armaroli N, et al.  
Photoinduced processes in multicomponent arrays containing transition metal complexes  
COORDIN CHEM REV 192: 671-682 SEP 1999
65. Treadway JA, Moss JA, Meyer TJ  
Visible region photooxidation on  $\text{TiO}_2$  with a chromophore-catalyst molecular assembly  
INORG CHEM 38: (20) 4386-4391 OCT 4 1999
66. Kintop JA, Machado WVM, Franco M, et al.  
Theoretical calculations of the nuclear magnetic shielding tensors and analysis of the C-13 NMR spectra of the tricyano(terpyridine)ruthenate(II) complex  
CHEM PHYS LETT 309: (1-2) 90-94 AUG 6 1999
67. Perez WJ, Lake CH, See RF, et al.  
In situ syntheses of trans-spanned octahedral ruthenium complexes. Crystal structures of trans- $[\text{Ru}(\text{Cl})(\text{trpy})\{\text{Ph}_2\text{PC}_6\text{H}_4\text{CH}_2\text{O}(\text{CO})(\text{CH}_2)_4(\text{CO})\text{OCH}_2\text{C}_6\text{H}_4\text{PPh}_2\}][\text{PF}_6]\text{center dot } 0.25\text{C}(6)\text{H}(5)\text{Me center dot } 0.5\text{CH}(2)\text{Cl}(2)$  and trans- $[\text{Ru}(\text{Cl})(\text{trpy})(\text{PPh}_3)_2][\text{BF}_4]\text{center dot } \text{CH}_2\text{Cl}_2$   
J CHEM SOC DALTON (14) 2281-2292 1999
68. Harriman A, Romero FM, Ziessel R, et al.  
Triplet energy transfer within closely spaced positional isomers of Ru/Os polypyridine-based heterodiads  
J PHYS CHEM A 103: (28) 5399-5408 JUL 15 1999
69. Pyo S, Perez-Cordero E, Bott SG, et al.  
Crystal structure of  $[\text{Ru}(\text{terpy})_2]$ : A new crystalline material from the reductive electrocrystallization of  $[\text{Ru}(\text{terpy})_2](2+)$   
INORG CHEM 38: (14) 3337-3343 JUL 12 1999
70. Cardenas DJ, Collin JP, Gavina P, et al.  
Synthesis, x-ray structure, and electrochemical and excited-state properties of multicomponent complexes made of a  $[\text{Ru}(\text{Terpy})(2)](2+)$  unit covalently linked to a [2]-catenate moiety. Controlling the energy-transfer direction by changing the catenate metal ion  
J AM CHEM SOC 121: (23) 5481-5488 JUN 16 1999
71. Santos JP, Zanicuelli MED, Batalini C, et al.  
Palmitic acid and aquo-ruthenium complex monolayers at the liquid-air interface and electroactive Langmuir-Blodgett films  
THIN SOLID FILMS 349: (1-2) 238-243 JUL 30 1999

72. Ribou AC, Wada T, Sasabe H  
Synthesis, characterization and optical properties of novel carbazole-ruthenium compounds: carbazole as a new building block?  
INORG CHIM ACTA 288: (2) 134-141 MAY 30 1999
73. Zadykiewicz J, Potvin PG  
Mono- and dinuclear ruthenium(II) complexes of 2,6-di(pyrazol-3-yl)pyridines: Deprotonation, functionalization, and supramolecular association  
INORG CHEM 38: (10) 2434-2441 MAY 17 1999
74. Farrer BT, Thorp HH  
Driving force and isotope dependence of the kinetics of proton-coupled electron transfer in oxoruthenium(IV) polypyridyl complexes  
INORG CHEM 38: (10) 2497-2502 MAY 17 1999
75. Hutchison K, Morris JC, Nile TA, et al.  
Spectroscopic and photophysical properties of complexes of 4'-ferrocenyl-2,2':6',2''-terpyridine and related ligands  
INORG CHEM 38: (10) 2516-2523 MAY 17 1999
76. Schlicke B, Belser P, De Cola L, et al.  
Photonic wires of nanometric dimensions. Electronic energy transfer in rigid rodlike Ru(bpy)<sub>3</sub><sup>2+</sup>-ph<sub>n</sub>-Os(bpy)<sub>3</sub><sup>2+</sup> compounds (ph=1,4-phenylene; n=3, 5, 7)  
J AM CHEM SOC 121: (17) 4207-4214 MAY 5 1999
77. Chamchoumis CM, Potvin PG  
A singly stranded, helical di-ruthenium(II) complex of a novel 6,6-ethynyl-linked bis(terpyridine) ligand. Distortion of the ethyne linkage and inversion of helicity  
J CHEM SOC DALTON (9) 1373-1374 MAY 7 1999
78. Lebeau EL, Meyer TJ  
Oxidation of benzyl alcohol by a dioxo complex of ruthenium(VI)  
INORG CHEM 38: (9) 2174-2181 MAY 3 1999
79. Zadykiewicz J, Potvin PG  
Structural studies on pyrazolylpyridine ligands and complexes. 2. Comparisons between bispyrazolopyridine linkage isomers and with 2,2':6',2''-terpyridine  
J COORD CHEM 47: (3) 395-407 1999
80. Gulyas PT, Smith TA, Paddon-Row MN  
Synthesis, electrochemistry and photophysics of rigid norbornylogous-bridged complexes of ruthenium and osmium  
J CHEM SOC DALTON (8) 1325-1335 APR 21 1999
81. Craig DC, Scudder ML, McHale WA, et al.  
Structural studies of complexes of tridentate terimine systems. Crystal structure of bis(2,2':6',2''-terpyridine)ruthenium(II) perchlorate hydrate, bis(2,2':6',2''-terpyridine)osmium(II) perchlorate hemihydrate and bis((1,10-phenanthroline-2-yl)(pyridin-2-yl)amine)iron(II) tetrafluoroborate dihydrate  
AUST J CHEM 51: (12) 1131-1139 1998
82. Chichak K, Branda NR  
Self-assembly of a linear multicomponent porphyrin array through axial coordination  
CHEM COMMUN (6) 523-524 MAR 21 1999
83. Catalano VJ, Kurtaran R, Heck RA, et al.  
Bdmp complexes of Ru(II) as structural analogs for Ru(II)-2,2':6',2''-terpyridine species (where bdmp is 2,6-bis(3,5-dimethyl-N-pyrazoyl)pyridine  
INORG CHIM ACTA 286: (2) 181-188 MAR 15 1999
84. Ziegler M, Monney V, Stoeckli-Evans H, et al.  
Complexes of new chiral terpyridyl ligands. Synthesis and characterization of their ruthenium(II) and rhodium(III) complexes  
J CHEM SOC DALTON (5) 667-675 MAR 7 1999
85. Heitzler FR, Neuburger M, Zehnder M, et al.  
Synthesis, H-1/C-13 NMR spectroscopic and structural studies of sterically induced internal dynamics in novel mono- and di-ruthenium(II) 2,2':6',2''-terpyridine complexes of 2,3-bis(2,2'-bipyridin-6-yl)pyrazine  
J CHEM SOC DALTON (4) 565-574 FEB 21 1999
86. Iashgari K, Kritikos M, Norrestam R, et al.  
Bis(terpyridine)ruthenium(II) bis(hexafluorophosphate) diacetonitrile solvate  
ACTA CRYSTALLOGR C 55: 64-67 Part 1 JAN 15 1999
87. Flamigni L, Barigelletti F, Armaroli N, et al.  
Triplet-triplet energy transfer between porphyrins linked via a ruthenium(II) bis(terpyridine) complex  
INORG CHEM 38: (4) 661-667 FEB 22 1999
88. Storrer GD, Takada K, Abruna HD  
Catechol-pendant terpyridine complexes: Electrodeposition studies and electrocatalysis of NADH oxidation  
INORG CHEM 38: (3) 559-565 FEB 8 1999
89. Constable EC, Housecroft CE, Schneider AG  
A clash of cultures: metal carbonyl functionalized Werner complexes  
J ORGANOMET CHEM 573: (1-2) 101-108 JAN 31 1999
90. Newkome GR, He EF, Godinez LA, et al.  
Neutral highly branched metallomacromolecules: incorporation of a (2,2':6',2''-terpyridine)ruthenium(II) complex without external counterions  
CHEM COMMUN (1) 27-28 JAN 7 1999
91. Bushell KL, Couchman SM, Jeffery JC, et al.  
Stepwise synthetic strategy for the preparation of trinuclear complexes of bis(terpyridyl) bridging ligands containing azacrown macrocyclic spacer groups  
J CHEM SOC DALTON (20) 3397-3403 OCT 21 1998
92. Fung WH, Yu WY, Che CM  
Mechanistic investigation of the oxidation of aromatic alkenes by monooxoruthenium(IV). Asymmetric alkene epoxidation by chiral monooxoruthenium(IV) complexes  
J ORG CHEM 63: (22) 7715-7726 OCT 30 1998
93. Couchman SM, Dominguez-Vera JM, Jeffery JC, et al.  
Structures, electrochemical and spectroscopic properties of ternary ruthenium(II)-polypyridyl complexes with additional carboxylate, biguanide or sulfonamide donors  
POLYHEDRON 17: (20) 3541-3550 1998
94. Sasaki I, Daran JC, Ait-Haddou H, et al.  
New annelated 2,2':6',2''-terpyridines and their Ru(II) complexes: synthesis and characterisation  
INORG CHEM COMMUN 1: (9) 354-357 SEP 1998
95. Seok WK, Moon SW, Kim MY  
NMR study on Ru(II) complexes containing 2,2':6',2''-terpyridine  
B KOR CHEM SOC 19: (11) 1207-1210 NOV 20 1998
96. Indelli MT, Bignozzi CA, Scandola F, et al.

Design of long-lived Ru(II) terpyridine MLCT states. Tricyano terpyridine complexes  
INORG CHEM 37: (23) 6084-6089 NOV 16 1998

97. Pramanik NC, Bhattacharya S  
The chemistry of  $[Ru(trpy)(Q)_x]^{n+}$  (trpy = 2,2',2''-terpyridine; Q = the quinolin-8-olate anion; X = Cl<sup>-</sup>, H<sub>2</sub>O, MeCN and N-3(-); n = 0 and 1)  
TRANSIT METAL CHEM 23: (4) 429-434 AUG 1998

98. Seok WK, Son YJ, Moon SW, et al.  
The comparative study in the oxygen atom transfer reaction by ruthenium mono-oxo complexes  
B KOR CHEM SOC 19: (10) 1084-1090 OCT 20 1998

99. Walsh JL, McCracken R, McPhail AT  
Preparation and X-ray crystal structure study of a polypyridyl ruthenium(II) complex containing a dehydrodithizone ligand  
POLYHEDRON 17: (18) 3221-3226 1998

100. Tsuge K, Tanaka K  
First artificial energy conversion from proton gradient to electricity  
CHEM LETT (10) 1069-1070 OCT 1998

101. Ferrere S, Gregg BA  
Chloride oxidation catalysis by a polymeric oxide derived from  $[Ru(4,4'$ -dimethyl-2,2'-bipyridine)(Cl)(3)(H<sub>2</sub>O)]  
J CHEM SOC FARADAY T 94: (18) 2827-2833 SEP 21 1998

102. Jing BW, Zhang H, Zhang MH, et al.  
Ruthenium(II) thiocyanate complexes containing 4'-(4-phosphonatophenyl)-2,2':6',2''-terpyridine: synthesis, photophysics and photosensitization to nanocrystalline TiO<sub>2</sub> electrodes  
J MATER CHEM 8: (9) 2055-2060 SEP 1998

103. Flamigni L, Barigelletti F, Armaroli N, et al.  
Photoinduced processes in highly coupled multicomponent arrays based on a ruthenium(II)bis(terpyridine) complex and porphyrins  
CHEM-EUR J 4: (9) 1744-1754 SEP 1998

104. Di Bilio AJ, Dennison C, Gray HB, et al.  
Electron transfer in ruthenium-modified plastocyanin  
J AM CHEM SOC 120: (30) 7551-7556 AUG 5 1998

105. Hartshorn CM, Steel PJ  
Cyclometalated compounds. XI. Single and double cyclometalations of poly(pyrazolylmethyl)benzenes  
ORGANOMETALLICS 17: (16) 3487-3496 AUG 3 1998

106. Albano G, Balzani V, Constable EC, et al.  
Photoinduced processes in 4'-(9-anthryl)-2,2':6',2''-terpyridine, its protonated forms and Zn(II), Ru(II) and Os(II) complexes  
INORG CHIM ACTA 277: (2) 225-231 AUG 3 1998

107. Seok WK, Yim SB, Klapotke TM, et al.  
Synthesis, structural characterization and semiempirical calculations of the ruthenium azide complex  $[Ru(tpy)(PPh_3)_2(N-3)] [ClO_4]$   
J ORGANOMET CHEM 559: (1-2) 165-171 MAY 29 1998

108. Lee JD, Vrana LM, Bullock ER, et al.  
A tridentate-bridged ruthenium-rhodium complex as a stereochemically defined light-absorber-electron-acceptor dyad  
INORG CHEM 37: (14) 3575-3580 JUL 13 1998

109. Islam A, Ikeda N, Yoshimura A, et al.

Nonradiative transition of phosphorescent charge-transfer states of ruthenium(II)-to-2,2'-biquinoline and ruthenium(II)-to-2,2':6',2''-terpyridine in the solid state  
INORG CHEM 37: (12) 3093-3098 JUN 15 1998

110. Constable EC, Housecroft CE, Johnston LA  
Dicobalt cluster-functionalized 2,2':6',2''-terpyridine ligands, ruthenium(II) complexes with covalently linked C<sub>2</sub>Co<sub>2</sub>(CO)<sub>6</sub> units  
INORG CHEM COMMUN 1: (2) 68-70 FEB 1998

111. Kurihara M, Daniele S, Tsuge K, et al.  
Synthesis and characterization of ruthenium terpyridine dioxolene complexes: Resonance equilibrium between Ru-III-catechol and Ru-II-semiquinone forms  
B CHEM SOC JPN 71: (4) 867-875 APR 1998

112. Pramanik NC, Pramanik K, Ghosh P, et al.  
Chemistry of  $[Ru(tpy)(pap)(L')^{(n+)}$  (tpy = 2,2',6',2''-terpyridine; pap = 2-(phenylazo)pyridine; L' = Cl<sup>-</sup>, H<sub>2</sub>O, CH<sub>3</sub>CN, 4-picoline, N-3(-); n = 1,2. X-ray crystal structure of  $[Ru(tpy)(pap)(CH_3CN)](ClO_4)_2$  and catalytic oxidation of water to dioxygen by  $[Ru \dots (tpy)(pap)(H_2O)](2+)$   
POLYHEDRON 17: (9) 1525-1534 1998

113. Catalano VJ, Heck RA, Immoos CE, et al.  
Steric modulation of electrocatalytic benzyl alcohol oxidation by  $[Ru(tpy)(R(2)dppi)(O)](2+)$  complexes  
INORG CHEM 37: (9) 2150-2157 MAY 4 1998

114. Cifan SA, Hondros DP, Thorp HH  
Quenching of guanine oxidation by oxoruthenium(IV): Effects of divalent cations on chemical nuclease studies  
INORG CHEM 37: (7) 1598-1601 APR 6 1998

115. Jing BW, Wang WQ, Zhang MH, et al.  
Polypyridine ruthenium(II) complexes containing mixed ligands. Synthesis, spectroscopic and photophysical and electrochemical properties  
DYES PIGMENTS 37: (2) 177-186 APR 15 1998

116. Ronco SE, Thompson DW, Gahan SL, et al.  
Synthesis of, characterization of, and photoinduced processes in polymetallic triad complexes containing Fe(II), Ru(II), and Rh(III) metal centers  
INORG CHEM 37: (8) 2020-2027 APR 20 1998

117. Jones SW, Vrana LM, Brewer KJ  
Using spectroelectrochemistry to probe the light absorbing properties of polymetallic complexes containing the tridentate bridging ligand 2,3,5,6-tetrakis(2-pyridyl)pyrazine  
J ORGANOMET CHEM 554: (1) 29-40 MAR 5 1998

118. Cheung STC, Fung AKM, Lam MHW  
Visible photosensitization of TiO<sub>2</sub> - Photodegradation of CCl<sub>4</sub> in aqueous medium  
CHEMOSPHERE 36: (11) 2461-2473 MAY 1998

119. Collin JP, Gavina P, Heitz V, et al.  
Construction of one-dimensional multicomponent molecular arrays: Control of electronic and molecular motions  
EUR J INORG CHEM (1) 1-14 JAN 1998

120. Takada K, Storrier GD, Pariente F, et al.  
EQCM studies of the redox processes during and after electropolymerization of films of transition-metal complexes of vinylterpyridine  
J PHYS CHEM B 102: (8) 1387-1396 FEB 19 1998



121. Carter PJ, Cheng CC, Thorp HH  
Oxidation of DNA and RNA by oxoruthenium(IV) metallointercalators: Visualizing the recognition properties of dipyrrophenazine by high-resolution electrophoresis  
J AM CHEM SOC 120: (4) 632-642 FEB 4 1998
122. Norrby T, Borje A, Akermark A, et al.  
Synthesis, structure, and photophysical properties of novel ruthenium(II) carboxypyridine type complexes  
INORG CHEM 36: (25) 5850-5858 DEC 3 1997
123. Zakeeruddin SM, Nazeeruddin MK, Pechy P, et al.  
Molecular engineering of photosensitizers for nanocrystalline solar cells: Synthesis and characterization of Ru dyes based on phosphonated terpyridines  
INORG CHEM 36: (25) 5937-5946 DEC 3 1997
124. Mamo A, Steffo I, Poggi A, et al.  
Ruthenium(II) and osmium(II) complexes with new terdentate polyquinoline and cyclometalating ligands. Synthesis, NMR characterization, luminescence properties, and electrochemical behavior  
NEW J CHEM 21: (11) 1173-1185 NOV 1997
125. Hammarstrom L, Barigelletti F, Flamigni L, et al.  
A study on delocalization of MLCT excited states by rigid bridging ligands in homometallic dinuclear complexes of ruthenium(II)  
J PHYS CHEM A 101: (48) 9061-9069 NOV 27 1997
126. Bryan CD, Bryan TA, Cordes AW, et al.  
Structure of chlorohydroxynitrosyl(terpyridine)ruthenium(II) hexafluorophosphate  
J CHEM CRYSTALLOGR 27: (7) 413-415 JUL 1997
127. Vrana LM, Brewer KJ  
A new class of light absorber-electron acceptor dyad  
J PHOTOCH PHOTOBIO A 109: (3) 201-211 SEP 30 1997
128. Nishiyama H, Shimada T, Itoh H, et al.  
Novel ruthenium-pyridinedicarboxylate complexes of terpyridine and chiral bis(oxazolonyl)pyridine: a new catalytic system for alkene epoxidation with [bis(acetoxy)iodo]benzene as an oxygen donor  
CHEM COMMUN (19) 1863-1864 OCT 7 1997
129. Indelli MT, Scandola F, Flamigni L, et al.  
Photoinduced electron transfer in ruthenium(II)-rhodium(III) terpyridine dyads  
INORG CHEM 36: (19) 4247-4250 SEP 10 1997
130. Haire GR, Leadbeater NE, Lewis J, et al.  
Photochemistry of [Ru(CO)5] with nitrogen heterocycles  
J CHEM SOC DALTON (17) 2997-3003 SEP 7 1997  
Yam VWW, Lee VWM  
Synthesis, emission, electrochemistry and cation-binding studies of ruthenium(II)-diimine-crown and -terpyridine-crown complexes  
J CHEM SOC DALTON (17) 3005-3010 SEP 7 1997
131. Hissler M, Zissel R  
Versatile ruthenium(II) metallo-synthons for the stepwise construction of ordered networks  
NEW J CHEM 21: (6-7) 843-846 JUN-JUL 1997
132. Flamigni L, Armaroli N, Barigelletti F, et al.  
Photoinduced processes in dyads made of a porphyrin unit and a ruthenium complex  
J PHYS CHEM B 101: (31) 5936-5943 JUL 31 1997
133. Jahng Y, Thummel RP, Bott SG  
Formation of ruthenium(II) complexes with unsymmetrical terdentate ligands  
INORG CHEM 36: (14) 3133-3138 JUL 2 1997
134. Cardenas DJ, Sauvage JP  
Templating and clipping coordination reactions leading to heteronuclear trimetallic complexes containing interlocking rings  
INORG CHEM 36: (13) 2777-2783 JUN 18 1997
135. Rao KM, Rao CRK, Zacharias PS  
Synthesis and molecular structure of [CpRu(PPh3)(Phterpy-N,N')]Cl complex: Hdentate nature of Phterpy and diterpy  
POLYHEDRON 16: (14) 2369-2374 1997
136. Fagalde F, deKatz NDL, Katz NE  
Base hydrolysis of acetonitrile coordinated to a ruthenium(II) polypyridine complex  
POLYHEDRON 16: (11) 1921-1923 1997
137. Churchill MR, Krajkowski LM, Szczepura LF, et al.  
Crystal structure of mer,trans-[Ru(NO2)(trpy)(PPh3)2][PF6]: A "problem structure"  
J CHEM CRYSTALLOGR 26: (12) 853-859 DEC 1996
138. Cardenas DJ, Gavina P, Sauvage JP  
Construction of interlocking and threaded rings using two different transition metals as templating and connecting centers: Catenanes and rotaxanes incorporating Ru(terpy)(2)-units in their framework  
J AM CHEM SOC 119: (11) 2656-2664 MAR 19 1997
139. Thompson AMWC, Smailes MCC, Jeffery JC, et al.  
Ruthenium tris-(bipyridyl) complexes with pendant protonatable and deprotonatable moieties: pH sensitivity of electronic spectral and luminescence properties  
J CHEM SOC DALTON (5) 737-743 MAR 7 1997
140. Barigelletti F, Flamigni L, Collin JP, et al.  
Vectorial transfer of electronic energy in rod-like ruthenium-osmium dinuclear complexes  
CHEM COMMUN (4) 333-338 FEB 21 1997
141. Jahng Y, Moon SW, Thummel RP  
Synthesis and properties of terdentates with extra pyridine ring and their Ru(II) complexes  
B KOR CHEM SOC 18: (2) 174-179 FEB 20 1997
142. Szalda DJ, Fagalde F, Katz NE  
Pentaammine-2 kappa N-5-(mu-4,4'-bipyridine-1 kappa N:2 kappa N')(2,2'-bipyridine-1 kappa(2),N,N')-(2,2':6',2"-terpyridine-1 kappa N-3,N',N")diruthenium tetrakis(hexafluorophosphate) acetonitrile solvate  
ACTA CRYSTALLOGR C 52: 3013-3016 Part 12 DEC 15 1996
143. Karlen T, Dani P, Grove DM, et al.  
New arylruthenium(II) complexes of the P,C,P'-coordinating terdentate monoanionic aryl ligands [C6H2(CH2PPh2)(2)-2,6-R-4](-) (PCP-R-4; R=Ph,H). Synthesis of 16-electron species [Ru(II)X(PCP-R-4)(PPh3)] (X=Cl,I,OTf) and their reactivity toward the neutral terdentate N-donor ligand 2,2':6',2"-terpyridine . . . (terpy)  
ORGANOMETALLICS 15: (26) 5687-5694 DEC 24 1996
144. Liang YY, Baba AI, Kim WY, et al.  
Intramolecular exchange energy transfer in a bridged bimetallic transition metal complex: Calculation of rate constants using emission spectral fitting parameters  
J PHYS CHEM-US 100: (47) 18408-18414 NOV 21 1996

145. Thompson AMWC, McCleverty JA, Ward MD  
Multinucleating ligands from multiple palladium(0)-catalysed cross-coupling reactions - Synthesis and characterisation of a trinuclear cyclometallated ruthenium(II) complex and a hexanuclear EPR-active molybdenum complex  
INORG CHIM ACTA 250: (1-2) 29-34 SEP 1996
146. Steenwinkel P, James SL, Grove DM, et al.  
New ruthenium(II) complexes of functionalized monoanionic aryldiamine N,C,N'-terdentate ligands: Syntheses of [Ru-II{2,6-(Me(2)NCH(2))(2)-4-R-C6H2)-(terpy)}Cl-(-); X-ray structure of a dimeric organolithium compound, [Li{2,6-(Me(2)NCH(2))(2)-4-Ph-C6H2}](2)  
CHEM-EUR J 2: (11) 1440-1445 NOV 1996
147. Whittle B, Batten SR, Jeffery JC, et al.  
Ruthenium(II) complexes of some new polynucleating ligands incorporating terpyridyl and macrocyclic aza-crown binding sites  
J CHEM SOC DALTON (22) 4249-4255 NOV 21 1996
148. Hanan GS, Arana CR, Lehn JM, et al.  
Coordination arrays: Synthesis and characterisation of rack-type dinuclear complexes  
CHEM-EUR J 2: (10) 1292-1302 OCT 1996
149. Balzani V, Barigelletti F, Belser P, et al.  
Rigid rodlike dinuclear Ru/Os complexes of a novel bridging ligand. Intercomponent energy and electron-transfer processes  
J PHYS CHEM-US 100: (42) 16786-16788 OCT 17 1996
150. Churchill MR, See RF, Bessel CA, et al.  
Crystal structure of mer,trans-[Ru(NO<sub>2</sub>)(trpy)(PPr<sub>3</sub>)<sub>2</sub>][ClO<sub>4</sub>], a species with disordered PPr<sub>3</sub> and NO<sub>2</sub> ligands  
J CHEM CRYSTALLOGR 26: (8) 543-551 AUG 1996
151. Schoonover JR, Ni JF, Roecker L, et al.  
Structural and resonance Raman studies of an oxygen-evolving catalyst. Crystal structure of [(bpy)<sub>2</sub>(H<sub>2</sub>O)RuIIORuI(OH)(bpy)<sub>2</sub>](ClO<sub>4</sub>)<sub>4</sub>  
INORG CHEM 35: (20) 5885-5892 SEP 25 1996
152. Yanagida S, Ogata T, Kuwana Y, et al.  
Synthesis of 2,2':5',2''-terpyridine and 2,2':5',2''-5'',2'''-quaterpyridine and their photocatalysis of the reduction of water  
J CHEM SOC PERK T 2 (9) 1963-1969 SEP 1996
153. Hasenknopf B, Hall J, Lehn JM, et al.  
Linear tris-terpyridines and their trinuclear Ru(II) complexes: Synthesis, absorption spectra, and excited state properties  
NEW J CHEM 20: (7-8) 725-730 JUL-AUG 1996
154. Gulyas PT, Hambley TW, Lay PA  
The crystal structure of (2,2'-bipyridine)(pyrazine)(2,2':6',2''-terpyridine)ruthenium(II) hexafluorophosphate  
AUST J CHEM 49: (4) 527-532 1996
155. Barigelletti F, Flamigni I., Guardigli M, et al.  
Modulation of the luminescence properties of a ruthenium-terpyridine complex by protonation of a remote site  
CHEM COMMUN (11) 1329-1330 JUN 7 1996
156. Bonhote P, Moser JE, Vlachopoulos N, et al.  
Photoinduced electron transfer and redox-type photochromism of a TiO<sub>2</sub>-anchored molecular diad  
CHEM COMMUN (10) 1163-1164 MAY 21 1996
157. Constable EC, Dunne SJ, Rees DGF, et al.  
Reversible cyclometallation at a ruthenium(II) centre  
CHEM COMMUN (10) 1169-1170 MAY 21 1996
158. Tzalis D, Tor Y  
Coordination compounds as building blocks: Single-step synthesis of multi-ruthenium(II) complexes  
CHEM COMMUN (9) 1043-1044 MAY 7 1996
159. Dovletoglou A, Adeyemi SA, Meyer TJ  
Coordination and redox chemistry of substituted-polypyridyl complexes of ruthenium  
INORG CHEM 35: (14) 4120-4127 JUL 3 1996
160. Grossshenny V, Harriman A, Hissler M, et al.  
Intramolecular triplet energy transfer in alkyne-bridged Ru-Os multinuclear complexes: Switching between dipole-dipole and electron-exchange mechanisms  
J CHEM SOC FARADAY T 92: (12) 2223-2238 JUN 21 1996
161. Im SG, Sykes AG  
Kinetic studies on the redox reactions of Clostridium pasteurianum rubredoxin  
J CHEM SOC DALTON (11) 2219-2222 JUN 7 1996
162. Sinha PK, Chakravarty J, Bhattacharya S  
Ruthenium phenolates: Synthesis, characterization and reactivities of a group of salicylaldiminato and 2-(aryloxy)phenolato complexes of ruthenium  
POLYHEDRON 15: (17) 2931-2938 1996
163. Ho PKK, Peng SM, Wong KY, et al.  
Syntheses, structures and electrochemical properties of single and double helical inorganic complexes containing new polypyridine ligands  
J CHEM SOC DALTON (9) 1829-1834 MAY 7 1996
164. Thorp HH, McKenzie RA, Lin PN, et al.  
Cleavage of functionally relevant sites in ferritin mRNA by oxidizing metal complexes  
INORG CHEM 35: (10) 2773-2779 MAY 8 1996
165. Cheng WC, Yu WY, Zhu J, et al.  
Chiral ruthenium(IV)-oxo complexes. Structure, reactivities of [Ru(terpy)(N boolean AND NO)(2+)] (N boolean and N=N,N',N'-teramethyl-1,2-diaminocyclohexane) and [Ru(Me<sub>3</sub>tacn)(cbpy)O]<sup>2+</sup> (cbpy=3,3'-[(4S-trans)-1,3-dioxolane-4,5-dimethyl]-2,2'-bipyridine)  
INORG CHIM ACTA 242: (1-2) 105-113 FEB 15 1996
166. Goll JG, Thorp HH  
Oxidation of DNA by trans-dioxoruthenium(VI) complexes: Self-inhibition of DNA cleavage by metal complexes  
INORG CHIM ACTA 242: (1-2) 219-223 FEB 15 1996
167. Ponce A, Bachrach M, Farmer PJ, et al.  
Intramolecular electron transfer in cyanide-bridged ruthenium dimers  
INORG CHIM ACTA 243: (1-2) 135-140 FEB 29 1996
168. Bardwell DA, Thompson AMWC, Jeffery JC, et al.  
New tricks for an old ligand: Cyclometallated and didentate coordination of 2,2':6',2''-terpyridine to ruthenium(II)  
J CHEM SOC DALTON (6) 873-878 MAR 21 1996
169. Szczepura LF, Kubow SA, Leising RA, et al.  
Synthesis, characterization and redox properties of mixed phosphine nitroruthenium(II) complexes. Crystal structure of trans-[Ru(NO)<sub>2</sub>(terpy)-(PMe<sub>3</sub>)(PPh<sub>3</sub>)] [ClO<sub>4</sub>].center dot H<sub>2</sub>O  
J CHEM SOC DALTON (7) 1463-1470 APR 7 1996
170. Schneider S, Brehm G, Prenzel CJ, et al.

Vibrational spectra, normal coordinate analysis and excited-state lifetimes for a series of polypyridylruthenium(II) complexes  
J RAMAN SPECTROSC 27: (2) 163-175 FEB 1996

171. Timpson CJ, Bignozzi CA, Sullivan BP, et al.  
Influence of solvent on the spectroscopic properties of cyano complexes of ruthenium(II)  
J PHYS CHEM-US 100: (8) 2915-2925 FEB 22 1996

172. Sutter JP, James SL, Steenwinkel P, et al.  
Versatile N,C,N coordination behavior of a monoanionic aryldiamine ligand in ruthenium(II) complexes: Syntheses and crystal structures of [Ru-II(C<sub>6</sub>H<sub>3</sub>(CH<sub>2</sub>NMe<sub>2</sub>)<sub>2</sub>-2,6)X(L)] (L equals norbornadiene, X=Cl, SO<sub>2</sub>CF<sub>3</sub>; L=PPh<sub>3</sub>, X=I) and [Ru-II(C<sub>6</sub>H<sub>3</sub>(CH<sub>2</sub>NMe<sub>2</sub>)<sub>2</sub>-2,6)(2,2':6:2"-terpyridine)]Cl  
ORGANOMETALLICS 15: (3) 941-948 FEB 6 1996

173. Navarro M, Galembeck SE, Romero JR, et al.  
Redox and spectral properties of [Ru(trpy)I.(H<sub>2</sub>O)](ClO<sub>4</sub>)<sub>2</sub> [trpy=2,2':6:2"-terpyridine; I=4,4'-(OMe)<sub>2</sub>bpy;4,4'-(NO<sub>2</sub>)<sub>2</sub>bpy]: A comparative computational study  
POLYHEDRON 15: (9) 1531-1537 MAY 1996

174. Vogler LM, Brewer KJ  
Building block approach to the construction of long-lived osmium(II) and ruthenium(II) multimetallic complexes incorporating the tridentate bridging ligand 2,3,5,6-tetrakis(2-pyridyl)pyrazine  
INORG CHEM 35: (4) 818-824 FEB 14 1996

175. Barigelletti F, Flamigni L, Guardigli M, et al.  
Energy transfer in rigid Ru(II)/Os(II) dinuclear complexes with biseyclometalating bridging ligands containing a variable number of phenylene units  
INORG CHEM 35: (1) 136-142 JAN 3 1996

176. Indelli MT, Scandola F, Collin JP, et al.  
Photoinduced electron and energy transfer in rigidly bridged Ru(II)-Rh(III) binuclear complexes  
INORG CHEM 35: (2) 303-312 JAN 17 1996

177. Chotalia R, Constable EC, Hannon MJ, et al.  
Hypodentate ligands - systematic approaches to complexes containing didentate 2,2'/6:2"-terpyridine (terpy) and the crystal and molecular-structures of [Ru(bipy-N,N')<sub>2</sub>(terpy-N,N')][PF<sub>6</sub>]<sub>2</sub> and [Ru(bipy-N,N')<sub>2</sub>(bterpy-N,N')][PF<sub>6</sub>]<sub>2</sub> (bipy=2,2'-bipyridine, bterpy=6-bromo-2,2'/6:2"-terpyridine . . .)  
J CHEM SOC DALTON (22) 3571-3580 NOV 21 1995

178. Boelrijk AEM, Jorna AMJ, Reedijk J  
Oxidation of octyl alpha-d-glucopyranoside to octyl alpha-d-glucuronic acid, catalyzed by several ruthenium complexes, containing a 2-(phenyl) azopyridine or a 2-(nitrophenyl)azopyridine ligand  
J MOL CATAL A-CHEM 103: (2) 73-85 OCT 28 1995

179. Toyohara K, Nagao H, Mizukawa T, et al.  
Ruthenium formyl complexes as the branch point in 2-electron and multielectron reductions of CO<sub>2</sub>  
INORG CHEM 34: (22) 5399-& OCT 25 1995

180. Lavagnoli LV, Navarro M, Degiovani WF, et al.  
Electrocatalytic oxidation of organic substrates in a biphasic system using a ruthenium(IV) complex  
QUIM NOVA 18: (2) 157-159 MAR-APR 1995

181. Novakova O, Kasparkova J, Vrana O, et al.  
Correlation between cytotoxicity and dna-binding of polypyridyl ruthenium complexes  
BIOCHEMISTRY-US 34: (38) 12369-12378 SEP 26 1995

182. Credi A, Balzani V, Campagna S, et al.  
Photophysical properties of a dinuclear rack-type Ru(II) complex and of its components  
CHEM PHYS LETT 243: (1-2) 102-107 SEP 8 1995

183. Dekatz NDL, Fagalde F, Katz NE  
Nitrile hydrolysis induced by oxidation of a dinuclear diruthenium complex  
POLYHEDRON 14: (20-21) 3111-3114 SEP 1995

184. Barigelletti F, Flamigni L, Balzani V, et al.  
Luminescence properties of rigid, rod-like, dichromophoric species - dinuclear ru-os terpyridine-type complexes with 2.4 nm metal-to-metal distance  
NEW J CHEM 19: (7) 793-798 JUL 1995

185. Rezvani AR, Evans CEB, Crutchley RJ  
Strong metal-metal coupling in a dinuclear (terpyridine)(bipyridine)ruthenium mixed-valence complex incorporating the bridging ligand 1,4-dicyanamudobenzene dianion  
INORG CHEM 34: (18) 4600-4604 AUG 30 1995

186. Szczepura LF, Maricich SM, See RF, et al.  
Synthesis, characterization, and reactivity of an oxoruthenium(iv) complex containing a bis(oxazoline) ligand - crystal-structure of [Ru(s-bpop)(Cl)(trpy)](BF<sub>4</sub>)  
INORG CHEM 34: (16) 4198-4205 AUG 2 1995

187. Seok WK, Kim MY, Yokomori Y, et al.  
Mechanistic studies on the oxidation of triphenylphosphine by [(trpy)(bpy)Ru-IV=O]<sup>2+</sup>: structure of the parent complex [(trpy)(bpy)Ru-II-OH<sub>2</sub>]<sup>2+</sup>  
B KOR CHEM SOC 16: (7) 619-624 JUL 20 1995

188. Constable EC, Thompson AMW, Cherryman J, et al.  
2,2'/6',4"-terpyridine - a cyclometalating analog of 2,2'/6:2"-terpyridine for metallosupramolecular chemistry  
INORG CHIM ACTA 235: (1-2) 165-171 JUL 1995

189. Coe BJ, Thompson DW, Culbertson CT, et al.  
Synthesis and photophysical properties of mono(2,2',2"-terpyridine) complexes of ruthenium(ii)  
inorg chem 34: (13) 3385-3395 jun 21 1995

190. Holbrey JD, Tiddy GJT, Bruce DW  
Amphiphilic terpyridine complexes of ruthenium and rhodium displaying lyotropic mesomorphism  
J CHEM SOC DALTON (11) 1769-1774 JUN 7 1995

191. Maestri M, Armaroli N, Balzani V, ET AL.  
Complexes of the ruthenium(ii)-2,2'/6',2"-terpyridine family - effect of electron-accepting and electron-donating substituents on the photophysical and electrochemical properties  
INORG CHEM 34: (10) 2759-2767 MAY 10 1995

192. Fagalde F, Katz NE  
Distance dependence of intramolecular electron-transfer parameters in mixed-valence asymmetric complexes of ruthenium  
POLYHEDRON 14: (9) 1213-1220 MAY 1995

193. Constable EC, Thompson AMWC  
Strategies for the assembly of homo-nuclear and hetero-nuclear metallosupramolecules containing 2,2'/6',2"-terpyridine metal-binding domains  
J CHEM SOC DALTON (10) 1615-1627 MAY 21 1995

194. Gerli A, Reedijk J, Lakin MT, et al.

- Redox properties and electrocatalytic activity of the oxo aqua system  $[\text{Ru}(\text{terpy})(\text{bpz})(\text{O})]^{2+}/[\text{Ru}(\text{Terpy})(\text{bpz})(\text{H}_2\text{O})]^{2+}$  - X-RAY crystal-structure of  $[\text{Ru}(\text{terpy})(\text{bpz})\text{Cl}]\text{PF}_6$ -center-dot-mecn (terpy=2,2',2''-terpyridine bpz=2,2'-bipyrazine)  
INORG CHEM 34: (7) 1836-1843 MAR 29 1995
195. Vanvliet PM, Toekimin SMS, Haasnoot JG, et al. mer- $[\text{Ru}(\text{terpy})\text{Cl}_3]$  (terpy=2,2',6',2''-terpyridine) shows biological activity, forms interstrand cross-links in dna and binds 2 guanine derivatives in a trans configuration  
INORG CHIM ACTA 231: (1-2) 57-64 MAR 15 1995
196. Whittle B, Everest NS, Howard C, et al. Synthesis and electrochemical and spectroscopic properties of a series of binuclear and trinuclear ruthenium and palladium complexes based on a new bridging ligand containing terpyridyl and catechol binding-sites  
INORG CHEM 34: (8) 2025-2032 APR 12 1995
197. Bardwell DA, Jeffery JC, Schatz E, et al. Conventional and cyclometalated complexes of ruthenium(II) with ambidentate terdentate ligands displaying n-3 or n2c binding modes  
J CHEM SOC DALTON (5) 825-834 MAR 7 1995
198. Hissler M, Ziessel R. Heteropolynuclear complexes containing multiple redox and chromophoric moieties - sigma-alkynyl-bipyridine or sigma-alkynyl-terpyridine derivatives of platinum(II)  
J CHEM SOC DALTON (5) 893-896 MAR 7 1995
199. Cheng CC, Goll JG, Neyhart GA, et al. Relative rates and potentials of competing redox processes during DNA cleavage - oxidation mechanisms and sequence-specific catalysis of the self-inactivation of oxometal oxidants by dna  
J AM CHEM SOC 117: (11) 2970-2980 MAR 22 1995
200. Rasmussen SC, ronco SE, Mlsna DA, et al. Ground-state and excited-state properties of ruthenium(II) complexes containing tridentate azine ligands,  $\text{Ru}(\text{tpy})(\text{bpy})\text{I}^{2+}$ , where I is a polymerizable acetylene  
INORG CHEM 34: (4) 821-829 FEB 15 1995
201. Neyhart GA, Cheng CC, Thorp HH. Kinetics and mechanism of the oxidation of sugars and nucleotides by oxoruthenium(IV) - model studies for predicting cleavage patterns in polymeric dna and rna  
J AM CHEM SOC 117: (5) 1463-1471 FEB 8 1995
202. Esmadi FT, Alhamid AJ. reaction of sulfur-dioxide with chlorocarbonyls of ruthenium, rhodium and iridium  
TRANSIT METAL CHEM 19: (6) 571-574 DEC 1994
203. Romero FM, Ziessel R. Preparation of novel mixed tritopic oligopyridine ligands built with chelating spacers and using palladium(0) catalyzed coupling reactions  
TETRAHEDRON LETT 35: (49) 9203-9206 DEC 5 1994
204. Ward MD. A Binuclear Ruthenium(II) Complex Of 2,2'/3',2''/6'',2'''-Quater-Pyridine Containing Ru5cl And Cyclometalated Ru5c Fragments Linked By A Bridging (N,C-Donor) Pyridyl Residue  
J CHEM SOC DALTON (21) 3095-3098 NOV 7 1994
205. Yu WY, Cheng WC, Che CM, et al. Synthesis, Redox Properties And Reactivities Of Ruthenium(II) Complexes Of 1,1'-Biisoquinoline (Biqn) And X-Ray Crystal-Structure Of  $[\text{Ru}(\text{Terpy})(\text{Biqn})(\text{Cl})]\text{ClO}_4$  (Terpy=2,2',6',2''-Terpyridine)  
POLYHEDRON 13: (21) 2963-2969 NOV 1994
206. Spek AL, Gerli A, Reedijk J. (2,2'-Biquinoline-Kappa-2n,N')Chloro-(2,2',6'2''-Terpyridine-Kappa-3n,N',N'')-Ruthenium(II) Hexafluorophosphate,  $[\text{RuCl}(\text{C}_{18}\text{H}_{12}\text{N}_2)(\text{C}_{15}\text{H}_{11}\text{N}_3)]\text{PF}_6$   
ACTA CRYSTALLOGR C 50: 394-397 Part 3 MAR 15 1994
207. Constable EC, Thompson AMWC. Novel Didentate 2,2'-6',2''-Terpyridine Complexes Of Ruthenium(II)  
INORG CHIM ACTA 223: (1-2) 177-179 AUG 1994
208. Barigelletti F, Flamigni L, Balzani V, et al. Rigid Rod-Like Dinuclear Ru(II) Os(II) Terpyridine-Type Complexes - Electrochemical-Behavior, Absorption-Spectra, Luminescence Properties, And Electronic-Energy Transfer Through Phenylene Bridges  
J AM CHEM SOC 116: (17) 7692-7699 AUG 24 1994
209. Vogler LM, Franco C, Jones SW, et al. Ruthenium Chromophores Containing Terpyridine And A Series Of Polyazine Bridging Ligands  
INORG CHIM ACTA 221: (1-2) 55-59 JUN 15 1994
210. Nagao H, Mizukawa T, Tanaka K. Carbon-carbon bond formation in the electrochemical reduction of carbon-dioxide catalyzed by a ruthenium complex  
INORG CHEM 33: (15) 3415-3420 JUL 20 1994
211. Beley M, Chodorowski S, Collin JP, et al. Luminescent dinuclear complexes containing ruthenium(ii)-terpyridine-type and osmium(II)-terpyridine-type chromophores bridged by a rigid bis-cyclometalating ligand  
INORG CHEM 33: (12) 2543-2547 JUN 8 1994
212. Barigelletti F, Flamigni L, Balzani V, et al. Intramolecular energy-transfer through phenyl bridges in rod-like dinuclear ru(II)/os(II) terpyridine-type complexes  
COORDIN CHEM REV 132: 209-214 MAY 1994
213. Smith SR, Neyhart GA, Kalsbeck WA, et al. electronic-properties of aquapolyterpyridyl ruthenium complexes bound to DNA  
NEW J CHEM 18: (3) 397-406 MAR 1994
214. Constable EC, Edwards AJ, Martinezmanez R, et al. Complexes Containing Ferrocenyl Groups As Redox Spectators - Synthesis, Molecular-Structure And Coordination Behavior Of 4'-Ferrocenyl-2,2',6',2''-Terpyridine  
J CHEM SOC DALTON (5) 645-650 MAR 7 1994
215. Bhattacharya S. Synthesis, Characterization And Reactivity Of A Ruthenium-Quinone Complex  
POLYHEDRON 13: (3) 451-456 FEB 1994
216. Ishitani O, Inoue N, Koike K, et al. A Novel Type Of Hydride-Transfer Photocatalysis By Ru-II-Pyridine Complexes - Regiocontrolled Reduction Of An NAD(P) Model-Compound By Triethylamine  
J CHEM SOC CHEM COMM (4) 367-368 FEB 21 1994
217. Farlow B, Nile TA, Walsh JL, et al.

Synthesis, X-Ray Structural Determination And Coordination Chemistry Of 4'-Ferrocenyl-2,2'/6',2"-Terpyridine  
POLYHEDRON 12: (23) 2891-2894 DEC 1993

218. Doveloglou A, Meyer TJ  
Mechanism Of Cis-Directed 4-Electron Oxidation By A Trans-Dioxo Complex Of Ruthenium(VI)  
J AM CHEM SOC 116: (1) 215-223 JAN 12 1994
219. Bessel CA, Margarucci JA, Acquaye JH, et al.  
Steric Ligand Effects Of 6 Bidentate Bipyridyl Ligands  
INORG CHEM 32: (25) 5779-5784 DEC 8 1993
220. Beley M, Collin JP, Sauvage JP  
Highly Coupled Mixed-Valence Dinuclear Ruthenium And Osmium Complexes With A Bis-Cyclometalating Terpyridine Analog As Bridging Ligand  
INORG CHEM 32: (21) 4539-4543 OCT 13 1993
221. Constable EC, Thompson AMWC, Greulich S  
Novel Synthesis Of A Doubly Cyclometalated Diruthenium Complex With Strongly Coupled Metal Centers  
J CHEM SOC CHEM COMM (18) 1444-1446 SEP 21 1993
222. Umeda K, Nakamura A, Toda F  
Catalytic Mechanism And Activity Of Bis(2,2' 6',2"-Terpyridine) Rhodium(III) For The Reduction Of NAD<sup>+</sup> Into NADH In A Photosensitized Reaction System  
B CHEM SOC JPN 66: (8) 2260-2267 AUG 1993
223. Xiao XM, Haga MA, Matsumurainoue T, et al.  
Synthesis And Proton Transfer-Linked Redox Tuning Of Ruthenium(II) Complexes With Tridentate 2,6-Bis(Benzimidazol-2-Yl)Pyridine Ligands  
J CHEM SOC DALTON (16) 2477-2484 AUG 21 1993
224. Nagao H, Mizukawa T, Tanaka K  
Carbon-Carbon Bond Formation In Multielectron Reduction Of Carbon-Dioxide Catalyzed By [Ru(Bpy)(Trpy)(Co)]<sup>2+</sup> (Bpy = 2,2'-Bipyridine Trpy = 2,2'/6',2"-Terpyridine)  
CHEM LETT (6) 955-958 JUN 1993
225. Bessel CA, See RF, Jameson DL, et al.  
Synthesis And Characterization Of Ruthenium Complexes Which Utilize A New Family Of Tridentate Ligands Based Upon 2,6-Bis(Pyrazol-1-Yl)Pyridine  
J CHEM SOC DALTON (10) 1563-1576 MAY 21 1993
226. Neyhart GA, Grover N, Smith SR, et al.  
Binding And Kinetics Studies Of Oxidation Of DNA By Oxoruthenium(IV)  
J AM CHEM SOC 115: (11) 4423-4428 JUN 2 1993
227. Altabef AB, Degallo SBR, Folquer ME, et al.  
Dinuclear Complexes Of (2,2'-Bipyridine)(2,2'/6',2"-Terpyridine)-Ruthenium(II) Bonded Through Cyanide To Pentaammineruthenium(II/III) Groups  
TRANSIT METAL CHEM 18: (3) 319-322 JUN 1993
228. Ward MD  
Synthesis And Coordination Chemistry Of 2,2'/4',2''/6'',2'''-Quaterpyridine, An Asymmetric Bridging Ligand With Inequivalent Bipyridyl Binding-Sites  
J CHEM SOC DALTON (8) 1321-1325 APR 7 1993
229. Islam MS, Uddin MM  
Mixed-Ligand Complexes Of Chromium(III) And Ruthenium(III) Ions With Imides And Amines  
SYN REACT INORG MET 22: (9) 1303-1315 1992

230. Collin JP, Laine P, Launay JP, et al.  
Long-Range Coupling In A Mixed-Valence Diruthenium Complexes Containing Bis-Terpyridine Ligands Of Various Lengths As Bridges  
J CHEM SOC CHEM COMM (5) 434-435 MAR 7 1993
231. Vogler LM, Scott B, Brewer KJ  
Investigation Of The Photochemical, Electrochemical, And Spectroelectrochemical Properties Of An Iridium(III) Ruthenium(II) Mixed-Metal Complex Bridged By 2,3,5,6-Tetrakis(2-Pyridyl)Pyrazine  
INORG CHEM 32: (6) 898-903 MAR 17 1993
232. Fagalde F, Katz NE  
Preparation And Spectroscopic, Electrochemical And Photophysical Properties Of Mononuclear, Dinuclear And Mixed-Valence Species Derived From The Photosensitizing Group (2,2'-Bipyridine)(2,2' - 6',2"-Terpyridine)Ruthenium(II)  
J CHEM SOC DALTON (4) 571-575 FEB 21 1993
233. Gupta N, Grover N, Neyhart GA, et al.  
Synthesis and properties of new dna cleavage agents based on oxoruthenium(IV)  
INORG CHEM 32: (3) 310-316 FEB 3 1993
234. Constable EC, Thompson AMWC  
Multinucleating 2,2'/6',2"-terpyridine ligands as building-blocks for the assembly of coordination polymers and oligomers  
J CHEM SOC DALTON (24) 3467-3475 DEC 21 1992
235. Griffith WP, Jolliffe JM  
Studies on transition-metal nitrido and oxo complexes .14. Carboxylato oxo-osmium(VI) and oxo-ruthenium(VI) complexes and their reactions  
J CHEM SOC DALTON (24) 3483-3488 DEC 21 1992
236. Arana CR, Abruna HD  
Monomeric and oligomeric complexes of ruthenium and osmium with tetra-2-pyridyl-1,4-pyrazine (tppz)  
INORG CHEM 32: (2) 194-203 JAN 20 1993
237. Constable EC, Thompson AMWC, Tocher DA, et al.  
Synthesis, characterization and spectroscopic properties of ruthenium(II)-2,2'-6',2"-terpyridine coordination triades x-ray structures of 4'-(n,n-dimethylamino)-2,2'-6',2"-terpyridine and bis(4'-(N,N-dimethylamino)-2,2'-6',2"-terpyridine . . . )ruthenium(II) hexafluorophosphate acetonitrile solvate  
NEW J CHEM 16: (8-9) 855-867 AUG-SEP 1992
238. Steed JW, Tocher DA  
Mononuclear, binuclear and trinuclear bis(allyl) complexes of ruthenium(IV) containing n-donor ligands  
POLYHEDRON 11: (21) 2729-2737 NOV 1992
239. Dash R, Potvin PG  
short syntheses of rigid acyclic or macrocyclic poly-imine ligands and their use in Ru(II), Fe(III), and alkali-metal complexation  
CAN J CHEM 70: (8) 2249-2255 AUG 1992
240. Constable EC, Thompson AMWC, Armaroli N, et al.  
Ligand substitution patterns control photophysical properties of ruthenium(II)-2,2',6',2"-terpyridine complexes - room-temperature emission from [ru(tpy)<sub>2</sub>]<sup>2+</sup> analogs  
POLYHEDRON 11: (20) 2707-2709 OCT 1992
241. Gupta N, Grover N, Neyhart GA, et al.  
[RuO(DPPZ)(tpy)]<sup>2+</sup> - a dna cleavage agent with high dna affinity  
ANGEW CHEM INT EDIT 31: (8) 1048-1050 AUG 1992

242. Degiovani WF, Deronzier A  
Electrochemical preparation and behavior of poly(pyrrole-  
[Ru(trpy)(bpy)(OH<sub>2</sub>)<sup>2+</sup>] (trpy = 2,2',6',2"-terpyridine) (bpy = 2,2'-  
bipyridine) films - application to the electrocatalytic oxidation of  
alcohols  
J ELECTROANAL CHEM 337: (1-2) 285-298 OCT 10 1992
243. Grover N, Gupta N, Singh P, et al.  
Studies of electrocatalytic dna cleavage by oxoruthenium(IV) - x-  
ray crystal-structure of [Ru(tpy)(tmen)OH<sub>2</sub>](ClO<sub>4</sub>)<sub>2</sub> (tmen =  
N,N,N',N'-tetramethylethylenediamine, tpy = 2,2',2"-terpyridine)  
INORG CHEM 31: (11) 2014-2020 MAY 27 1992
244. Adeyemi SA, Dovletoglou A, Guadalupe AR, et al.  
redox and spectral properties of the 4-electron oxidant trans-  
[Ru(tpy)(O)<sub>2</sub>(H<sub>2</sub>O)](ClO<sub>4</sub>)<sub>2</sub>  
INORG CHEM 31: (8) 1375-1383 APR 15 1992
245. Constable EC, Thompson AMWC  
A new ligand for the self assembly of starburst coordination  
oligomers and polymers  
J CHEM SOC CHEM COMM (8) 617-619 APR 15 1992
246. Brewer KJ, Vogler I.M  
the investigation of the spectroscopy and electrochemistry of a  
tridentate bridged mixed-metal complex of the form  
[(tpy)Ru(tpp)IrCl<sub>3</sub>]<sup>2+</sup> (tpy=2,2',6',2"-terpyridine, tpp=2,3,5,6-  
tetrakis(2'-pyridyl)pyrazine)  
ABSTR PAP AM CHEM S 203: 250-INOR Part 2 APR 5 1992
247. Amouyal E, Mouallembahout M  
Photophysical study of tolylterpyridine complexes - intramolecular  
electron-transfer in an osmium(II)dyad  
J CHEM SOC DALTON (3) 509-513 FEB 1992
248. Hayes MA, Meckel C, Schatz E, et al.  
derivatives of tris(2,2'-bipyridine)ruthenium(II) with pendant  
pyridyl or phenol ligands  
J CHEM SOC DALTON (4) 703-708 FEB 1992
249. Pramanik A, Bag N, Chakravorty A  
Synthesis, characterization and structure of the salicylate salt of  
[Ru(terpy)(pph<sub>3</sub>)<sub>2</sub>]<sup>+</sup> (terpy = 2,2'-6',2"-terpyridine)  
J CHEM SOC DALTON (1) 97-99 JAN 1992
250. Collin JP, Guillerez S, Sauvage JP, et al.  
Photoinduced charge separation in dyads and triads containing a  
ruthenium(II)-bis-terpyridine or osmium(II)-bis-terpyridine  
photosensitizer covalently linked to electron-donor and acceptor  
groups  
COORDIN CHEM REV 111: 291-296 DEC 6 1991
251. Benaltabef A, Degallo SBR, Folquer ME, et al.  
Syntheses and characterization of new mononuclear and dinuclear  
complexes derived from ruthenium polypyridines  
INORG CHIM ACTA 188: (1) 67-70 OCT 1 1991
252. Bessel CA, See RF, Jameson DL, et al.  
Synthesis, characterization and crystal-structure of trans-[2,6-  
bis(3-phenylpyrazol-1-yl-kappa-n<sub>2</sub>)pyridine-kappa-  
n]chlorobis(trimethylphosphine)ruthenium(II) perchlorate -  
evidence for meridional steric crowding  
J CHEM SOC DALTON (11) 2801-2805 NOV 1991
253. Beley M, Collin JP, Sauvage JP, et al.  
Photophysical and photochemical properties of ruthenium and  
osmium complexes with substituted terpyridines  
J CHEM SOC DALTON (11) 3157-3159 NOV 1991
254. Collin JP, Guillerez S, Sauvage JP, et al.  
Photoinduced processes in dyads and triads containing a  
ruthenium(II) bis(terpyridine) photosensitizer covalently linked to  
electron-donor and acceptor groups  
INORG CHEM 30: (22) 4230-4238 OCT 30 1991
255. Amouyal E, Mouallembahout M, Calzaferri G  
evidence for charge localization in the excited-state of a  
bis(terpyridyl)complex of ruthenium (II)  
CR ACAD SCI II 313: (10) 1129-1133 NOV 7 1991
257. Collin JP, Beley M, Sauvage JP, et al.  
a room-temperature luminescent cyclometallated ruthenium(II)  
complex of 6-phenyl-2,2'-bipyridine  
INORG CHIM ACTA 186: (1) 91-93 AUG 1 1991
258. Che CM, Ho C, Lau TC  
Tuning the reactivities of ruthenium-oxo complexes with robust  
ligands - a ruthenium(IV)-oxo complex of 6,6'-dichloro-2,2'-  
bipyridine as an active oxidant for stoichiometric and catalytic  
organic oxidation  
J CHEM SOC DALTON (8) 1901-1907 AUG 1991
259. Liang XQ, Suwanrumpha S, Freas RB  
Fast-atom-bombardment tandem mass-spectrometry of  
(polypyridyl)ruthenium(II) complexes  
INORG CHEM 30: (4) 652-658 FEB 20 1991
260. Hecker CR, Fanwick PE, Mcmillin dr  
Evidence for dissociative photosubstitution reactions of  
[Ru(trpy)(bpy)(NCCH<sub>3</sub>)<sup>2+</sup>] - crystal and molecular-structure of  
[Ru(trpy)(bpy)(py)](PF<sub>6</sub>)<sub>2</sub>·(CH<sub>3</sub>)<sub>2</sub>CO  
INORG CHEM 30: (4) 659-666 FEB 20 1991
261. Greene DL, Mingos DMP  
application of microwave dielectric loss heating effects for the  
rapid and convenient synthesis of ruthenium(II) polypyridine  
complexes  
TRANSIT METAL CHEM 16: (1) 71-72 FEB 1991
262. Hecker CR, Gushurst AKI, Mcmillin DR  
Phenyl substituents and excited-state lifetimes in ruthenium(II)  
terpyridyls  
INORG CHEM 30: (3) 538-541 FEB 6 1991

**Appendix II**  
**“Publications and presentation”**

## Publications and Presentations

### Publications

- Duati M, Fanni S, Vos J G *Inorg. Chem Comm.* 2000, 3, 68
- Rau S, Ruben, M, Buttner T, Temme C, Dautz S, Gorls H, Rudolph M, Walther D, Duati M, O'Connor C, Vos J G, *J. Chem Soc. Dalton Trans.* 2000, 3649
- Rau S, Buttner T, Temme C, Ruben, M, Gorls H, Walther D, Duati M, Fanni S, Vos J G, *Inorg. Chem.* 2000, 39, 1621

### Talk & Poster

- September, 2000 Castiglion della Pescaia, Firenze IT  
**6<sup>th</sup> Scuola di Chimica Inorganica per Dottorandi**
- Price as best Talk
- May, 2000 UCC, Cork IE  
**52<sup>nd</sup> Irish Colloquium of chemistry**
- Price as best Inorganic Talk
- April, 2000 DCU, Dublin, IE  
**Internal Talk**  
talk
- February, 2000 Dublin, IE  
**TMR meeting**  
talk
- July, 1999 Lipari, IT  
**13<sup>th</sup> ISPPCC**  
Poster.
- May, 1999 Upsala, SE  
**Young Researcher TMR meeting**  
Talk.





ELSEVIER

# A new luminescent Ru(terpy) complex incorporating a 1,2,4-triazole based $\sigma$ -donor ligand

Marco Duati, Stefano Fanni, Johannes G. Vos\*

*Inorganic Chemistry Research Centre, School of Chemical Sciences, Dublin City University, Dublin 9, Ireland*

Received 22 November 1999

## Abstract

The mononuclear compound [Ru(terpy)L], where H<sub>2</sub>L is 2,6-bis(1,2,4-triazol-3-yl)pyridine, shows an emission lifetime of 65 ns, about 300 times longer than that observed for the parent [Ru(terpy)<sub>3</sub>]<sup>2+</sup> complex. ©2000 Published by Elsevier Science S.A. All rights reserved.

**Keywords:** Luminescence; Ruthenium complexes; Terpyridine complexes; Triazole complexes

## 1. Introduction

Ruthenium polypyridine complexes are widely used as photosensitisers in covalently linked multicomponent systems. Their photophysical properties make them ideal candidates as building blocks for the design of supramolecular species performing complex light induced functions [1].

The polypyridyl ligands employed are mainly derivatives or analogues of the *bidentate* 2,2'-bipyridine or derivatives or analogues of the *tridentate* 2,6,2''-terpyridine (terpy) [1–3]. Tridentate terpyridine-type ligands are ideal from a geometrical point of view as they can form achiral complexes for which the C<sub>2v</sub> symmetry is not affected by substitution in the 4 position of the terpy ligands. Furthermore, the 'rod-like' geometry of these complexes offers the best spatial arrangement for the synthesis of triads or molecular wires. However, the very short excited-state lifetime and weak luminescence intensity of [Ru(terpy)<sub>3</sub>]<sup>2+</sup> at room temperature, represent a severe limitation to the application of this complex as photosensitiser. Improvement of the photophysical properties of terpy-based Ru(II) complexes is therefore currently the object of intensive studies [4–8]. As a contribution to these studies, we report the new [RuL(terpy)] mononuclear complex, where H<sub>2</sub>L is 2,6-bis(1,2,4-triazol-3-yl)pyridine, which exhibits a remarkable 300-fold increase of the emission lifetime when compared with the parent compound [Ru(terpy)<sub>3</sub>]<sup>2+</sup>.

## 2. Experimental

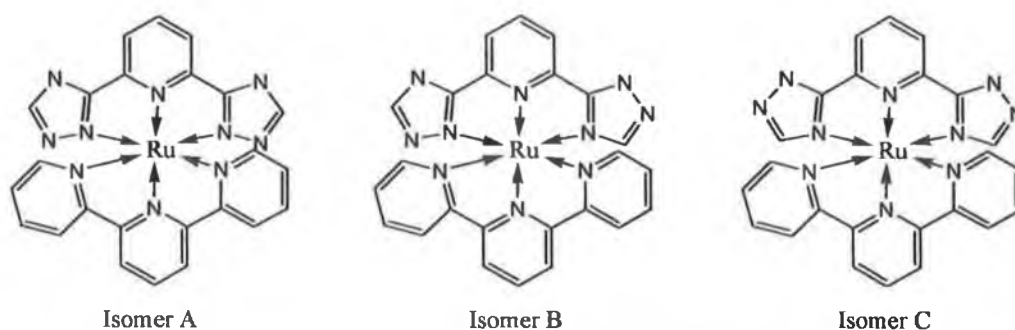
2,6-Bis(1,2,4-triazol-3-yl)pyridine was synthesised, in high yield, following the literature pathway [9,10] for similar compounds.

The Ru(terpy) complex was obtained by heating [Ru(terpy)]Cl<sub>3</sub> and a stoichiometric amount of the ligand H<sub>2</sub>L in water containing a slight molar excess of NaOH and a few drops of *N*-ethylmorpholine. The reaction mixture was refluxed for 2 h; the dark green solution was concentrated, acidified to pH 3 with HCl and an excess of NH<sub>4</sub>PF<sub>6</sub> was added. Purification by column chromatography on alumina (acetonitrile/methanol 50:50) gave a 30% yield.

In agreement with the literature [11,12], three different isomers were found (Scheme 1). Isomers A (10%) and B (60%) were eluted from a neutral alumina column using acetonitrile followed by the elution of the isomer C (30%) using methanol. The identification of the three isomers is based on the chemical shift of the triazole proton in the NMR.

Since isomer C is most easily purified all further studies were carried out using this species, both A and B yield however very similar results. Elemental analysis suggests that a mixture of monoprotonated/deprotonated (80:20) isomers is formed after recrystallisation of C from acetone/water. [Ru(terpy)(HL)] [PF<sub>6</sub>]:[Ru(terpy)(L)] (80:20): *Anal. Calc.*: C, 43.52; H, 2.56; N, 21.15. *Found*: C, 43.7; H, 2.60; N, 21.03%. <sup>1</sup>H NMR:  $\delta_{11}$  (CD<sub>3</sub>OD, NaOD) 8.6 (2H, q), 8.4 (2H, q), 8.2 (H, m), 8.1 (3H, m), 7.73 (2H, t), 7.6 (H, d), 7.25 (2H, t of d), 7.06 (2H, m), 6.98 (H, d). To ensure full

\* Corresponding author. Tel. +353 1 704 5307; fax: +353 1 704 5503, e-mail: han.vos@dcu.ie

Scheme 1. Possible coordination isomers for  $[\text{Ru}(\text{terpy})\text{L}]$ .

deprotonation of the complex all measurements reported in this communication were carried out in basic media.

### 3. Results and discussion

The UV–Vis absorption spectrum of the complex  $[\text{Ru}(\text{terpy})\text{L}]$ , isomer C, in basic ethanol shows an intense metal-to-ligand-charge-transfer (MLCT) band at 480 nm (Fig. 1(a)), with a molar extinction coefficient of  $7900 \text{ M}^{-1} \text{ cm}^{-1}$ . The bands at 275, 309 and 380 are assigned to the intra ligand  $\pi-\pi^*$  transition of the ligands. The small but distinct shoulders at 626, 579 nm have not yet been assigned.

When excited within the MLCT absorption band at 298 K, in a basic ethanol solution, the complex exhibits a strong emission with a single band centred at 700 nm (Fig. 1(b)) and a lifetime of  $65 (\pm 3) \text{ ns}$ . Protonation of the triazole rings results in a total quenching of the emission. Based on results reported in the literature for other ruthenium polypyridyl complexes containing 1,2,4-triazole containing ligands this emission is more than likely terpy based and the bistriazolopyridine ligand acts as a spectator ligand [13]. The emission lifetime measured for this compound represents an increase by two orders of magnitude with respect to  $[\text{Ru}(\text{terpy})_2]^{2+}$  (Table 1). It is therefore clear that the use of the triazolato

Table 1  
Electronic properties<sup>a</sup>

	Absorption	Emission	
	$\lambda_{\text{max}}/\text{nm}$ ( $\epsilon \times 10^{-4}/\text{M}^{-1} \text{ cm}^{-1}$ )	$\lambda_{\text{max}}/\text{nm}$	$\tau/\text{ns}$
$[\text{Ru}(\text{terpy})_2]^{2+}$ <sup>b,c</sup>	474 (10.4)	629	0.25
$[\text{Ru}(\text{terpy})(\text{L})]$ <sup>d</sup>	480 (7.9)	701	65

<sup>a</sup> Room temperature, de-aerated solution.

<sup>b</sup> Ref. [8].

<sup>c</sup> Acetonitrile.

<sup>d</sup> Ethanol.

ligand dramatically extends the lifetime of the  $^3\text{MLCT}$  excited state of the  $\text{Ru}(\text{II})(\text{terpy})$  complex. This is likely to originate from the raising of the  $^3\text{MC}$  states following the replacement of the weak field terpyridine ligand by a strong  $\sigma$ -donor ligand. The absorption and emission spectra show also interesting solvatochromic properties (see Table 2), similar to these observed for  $[\text{Ru}(\text{terpy})\text{CN}_3]$  [8]. This solvent dependence may be used to further manipulate the photophysical properties of the compound.

### 4. Conclusions

This communication describes an alternative strategy to extend the lifetime of the triplet state in terpy-type ruthenium

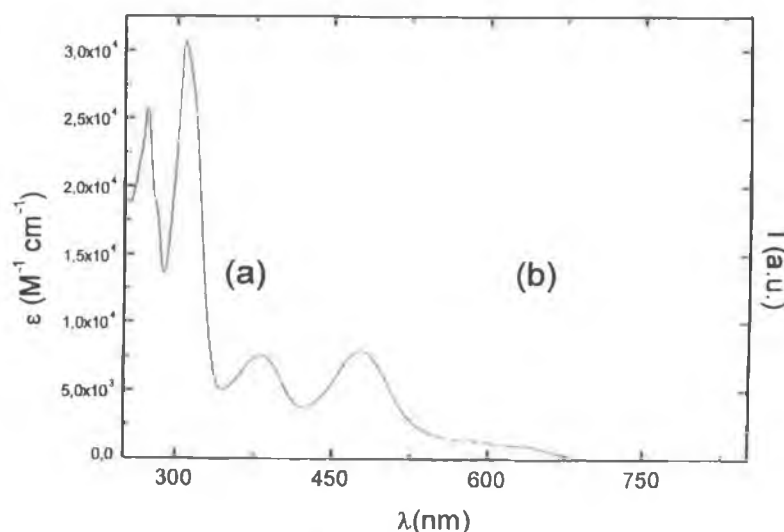


Fig. 1. Absorption (a) and emission (b) spectra of  $[\text{Ru}(\text{terpy})(\text{L})]$  in basic ethanol solution: excitation was at 474 nm.

Table 2  
Absorption and emission properties of [Ru(terpy)L] in different solvents

	Solvent (acceptor no.)						
	H <sub>2</sub> O (58.4) <sup>a</sup>	MeOH (41.3)	EtOH (37.1)	CH <sub>3</sub> CN (19.3)	DMSO (19.3)	DMF (16.0)	(CH <sub>3</sub> ) <sub>2</sub> CO (12.5)
$\lambda_{\text{max}}^{\text{abs}}/\text{nm}$ (298 K) <sup>b</sup>	472	473.5	480.5	488	494	495	493
$\lambda_{\text{max}}^{\text{em}}/\text{nm}$ (298 K)	692	693.7	700.9	740	741.8	752.3	734.8
$\lambda_{\text{max}}^{\text{em}}/\text{nm}$ (77 K)	663 <sup>c,d</sup>		666 <sup>d,e</sup>			697 <sup>c,d</sup>	

<sup>a</sup> Acceptor numbers were taken from Ref. [12].

<sup>b</sup> Low-energy band.

<sup>c</sup> 9 M LiCl glass.

<sup>d</sup> EtOH:MeOH (4:1) glass.

<sup>e</sup> DMF:CH<sub>2</sub>CL<sub>2</sub> glass.

<sup>f</sup> High energy band.

60 63 5 76 80

complexes. Usually, delocalisation of the emitting state is used to increase the lifetime of terpy based excited states [4–7]. In our approach we have raised the deactivating <sup>3</sup>MC state instead. To the best of our knowledge there is only one other compound, namely [Ru(terpy)CN<sub>3</sub>], where a similar approach has been taken [8]. With the ligand introduced in this contribution an increased stability is expected for the terpy complex, since monodentate cyano ligands tend to be more labile. In addition, the well-defined synthetic pathways that exist for pyridyltriazole compounds [10,11] enable many modifications for these ligands. This should facilitate the synthesis of dinuclear complexes with bridging triazole ligands. Finally, the combination of this approach with thiophene [7] or alkyne [6] containing terpy ligands is expected to yield multinuclear systems with even longer emission lifetimes, which could find applications as photosensitisers in rod-like molecular assemblies.

### Acknowledgements

The authors wish to thank the EC TMR Programme (Contracts CT96-0031 and CT96-0076) for financial support.

### References

- [1] V. Balzani, F. Scandola, *Supramolecular Photochemistry*, Ellis Horwood, Chichester, UK, 1991.
- [2] V. Balzani, A. Juris, M. Venturi, S. Campagna, S. Serroni, *Chem. Rev.* 96 (1996) 759.
- [3] A. Harriman, R. Ziessel, *Coord. Chem. Rev.* 171 (1998) 331.
- [4] F. Barigelletti, L. Flamigni, V. Balzani, J.-P. Colin, J.-P. Savage, A. Sour, E.C. Constable, A.M.W. Cargill Thompson, *J. Am. Chem. Soc.* 116 (1994) 7692.
- [5] M. Maestri, N. Armaroli, V. Balzani, E.C. Constable, A.M.W. Cargill Thompson, *Inorg. Chem.* 34 (1995) 2759.
- [6] V. Grosshenny, A. Harriman, R. Ziessel, *Angew. Chem., Int. Ed. Engl.* 33 (1995) 1100.
- [7] E.C. Constable, C.E. Housecroft, E.R. Schofield, S. Encinas, N. Armaroli, F. Barigelletti, L. Flamigni, E. Figgemeier, J.G. Vos, *Chem. Commun.* (1999), 869.
- [8] M.T. Indelli, C.A. Bignozzi, F. Scandola, J.-P. Colin, *Inorg. Chem.* 46 (1998) 6084.
- [9] R. Hage, J.G. Haasnoot, J. Reedijk, R. Wang, J.G. Vos, *Inorg. Chem.* 30 (1991) 3263.
- [10] K.H. Suyiyarto, D.C. Craig, A.D. Rae, H.A. Goodwin, *Aust. J. Chem.* 46 (1993) 1269.
- [11] H.P. Hughes, J.G. Vos, *Inorg. Chem.* 34 (1995) 4001.
- [12] M.G.B. Drew, M.J. Hudson, P.B. Iverson, C. Madic, M.L. Rusel, *J. Chem. Soc., Dalton Trans.* (1999) 2433.
- [13] H.P. Hughes, D. Martin, S. Bell, J.J. McGarvey, J.G. Vos, *Inorg. Chem.* 32 (1993) 4402.

## A Bibenzimidazole-Containing Ruthenium(II) Complex Acting as a Cation-Driven Molecular Switch

Sven Rau, Torsten Büttner, Christian Temme,  
Mario Ruben, Helmar Görls, and Dirk Walther\*

Institut für Anorganische und Analytische Chemie,  
Friedrich-Schiller-Universität, 07743 Jena, Germany

Marco Duati, Stefano Fanni, and Johannes G. Vos\*

Inorganic Chemistry Research Centre, School of Chemical  
Sciences, Dublin City University, Dublin 9, Ireland

Received October 19, 1999

### Introduction

Multinuclear ruthenium polypyridyl complexes are currently the subject of extensive investigations, their photophysical properties making them ideal components for photochemically and electrochemically driven molecular devices.<sup>1</sup> Among these compounds, mononuclear ruthenium complexes containing biimidazole or bibenzimidazole (bibzimH<sub>2</sub>) type ligands<sup>2</sup> have been shown to be excellent building blocks for the synthesis of heteronuclear complexes of the type {(bpy)<sub>n</sub>Ru[(bibzim)M-(bpy)<sub>2</sub>]<sub>3-n</sub>}<sup>m+</sup> (M = Ru, Os, Ni, Co).<sup>3–5</sup> This behavior makes these complexes prime candidates for application as luminophores for the detection of metal ions. The luminophore approach to the development of sensors has been widely used.<sup>6</sup> Ruthenium polypyridyl complexes have been proposed as luminescent sensors for the detection of anions.<sup>7</sup>

In this contribution, we wish to report the interaction of the nonluminescent compound [Ru(tbbpy)<sub>2</sub>(bibzim)], **1** (see Figure 1), with a series of metal ions in solution. The results obtained show that the emission of **1** is switched on by the presence of metal ions such as Zn(II), Mg(II), and Cu(I). It is also shown that both the emission intensity and the emission wavelength are dependent on the concentration and the nature of the metal ion. Comparable results regarding the tuning of the emission maxima were recently obtained for substituted phenanthrolines.<sup>8</sup> To the best of our knowledge, there is only one other example where the emission intensity of a ruthenium complex is increased by binding of another metal.<sup>9</sup> The X-ray structure of

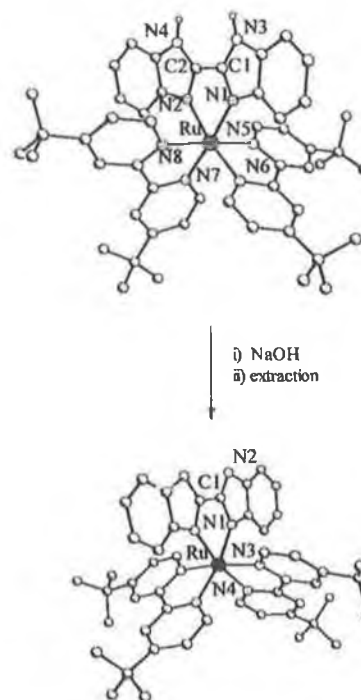


Figure 1. Synthesis of **1** from **2**. Anions, solvent molecules, and protons, except for the N3 and the N4 hydrogen in **2**, omitted from the X-ray structures for clarity.

**1** and of its protonated analogue [Ru(tbbpy)<sub>2</sub>(bibzimH<sub>2</sub>)]<sup>2+</sup>, **2**, are also reported.

### Experimental Section

**Methods and Materials.** All synthetic work was performed using Schlenk techniques. Emission and absorption spectra were recorded using septum-equipped luminescent cells (Hellma). THF was dried and distilled over sodium/benzophenone. CH<sub>3</sub>CN was dried over CaH<sub>2</sub> and distilled, and all other solvents were distilled prior to use. NMR spectra were recorded using Bruker 400 and 200 MHz spectrometers. UV–vis spectra were obtained using a Varian Cary 1 UV–vis or a Shimadzu UV 3100 UV–vis–NIR spectrometer. Emission spectra were not corrected and were recorded using a Perkin-Elmer LS50B spectrometer equipped with a Hamamatsu R928 red-sensitive detector. Luminescent lifetimes were measured by employing a Spectra Physics Nd:YAG frequency-tripled, Q-switched laser as the excitation source, coupled in a right-angled configuration with an Oriol iCCD. Laser power was measured as 30 mJ/20 ns pulse. IR spectra were recorded using a Perkin-Elmer 2000 FT-IR spectrometer. Elemental analyses were performed by the Microanalytical Laboratory of the University Jena. RuCl<sub>3</sub>·3H<sub>2</sub>O, 4-*tert*-butylpyridine, MgCl<sub>2</sub>, ZnCl<sub>2</sub>, ZnEt<sub>2</sub>, 1,2-diaminobenzene (Aldrich), oxamide (Fluka), Cu(CH<sub>3</sub>CN)<sub>4</sub>BF<sub>4</sub>, and Pd(CH<sub>3</sub>CN)<sub>2</sub>Cl<sub>2</sub> (ABCR) were used as purchased without further purification. Ru(tbbpy)<sub>2</sub>Cl<sub>2</sub>,<sup>10</sup> tbbpy,<sup>10</sup> and bibzimH<sub>2</sub><sup>11</sup> were prepared by literature methods.

**Synthesis of [Ru(tbbpy)<sub>2</sub>(bibzimH<sub>2</sub>)]Cl<sub>2</sub> (**2**).** The synthesis was performed using standard procedures<sup>2</sup> with 265 mg (1.13 mmol) of bibzimH<sub>2</sub> and 510 mg (0.71 mmol) of Ru(tbbpy)<sub>2</sub>Cl<sub>2</sub>. Crystals of **2** suitable for X-ray studies were grown from an acetonitrile solution of [Ru(tbbpy)<sub>2</sub>(bibzimH<sub>2</sub>)]Cl<sub>2</sub>. To obtain the complex as its perchlorate, the product was redissolved in water and precipitated by the addition of aqueous LiClO<sub>4</sub>. Note! Perchlorates are potentially explosive. Yield: 740 mg (0.64 mmol). Anal. Calcd. for [Ru(tbbpy)<sub>2</sub>(bibzimH<sub>2</sub>)](ClO<sub>4</sub>)<sub>2</sub>·2H<sub>2</sub>O·Me<sub>2</sub>CO: C, 54.60; H, 5.84; N, 9.62. Found: C, 54.70;

(10) Hadda, T. B.; Le Bozec, H. *Polyhedron* 1988, 7, 575.

(11) Lane, E. S. *J. Chem. Soc.* 1955, 1079.

(1) (a) Balzani, V.; Scandola, F. *Supramolecular Photochemistry*; Ellis Horwood: Chichester, U.K., 1991. (b) Sun, L.; Berglund, H.; Davydov, R.; Norrby, T.; Hammarström, L.; Korall, P.; Börje, A.; Philouze, C.; Berg, K.; Tran, A.; Andersson, M.; Stenhagen, G.; Mårtensson, J.; Almgren, M.; Styring, S.; Åkermark, A. *J. Am. Chem. Soc.* 1997, 119, 6996.

(2) (a) Haga, M. *Inorg. Chim. Acta* 1980, 45, L183. (b) Haga, M. *Inorg. Chim. Acta* 1983, 75, 29.

(3) Haga, M.; Matsumura-Inoue, T.; Yamabe, S. *Inorg. Chem.* 1987, 26, 4148.

(4) Rillema, D. P.; Sahai, R.; Matthews, P.; Edwards, A. K.; Shaver, R. J.; Morgan, L. *Inorg. Chem.* 1990, 29, 167.

(5) Haga, M.; Ali, Md. M.; Arakawa, R. *Angew. Chem., Int. Ed. Engl.* 1996, 35, 76.

(6) (a) de Silva, A. P.; Gunaratne, H. Q. N.; Gunnlaugsson, T.; Huxley, A. J. M.; McCoy, C. P.; Rademacher, J. T.; Rice, T. E. *Chem. Rev.* 1997, 97, 1515. (b) Voyer, N.; Maltais, F. *Adv. Mater.* 1993, 5, 568.

(7) Becr, P. D.; Cadman, J. *New J. Chem.* 1999, 23, 347.

(8) Joshi, H. S.; Jamshidi, R.; Tor, Y. *Angew. Chem., Int. Ed. Engl.* 1999, 38, 2721.

(9) Barigelletti, F.; Flamingi, L.; Calogero, G.; Hammarström, L.; Sauvage, J.-P.; Collin, J.-P. *J. Chem. Soc., Chem. Commun.* 1998, 2333.

**Table 1.** ESI-MS and Photophysical Data for Investigated Complexes Based on **1**

	$\lambda_{\text{max}}$ , nm	$\lambda_{\text{em}}$ , nm	$\tau$ , ns	ESI-MS signal ( $m/z$ )
[Ru(tbbpy) <sub>2</sub> (bibzim)] <sup>0</sup>	580			[Ru(tbbpy) <sub>2</sub> (bibzimH)] <sup>+</sup> (871)
[Ru(tbbpy) <sub>2</sub> (bibzimH <sub>2</sub> )]Cl <sub>2</sub>	480	645	130	[Ru(tbbpy) <sub>2</sub> (bibzimH)] <sup>+</sup> (871)
[{Ru(tbbpy) <sub>2</sub> } <sub>2</sub> (bibzim)](PF <sub>6</sub> ) <sub>2</sub>	510	700	70	[{Ru(tbbpy) <sub>2</sub> } <sub>2</sub> (bibzim)](PF <sub>6</sub> ) <sup>+</sup> (1654)
[Ru(tbbpy) <sub>2</sub> (bibzim)ZnCl <sub>2</sub> ]	500	675	80	[Ru(tbbpy) <sub>2</sub> (bibzim)ZnCl] <sup>+</sup> (971)
[Ru(tbbpy) <sub>2</sub> (bibzim)ZnEt <sub>2</sub> ]	510	675	<i>a</i>	[Ru(tbbpy) <sub>2</sub> (bibzim)ZnEt] <sup>+</sup> (963)
[{Ru(tbbpy) <sub>2</sub> (bibzim)} <sub>2</sub> ZnCl <sub>2</sub> ]	530	710	<i>a</i>	[{Ru(tbbpy) <sub>2</sub> (bibzim)} <sub>2</sub> ZnCl] <sup>+</sup> (1841)
[Ru(tbbpy) <sub>2</sub> (bibzim)CuBF <sub>4</sub> ]	500	685	60	<i>a</i>
[Ru(tbbpy) <sub>2</sub> (bibzim)MgCl <sub>2</sub> ]	500	675	40	
[Ru(tbbpy) <sub>2</sub> (bibzim)NiBr <sub>2</sub> ]	505			[Ru(tbbpy) <sub>2</sub> (bibzim)NiBr] <sup>+</sup> (1009)
[Ru(tbbpy) <sub>2</sub> (bibzim)CoBr <sub>2</sub> ]	492			[Ru(tbbpy) <sub>2</sub> (bibzim)CoBr] <sup>+</sup> (1010)
[Ru(tbbpy) <sub>2</sub> (bibzim)PdCl <sub>2</sub> ]	462			[Ru(tbbpy) <sub>2</sub> (bibzim)PdCl] <sup>+</sup> (1012)

<sup>a</sup> Not measured.

H, 5.90; N, 9.88. <sup>1</sup>H NMR for [Ru(tbbpy)<sub>2</sub>(bibzimH<sub>2</sub>)]Cl<sub>2</sub> (CH<sub>3</sub>CN-*d*<sub>3</sub>;  $\delta$  ppm): 8.55 (1H, s), 8.45 (1H, s), 7.78 (3H, m), 7.47 (1H, d), 7.31 (2H, m), 7.01 (1H, t), 5.64 (1H, d), 1.46 (9H, s); 1.34 (9H, s). ES-MS ( $m/z$ ): 871 (M - H<sup>+</sup> - 2Cl).

**Synthesis of [Ru(tbbpy)<sub>2</sub>(bibzim)] (1).** A 500 mg sample of [Ru(tbbpy)<sub>2</sub>(bibzimH<sub>2</sub>)]Cl<sub>2</sub>, **2**, was dissolved in ca. 200 mL of methanol. A 200 mL portion of a 5 M aqueous NaOH solution was added, and the violet mixture was stirred at room temperature for 15 min. The solution was then extracted three times with CH<sub>2</sub>Cl<sub>2</sub>, and the organic layers were combined. The solvent was immediately removed by vacuum distillation at room temperature. A small sample was crystallized from dry CH<sub>3</sub>CN to yield X-ray-suitable crystals. ES-MS ( $m/z$ ): 871 (M + H<sup>+</sup>). FT-IR spectra (Nujol emulsion and KBr disk) showed no NH or OH signals. <sup>1</sup>H NMR (THF-*d*<sub>6</sub>;  $\delta$ , ppm): 8.56 (1H, s), 8.45 (1H, s), 7.85 (2H, m), 7.40 (2H, m), 7.26 (1H, d), 6.66 (1H, t), 6.37 (1H, t), 5.38 (1H, d), 1.45 (9H, s), 1.30 (9H, s).

**Investigation of the Luminescence Properties of Mixed-Metal Solutions Containing 1.** A 9 mL portion of a concentrated solution of the corresponding metal compound in THF was added to 1 mL of a 10<sup>-4</sup> M THF solution of **1**. The resulting mixture was stirred for 30 min and then was analyzed by UV-vis and emission spectrometry. To investigate the concentration dependence of the luminescence, a dilute zinc solution (5.4 × 10<sup>-3</sup> M) was gradually added via a microsyringe to 10 mL of a 10<sup>-5</sup> M solution of **1**. All mixtures obtained were analyzed by electrospray mass spectrometry as described below.

**X-ray Structure Determinations.** The intensity data for the crystals of compounds **1** and **2** were collected on a Nonius KappaCCD diffractometer at *T* = -90 °C, using graphite-monochromated Mo K $\alpha$  radiation. Data were corrected for Lorentz and polarization effects but not for absorption.<sup>12</sup>

The structures were solved by direct methods (SHELXS<sup>13</sup>) and refined by full-matrix least-squares techniques against *F*<sub>o</sub><sup>2</sup> (SHELXL-97<sup>14</sup>). Two *tert*-butyl groups of **2** were found to be disordered, but the disorder could be solved. For **2**, the hydrogen atoms of the amine group in the bibenzimidazole system were located by a difference Fourier synthesis and refined isotropically. All other hydrogen atoms were included at calculated positions with fixed thermal parameters. All non-hydrogen atoms were refined anisotropically.<sup>14</sup> XP (SIEMENS Analytical X-ray Instruments, Inc.) was used for structure representations.

**Mass Spectroscopy.** Mass spectra were recorded on a Finnigan MAT 95 XL spectrometer. In the ESI process, the sample used for the photochemical investigation (ca. 10<sup>-5</sup> M solution in THF) was introduced into the ESI ion source with a Harvard Apparatus syringe infusion pump, model 22, with a flow rate of 5–20  $\mu$ L/min. The positive-ion ES mass spectra were obtained with potentials of 3–4 kV applied to the electrospray needle. The resolution was usually about 2000 at  $m/z$  750.

## Results and Discussion

Compound **2** was prepared using standard synthetic methods.<sup>2</sup> The deprotonated complex **1** was then obtained conveniently by reaction of **2** with NaOH and subsequent extraction with dichloromethane. 4,4'-*tert*-Butyl-2,2'-bipyridyl was used to improve the solubility of the compounds in organic solvents

such as THF. The molecular structures of compounds **1** and **2** as obtained from X-ray analysis are shown in Figure 1.

As expected, Ru(II) possesses in both cases a distorted octahedral coordination sphere. Except for a widened N–C–N angle of 117.2(3)° at the bridging carbon of the bibenzimidazole ligand in **1** compared with 113.2(3)° in **2**, no significant structural changes are induced through the deprotonation. Ruthenium–nitrogen (tbbpy) distances in both **1** and **2** are ~2.045 Å (except in **2**, where Ru–N6 = 2.024(2) Å) and are within the range expected, whereas ruthenium–nitrogen (bibzim) distances are 2.094(2) Å for **2** and 2.101(3) Å for **1**.<sup>15</sup>

Deprotonation of **2** yields a significant bathochromic shift in the absorption spectrum of about 100 nm and also results in a total quenching of emission (see Table 1). Addition of a series of various metal salts to **1** in THF results in a hypsochromic shift of the absorption maxima from 580 to ca. 500 nm, depending on the nature of the metal ion (see Table 1). In addition, the luminescence is "switched on" upon addition of ZnCl<sub>2</sub>, ZnEt<sub>2</sub>, MgCl<sub>2</sub>, or Cu(CH<sub>3</sub>CN)<sub>4</sub>BF<sub>4</sub>. Interestingly, the wavelength of the emission maximum is metal dependent, varying from 670 nm for Mg(II) to 710 nm for the trinuclear ZnCl<sub>2</sub> complex (see Figure 2). Upon addition of metal salts such as NiCl<sub>2</sub> and PdBr<sub>2</sub>, a hypsochromic shift in the absorption spectra is observed as well but no emission is detected, which is in contrast to recently published data for a Ru–Pd complex.<sup>16</sup> These results, especially for ZnEt<sub>2</sub>, show that the spectral changes cannot be explained by protonation of the imidazole ring. The maxima observed for both absorption and emission spectra are however quite similar to those found for the Ru–Ru dimer (see Table 1).

The spectroscopic changes observed can, therefore, be attributed to binding of the transition metal ions to the free bibenzimidazole binding site. In this case, we can expect 1:1, 1:2, or 1:3 complexes to be formed. To identify the compositions of the compounds obtained, electrospray mass spectrometry was carried out on the reaction mixtures. The results obtained are given in Table 1. The mass spectral data clearly indicate the compositions of the metal complexes. All reaction mixtures, except for those of magnesium species, show a signal that can be attributed to a binuclear species with an overall charge of

- (12) Otwinowski, Z.; Minor, W. *Methods Enzymol.* **1997**, *276*, 307–326.  
 (13) Sheldrick, G. M. *Acta Crystallogr., Sect. A* **1990**, *46*, 467.  
 (14) Sheldrick, G. M. SHELXL-97. University of Gottingen, Germany, 1993.  
 (15) (a) Haga, M.; Ali, Md. M.; Koseki, S.; Fujimoto, K.; Yoshimura, A.; Nozaki, K.; Ohno, T.; Nakajima, K.; Stufkens, D. J. *Inorg. Chem.* **1996**, *35*, 3335 (b) Majumdra, P.; Peng, S.; Goswami, S. *J. Chem. Soc., Dalton Trans.* **1998**, 1569.  
 (16) For an emitting ruthenium palladium complex, see: Yam, V. W.-W.; Lee, V. W.-M.; Cheung, K.-K. *J. Chem. Soc., Chem. Commun.* **1994**, 2075.

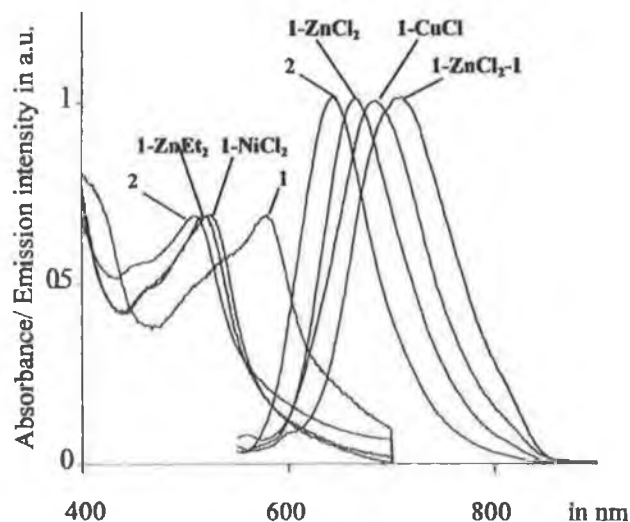


Figure 2. Selected UV-vis and emission spectra recorded in THF for some of the heteronuclear complexes discussed in the text.

+1, resulting from the loss of one counterion. This observation suggests that when an excess of metal ions is present, a 1:1 complex is obtained. Also organometallic complexes are found to bind. **1** forms a complex with  $\text{ZnEt}_2$  that has properties very similar to those observed for its  $\text{ZnCl}_2$  analogue. The absorption maximum is slightly shifted, but this organometallic complex emits at the same wavelength as the  $1\text{-ZnCl}_2$  complex (see Table 1).

If **1** is reacted with small amounts of  $\text{ZnCl}_2$  (up to 3 equiv/ equiv of **1**), the absorption maximum gradually shifts from 580 to 530 nm and at the same time a rise of the emission at 710 nm is observed. This represents a bathochromic shift of 30 nm in both absorption and emission wavelength maxima with respect to those observed at high  $\text{ZnCl}_2\text{:1}$  ratios, suggesting that, at low zinc concentrations, a trinuclear complex is formed as shown in Figure 3. This hypothesis is confirmed by electrospray mass spectroscopy, which indicates that, at low zinc concentrations, a product with the composition  $\{[\text{Ru}(\text{tbbpy})_2(\text{bibzim})]_2\text{ZnCl}_2\}$  is formed. When **1** is reacted with more than a  $10^4$ -fold excess of  $\text{ZnCl}_2$  a complex of the composition  $\{[\text{Ru}(\text{tbbpy})_2(\text{bibzim})]\text{ZnCl}_2\}$  is obtained (see Figure 3).

One of the most striking observations is that the maxima of both absorption and emission spectra are dependent on the nature and concentration of the metal ion added. The absorption features of ruthenium polypyridyl complexes in the visible region are explained by the presence of a singlet metal-to-ligand charge transfer ( $^1\text{MLCT}$ ) transition, while the emission is normally assumed to occur from a  $^3\text{MLCT}$  state. The shifts observed in both absorption and emission spectra indicate therefore that the energies of both the  $^1\text{MLCT}$  and the  $^3\text{MLCT}$  transitions are affected by binding of the transition metal ions. In all cases, the absorption maxima are shifted to higher energy than observed in the spectra of **1**. All are however at lower energy than found for **2**. The emission wavelengths follow a similar trend.

An initial interpretation of these results suggests that the behavior observed can be explained by a stabilization of the metal-based ground state in the heteronuclear compounds with respect to **1**. This is not unexpected, and such behavior has been

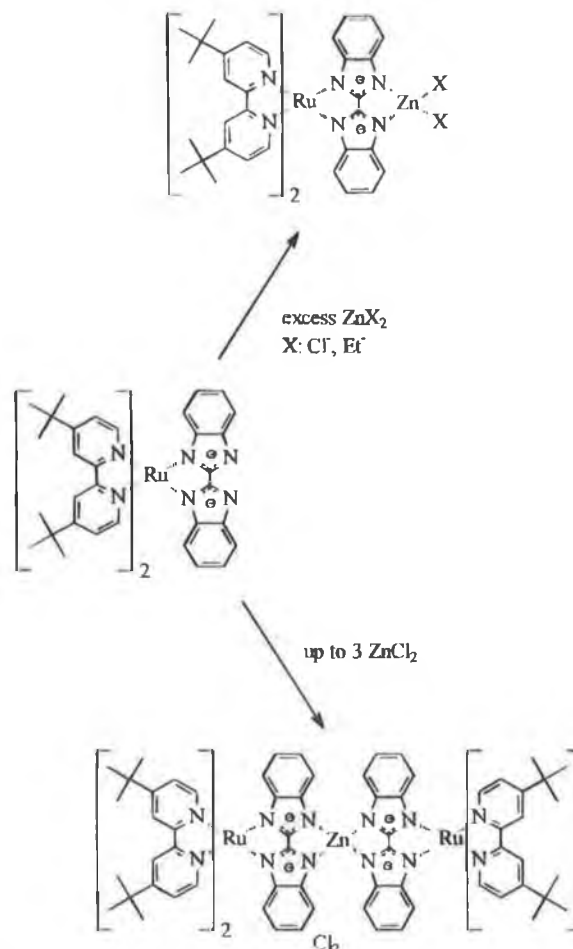


Figure 3. Proposed pathways for the reactions of **1** with different zinc compounds.

observed for other complexes with negatively charged bridges.<sup>3,17</sup> The emission observed can then be explained by the increased energy gap between the emitting triplet state and the ground state. This increased energy gap is expected not only to shift the emission to higher energy but also to increase the emission lifetime. The variations in emission and absorption energies are therefore measures of the electron-withdrawing properties of the metal ions added. However, a second factor that needs to be taken into account is the location of the deactivating triplet metal-centered ( $^3\text{MC}$ ) state. Upon binding of a second metal ion, the energy of this state will be reduced, since the electron density on the negatively charged bridge is now shared by two metal centers, leading to a decrease of the emission lifetime. This is, for example, clearly the case for the mononuclear and dinuclear  $\text{Ru}(\text{bpy})_2$  complexes of the ligand 3,5-bis(pyridin-2-yl)-1,2,4-triazole (Hbpt). For this ligand, which deprotonates upon binding, forming bpt, the emission shifts to higher energy upon binding of a second ruthenium center, but the emission lifetime decreases from 160 to 100 ns because of a lowering of the  $^3\text{MC}$  level.<sup>18</sup> The emission lifetimes observed for these complexes will therefore be governed by both the energy gap law and by the relative energies of the emitting triplet state and the deactivating  $^3\text{MC}$  state.

In conclusion, we report here a neutral ruthenium complex that can act as a ligand for different metal centers, thus creating different hetero- and heterotrinnuclear complexes. Also, organometallic compounds such as  $\text{ZnEt}_2$  can be complexed by **1**, which might allow the tuning of the reactivity of the  $\text{Zn-Et}$  bond through the interaction with the ruthenium complex. The

(17) Hage, R.; Haasnoot, J. G.; Nieuwenhuis, H. A.; Reedijk, J.; De Ridder, D. J. A.; Vos, J. G. *J. Am. Chem. Soc.* **1990**, *112*, 9245.

(18) Barigelletti, F.; De Cola, L.; Balzani, V.; Hage, R.; Haasnoot, J. G.; Reedijk, J.; Vos, J. G. *Inorg. Chem.* **1989**, *28*, 4346.

heteronuclear bibenzimidazole complexes show a remarkable "2-fold" tunability. The emission, which can be "switched on" by complexation with closed-shell metal ions such as  $Zn^{2+}$  and  $Mg^{2+}$ , can also be "fine-tuned" in both *wavelength* ( $\lambda_{max}$ ) and *intensity* ( $\tau$ ) simply by choosing a suitable metal ion. These properties are very promising in view of the continuing search for components to be used in molecular-level devices and might also lead to the design of novel luminescence-based sensors.

**Acknowledgment.** S.R. and M.R. acknowledge the Studienstiftung des Deutschen Volkes for Ph.D. grants. Financial

support from the Deutsche Forschungsgemeinschaft (Grant SFB 436) is gratefully acknowledged. M.D., S.F., and J.G.V. thank the EC TMR Programme (Grants CT96-0031 and CT96-0076) for financial assistance.

**Supporting Information Available:** X-ray crystallographic files, in CIF format, for the structures of **1** and **2**. This material is available free of charge via the Internet at <http://pubs.acs.org>.

IC991225H

# DALTON

Incorporating *Acta Chemica Scandinavica*

---

An international journal  
of inorganic chemistry

REPRINT

*With the  
Compliments of the Author*



# Bis(R-bipyridyl)ruthenium bibenzimidazole complexes (R = H, Me or Bu<sup>t</sup>): supramolecular arrangement *via* hydrogen bonds, photo- and electro-chemical properties and reactivity towards carbon dioxide

Sven Rau,<sup>a</sup> Mario Ruben,<sup>a</sup> Torsten Büttner,<sup>a</sup> Christian Temme,<sup>a</sup> Sylvana Dautz,<sup>a</sup> Helmar Görls,<sup>a</sup> Manfred Rudolph,<sup>a</sup> Dirk Walther,<sup>\*a</sup> Andre Brodkorb,<sup>b</sup> Marco Duati,<sup>c</sup> Christine O'Connor<sup>c</sup> and Johannes G. Vos<sup>\*c</sup>

<sup>a</sup> Institut für Anorganische und Analytische Chemie, Friedrich-Schiller-University, 07743 Jena, Germany

<sup>b</sup> Laboratoire de Chimie Organique Physique, CP 160180, Université Libre de Bruxelles, 1050 Bruxelles, Belgium

<sup>c</sup> Inorganic Chemistry Research Centre, School of Chemical Sciences, Dublin City University, Dublin 9, Ireland

Received 18th May 2000, Accepted 24th August 2000

First published as an Advance Article on the web 28th September 2000

Complexes of the type  $[\text{Ru}(\text{H}_2\text{bibzim})(\text{R}-\text{bpy})_2\text{X}_2 \cdot n\text{H}_2\text{O}$  (R = H, 2,2'-bipyridine, bpy, X =  $\text{CF}_3\text{SO}_3^-$  **1**; R = Me, 4,4'-dimethyl-2,2'-bipyridine, dmbpy, X =  $\text{PF}_6^-$  **2**; R = *tert*-butyl, 4,4'-di-*tert*-butyl-2,2'-bipyridine, tbbpy, X =  $\text{Cl}^-$  **3**; H<sub>2</sub>bibzim = 1,1'-bibenzimidazole) containing two NH functions acting as hydrogen bond donors formed different spatially highly organised supramolecular assemblies with water. X-Ray investigation revealed that the nature of the counter ion influences the hydrogen bonding pattern and extent of spatial organisation. In **2** one dimensional chains of hydrogen bonded water could be found. In the deprotonated complex  $[\text{Ru}(\text{bibzim})(\text{tbbpy})_2]$  **4** water molecules serve as hydrogen bond donors. The diastereomeric forms **5a/5b** of the homodinuclear ruthenium complex  $[\{\text{Ru}(\text{tbbpy})_2\}_2(\text{bibzim})][\text{PF}_6]_2$  could be separated. No differences in their photophysical properties could be detected. The X-ray investigation of **5a** and  $[\{\text{Ru}(\text{bpy})_2\}_2(\text{bibzim})][\text{PF}_6]_2$  **6** showed little influence of peripheral substitution on structural properties. Complexes **3–5** exhibit activity in electrochemical CO<sub>2</sub> reduction which can be tuned by variation of the degree of protonation of the bibenzimidazole.

## Introduction

The chemistry of polypyridine ruthenium(II) complexes bridged by bi- or tri-dentate ligands<sup>1</sup> has received much attention in connection with the construction of molecular electronic devices.<sup>2</sup> Suitable bridging ligands are for example bipyrimidine,<sup>3</sup> substituted pyrazines,<sup>4</sup> substituted bipyridines<sup>5</sup> and biimidazoles.<sup>6</sup> In the last few years ruthenium polypyridyl complexes based on benzimidazole moieties have been investigated in detail.<sup>7</sup> These studies have concentrated on the spectroscopic and electrochemical properties of these complexes. The presence of the acidic imidazole proton allows deprotonation of the complexes and this results in a rich chemistry where changes in pH can be used to determine the electrochemical and photophysical properties of the compounds.<sup>8</sup> This, deprotonation of bibenzimidazole for instance allows for the formation of di- and oligo-nuclear complexes.<sup>9</sup> Additionally, ruthenium benzimidazole complexes can be used as catalysts for the electrochemical reduction of CO<sub>2</sub><sup>10</sup> and their application as proton driven molecular switches has been reported.<sup>11</sup> Recently we have found that a substituted, deprotonated bibenzimidazole can act as a metal sensor.<sup>12</sup>

Considering the large number of studies carried out on ruthenium compounds in solution it is surprising that there has been much less interest in the study of these compounds in well defined solid state environments.<sup>13–15</sup> The presence of the imidazole nitrogen atoms in benzimidazole complexes in both their protonated and deprotonated state should be an ideal building block for the construction of solid state supramolecular

structures based on hydrogen bonding. Our interest in these compounds is twofold. First we would like to use the imidazole unit as a building block for the construction of well defined solid state structures. Secondly we are interested to see whether the known dependence of photophysical properties on the stereochemistry of ruthenium complexes<sup>16</sup> is also valid for bibenzimidazole based systems.

In this contribution we report on a number of syntheses and crystal structures of benzimidazole containing ruthenium polypyridyl complexes. The structures obtained show some well defined hydrogen bonding patterns. We also show that the separation of the stereoisomers of the homodinuclear complexes is possible and that the photophysical properties of these isomers are independent of their stereochemistry. In addition we report on the catalytic properties of these compounds for the electrochemical reduction of CO<sub>2</sub>. All compounds obtained are fully characterized by X-ray crystallography, NMR, UV-vis and emission spectroscopy.

## Experimental

### Materials

All synthetic work was performed using Schlenk techniques. Emission and absorption spectra were recorded using septum equipped luminescent cells (Hellma) in spectroscopic acetonitrile (Fluka) and THF (Aldrich). THF was dried and distilled over sodium benzophenone, CH<sub>3</sub>CN was dried over CaH<sub>2</sub> and distilled; all other solvents were distilled prior to use

[Ru(COD)Cl<sub>2</sub>]<sub>n</sub>,<sup>17</sup> bibenzimidazole (H<sub>2</sub>bibzim),<sup>18</sup> 4,4'-di-*tert*-butyl-2,2'-bipyridine (tbbpy),<sup>19</sup> Ru(bpy)<sub>2</sub>Cl<sub>2</sub>,<sup>20</sup> Ru(dmbpy)<sub>2</sub>-Cl<sub>2</sub> (dmbpy = 4,4'-dimethyl-2,2'-bipyridine),<sup>21</sup> [Ru(bibzim)-(tbbpy)<sub>2</sub>]<sup>12</sup> and [Ru(bpy)<sub>2</sub>]<sub>2</sub>(bibzim)[PF<sub>6</sub>]<sub>2</sub><sup>7</sup> were synthesized using literature methods. Oxalic acid and NH<sub>4</sub>ClO<sub>4</sub> (Fluka) were used without further purification.

### Preparations

[Ru(tbbpy)<sub>2</sub>Cl<sub>2</sub>]. 12.08 g (0.043 mol) [Ru(COD)Cl<sub>2</sub>]<sub>n</sub> and 23.2 g (0.086 mol) tbbpy were refluxed in 40 cm<sup>3</sup> DMF for 72 h. The DMF and cycloocta-1,5-diene were removed by vacuum distillation and the resulting black microcrystalline compound was dried under vacuum for 2 h. The complex was purified by Soxhlet extraction with toluene. The toluene was removed and the resulting dark microcrystalline compound dried under vacuum for 3 h. Yield: 78%. <sup>1</sup>H NMR (acetone-d<sub>6</sub>): δ 10.02 (1 H, d, H6), 8.54 (1 H, s, H3), 8.42 (1 H, s, H3a), 7.68 (1 H, d, H5), 7.48 (1 H, d, H6a), 7.08 (1 H, d, H5a), 1.51 (9 H, s, *t*-butyl) and 1.31 (9 H, s, *t*-butyl). UV (THF) λ<sub>max</sub> = 583 nm. MS: *m/z* = 708 (corresponding isotope pattern for C<sub>36</sub>H<sub>48</sub>-N<sub>4</sub>Cl<sub>2</sub>Ru).

[Ru(H<sub>2</sub>bibzim)(R-bpy)<sub>2</sub>]<sub>2</sub>X<sub>2</sub> 1–3. These were synthesized using standard procedures.<sup>7,9</sup> **CAUTION:** perchlorates are potentially explosive. After removal of the solvent 10 cm<sup>3</sup> water were added followed by a concentrated aqueous solution of NH<sub>4</sub>PF<sub>6</sub>, LiCF<sub>3</sub>SO<sub>3</sub> or LiClO<sub>4</sub> respectively. If no counter ion source was added the complex was obtained as its dichloride and purified using the same techniques. The resulting precipitate was filtered off, redissolved in acetonitrile, filtered and then the solvent was removed. Yields were above 90% for all compounds. ES-MS: [Ru(H<sub>2</sub>bibzim)(bpy)<sub>2</sub>][PF<sub>6</sub>]<sub>2</sub> 1, *m/z* = 647 (corresponding isotope pattern for C<sub>34</sub>H<sub>25</sub>N<sub>8</sub>Ru); [Ru(H<sub>2</sub>bibzim)(dmbpy)<sub>2</sub>][PF<sub>6</sub>]<sub>2</sub> 2, *m/z* = 702 (corresponding isotope pattern for C<sub>38</sub>H<sub>33</sub>N<sub>8</sub>Ru); [Ru(H<sub>2</sub>bibzim)(tbbpy)<sub>2</sub>][PF<sub>6</sub>]<sub>2</sub> 3, *m/z* = 871 (corresponding isotope pattern for C<sub>50</sub>H<sub>57</sub>N<sub>8</sub>Ru). The compounds were also characterized using <sup>1</sup>H NMR (Table 2), UV-vis and emission (Table 3) and cyclic voltammetry (Table 3). Suitable crystals for X-ray crystallography were obtained by slow evaporation of an acetone-water solution (1:1) of 1 and 2 and of an acetonitrile-water solution (1:1) of 3.

[Ru(bibzim)(tbbpy)<sub>2</sub>] 4. This was recrystallized from an acetone-water (50:50) solution as the dihydrate.

[Ru(tbbpy)<sub>2</sub>]<sub>2</sub>(bibzim)[PF<sub>6</sub>]<sub>2</sub> 5. This was synthesized using 369 mg of [Ru(tbbpy)<sub>2</sub>Cl<sub>2</sub>] (0.52 mmol) and 61 mg (0.26 mmol) H<sub>2</sub>bibzim refluxed with 2 cm<sup>3</sup> triethylamine for 20 h in 100 cm<sup>3</sup> ethanol-water (1:1). The solution was allowed to cool, filtered and the solvent removed. The dark residue was redissolved in 10 cm<sup>3</sup> of water. A concentrated aqueous solution of NH<sub>4</sub>PF<sub>6</sub> was added. The resulting precipitate was filtered off and redissolved in 100 cm<sup>3</sup> acetone-water (1:1) and left to recrystallize. The precipitate was filtered off and analysed by <sup>1</sup>H NMR spectroscopy. Two isomers could be identified. The precipitate was purified by recrystallization and two pure fractions of the complex could be separated. Alternatively [Ru(bibzim)-(tbbpy)<sub>2</sub>] can be refluxed with one equivalent of [Ru(tbbpy)<sub>2</sub>Cl<sub>2</sub>] in ethanol-water (1:1) for 8 h and the resulting compound treated in the same way as described for the former synthesis. Yield for both methods: 0.25 mmol (96%). After obtaining the pure fractions recrystallization from acetone water (50:50) yielded suitable crystals for X-ray diffraction for the *meso* isomer 5a. <sup>1</sup>H NMR, see Table 2. UV-vis, electrochemical data and emission, see Table 3.

[Ru(bpy)<sub>2</sub>]<sub>2</sub>(bibzim)[PF<sub>6</sub>]<sub>2</sub> 6. This was crystallized by slow evaporation of an acetonitrile water solution (50:50) of the diastereomeric mixture.

### Instrumentation

NMR spectra were recorded using Bruker 400 and 200 MHz spectrometers, UV-VIS spectra using a Varian Cary 1 UV-vis or a Shimadzu UV 3100 UV-vis-NIR spectrometer. Emission spectra are not corrected and were recorded using a Perkin-Elmer LS50B spectrometer equipped with a Hamamatsu R928 red sensitive detector. IR spectra were recorded using a Perkin-Elmer 2000 FT-IR spectrometer.

### Lifetime measurements

Luminescent lifetimes were measured employing a Spectra Physics Nd-YAG frequency tripled, Q-switched laser as excitation source coupled in a right angled configuration to an Oriol iCCD; laser power was measured as 30 mJ per 20 ns pulse. The single photon counting (SPC) measurements for the dinuclear complexes were performed with an Edinburgh Instruments FL-900 spectrofluorimeter equipped with a nitrogen filled discharge lamp and a Peltier-cooled Hamamatsu R-928 PM tube. The emission decays were analysed with the Edinburgh Instruments software (version 3.0), based on non-linear least squares regression using a modified Marquardt algorithm.

### Electrochemical equipment

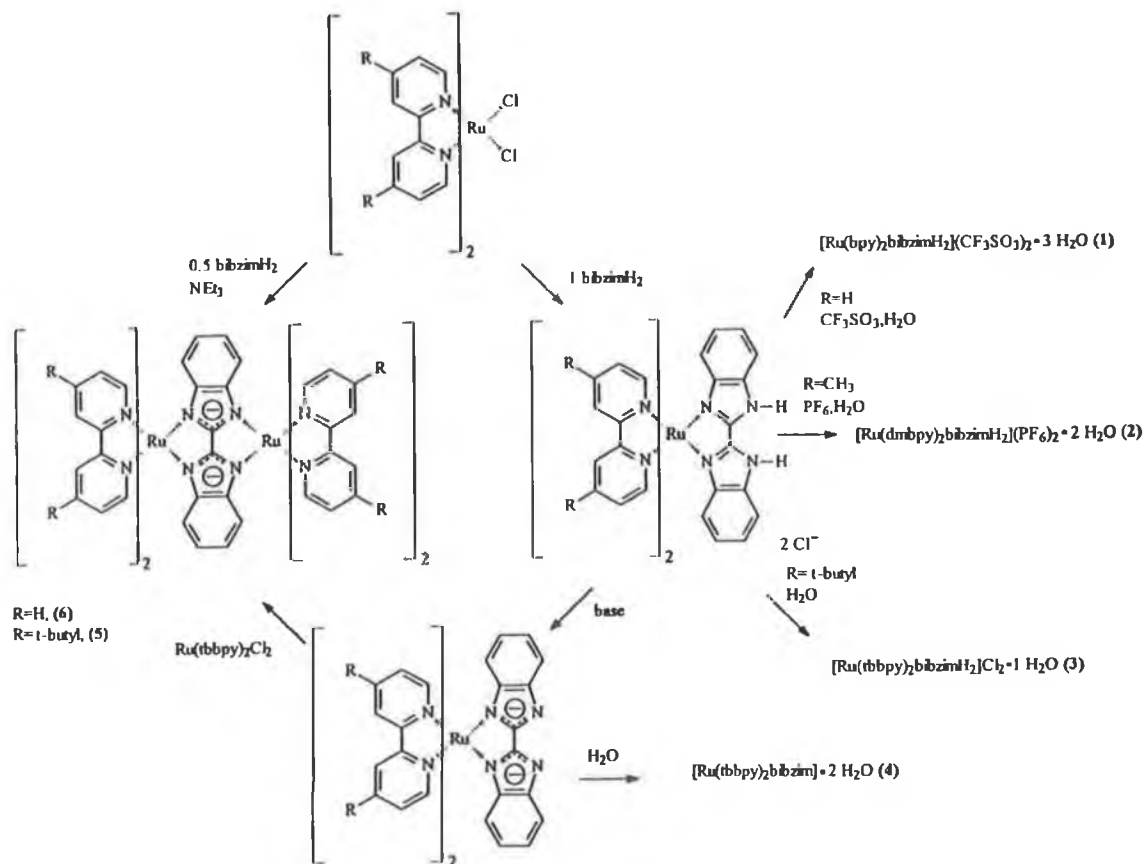
The cyclic voltammetric measurements were made with a home built computer controlled instrument based on the DAP-3200a data acquisition board (DATALOG Systems) as well as with the Autolab PG Stat 20 (Metrohm). The experiments were performed in a three electrode cell under a blanket of solvent saturated argon or carbon dioxide respectively. The ohmic resistance which had to be compensated for was obtained by measuring the impedance of the system at potentials where the faradaic current was negligibly small. Background correction was accomplished by subtracting the current curves of the blank electrolyte (containing the same concentration of supporting electrolyte) from the experimental curve. The reference was an Ag-AgCl electrode in acetonitrile containing 0.25 M tetra-*n*-butylammonium chloride but for convenience all potentials were finally referenced to the SCE<sup>22</sup> throughout. Exhaustive electrolyses of complexes were performed with 0.001 M solutions of the complexes in dried acetonitrile with 1 M tetra-*n*-butylammonium perchlorate as supporting electrolyte using a Bank potentiostat. Solvent and mercury were removed and the complex resuspended in 2 cm<sup>3</sup> water followed by extraction with 2 cm<sup>3</sup> CHCl<sub>3</sub>. Oxalate was determined in the aqueous phase. The yield of oxalate was determined using a Knauer HPLC system with a C<sub>18</sub> column and 5% H<sub>3</sub>PO<sub>4</sub> as mobile phase, equipped with a Knauer absorbance detector UV-1 set at 208 nm calibrated with a solution of oxalic acid. Oxalic acid was additionally identified by subtracting IR spectra of the complex in solution before and after the electrolysis where the band at 1645 cm<sup>-1</sup> was assigned to oxalic acid.

### Mass spectroscopy

The mass spectra were recorded using a SSQ 170, Finnigan MAT, electrospray mass spectra on a Finnigan MAT, MAT 95 XL instrument. In the ESI process the sample used for the photochemical investigation (*ca.* 10<sup>-5</sup> M solution in THF) was introduced into the ESI ion source with a Harvard Apparatus syringe infusion pump, Model 22, with a flow rate of 5–20 l min<sup>-1</sup>. The positive ES mass spectra were obtained with voltages of 3–4 kV applied to the electrospray needle. The resolution was usually about 2000 at *m/z* = 750.

### Crystal structure determination

The intensity data for the compounds were collected on a Nonius KappaCCD diffractometer, using graphite-monochrom-



Scheme 1 Synthesis of the complexes 1–6.

ated Mo-K $\alpha$  radiation. Data were corrected for Lorentz and polarization effects, but not for absorption.<sup>23</sup> The structures were solved by direct methods (SHELXS<sup>24</sup>) and refined by full-matrix least squares techniques against  $F_o^2$  (SHELXL 97<sup>25</sup>). For the compound **2** the hydrogen atoms of the "amine group" and the water molecules were located by Fourier difference synthesis and refined isotropically. All other hydrogen atoms were included at calculated positions with fixed thermal parameters. All non-hydrogen atoms were refined anisotropically.<sup>25</sup> XP (Siemens Analytical X-Ray Instruments, Inc.) was used for structure representations.

**Crystal data.**  $[\text{Ru}(\text{H}_2\text{bibzim})(\text{bpy})_2][\text{CF}_3\text{SO}_3]_2 \cdot 3\text{H}_2\text{O}$  **1**.  $\text{C}_{36}\text{H}_{26}\text{F}_6\text{N}_8\text{O}_6\text{RuS}_2$ ,  $M_r = 999.34 \text{ g mol}^{-1}$ , monoclinic, space group  $C2/c$ ,  $a = 22.0290(10)$ ,  $b = 16.2900(10)$ ,  $c = 13.3542(6) \text{ \AA}$ ,  $\beta = 122.214(2)^\circ$ ,  $V = 4054.5(4) \text{ \AA}^3$ ,  $T = -90^\circ\text{C}$ ,  $Z = 4$ ,  $\mu(\text{Mo-K}\alpha) = 5.81 \text{ cm}^{-1}$ , 20269 reflections measured, 4590 independent reflections,  $R_{\text{int}} = 0.101$ , 3531 reflections with  $F_o > 4\sigma(F_o)$ ,  $R1_{\text{obs}} = 0.095$ ,  $wR2_{\text{obs}} = 0.222$ ,  $R1_{\text{all}} = 0.128$ ,  $wR2_{\text{all}} = 0.241$ .

$[\text{Ru}(\text{H}_2\text{bibzim})(\text{dmbpy})_2][\text{PF}_6]_2 \cdot 2\text{H}_2\text{O} \cdot 2\text{C}_3\text{H}_6\text{O}$  **2**.  $\text{C}_{38}\text{H}_{34}\text{F}_{12}\text{N}_8\text{P}_2\text{Ru} \cdot 2\text{C}_3\text{H}_6\text{O} \cdot 2\text{H}_2\text{O}$ ,  $M_r = 1145.93 \text{ g mol}^{-1}$ , monoclinic, space group  $C2/c$ ,  $a = 22.7551(5)$ ,  $b = 23.9120(5)$ ,  $c = 9.6410(3) \text{ \AA}$ ,  $\beta = 112.708(3)^\circ$ ,  $V = 4839.2(2) \text{ \AA}^3$ ,  $T = -90^\circ\text{C}$ ,  $Z = 4$ ,  $\mu(\text{Mo-K}\alpha) = 4.88 \text{ cm}^{-1}$ , 6467 reflections measured, 3362 independent,  $R_{\text{int}} = 0.018$ , 3075 with  $F_o > 4\sigma(F_o)$ ,  $R1_{\text{obs}} = 0.042$ ,  $wR2_{\text{obs}} = 0.123$ ,  $R1_{\text{all}} = 0.0467$ ,  $wR2_{\text{all}} = 0.133$ .

$[\text{Ru}(\text{H}_2\text{bibzim})(\text{tbbpy})_2]\text{Cl}_2 \cdot \text{H}_2\text{O} \cdot 2\text{C}_3\text{H}_6\text{O}$  **3**. Described previously.<sup>12</sup>

$[\text{Ru}(\text{bibzim})(\text{tbbpy})_2] \cdot 2\text{H}_2\text{O} \cdot \text{C}_3\text{H}_6\text{O}$  **4**.  $\text{C}_{50}\text{H}_{56}\text{N}_8\text{Ru} \cdot \text{C}_3\text{H}_6\text{O} \cdot 2\text{H}_2\text{O}$ ,  $M_r = 964.21 \text{ g mol}^{-1}$ , monoclinic, space group  $C2/c$ ,  $a = 11.7219(5)$ ,  $b = 17.5925(8)$ ,  $c = 24.522(1) \text{ \AA}$ ,  $\beta = 101.083(3)^\circ$ ,  $V = 4962.6(4) \text{ \AA}^3$ ,  $T = -90^\circ\text{C}$ ,  $Z = 4$ ,  $\mu(\text{Mo-K}\alpha) = 3.66 \text{ cm}^{-1}$ , 5809 reflections measured, 3209 independent,  $R_{\text{int}} = 0.045$ , 3082 with  $F_o > 4\sigma(F_o)$ ,  $R1_{\text{obs}} = 0.053$ ,  $wR2_{\text{obs}} = 0.148$ ,  $R1_{\text{all}} = 0.069$ ,  $wR2_{\text{all}} = 0.174$ .

$[\{\text{Ru}(\text{tbbpy})_2\}_2(\text{bibzim})][\text{PF}_6]_2 \cdot 6\text{C}_3\text{H}_6\text{O}$  **5a**.  $\text{C}_{86}\text{H}_{104}\text{F}_{12}\text{N}_{12}\text{P}_2\text{Ru}_2 \cdot 6\text{C}_3\text{H}_6\text{O}$ ,  $M_r = 2146.36 \text{ g mol}^{-1}$ , triclinic, space group  $P1$ ,  $a = 12.3749(3)$ ,  $b = 14.4512(4)$ ,  $c = 16.6108(5) \text{ \AA}$ ,  $\alpha = 80.763(2)$ ,  $\beta = 88.971(2)$ ,  $\gamma = 75.717(2)^\circ$ ,  $V = 2840.7(1) \text{ \AA}^3$ ,  $T = -90^\circ\text{C}$ ,  $Z = 1$ ,  $\mu(\text{Mo-K}\alpha) = 3.67 \text{ cm}^{-1}$ , 20676 reflections measured, 11432 independent,  $R_{\text{int}} = 0.047$ , 9084 with  $F_o > 4\sigma(F_o)$ ,  $R1_{\text{obs}} = 0.063$ ,  $wR2_{\text{obs}} = 0.155$ ,  $R1_{\text{all}} = 0.085$ ,  $wR2_{\text{all}} = 0.168$ .

$[\{\text{Ru}(\text{bpy})_2\}_2(\text{bibzim})][\text{PF}_6]_2 \cdot 3\text{C}_2\text{H}_3\text{N} \cdot 2\text{H}_2\text{O}$  **6**.  $\text{C}_{54}\text{H}_{40}\text{F}_{12}\text{N}_{12}\text{P}_2\text{Ru}_2 \cdot 3\text{C}_2\text{H}_3\text{N} \cdot 2\text{H}_2\text{O}$ ,  $M_r = 1508.25 \text{ g mol}^{-1}$ , monoclinic, space group  $C2/c$ ,  $a = 24.474(2)$ ,  $b = 13.921(1)$ ,  $c = 19.433(1) \text{ \AA}$ ,  $\beta = 106.843(3)^\circ$ ,  $V = 6336.9(8) \text{ \AA}^3$ ,  $T = -90^\circ\text{C}$ ,  $Z = 4$ ,  $\mu(\text{Mo-K}\alpha) = 6.19 \text{ cm}^{-1}$ , 8224 reflections measured, 4504 independent,  $R_{\text{int}} = 0.045$ , 3666 with  $F_o > 4\sigma(F_o)$ ,  $R1_{\text{obs}} = 0.048$ ,  $wR2_{\text{obs}} = 0.125$ ,  $R1_{\text{all}} = 0.0635$ ,  $wR2_{\text{all}} = 0.141$ .

CCDC reference number 186/2160.

See <http://www.rsc.org/suppdata/dt/b0/b003992f/> for crystallographic files in .cif format.

## Results and discussion

### Synthesis of complexes 1–6

All complexes could be obtained *via* standard procedures starting from the corresponding precursor  $[\text{Ru}(\text{R-bpy})_2\text{Cl}_2]$  (Scheme 1).<sup>7</sup> The complexes with  $\text{R} = \text{H}$  and  $\text{CH}_3$  were synthesized according to literature methods.<sup>20,21</sup> However, in our hands the synthesis of the *tert*-butyl substituted complex did not proceed along standard procedures with reproducible relatively high yields. Instead of  $[\text{Ru}(\text{tbbpy})_2\text{Cl}_2]$  large quantities of  $[\text{Ru}(\text{tbbpy})_2\text{Cl}_2]$  were obtained. For this reason we developed a new route which is based on separation of the reduction and complex formation into a two step synthesis. In the first step  $\text{RuCl}_3(\text{H}_2\text{O})_x$  was treated with cycloocta-1,5-diene to form the polymeric ruthenium(II) complex  $\text{RuCl}_2(\text{COD})_n$  in good yields.<sup>17</sup> Refluxing of the polymeric compound with tbbpy in DMF and subsequent purification by extraction in step 2 resulted in the pure complex.

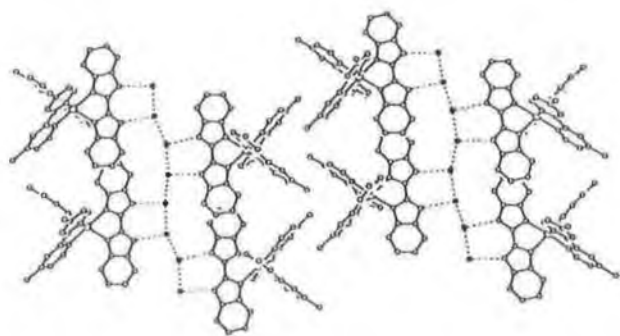


**Fig. 1** Supramolecular arrangement of  $[\text{Ru}(\text{H}_2\text{bibzim})(\text{dmbpy})_2]^{2+}$  **2** in the solid state; protons, anions and acetone molecules are omitted for clarity.

Complexation with bibenzimidazole yields the mono- or dinuclear compound depending on the molar ratio employed (Scheme 1). The dinuclear complex **5** was also accessible if the mononuclear complex was deprotonated, isolated and treated with one equivalent of  $[\text{Ru}(\text{tbbpy})_2\text{Cl}_2]$ . Complexes **1–4** yield supramolecular structures characterized by different hydrogen bonding networks, synthesized according to Scheme 1.

#### Crystal structures of complexes **1–6**

The complexes,  $[\text{Ru}(\text{bpy})_2(\text{H}_2\text{bibzim})][\text{CF}_3\text{SO}_3]_2 \cdot 3\text{H}_2\text{O}$  **1**,  $[\text{Ru}(\text{H}_2\text{bibzim})(\text{dmbpy})_2][\text{PF}_6]_2 \cdot 2\text{H}_2\text{O}$  **2**,  $[\text{Ru}(\text{H}_2\text{bibzim})(\text{tbbpy})_2]\text{Cl}_2 \cdot \text{H}_2\text{O}$  **3**,  $[\text{Ru}(\text{bibzim})(\text{tbbpy})_2] \cdot 2\text{H}_2\text{O}$  **4**, *meso*- $[\text{Ru}(\text{tbbpy})_2]_2(\text{bibzim})][\text{PF}_6]_2$  **5a** and *meso*- $[\text{Ru}(\text{bpy})_2]_2(\text{bibzim})][\text{PF}_6]_2$  **6** could be obtained as single crystals suitable for X-ray investigation. Their solid state structures are displayed in Figs. 1–6. All investigated complexes possess a distorted octahedral co-ordination geometry at the ruthenium centre. The ruthenium–bipyridine distances are within the expected range and are within experimental errors invariant towards the different substitution at the 4 position. A similar result has been obtained by Rillema *et al.* for tris chelates of ruthenium(II) with bipyridine, bipyrimidine and bipyrazine.<sup>26</sup> The ruthenium–bibenzimidazole distances are longer than the ruthenium–bipyridine distances and proved to be invariant to changes of the degree of protonation of the bibenzimidazole. They are, however, elongated in the dinuclear complexes with respect to the mononuclear complexes (Table 1).

#### Mononuclear complexes **1–4** and their supramolecular aspects.

In the solid state all these mononuclear complexes are accompanied by water and solvent molecules in the asymmetric unit. We could not however find any interaction between solvent molecules like acetone or acetonitrile with the complex cation.  $[\text{Ru}(\text{H}_2\text{bibzim})(\text{dmbpy})_2][\text{PF}_6]_2 \cdot 2\text{H}_2\text{O}$  **2** was formed by slow crystallisation from an acetone–water solution. The Ru–N<sub>dmbpy</sub> distances are somewhat longer than in  $[\text{Ru}(\text{H}_2\text{bibzim})(\text{tbbpy})_2]^{2+}$  **3**<sup>12</sup> (Table 1) and are within experimental errors the same as for the  $[\{\text{Ru}(\text{dmbpy})_2\}_2(\text{bpym})\}^{4+}$  (bpym = 2,2'-bipyrimidine) system.<sup>3</sup> The bibenzimidazole ligand in **2** is slightly bent around the ruthenium centre. This is reflected in the angle of 166.6° resulting from two lines constructed from the centroid of the benzene ring of one half of the ligand and the corresponding bridging carbon atom. Both benzimidazole rings exhibit a slight torsion angle towards each other of 4.3°. Both N–H functions of the bibenzimidazole ligand serve as hydrogen bond donors for water molecules resulting in a nitrogen–oxygen distance of 2.811(5) Å. One water molecule which is spatially fixed by the N–H hydrogen bond forms a hydrogen bond to the neighbouring molecule (O...O distance 2.762(5) Å) which is also fixed by a N–H hydrogen bond from the same complex, see Fig. 1. The next water molecule forms a hydrogen bond to a neighbouring water molecule which is in turn hydrogen bonded by a N–H function (O...O distance

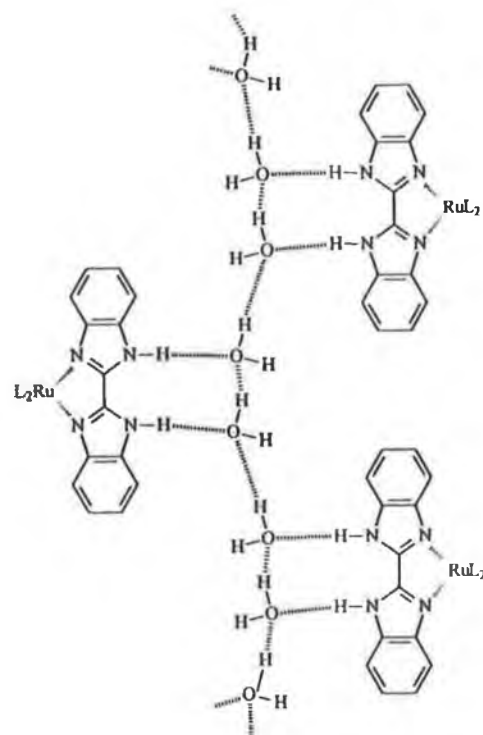


**Fig. 2** Graphical representation of the supramolecular arrangement of complex **2** in the solid state; anions and acetone molecules are omitted for clarity.

2.778(5) Å) of another molecule of **2**. The next  $[\text{Ru}(\text{H}_2\text{bibzim})(\text{dmbpy})_2]^{2+}$  of the same strand is 3.976 Å above the plane formed by the bibenzimidazole ligand of the first complex and its hydrogen bonded water.

This structural principle continues throughout the whole crystal and directs this highly ordered spatial orientation in such a way that the  $\Delta$  enantiomer and the  $\Lambda$  enantiomer form separated strings which are interconnected by a one dimensional chain of water molecules (Fig. 2) and the complexes together with the water molecules are arranged in a step like manner. There are only a few examples in the literature where single molecules are interconnected by one dimensional chains of water<sup>27</sup> none of them being a ruthenium polypyridyl complex; even so there are a few ruthenium complexes displaying more complicated hydrogen bond networks involving water.<sup>28</sup> Crystal structures of ruthenium polypyridyl complexes containing the benzimidazole fragment display limited hydrogen bonding patterns.<sup>13</sup> If nuclear base substituted bipyridine ligands are employed structurally highly organized architectures can be obtained by suitable interaction of the heterocyclic moieties.<sup>29</sup>

In contrast to complex **2** the closely related  $[\text{Ru}(\text{H}_2\text{bibzim})(\text{bpy})_2][\text{CF}_3\text{SO}_3]_2 \cdot 3\text{H}_2\text{O}$  **1**, shows a completely different hydrogen bonding network (Fig. 3). Similarly to **2**, both of the protonated secondary amine functions of the bibenzimidazole are within hydrogen bonding distance to one water respectively. In contrast to the former, both water molecules are not within hydrogen bonding distance towards each other. They are however both in hydrogen bonding distance to a third water molecule and to an oxygen from a triflate counter ion ( $\text{CF}_3\text{SO}_3^-$ ) respectively. The third water molecule is in hydrogen bonding distance to the oxygens from two different triflate counter ions. One ruthenium complex unit is therefore incorporated in a hydrogen bonding network involving three water and four triflate molecules. These triflates are also in hydrogen bonding distance to other water molecules which are in hydrogen bonding distance to another molecule of **1**. The complexes are therefore, *via* their N–H functions, interconnected by a complicated network involving (i) water molecules serving as hydrogen bond

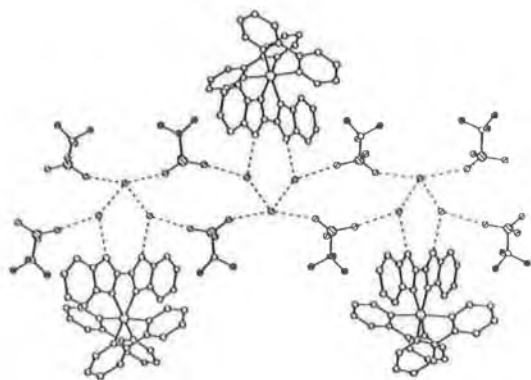


Fig. 3 Hydrogen bonding network of  $[\text{Ru}(\text{H}_2\text{bibzim})(\text{bpy})_2][\text{CF}_3\text{SO}_3]_2 \cdot 3\text{H}_2\text{O}$  **1** in the solid state; protons and acetone molecules are omitted for clarity.

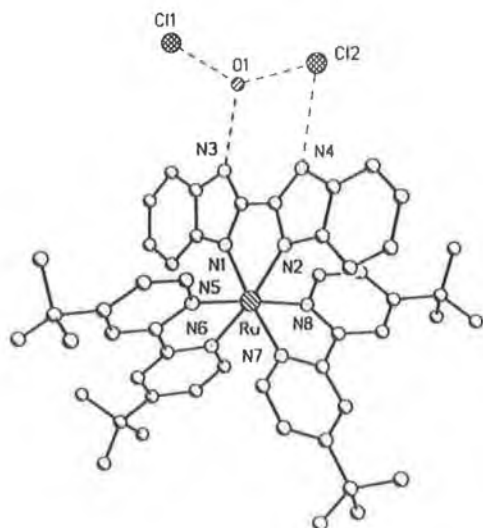


Fig. 4 Hydrogen bonding system of  $[\text{Ru}(\text{H}_2\text{bibzim})(\text{tbbpy})_2]\text{Cl}_2 \cdot \text{H}_2\text{O}$  **3** in the solid state; protons and acetonitrile molecules are omitted for clarity.

acceptors for N–H and O–H donors and (ii) triflate molecules serving as hydrogen bond acceptors for O–H hydrogen bond donors from water molecules connected to different ruthenium complexes.

Changing the counter ion from hexafluorophosphate to triflate clearly influences the degree of spatial orientation and order. Additionally, chloride represents a suitable counter ion which is, in copper complexes of bibenzimidazole,<sup>30</sup> known to interact directly with the N–H function of the bibenzimidazole. A ruthenium bibenzimidazole complex would therefore have the opportunity to interact either with water or chloride ions.

In a recent communication<sup>12</sup> we reported internal structural parameters of  $[\text{Ru}(\text{H}_2\text{bibzim})(\text{tbbpy})_2]\text{Cl}_2 \cdot \text{H}_2\text{O}$  **3**. In order to compare the supramolecular aspects of **3** with those of **1** and **2** we discuss here the hydrogen bonding network displayed by **3**. In the solid state both N–H functions are protonated and act as hydrogen bond donors (Fig. 4). In contrast to the previous two structures of **1** and **2** one hydrogen bond is formed to a counter ion Cl<sup>-</sup> ( $\text{N} \cdots \text{Cl}$  3.080(4) Å), the second to a molecule of water which is displaced over two positions and the discussion will use the weighted position ( $\text{N} \cdots \text{O}$  2.626(4) Å). The water serves as hydrogen bond donor to the N–H bonded Cl<sup>-</sup> ( $\text{O} \cdots \text{Cl}^-$  3.039(4) Å) and to the second Cl<sup>-</sup> with an oxygen–chloride distance of 3.022(4) Å. Even so the bibenzimidazole ligand does serve as a hydrogen bond donor; similar to the former systems, no further supramolecular aggregation could be observed.

When we go from the bibenzimidazole **1–3** to the bibenzimidazolates complexes the question arises as to how the trans-

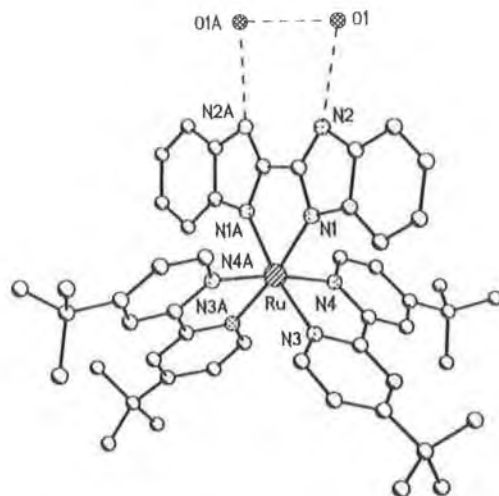


Fig. 5 Hydrogen bonding network of  $[\text{Ru}(\text{bibzim})(\text{tbbpy})_2] \cdot 2\text{H}_2\text{O}$  **4**, protons and acetone molecules are omitted for clarity.

formation of the secondary amine functions to amide functions influences the hydrogen bonding network. If  $[\text{Ru}(\text{bibzim})(\text{tbbpy})_2]$  **4** is crystallized from neat acetonitrile no supramolecular assemblies can be observed.<sup>12</sup> However when the same complex is crystallized from an acetone–water mixture two molecules of water are 2.819(5) Å, within hydrogen bonding distance, to the nitrogens of the deprotonated bibenzimidazole ligand and 3.036(5) Å towards each other as well (Fig. 5). This hydrogen bonding interaction does not seem to affect internal structural parameters of the ruthenium complex.

It seems reasonable to assume that the water molecules serve as hydrogen bond donors towards the negatively polarized bibenzimidazole nitrogens. Additionally one molecule of water serves as hydrogen bond donor for the second water molecule. This system could, in principle, form aggregates similar to **1** and **2**. However, the transformation of the bibenzimidazole unit from a hydrogen-bond donor to an acceptor seems to prevent similar supramolecular arrangements. Even so the degree of protonation does not seem to affect internal structural parameters although it does strongly influence the supramolecular structure of the mentioned complexes.

**Binuclear complexes.** Deprotonation of the bibenzimidazole ligand turns the corresponding complex into a very reactive metallo ligand.<sup>12</sup> The combination of two octahedral complex fragments in one molecule ultimately leads to three diastereomeric isomers the *meso* form  $\Delta\Lambda$  and the  $\Delta\Delta$ ,  $\Lambda\Lambda$  isomers whose racemic mixture is referred to as *rac*. The problem stays at a relatively simple level if symmetric bridging ligands are employed. *meso*- $[\{\text{Ru}(\text{tbbpy})_2\}_2(\text{bibzim})][\text{PF}_6]_2$  **5a** and *meso*- $[\{\text{Ru}(\text{bpy})_2\}_2(\text{bibzim})][\text{PF}_6]_2$  **6** belong to this group.

The *tert*-butyl substituted homodinuclear complex **5a** could be crystallized from a solution of a purified fraction by slow evaporation of the solvent. Its molecular structure is depicted in Fig. 6. The Ru–N<sub>tbbpy</sub> distances of 2.040(3) to 2.065(3) Å are not significantly different from those in the related mononuclear complexes described above and correlate well with values reported for the related biimidazolates (biim) complex.<sup>6</sup> The Ru–N<sub>bibzim</sub> distances are at 2.164(3) Å significantly longer than in the investigated mononuclear complexes.

The homodinuclear complex *meso*- $[\{\text{Ru}(\text{bpy})_2\}_2(\text{bibzim})][\text{PF}_6]_2$  **6** could be crystallized from a mixture of the diastereomeric isomers by slow evaporation of an acetonitrile solution. The Ru–N<sub>bpy</sub> distances of 2.021(4) to 2.043(4) Å are not significantly different from the related mononuclear complexes described above and correlate well with the values recently reported for *meso*- $[\{\text{Ru}(\text{bpy})_2\}_2(\text{biim})][\text{ClO}_4]_2$ .<sup>6</sup> The Ru–N<sub>bibzim</sub> distances are, however, at 2.139(4) Å significantly longer than in the investigated mononuclear complexes<sup>12</sup> but correlate well

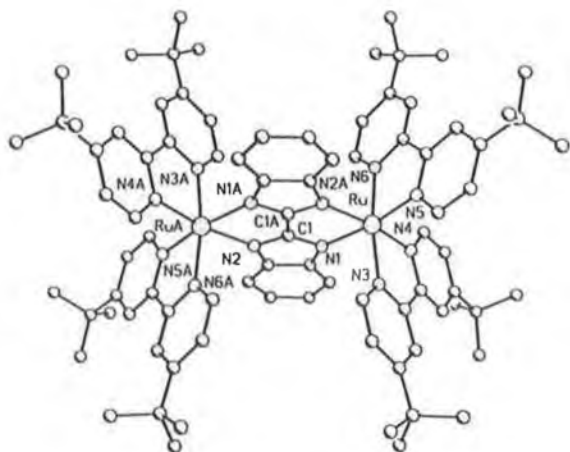


Fig. 6 Structure of *meso*-[(Ru(tbbpy)<sub>2</sub>)<sub>2</sub>(bibzim)](PF<sub>6</sub>)<sub>2</sub> 5a; protons, anions and solvent molecules are omitted for clarity.

with the values reported for the dinuclear biimidazolate complex. They also seem to be slightly shorter compared to those of 5a. The bibenzimidazole ligand in both dinuclear complexes is not bent around a single ruthenium and no torsion angle between the benzimidazole moieties could be observed.

The structural evidence implies that upon going from the mononuclear to the dinuclear complexes a weakening of the bonding interaction between the ruthenium(II) centre and the bridging bibenzimidazole occurs. If bibenzimidazole is acting as a bridging ligand it is double deprotonated and turns into a much stronger  $\sigma$  donor.<sup>7</sup> The increased  $\sigma$  donor strength might cause a decrease of the acceptor abilities. However since the ruthenium–bibenzimidazole distances in the mononuclear deprotonated complex 4<sup>12</sup> are much shorter than in the dinuclear complexes differences in the ligand properties cannot fully explain the differences in bond lengths for the mono- and di-nuclear complexes observed in the structural data obtained from X-ray investigations. Comparing the data obtained it is evident that substitution at the 4 position of the peripheral bipyridine system has no significant influence on structural parameters of the ruthenium complexes (see Table 1).

### NMR spectroscopy of complexes 1–3 and 5

NMR spectroscopy has proved to be a useful tool in the structural characterization of ruthenium polypyridyl complexes<sup>31</sup> but with a few exceptions<sup>32</sup> has not been used to any great extent in the structural characterization of polypyridyl ruthenium bibenzimidazole complexes. The protonated mononuclear complexes [Ru(H<sub>2</sub>bibzim)(bpy)<sub>2</sub>]<sup>2+</sup> 1, [Ru(H<sub>2</sub>bibzim)(dmbpy)<sub>2</sub>]<sup>2+</sup> 2 and [Ru(H<sub>2</sub>bibzim)(tbbpy)<sub>2</sub>]<sup>2+</sup> 3 exhibit C<sub>2</sub> symmetry in solution. The protons of the secondary amine function of the bibenzimidazole ligand are not detectable in CD<sub>2</sub>Cl<sub>2</sub>, DMSO, acetone or acetonitrile and a direct investigation into its involvement in hydrogen bonding was therefore precluded. While the chemical shifts of the aromatic bibenzimidazole protons are almost unaffected by either different substitution or solvent (Table 2), the bipyridine based protons exhibit a large shift on changing the deuterated solvents from acetone to acetonitrile. It is very unlikely that these shifts are due to interaction of the secondary amine protons of bibenzimidazole with solvent molecules since similar shifts have been observed for [Ru(tbbpy)<sub>3</sub>]<sup>2+</sup> (Table 2).

The NMR spectra of the diastereomeric forms of complex 5 are different (Fig. 7). The signals for one pyridine system remain relatively unchanged in both forms, however, the positions of the H5b and H6b protons of the other pyridine moiety are considerably shifted upfield in the spectrum of the *rac* fraction if compared with that of the *meso* form (Table 2). This is consistent with results obtained for the strongly related [(Ru(dmbpy)<sub>2</sub>)<sub>2</sub>(bpm)]<sup>4+</sup> system<sup>3</sup> and has been explained in terms

Table 1 Selected bond lengths (Å) and angles (°) of [Ru(H<sub>2</sub>bibzim)(bpy)<sub>2</sub>](CF<sub>3</sub>SO<sub>3</sub>)<sub>2</sub> 1, [Ru(H<sub>2</sub>bibzim)(dmbpy)<sub>2</sub>](PF<sub>6</sub>)<sub>2</sub> 2, [Ru(H<sub>2</sub>bibzim)(tbbpy)<sub>2</sub>](PF<sub>6</sub>)<sub>2</sub> 3, [Ru(bibzim)(tbbpy)<sub>2</sub>]<sub>2</sub>(bibzim)](PF<sub>6</sub>)<sub>2</sub> 5a and *meso*-[(Ru(tbbpy)<sub>2</sub>)<sub>2</sub>(bibzim)](PF<sub>6</sub>)<sub>2</sub> 6

	1	2	3	4	5a	6
Ru–N(bpy)	2.046(6)	2.045(3)	2.024(2)	2.055(4)	2.040(3)	2.021(4)
Ru–N(bibzim)	2.100(6)	2.088(3)	2.094(2)	2.099(4)	2.160(3)	2.135(4)
N(bpy)–Ru–N(bpy)	78.6(2)	78.66(11)	78.08(9)	78.95(14)	78.81(13)	79.0(2)
N(bibzim)–Ru–N(bibzim)	77.4(3)	77.3(2)	77.14(9)	77.0(2)	80.89(12)	81.3(2)
Bending angle of bibzim	166.1	166.6	166.3	169.3	180	180
Torsion angle of bibzim	4.5	4.3	3.8	1.2	1.3	0.4
N–C–N angle of bibzim	113.0(5)	112.3(3)	113.2(3)	116.8(5)	117.9(3)	118.0(4)

**Table 2**  $^1\text{H}$  NMR data of complexes 1–3, 5 and  $[\text{Ru}(\text{tbbpy})_2][\text{PF}_6]_2$  A in acetone- $d_6$  and acetonitrile- $d_3$ 

Proton	Chemical shifts in acetone- $d_6$					Chemical shifts in acetonitrile- $d_3$				
	1	2	3	5a	5b	A	1	2	3	A
H3a	8.84	8.57	8.83	8.76	8.76	8.86	8.52	8.37	8.51	8.46
H3b	8.80	8.46	8.72	8.68	8.73		8.43	8.28	8.42	
H6a	8.27	7.94	7.96	8.16	8.09	7.82	7.97	7.80	7.87	7.55
H6b	8.16	7.80	8.02	8.32	7.78		7.97	7.71	7.76	
H5b	8.05	7.18	7.61	7.70	7.29		7.38	7.11	7.35	
H3BL	7.82	7.80	7.80	6.66/5.66 <sup>a</sup>	6.66/5.66 <sup>a</sup>		7.78	7.71	7.76	
H5a	7.62	7.38	7.43	7.56	7.51	7.57	7.38	7.27	7.48	7.39
H4BL	7.44	7.38	7.38	6.66/5.66 <sup>a</sup>	6.66/5.66 <sup>a</sup>		7.38	7.37	7.43	
H5BL	7.08	7.02	7.02	6.66/5.66 <sup>a</sup>	6.66/5.66 <sup>a</sup>		7.05	7.03	7.06	
H6BL	5.87	5.86	5.78	6.66/5.66 <sup>a</sup>	6.66/5.66 <sup>a</sup>		5.76	5.83	5.68	
4 position	8.27 H4a	2.57 CH <sub>3</sub> a	1.47 C <sub>4</sub> H <sub>9</sub>	1.43 C <sub>4</sub> H <sub>9</sub>	1.43 C <sub>4</sub> H <sub>9</sub>	1.38 C <sub>4</sub> H <sub>9</sub>	8.11 H4a	2.57 CH <sub>3</sub> a	1.47 C <sub>4</sub> H <sub>9</sub>	1.39 C <sub>4</sub> H <sub>9</sub>
4 position	7.44 H4b	2.41 CH <sub>3</sub> b	1.33 C <sub>4</sub> H <sub>9</sub>	1.34 C <sub>4</sub> H <sub>9</sub>	1.38 C <sub>4</sub> H <sub>9</sub>		7.97 H4b	2.42 CH <sub>3</sub> b	1.35 C <sub>4</sub> H <sub>9</sub>	

<sup>a</sup> Owing to multiple peak overlap no assignment is possible.

**Table 3** Photo- and electro-chemical data in acetonitrile of complexes 1–6

Complex	$\lambda_{\text{max}}/\text{nm}$		Lifetime/ns	$E_{\text{ox}}/\text{V}$	$E_{\text{red}}/\text{V}$
	absorption	emission			
1	463 <sup>a</sup>	640 <sup>a</sup>	131 <sup>b</sup>	1.12 <sup>a</sup>	–1.53/–1.86 <sup>b</sup>
2	465	650	90	0.99	
3	473	648	120	0.99	ca. –0.7 to –1.2
4	580	—	—	0.39	–1.16/–1.25
5a	510	700	50	0.64/0.95	–1.07/–1.21
5b	510	700	60	0.64/0.95	–1.07/–1.21
6	505	695	60 <sup>b</sup>	0.76/1.04 <sup>a</sup>	–1.49/–1.78 <sup>b</sup>

<sup>a</sup> Ref. 7. <sup>b</sup> Ref. 9.

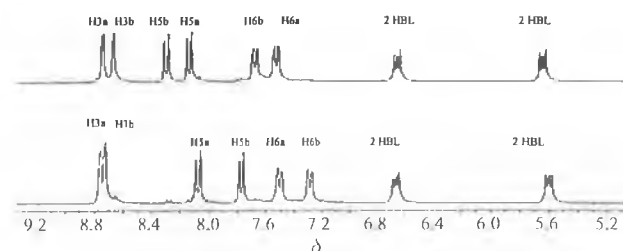


**Fig. 7**  $^1\text{H}$  NMR spectra of the *meso* (top) (5a) and *rac* (bottom) (5b) forms of  $[\{\text{Ru}(\text{tbbpy})_2\}_2(\text{bibzim})][\text{PF}_6]_2$  in acetone- $d_6$ .

of a greater anisotropic effect from the ring current of the adjacent bipyridine system experienced by H5b and H6b protons which are directly over the bridging ligand. The NMR spectrum of the first fraction was assigned to the *meso* form since crystals suitable for X-ray diffraction could be obtained from the purified fraction.

#### Photophysical and electrochemical properties of complexes 1–6

Alkyl substituents at bipyridine ligands should have an inductively electron donating effect on the aromatic system of the corresponding pyridine ring. In order to investigate the influence of substitution on the properties of the ruthenium complexes the oxidation potentials were determined. Alkyl substitution at the 4 position of the bipyridine ligand leads to a roughly 0.1 V shift towards lower oxidation potential of all mono- and di-nuclear complexes investigated which is in agreement with results obtained for  $[\{\text{Ru}(\text{dmbpy})_2\}_2(\text{bibzim})][\text{ClO}_4]_2$ <sup>33</sup> (Table 3). These results suggest that substitution with aliphatic groups has an influence on the electronic situation at the central metal atom. It seems likely that the +I effect of the alkyl substituent results in an increase of the electron density at the metal.

As expected, deprotonation of the bibenzimidazole ligand leads to a large shift of 0.6 V towards more negative potentials

for the oxidation of the ruthenium centre. This indicates an enhanced electron density at the metal centre induced by the deprotonation.

Substitution also influences the reduction properties which are related to the bipyridine system.<sup>5</sup> The most pronounced effect can be attributed to deprotonation of the bibenzimidazole ligand. The not well resolved reduction of the protonated complex is replaced by a two step wave for the deprotonated complex. However due to the complexity of the data obtained for the protonated complex no direct comparison of reduction potentials is possible. Haga investigated the non-substituted complex and did not find a large shift in reduction potentials for the protonated and deprotonated form.<sup>7</sup>

Owing to the intrinsic nature of the MLCT process an increase of the electron density at the ruthenium centre should also influence the photophysical properties of the complex. However, the absorption and emission properties of the complexes (Table 3) do not support this assumption. The mononuclear unsubstituted ruthenium complex 1 absorbs in the visible range at 463 nm. The emission is at 640 nm.<sup>7,9</sup> Whilst the absorption maxima of the series 1 to 3 do show a slight bathochromic shift, the wavelength of emission seems not to be affected at all (Table 3). An investigation of the lifetime of the excited state shows that all three mononuclear complexes have quite similar lifetimes (Table 3). An acetonitrile solution of the dried protonated complex 3 showed no differences to the above described values for absorption maximum and emission wavelength. However, if the same complex is dissolved in water a small bathochromic shift in the absorption maximum is observed and a bathochromic shift of 30 nm in the emission wavelength as well. A similar experiment with  $[\text{Ru}(\text{tbbpy})_2]^{2+}$  showed that the UV-vis spectrum and the wavelength of emission are nearly invariant changing from acetonitrile to water. Comparison indicates that different environments at the N–H functions in solution influence photophysical properties and that water also serves as a hydrogen bond acceptor in



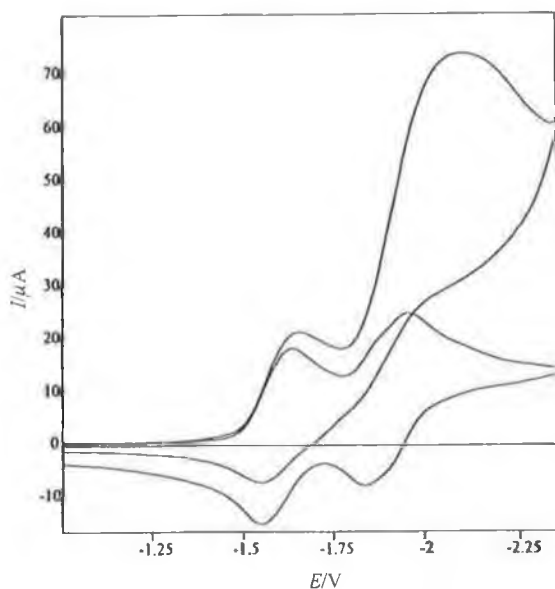


Fig. 8 Negative cyclic voltammogram of  $[\text{Ru}(\text{tbbpy})_2]_2(\text{bibzim})\text{[PF}_6\text{]}_2$  **5a/5b** in acetonitrile vs. SCE; (lower) two one electron reductions under an argon atmosphere; (upper) catalytic current enhancement under a  $\text{CO}_2$  atmosphere.

solution whereas acetonitrile does not interact to a great extent with the N–N functions.

As discussed earlier,<sup>12</sup> deprotonation of the bibenzimidazole forming **4** results in a loss of emission and bathochromic shift of the absorption maxima.

Both dinuclear *tert*-butyl substituted stereoisomers **5a/5b** absorb at 510 nm in the visible range and emit at 700 nm. Complex **6** absorbs at 505 nm and we determined the emission wavelength at 695 nm. Substitution of the pyridine ligand does not seem to influence photophysical properties to a great extent.

Most intriguing was the investigation into the lifetime of the excited state of the two sets of stereoisomers **5a/5b**. The lifetimes of the lowest excited states of both the *meso* and the *rac* isomer were  $60 \pm 2$  ns. The apparent absence of any influence of the stereochemistry on the lifetime of the lowest excited states in dinuclear bibenzimidazole complexes is in contrast to the observations made for stereoisomers of dinuclear HAT (hexa-azatriphenylene) based systems.<sup>16</sup> However in the latter emission occurs from the triplet MLCT ruthenium HAT state.<sup>14</sup> In the case of the dinuclear bibenzimidazole complexes the ancillary bipyridines<sup>7</sup> act as the luminophore. This might be a tentative explanation for the observed independence of the lifetime of the lowest excited state of the stereochemistry at the ruthenium. Comparison with literature values of excited state lifetimes obtained for the unsubstituted isomer **6**, of 60 ns<sup>9</sup> shows that also in the dinuclear complexes the substitution with *tert*-butyl groups has no pronounced influence on the excited state lifetime.

#### Electrochemical $\text{CO}_2$ reduction

Complexes **3**, **4** and a racemic mixture of **5a** and **5b** were investigated for their activity in electrochemical carbon dioxide reduction. Some ruthenium polypyridyl systems<sup>15</sup> exhibit a remarkable activity and selectivity in this process whereas others do not show any activity.<sup>10</sup> Since deprotonation of the bibenzimidazole ligand enhances its  $\sigma$ -donor properties an influence on the electrochemical reactivity can be envisaged.

All investigated complexes can be reduced and at least two reversible one electron reduction processes can be discerned whereas the protonated complex exhibits a much more complex behaviour. In the presence of  $\text{CO}_2$  an increase in the cathodic current can be observed for both steps (Fig. 8) for all three

compounds. The increase is relatively small for the first reduction step whereas a relatively strong increase for the second step can be observed. This indicates that the two electron reduced species is the most active catalyst which transforms the carbon dioxide. The degree of increase of the current is dependent on the complex. The protonated complex **3** exhibits only a relatively small increase in current. The deprotonated complex **4** is roughly twice as active judging from the current enhancement and the dinuclear complex **5a/5b** is even more active than the deprotonated mononuclear complex.

Preliminary investigation into the range of products obtained during an exhaustive reduction of carbon dioxide in a  $\text{CO}_2$  saturated 0.1 M acetonitrile solution of these complexes using **3** showed the production of carbon monoxide (1–2%) and oxalate (*ca.* 10%). If, however, the deprotonated complex **4** was employed oxalate was produced with 43% current efficiency beside some carbon monoxide (1–2%). The course of the reaction was monitored using UV-vis spectroscopy. The protonated complex showed in the initial phase a sharp decrease in the absorption and a shift in the maxima from 473 to 548 nm. This new band continued to decrease during the electrolysis and disappeared completely. For the deprotonated complex no such shifts could be observed however the absorption decreased. This result suggests that some electrical energy is consumed by transformation of the protonated complex. This significant relation between structure and reactivity even for the two mononuclear complexes together with their known interaction with water which might alter the range of products obtained<sup>10</sup> will be investigated in more detail.

#### Conclusion

This work represents to the best of our knowledge the first crystallographic investigation into supramolecular aspects of ruthenium bibenzimidazole complexes. The assembly of highly spatially ordered arrays of mononuclear ruthenium bibenzimidazole complexes is possible for **2** by exploiting the hydrogen bond donor activity of bibenzimidazole towards water. It could also be shown that the choice of counter ions influences the supramolecular structure in the solid state. The nature of the hydrogen bonding activity of ruthenium bibenzimidazole complexes can be reversed from donor to acceptor by deprotonation of the secondary amine which has only a small influence on internal structural parameters. However the resulting species although in principle capable of forming polymeric supramolecular structures bridged by water molecules remains isolated. The deprotonated complex **4** represents a reactive metallo ligand.<sup>12</sup>

By using two dimensional NMR it was also possible to show that two diastereomeric forms of the homodinuclear complexes exist (**5a/5b**) and can be separated. The lifetime of the lowest excited state proved to be independent of the stereochemistry at the ruthenium.

Alkyl substitution at the 4 position of the corresponding pyridine unit resulted in a negative shift of the oxidation potential of the ruthenium. It is possible to switch off the emission of complex **3** by deprotonation of the secondary amine function of the bibenzimidazole ligand.<sup>12</sup>

The mononuclear protonated complex **3**, its deprotonated analogue **4** and the dinuclear complex **5a/5b** are active catalysts in electrochemical carbon dioxide reduction. The reactivity and selectivity of the mononuclear complexes depends on the degree of protonation since **4** exhibits a nearly twofold enhancement of the catalytic current and a 300% increase in current efficiency in oxalate production if compared with that of **3**.

#### Acknowledgements

S. R. and M. R. acknowledge the "Studienstiftung des



Deutschen Volkes" for a Ph.D. grant. Financial support from the Deutsch Forschungsgemeinschaft (SFB 436) is gratefully acknowledged. M. D., C. O'C. and J. G. V. thank the EC TMR programme (grants number CT96-0031 and CT96-0076) for financial assistance.

## References

- 1 V. Balzani, A. Juris, M. Venturi, S. Campagna and S. Serroni, *Chem. Rev.*, 1996, **96**, 759; J. P. Sauvage, J. P. Collin, J. P. Chambron, S. Guillerez, C. Coudret, V. Balzani, F. Barigelletti, L. De Cola and L. Flamingi, *Chem. Rev.*, 1994, **94**, 993.
- 2 V. Balzani and F. Scandola, *Supramolecular Photochemistry*, Ellis Horwood, Chichester, 1991; L. Sun, H. Berglund, R. Davydov, T. Norrby, L. Hammarström, P. Korall, A. Börje, C. Philouze, K. Berg, A. Tran, M. Andersson, G. Stenhagen, J. Mårtensson, M. Almgren, S. Styring and B. Åkermark, *J. Am. Chem. Soc.*, 1997, **119**, 6996; G. S. Hanan, C. R. Arana, J. M. Lehn and D. Fenske, *Angew. Chem., Int. Ed. Engl.*, 1995, **34**, 1122; F. Barigelletti, L. Flamingi, V. Balzani, J. P. Collin, J. P. Sauvage, A. Sour, E. C. Constable and A. M. W. Cargill Thompson, *J. Am. Chem. Soc.*, 1994, **116**, 7692; A. Harriman and R. Ziessel, *Chem. Commun.*, 1996, 1707; F. Barigelletti, L. Flamingi, J. P. Collin and J. P. Sauvage, *Chem. Commun.*, 1997, 333.
- 3 N. C. Fletcher, P. C. Junk, D. A. Reitsma and F. R. Keene, *J. Chem. Soc., Dalton Trans.*, 1998, 133.
- 4 S. Serroni, G. Denti, S. Campagna, A. Juris, M. Ciano and V. Balzani, *Angew. Chem., Int. Ed. Engl.*, 1992, **31**, 1493.
- 5 A. J. Downard, G. E. Honey, L. F. Phillips and P. J. Steel, *Inorg. Chem.*, 1991, **30**, 2259.
- 6 P. Majumadra, S. Peng and S. Goswami, *J. Chem. Soc., Dalton Trans.*, 1998, 1569.
- 7 M. Haga, *Inorg. Chim. Acta*, 1980, **45**, L183; M. Haga, *Inorg. Chim. Acta*, 1983, **75**, 29; M. Haga, T. Matsumura-Inoue and S. Yamabe, *Inorg. Chem.*, 1987, **26**, 4148.
- 8 M. Haga and A. Tsunemitsu, *Inorg. Chim. Acta*, 1989, **164**, 137.
- 9 D. P. Rillema, R. Sahai, P. Matthews, A. K. Edwards, R. J. Shaver and L. Morgan, *Inorg. Chem.*, 1990, **29**, 167.
- 10 Md. M. Ali, H. Sato, T. Mizukawa, K. Tsuge, M. Haga and K. Tanaka, *Chem. Commun.*, 1998, 249.
- 11 M. Haga, Md. M. Ali and R. Arakawa, *Angew. Chem., Int. Ed. Engl.*, 1996, **35**, 76.
- 12 S. Rau, T. Büttner, C. Temme, M. Ruben, H. Görls, D. Walther, M. Duati, S. Fanni and J. G. Vos, *Inorg. Chem.*, 2000, **39**, 1621; for other ruthenium polypyridyl based sensors see A. P. de Silva, H. Q. N. Gunaratne, T. Gunnlaugsson, A. J. M. Huxley, C. P. McCoy, J. T. Rademacher and T. E. Rice, *Chem. Rev.*, 1997, **97**, 1515; F. Barigelletti, L. Flamingi, G. Calogero, L. Hammarström, J. P. Sauvage and J. P. Collin, *Chem. Commun.*, 1998, 2333.
- 13 M. Haga, M. M. Ali, S. Koseki, K. Fujimoto, A. Yoshimura, K. Nozaki, T. Ohno, K. Nakajima and D. J. Stufkens, *Inorg. Chem.*, 1996, **35**, 3335; D. Carmona, J. Ferrer, A. Mendoza, F. J. Lahoz, L. A. Oro, F. Viguri and J. Reyes, *Organometallics*, 1995, **14**, 2066; S. Baitalik, U. Flörke and K. Nag, *Inorg. Chem.*, 1999, **38**, 3296.
- 14 M. J. Uddin, A. Yoshimura and T. Ohno, *Bull. Chem. Soc. Jpn.*, 1999, **72**, 989.
- 15 S. S. Turner, C. Michaut, O. Kahn, L. Quahab, A. Lecas and E. Amouyal, *New J. Chem.*, 1995, **19**, 773; N. W. Alcock, P. R. Barker, J. M. Haider, M. J. Hannon, C. L. Painting, Z. Pikramenou, E. A. Plummer, K. Rissanen and P. Saarenketo, *J. Chem. Soc., Dalton Trans.*, 2000, 1447.
- 16 T. J. Rutherford, O. Van Gitje, A. Kirsch-De Mesmaeker and F. R. Keene, *Inorg. Chem.*, 1997, **36**, 4465; U. Knopf and A. v. Zelewsky, *Angew. Chem., Int. Ed.*, 1999, **38**, 302.
- 17 M. A. Bennett and G. Wilkinson, *Chem. Ind.*, 1959, 1516.
- 18 E. S. Lane, *J. Chem. Soc.*, 1955, 1079.
- 19 T. B. Hadda and H. Le Bozec, *Polyhedron*, 1988, **7**, 575.
- 20 B. P. Sullivan, D. J. Salmon and T. J. Meyer, *Inorg. Chem.*, 1978, **17**, 3334.
- 21 T. Togano, N. Nagano, M. Tsuchida, H. Kumakura, K. Hisamatsu, F. S. Howell and M. Mukaida, *Inorg. Chim. Acta*, 1992, **195**, 221.
- 22 *Gmelin Handbuch*, Erweiterungswerk for the 8th edition, Springer, Berlin-New York, 1974, B 14, A 1, ch. 2.4, pp. 80-89.
- 23 Z. Gwinowski and W. Minor, *Methods Enzymol.*, 1997, **276**.
- 24 G. M. Sheldrick, *Acta Crystallogr., Sect. A*, 1990, **46**, 467.
- 25 G. M. Sheldrick, SHELXL 97, University of Göttingen, 1997.
- 26 D. P. Rillema, D. S. Jones, C. Woods and H. A. Levy, *Inorg. Chem.*, 1992, **31**, 2935.
- 27 Thanks to Dr. Greg Shields, CCDC, for helping with the search for one dimensional water chains; J. P. Glusker, H. L. Carrell, H. M. Berman, B. Gallen and R. M. Peck, *J. Am. Chem. Soc.*, 1977, **99**, 595; R. Kaplonek, G. Fechtel, U. Baumeister and H. Hartung, *Z. Anorg. Allg. Chem.*, 1992, **617**, 161; E. Psillakis, J. C. Jeffery, J. A. McCleverty and M. D. Ward, *J. Chem. Soc., Dalton Trans.*, 1997, 1645.
- 28 M. Ruben, S. Rau, A. Skirl, K. Krause, D. Walther and J. G. Vos, *Inorg. Chim. Acta*, 2000, **303**, 206; C. Anderson and A. L. Beauchamp, *Inorg. Chem.*, 1995, **34**, 6065; C. Sudha, S. K. Mandal and A. R. Chakravarty, *Inorg. Chem.*, 1998, **37**, 270.
- 29 C. M. White, M. F. Gonzalez, D. A. Bardwell, L. H. Rees, J. C. Jeffery, M. D. Ward, N. Armaroli, G. Calogero and F. Barigelletti, *J. Chem. Soc., Dalton Trans.*, 1997, 1727.
- 30 S. de Souza Lemos, K. E. Bessler and E. Schulz Lang, *Z. Anorg. Allg. Chem.*, 1998, **624**, 701.
- 31 A. C. Lees, B. Evrard, T. E. Keyes, J. G. Vos, C. J. Kleverlaan, M. Alebbi and C. A. Bignozzi, *Eur. J. Inorg. Chem.*, 1999, 2309.
- 32 M. Haga, *Inorg. Chim. Acta*, 1983, **77**, L39.
- 33 M. Haga and A. M. Bond, *Inorg. Chem.*, 1991, **30**, 475.
- 34 A. Kirsch-De Mesmaeker, J. Jacquet, A. Masschelein, F. Vanhecke and K. Heremans, *Inorg. Chem.*, 1989, **28**, 2465.
- 35 F. R. Keene and B. P. Sullivan, in *Electrochemical and Electro-catalytical Reactions of Carbon Dioxide*, eds. B. P. Sullivan, K. Kirst and H. E. Guard, Elsevier, Amsterdam, 1993, ch. 5, pp. 118-144 and references cited therein.